UNCLASSIFIED

AD NUMBER
AD893335
NEW LIMITATION CHANGE

TO

Approved for public release, distribution unlimited

FROM

Distribution authorized to U.S. Gov't. agencies only; Test and Evaluation; 15 Feb 1972. Other requests shall be referred to Air Force Flight Dynamics Lab./FY, Wright-Patterson AFB, OH 45433.

AUTHORITY

Air Force Flight Dynamics Lab ltr dtd 27 Aug 1979

THIS PAGE IS UNCLASSIFIED

AFFDL-TR-71-22

A GUIDE FOR PREDICTING
THE AURAL DETECTABILITY OF AIRCRAFT

ERIC E. UNGAR, ET AL

BOLT BERANEK AND NEWMAN, INC.

TECHNICAL REPORT AFFDL-TR-71-22

MARCH 1972

AIR FORCE FLIGHT DYNAMICS LABORATORY
AIR FORCE SYSTEMS COMMAND
WRIGHT-PATTERSON AIR FORCE BASE, OHIO

NOTICE

When Government drawings, specifications, or other data are
used for any purpose other than in connection with a definitely
related Government procurement operation, the United States
Government thereby incurs no responsibility nor any obligation
whatsoever; and the fact that the Government may have formulated,
furnished, or in any way supplied the said drawings, specifica-
tions, or other data, is not to be regarded by implication or
otherwise as in any manner licensing the holder or any other per-
son or corporation, or conveying any rights or permission to man-
ufacture, use, or sell any patented invention that may in any way
be related thereto.

A GUIDE FOR PREDICTING
THE AURAL DETECTABILITY OF AIRCRA T

ERIC E. UNGAR, ET AL

Distribution limited to U.S. Government agencies only; test and evaluation; statement applied 15 February 1972. Other requests for this document must be referred to AF Flight Dynamics Laboratory/FY, Wright-Patterson AFB, Ohio 45433.

ABSTRACT

The concepts which underlie the detection of aircraft by the human ear are described. A scheme is delineated for predicting the range at which a given aircraft will first be heard by an "average" listener; this scheme is also applicable to comparing the aural detectabilities of alternate aircraft configurations and to identifying those components of the noise of a given configuration which bear prime responsibility for the aircraft's detectability. Means are presented for predicting the noise due to all sources likely to be significant for light aircraft, the attenuation of acoustic signals propagating from an aircraft to a listener on the ground, and the ability of a listener to detect an acoustic signal in the presence of background noise.

TABLE OF CONTENTS

page

LIST OF FIGURES

xiii

LIST OF SYMBOLS

A	area
A_b	total propeller blade area
A_j	area of jet
A_ℓ	Fourier coefficient of blade section profile
A_s	Fourier coefficient
B	bending stiffness of beam, or number of plates
C_D	drag coefficient
C_L	lift coefficient
D	flexural rigidity of plate, or jet diameter, or duct diameter
$D_1(r_1)$	maximum blade thickness at radius r_1
E	Young's modulus
F	force, or force component
F_d	drag force at effective radius
F_t	total thrust
G	Green's function
H	duct width
I	acoustic intensity, or moment of inertia
J_m	Bessel function of order m
L	duct length
L_d	detection level, or eddy decay distance
$L_{N,1}$	noise spectrum level
$L_{N,\Delta f}$	noise level in frequency band Δf
$L_{N,c}$	noise level in critical bands
L_{OA}	overall level
L_{OB}	level in octave band

L_p	sound pressure level
L_R	unlined duct length
L_S	lined duct length
$L_{S,1}$	spectrum level of signal
$L_{S,\Delta f_S}$	signal level in frequency band Δf_S
$L_{S,\theta}$	signal level in critical band
L_w	sound power level
ΔL	attenuation
ΔL_S	spreading loss
M	Mach number
M_d	rotational Mach number at effective radius
N	number of cylinders
N_t	number of teeth
P_j	pressure in jet
P_0	ambient pressure
Q	rate of mass displacement
R	distance from sound source
R_c	corrected detection range
R	reference distance
R_{min}	minimum range
R_u	uncorrected detection range
S	duct cross-sectional area
S_1	blade thickness function
T	total drag torque
T_{eff}	effective contact duration
U	free-stream velocity, or flow speed

U_a	absorptive duct perimeter
U_c	convection velocity
U_j	jet velocity
U_0	velocity of entering air
U_{tip}	tip speed of propeller or fan blade
$U_{0.7}$	blade speed at 0.7 radius
V_D	propeller disc volume
W	acoustic power
W_d	dissipated power
W_{in}	power input
W_m	mechanical power
W_{ref}	reference power $= 10^{-12}$ watts
X	distance from leading edge
X_S	distance at beginning of shadow zone
Y_b	point input admittance of beam
Y_c	point input admittance of beam-plate system
Y_d	point input admittance of plate
Z	duct wall impedance
Z_n	impedance of nth mode
a	propeller radius
a_d	effective propeller radius
a_m	propeller mean radius
a_z	effective propeller radius for thrust
a_ϕ	effective propeller radius for torque
b	chord length

b_L	lining thickness
c	speed of sound in air
c_b	speed of bending waves in beam
c_L	longitudinal wave velocity
c_p	speed of bending waves in plate
d	blade thickness
d_p	projected blade thickness
e	base of natural logarithms
f	frequency
f_B	blade passage frequency
f_D	frequency at which $\lambda = D$
f_F	firing frequency
f_{OB}	center frequency of octave band
f_{pk}	peak frequency
f_s	shaft rotation frequency
f_t	tooth contact frequency
Δf	frequency band
h	plate thickness
h_s	mean height of sound source and receiver
i	$\sqrt{-1}$
k	wavenumber
k_p	wavenumber of pressure disturbance
k_r	radial wavenumber
k_z	axial wavenumber
ℓ	index number, or mean free path
m_a	mass flow rate of air
m_b	mass per unit length of beam

m_f	mass flow rate of fuel
m_p	mass per unit area of plate
p	pressure or (rms) sound pressure
$p_{b\ell}$	root-mean-square pressure in boundary layer
p_{ref}	reference pressure = 2×10^{-4} dyn/cm^2 = 2×10^{-5} Newton/m^2
q	source density
r	radial coordinate, or distance, or c_p/c_b
s	harmonic number index
t	time
u_{rms}	root-mean-square fluctuating velocity
v	velocity amplitude
w	span-wise dimension of airfoil edge, or width of beam
x	Cartesian coordinate
z	axial coordinate
du/dz	vertical gradient of effective sound velocity

Ξ	flow resistance of lining per unit thickness
Φ_{ac}	spectrum of radiated acoustic pressure
Φ_d	eddy-decay spectrum function
Φ_f	fixed-location spectrum of pressure
Φ_f'	normalized Φ_f (see Eq. 14 of Appendix K)
Φ_p	pressure spectrum
Φ_3	cross-stream spectrum function
Ω	angular velocity
Ω_0, Ω_1	spherical angles

α	angle of attack, or absorption coefficient
α_I	radius of gyration

$\alpha_{c\ell}$ classical absorption coefficient

α_{mol} molecular absorption coefficient

α_s normalized Fourier coefficient of thrust force

α_{scat} attenuation coefficient for atmospheric scattering

α_{tot} total attenuation coefficient, or total absorption coefficient

α_z absorption coefficient for axial waves

β pitch angle

β_I B/D

β_ℓ Fourier coefficient for blade thickness function

δ boundary layer thickness, or diameter/wavelength ratio

δ_{te} trailing edge thickness

δ_w wake thickness

δ^* boundary layer displacement thickness

θ angle between propeller plane and line from propeller center to observer

θ_e angle of elevation

$\theta_c(f)$ critical band correction

θ_j angle from jet axis

θ_0 angle at sound source, subtended by duct end (see Fig. H1)

ε small angle

η acoustic conversion efficiency, or structural loss factor

λ acoustic wavelength

λ_b bending wavelength

λ_c wavelength at critical frequency

ν angle (see Fig. A2), or kinematic viscosity of air

ρ	density of air
ρ_s	density of structural material
τ	real part of duct propagation constant
τ_n	real part of propagation constant of *nth* duct mode
σ	acoustic radiation efficiency, or imaginary part of duct propagation constant
σ_{ac}	acoustic efficiency
σ_p	porosity of lining
σ_n	imaginary part of propagation constant of *nth* duct mode
ϕ	angular coordinate
ϕ_p	pressure correlation function
χ	structure factor of lining
ψ	angle between propeller blade and plane through hub and observation point (see Fig. B1)
ω	radian frequency
ω_B	blade passage radian-frequency $= \Omega B$

INTRODUCTION

PURPOSE AND SCOPE

It is desirable for all military aircraft to be impossible to detect by the enemy until it is too late for him to employ countermeasures or take evasive action. Modern high-speed strike or reconnaissance aircraft approach this ideal by flying at treetop level, but their high speeds limit their utility for certain missions. Consequently, there exists a continuing interest in slow-flying aircraft of minimum detectability.

Much is known about designing aircraft and countermeasures to reduce detectability by radar, optical and infrared means; also, all of these means tend to be useful only for very limited ranges against aircraft flying at treetop level. In contrast, the acoustic noise emanating from aircraft may be detected - and localized - at very considerable ranges, even by the unaided human ear. Thus, low-speed aircraft tend to be extremely vulnerable to aural detection by personnel on the ground.

Although there exists much information relevant to the design of "quiet" aircraft, this information is widely scattered throughout the literature and is generally inaccessible to the nonspecialist in acoustics. It is the purpose of the present report to provide a collection of information pertinent to the design of aircraft from the standpoint of minimum aural detection, and to present this information in a form in which it may be readily used without reference to a multitude of other documents.

A "quiet" aircraft must satisfy aural detectability specifications, in addition to the usual performance specifications (e.g., payload, range, speed). Generally, many different alternative configurations will satisfy the various requirements to various degrees, and the aircraft designer usually is faced with selecting the best compromises. The designer of an aircraft that must meet stringent aural detectability requirements will generally need to begin with a first-cut configuration designed on the basis of both performance and acoustic requirements; he must then evaluate the aural detectability of his initial design, identify what acoustic changes are required, modify or redesign the aircraft accordingly - and repeat the evaluation-modification cycle until he reaches an acceptable result.

The information provided in the present report may be used:
(1) to compare the aural detectabilities of alternate components
(in order to enable one to make favorable initial choices), (2)
to evaluate and compare the aural detectabilities of aircraft
designs, (3) to estimate the ranges at which aircraft may be de-
tected by ear, and (4) to identify what components of noise con-
tribute most to the aural detectability of a given design (and
thus what components of noise must be reduced in order to reduce
detectability). Although some hints are provided concerning tac-
tics (e.g., selection of favorable terrain and meteorological con-
ditions) for reducing the probability of aural detection and con-
cerning how one might obtain more precise detection-range predic-
tions for given situations, these topics are considered generally
beyond the scope of this report.

ORGANIZATION OF REPORT

The first of the following sections summarizes the basic
concepts involved in aural detectability analysis, presents com-
monly used acoustical quantities and notation, and indicates the
most important characteristics of these quantities. The second
section delineates a scheme for determining the range at which
an aircraft can first be heard, provides guidelines for obtaining
the information needed to apply this scheme, and illustrates its
use.

In the fourteen appendixes of this report are provided the
tools for implementing the suggested detection range estimation
scheme. These appendixes deal with the various noise sources
likely to be significant for light "quiet" aircraft, with the
ability of human listeners to detect an acoustic signal in the
presence of background noise, and with the attenuation acoustic
signals experience as they propagate through the atmosphere.
Each appendix attempts to provide the reader with some insight
into the basic processes; some appendixes - in particular those
which present newly developed information - even contain complete
derivations. Each appendix also includes, usually at its end,
specific directions for application of the given information.

SOME BASIC CONCEPTS

AURAL DETECTABILITY

Aural detectability involves three major considerations:

1. Characteristics of acoustic noise generated at the source,

2. Modifications experienced by acoustic signals as they propagate from the aircraft to listener locations on the ground,

3. Ability of human listeners to detect aircraft noise in their background noise environment.

A noise source may be described most conveniently in terms of its acoustic power spectrum (i.e., the frequency distribution of the acoustic power emitted by the source), its directivity (i.e., the variation of the acoustic power with direction as measured from reference axes attached to the source), and any time - variations of the spectrum and directivity. Because the noise sources associated with aircraft in steady flight are not likely to change with time, time-variations need not be considered here; rather slow variations, such as may result from maneuvers or changes in engine or propeller settings may be analyzed simply in terms of sequences of quasi-steady conditions.

In most military situations in which one is concerned with aural detection, enemy personnel may be located in any direction from the aircraft. One therefore would prefer to design such an aircraft so that there exist no directions in which the radiated sound is more intense than in others - except that one may wish to direct much of the noise upward, where there are no listeners, or possibly backward, where the noise heard at a fixed location on the ground after the aircraft has passed is likely to be less intense than when the aircraft is more nearly overhead. However, for most noise sources of interest here one can do little to change their directivity significantly. Although the various noise sources discussed later do have some inherent directivity characteristics, the directivity effects are generally not very pronounced. For this reason, and because consideration of directivity effects complicates the analysis and greatly increases the computational burden, directivity considerations are not emphasized here. (But directivity information has been included in the appendixes, as far as it is readily at hand, so that it may be available for more detailed analyses than those generally advocated here.)

As an acoustic signal travels away from a source, its energy is spread out over a larger area, so that less energy reaches a sensor (ear or microphone) of a given size. In addition, the atmosphere through which a signal propagates absorbs energy from it, again reducing the signal that reaches a given sensor. Atmospheric gradients also refract (deflect) signals, and may either reduce or increase the amount of energy reaching a sensor; the same is true of terrain and vegetation, which may reflect and/or absorb acoustic energy. An acoustic signal generally is described by its spectrum (frequency-distribution) of acoustic pressure; only spreading attenuates all frequency-components equally, the other attenuation effects generally are frequency-dependent.

A human listener can detect an acoustic signal only if it is strong enough to be above the threshold of sensitivity of his hearing system *and* if it is sufficiently intense so that he can distinguish it from the background noise that always reaches his ear (e.g., due to wind, rustling leaves, machinery, human activity). The hearing sensitivities of different individuals differ widely and are also affected by exposure to noise. Of course, any ear covering tends to reduce this sensitivity, whereas listening aids (even cupped hands) may enhance it. An individual's ability to detect an acoustic signal also depends on many psychological factors, such as fear and fatigue, whose effects cannot be readily predicted. The "masking" effect of background noise depends on the spectral (and time-dependent) character of both the noise and the signal. Prediction of whether a given signal will be detected (or better, of the probability that a given signal will be detected) under given conditions clearly is a very complex problem. Fortunately, this problem and most of its complexities may be by-passed here, since for purposes of evaluating alternate aircraft components and designs it suffices to consider an average listener under representative conditions.

ACOUSTICAL QUANTITIES

Sound Power Level and Sound Pressure Level

Because the values of sound power and sound pressure encountered in most acoustics problems extend over several orders of magnitude, it has become customary to represent these quantities in logarithmic terms. Thus, the sound power level L_W of a source which radiates acoustic power W is defined as*

$$L_W = 10 \log (W/W_{ref}) \tag{1}$$

_____

*All logarithms in this report refer to base 10.

4

where W_{ref} is a reference power. The internationally accepted standard value $W_{ref} = 10^{-12}$ watt $\approx 7.38 \times 10^{-13}$ ft lb/sec is used throughout this report. The power level L_W is a dimensionless quantity, but to indicate its logarithmic character and the fact that it is defined with a factor of 10, it is given the "units" of decibels (dB). Because different reference values have been used, it is also customary to indicate the reference value one uses. For example, the power level corresponding to an acoustic power of 2.0 watt would be written as $L_W = 123$ dB, re 10^{-12} watts.

The sound pressure level L_p corresponding to a mean-square acoustic pressure p^2 is defined in a manner similar to Eq. (1) as

$$L_p = 10 \log (p^2/p_{ref}^2) = 20 \log (p/p_{ref}) \qquad (2)$$

where p_{ref}^2 represents a reference mean-square pressure, and where p and p_{ref} represent the root-mean-square values that correspond to p^2 and p_{ref}^2. The internationally accepted standard reference value $p_{ref} = 0.0002$ microbar $= 0.0002$ dyne/cm^2 $= 2 \times 10^{-5}$ newton/m^2 $\approx 2 \times 10^{-10}$ atm $\approx 2.86 \times 10^{-9}$ psi is used throughout this report. Again, it is customary to append the "dB" designation to the sound pressure level and to indicate the reference quantity; for example, the pressure level corresponding to an acoustic pressure of $p = 10$ microbar would be written as $L_p = 94$ dB, re 0.0002 microbar.

In the foregoing definitions W and p may represent either the total power and mean-square pressure measured at all frequencies, or those same quantities measured in specified frequency bands. If these quantities are measured in bands and the resulting L_W and L_p values are plotted as a function of frequency (usually, the center frequency of the bands used), one obtains sound power and sound pressure spectra. Spectra are most often given in octave bands (which span a factor of 2 in frequency) and 1/3 octave bands (which span a factor of $2^{1/3}$ in frequency).

Dependence of Sound Pressure on Sound Power Level

The mean-square acoustic pressure(measured at a given frequency or in a given frequency band) at a given location with respect to a sound source is proportional to the acoustic power produced by that source (at the same frequency or in the same frequency band). In a free field, where no reflections occur, the acoustic pressure decreases with increasing distance from the source; at several wavelengths' distance from the source, the mean-square pressure varies inversely as the square of the distance from the source (because in essence the acoustic power emanating from the source is spread over a larger surface area and a sensor of a given area intercepts less of the power).

The aforementioned variation, when expressed logarithmically and with the appropriate constants, results in a simple expression for the sound pressure level L_p measured at a distance R from a nondirective source (i.e., a source that radiates uniformly in all directions) emitting sound with a sound power level L_w:

$$L_p(dB, re\ 0.0002\ microbar) = L_w(dB, re\ 10^{-12}watt) - 20\ log\ R - 0.5 \quad (3)$$

where R denotes the distance in feet.

Dependence of Levels on Bandwidth

It is often necessary to express levels given in bands of one width in terms of levels in bands of other widths. For signals whose narrow-band spectra are relatively flat within the broader (overlapping) bands Δf_1 and Δf_2, one may assume the power to be approximately uniformly distributed over frequency in the vicinity of the bands of concern. If W_1 represents the power in the band Δf_1 and W_2 that in Δf_2, then

$$W_1/\Delta f_1 = W_2/\Delta f_2 . \quad (4)$$

The power level L_{W1} in the band Δf_1 then is related to the level L_{W2} as

$$L_{W1} = L_{W2} + 10\ log\ (\Delta f_1/\Delta f_2) \quad (5)$$

If Δf_1 is an octave band and Δf_2 a 1/3-octave band of the same center frequency, then $\Delta f_1/\Delta f_2 = 3.0$ and $L_{W1} - L_{W2} \approx 5$ dB.

Multiple Sources

The total acoustic power radiated by several sources is equal to the sum of the individual contributions. This is true of the overall power (including all frequencies), as well as in any frequency band.

The mean-square pressure observed at a given location as the result of several sources similarly is equal to the sum of the individual mean-square contributions (overall, or in specified bands), provided that the various individual contributions are uncorrelated (i.e., not substantially in phase with each other)*

---

*For correlated signals, the total *root*-mean-square pressure is equal to the sum of the *root*-mean-square components.

Since it is unlikely that the noise components produced by different sources on an aircraft will be correlated, one may consider them generally uncorrelated for all practical purposes.

It is usually convenient to work only in terms of the levels, and to avoid converting from levels back to the basic quantities, combining these quantities as outlined above, and then converting the results again into levels. One may obtain the (power or pressure) level L_{comb} which corresponds to the combination of two components, one at level L_1 and one at L_2, by using the chart of Fig. 1. For example, by use of this chart one may determine very easily that a signal of 90 dB and one of 96 dB combine to produce a signal of 97 dB (*not* 186 dB!).

One may obtain the level corresponding to a combination of several signals by using the chart repetitively for two components at a time; the sequence of forming the two-at-a-time combinations is immaterial. For example, consider four levels: $L_1 = 60$ dB, $L_2 = 65$ dB, $L_3 = 66$ dB, $L_4 = 68$ dB. Then one finds $L_{1+2} = 66.2$ dB, $L_{3+4} = 70.1$ dB, and $L_{(1+2)+(3+4)} = 71.6$ dB; or

$$L_{(1+2)+3} = 69.0 \text{ dB}, \quad L_{[(1+2)+3]+4} = 71.6 \text{ dB}.$$

DETECTION RANGE CALCULATION

GENERAL APPROACH

The "aural detection range" of a given aircraft operating at specified conditions may be defined as the greatest distance at which an "average" listener on the ground can distinguish the aircraft sound from his ambient background noise environment. In order to estimate this detection range, one may proceed as follows:

1. Determine the frequency distribution of the acoustic power emitted by the aircraft, due to all sources;

2. Determine the "detection level spectrum", i.e., the sound pressure level spectrum of signals that the average listener can just detect in the presence of the ambient noise;

3. Calculate the distance within which the aircraft sound (at each frequency) reaches the level at which it can be detected by the listener. This process results in a frequency distribution of ranges, or a "detection range spectrum". The maximum of this spectrum then is the detection range.

This approach is illustrated graphically in Fig. 2, to which further reference will be made below.

ACOUSTIC POWER EMITTED BY AIRCRAFT

In order to determine the spectrum of the acoustic power generated by a given aircraft under specified operating conditions, one generally may proceed best by considering each noise source separately, and then combining the effects of all such sources. Where acoustic data directly pertinent to specific components (e.g., engines, propellers, or engine-propeller combinations) are available, this data should be used. If such data are not in hand, one may use the estimation techniques presented in the appendixes to this report.

For *propeller-drive aircraft,* one should consider the following sources (listed in the probable order of importance)*:

---

*Note: The capital letters preceding each noise component listed indicate the appendix which may be used to estimate the noise from that component.

1. Propeller
   A Rotational (pure-tone) noise
   B Vortex (broad-band) noise

2. Engine exhaust, intake, and casing
   C Piston engines
   D Rotating combustion engines
   E Turboshaft engines

3. Power transmission systems
   J Gears

4. Aerodynamic noise
   K Boundary layer turbulence
   K Movement through atmospheric turbulence
   K Turbulent wakes

5. Vibrating internal components
   L Radiation from point-excited surface structures

   For *jet-engine drive aircraft,* one should consider the fol-
lowing sources (again listed in the probable order of importance)*:

1. Propulsion system
   E Turbine exhaust, inlet, casing
   F Fan and compressor (pure-tone) noise
   G Jet exhaust flow
   H Effects of inlet and exhaust ducts

2. Aerodynamic noise
   K Boundary layer turbulence
   K Movement through atmospheric turbulence
   K Turbulent wakes

3. Vibrating internal components
   L Radiation from point-excited surface structures

   The upper part of Fig. 2 illustrates the acoustic power
spectra for an hypothetical propeller-driven aircraft. For the
sake of clarity, only two broad-band source-spectra (propeller
vortex noise and engine casing noise**) and pure tones from only
one source (propeller rotational noise) are shown. The figure
also shows the total broad-band noise spectrum, obtained by com-
bining the two contributions according to Fig. 1.

---

*Note: The capital letters preceding each noise component listed
 indicate the appendix which may be used to estimate the noise
 from that component.

**For this hypothetical aircraft, the exhaust was assumed to be well
 muffled, so that exhaust noise is effectively absent.

DETECTION LEVEL SPECTRUM

As discussed in Appendix N, the sound pressure level of an acoustic signal that a listener can just detect depends on the listener's threshold of hearing and on the ambient noise that surrounds him. The threshold of hearing for pure tones is slightly different from that for bands of noise, and a given (broad-band) background noise generally can mask a broad-band signal better than it can a pure tone. Therefore, one must treat pure-tone and broad-band signals separately.

Appendix N presents standard hearing threshold curves and indicates how one may determine the detection levels which correspond to given ambient noise spectra. (The detection level represents the sound pressure level of a signal which is just detectable against the background noise.) A signal is detectable if it exceeds at any frequency both the hearing threshold level and the detection level - thus, if it exceeds the higher of these two levels. A curve which at any frequency follows either the hearing threshold level curve or the detection level curve, whichever is higher, thus constitutes a "detection level spectrum", which a signal must exceed to be detectable.

Information on the ambient noise in some environments likely to be of interest in relation to quiet aircraft design is also presented in Appendix N, in terms of detection levels for pure-tone signals.

Figure 2 illustrates how one may derive pure-tone and octave-band detection level spectra from the hearing threshold curves and detection levels. The hearing threshold curves in Fig. 2 have been taken from Fig. N1. The pure tone detection level corresponds to nighttime data for a dense Panama jungle (from Fig. N4); the octave-band detection data has been derived from the pure-tone data with the aid of Fig. N2. The heavy solid and dashed curves then correspond to the detection level spectra, for pure-tones and octave-band noise, respectively.

DETECTION RANGE SPECTRUM

If one knows the spectrum of acoustic power levels L_w of the noise of an aircraft and also the spectrum of detection levels L_d applicable to given conditions, one may easily determine the distance over which each frequency-component of the aircraft noise must travel (in an ideal non-absorbing and non-scattering atmosphere) so that the sound pressure level of the signal is equal to the detection level. In view of Eq. (3), this distance R_u (ft) may be found from

$$20 \log R_u = L_w - L_d - 0.5 \approx L_w - L_d \qquad (6)$$

L_w and L_d are expressed in decibels, referred to the standard reference power and pressure, respectively. Because of the uncertainties usually involved in estimating L_w and L_d, one may usually neglect the 0.5 dB correction.

By applying Eq. (6) to each frequency component, one may arrive at a spectrum of "uncorrected detection ranges" R_u. The designation "uncorrected" implies that corrections for atmospheric and terrain attenuation effects have not yet been included.

If L_w and L_d are plotted to the same scale, as in Fig. 2, one may determine $20 \log R_u$ graphically, as shown in the figure. Again, one must carry out separate calculations for the pure-tone and for the broad-band noise components. The uncorrected detection range spectrum one obtains from Fig. 2 is shown as the dotted curve of Fig. 3 for broad-band noise and as the open circles for pure-tone noise. *

From the information presented in Figs. M1 though M3 (of Appendix M) one may estimate the total absorption coefficient α_{tot} (dB/ft) due to atmospheric and terrain effects at each frequency. From Fig. M4 or the corresponding relation (see last footnote of Appendix M) one may then correct the previously found "uncorrected detection range" spectrum, to obtain a spectrum of actual (corrected) detection range. The maximum of this spectrum determines the range at which the aircraft will first be heard under the specified conditions; by noting the frequency at which this maximum is found and referring back to the noise source spectra, one may then determine which noise component is primarily responsible for earliest aural detection of the aircraft - i.e., which noise component must be reduced to reduce the detection range significantly.

The solid curve and filled-in circles of Fig. 3 represent the corrected detection range spectrum for the octave-band and pure-tone noise components, respectively, as obtained from the uncorrected spectrum for certain conditions ($\alpha_{tot} \approx 0.02$ dB/ft). One finds that the maximum of the corrected range spectrum corresponds to $20 \log R_c \approx 70$ indicating that the aircraft will first be detected aurally at a range of about 3000 ft. One finds that the 160 Hz pure tone component of propeller rotational noise will be heard first. If this component can be reduced by a little more than 3 dB, then the 80 Hz tone becomes predominant, and the detection range is reduced to about 2000 ft. If all the propeller pure-tones could be eliminated (or reduced by 10 dB or more), the detection range would be about 1000 ft; with the noise components

---

*Appendix P presents an alternate method for determining R_u. This alternate method is preferable if recorded flyby noise data are available, or if there exists considerable uncertainty about whether a noise component should be considered as a pure-tone or broadband.

between 125 and 160 Hz being heard first. One notes from Fig. 2 that at these frequencies the noise is primarily engine casing noise; therefore, one would need to reduce the noise from this source in order to achieve any further reduction in detection range.
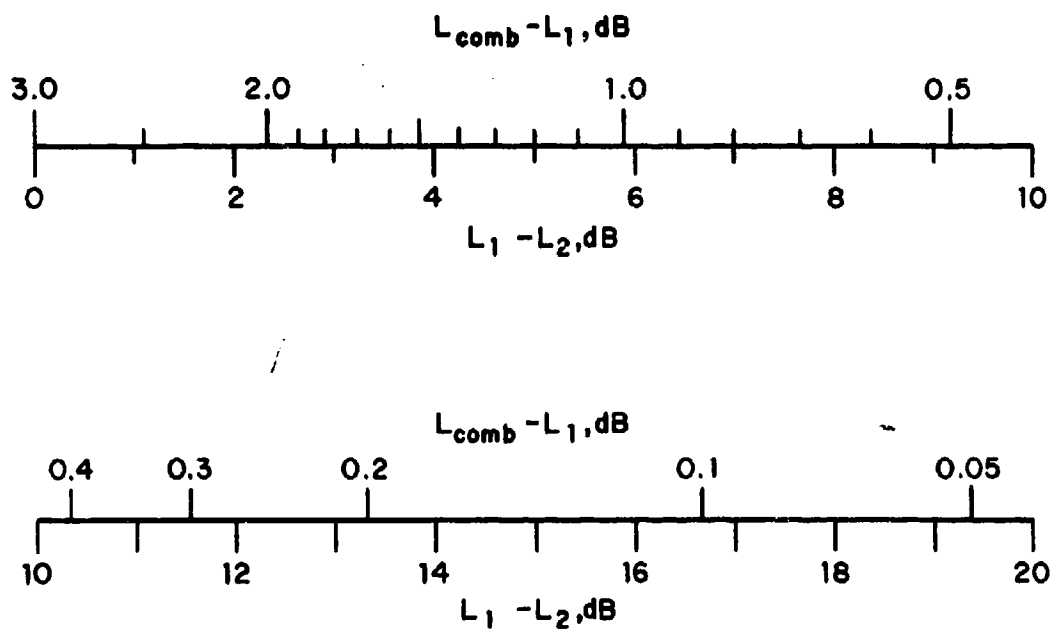
FIGURE 1   CHART FOR COMBINING TWO UNCORRELATED ACOUSTIC LEVELS,
            L₁ and L₂.   LEVELS MAY BE POWER LEVELS OR SOUND-
            PRESSURE LEVELS
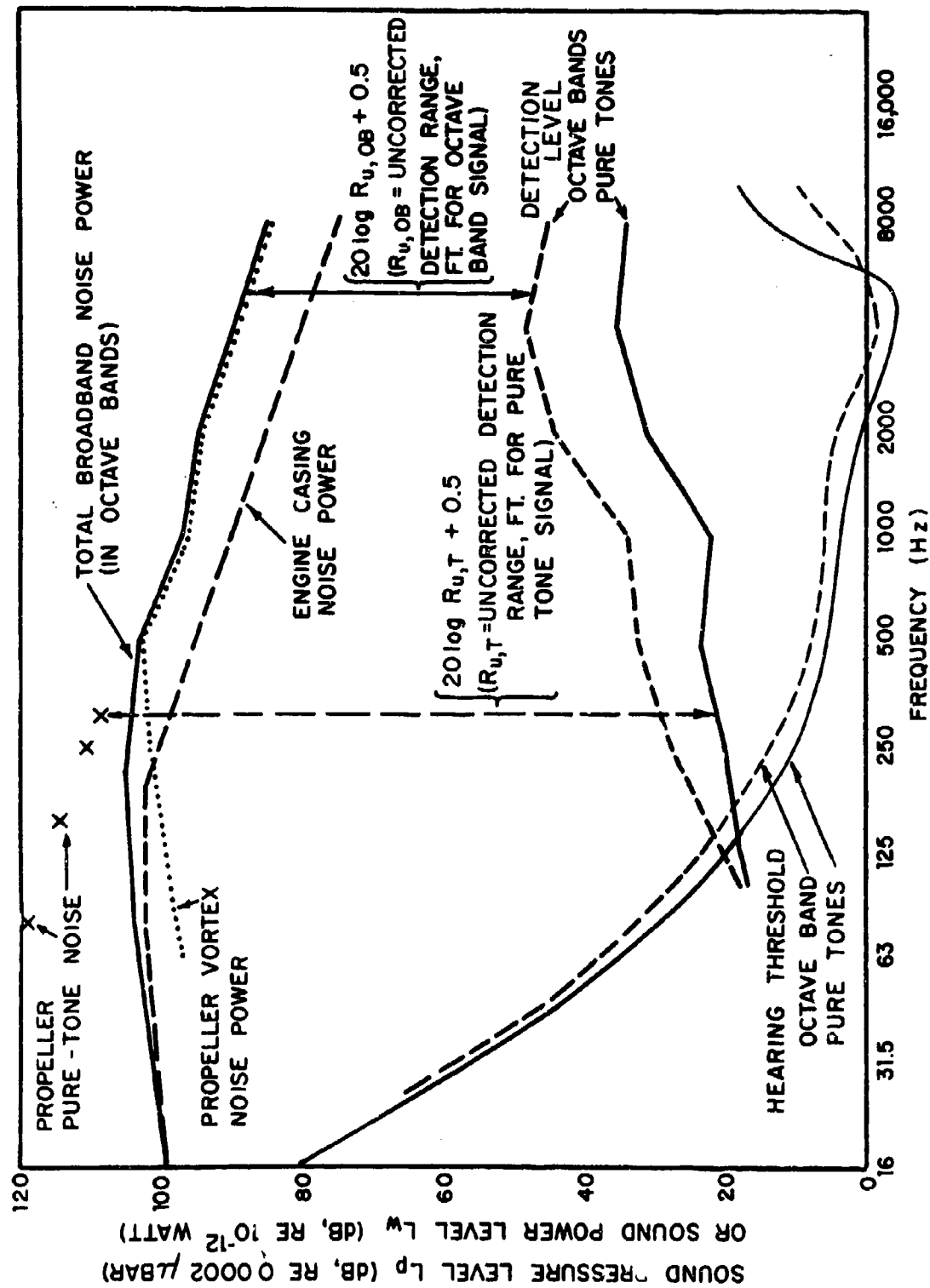
FIGURE 2   ILLUSTRATION OF DETECTION RANGE CALCULATION APPROACH
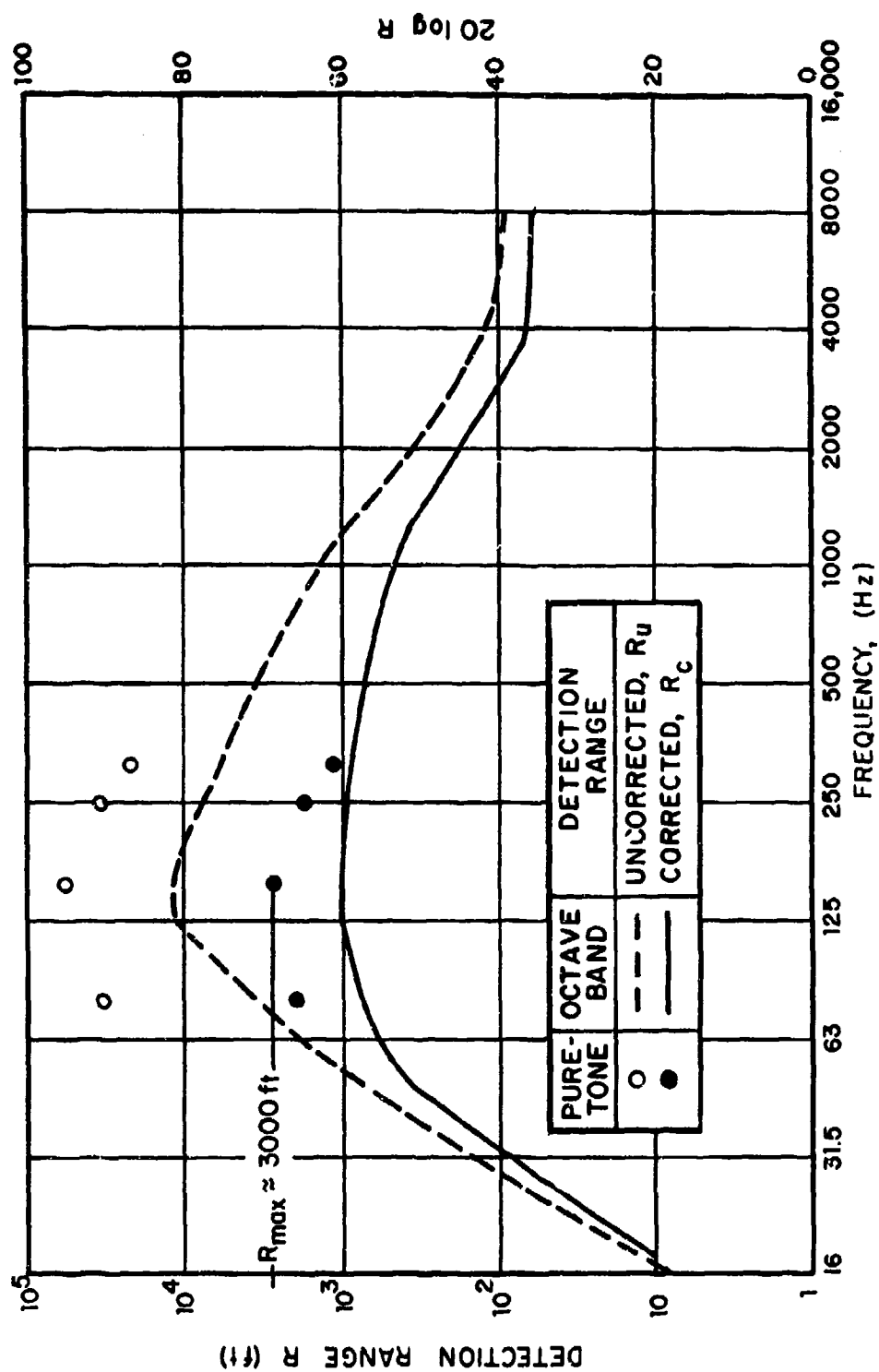
FIGURE 3   DETECTION RANGE SPECTRA CORRESPONDING TO FIGURE 2

APPENDIX A

ROTATIONAL NOISE OF PROPELLERS

DIPOLE SOUND

Early investigations of propeller noise (Ref. 1) showed that the lift and drag forces acting on the propeller blades give rise to equal and opposite inertia forces on the fluid medium, and these forces constitute arrays of acoustic dipole sources distributed over the propeller disk and rotating in the propeller plane at the propeller's angular velocity.

In order to analyze the acoustic effects of these dipole sources, it is convenient to treat first the case of a propeller having B blades, rotating at angular velocity Ω (but not advancing axially) with uniform inflow to the propeller. An element of the fluid medium at polar coordinate position r_1, ϕ_1 in the plane of the propeller is subjected to forces F_Z and F_ϕ as the propeller passes the element's location, which correspond to infinitesimal increments of the thrust and the drag on the propeller blade. When there is no propeller blade present at the position r_1, ϕ_1, there is no force exerted on the fluid.

The duration of each force pulse is determined by the local width of the propeller blade, projected onto the propeller disk plane, and by the propeller's rotational speed. The force on the fluid at a typical location then varies with time as shown in Fig. A1. If one expands such a periodic function in a Fourier series, one obtains a sum of harmonic functions whose frequencies are multiples of the blade passage frequency $\omega_B = \Omega B$.

One may express (see Ref. 2) the axial force distribution as

$$F_Z(t;r_1,\phi_1) = \sum_s A_s \exp[-is\omega_B(t-\phi_1/\Omega)]$$

$$= F_Z^0 \sum_{-\infty}^{\infty} \alpha_s \exp(isB\phi_1)\exp(-isB\Omega t) \tag{1}$$

where A_s and α_s are Fourier coefficients; s is the harmonic number index; F_Z^0 is the thrust force amplitude.

Similarly, the drag force distribution may be expressed as

$$F_\phi(t;r_1,\phi_1) = F^o_\phi \sum_{-\infty}^{+\infty} \alpha_s \exp(isB\phi_1)\exp(-isB\Omega t) \qquad (2)$$

As shown in Ref. 3, application of a concentrated force at a point in a fluid is equivalent to locating an acoustic dipole source at that point, with the dipole axis in the direction of the force. Thus, the double array of forces over the propeller disk due to thrust and drag gives rise to acoustic radiation from a double array of dipole sources, the thrust-related array having all sources aligned parallel to the propeller shaft and the drag-induced sources aligned parallel to the propeller plane.

To find the sound field produced by the previously given force distributions, one may use the Green's function for a dipole source of unit strength in the z-direction and of sinusoidal frequency ω, (Ref. 2)

$$G_{1z} = - ik\cos\nu \; \frac{e^{ikr}}{4\pi r} \sum_{m=-\infty}^{+\infty} i^m J_m(kr_1 \sin\nu)e^{im(\phi-\phi_1)}e^{-i\omega t} \qquad (3)$$

where the distances r and r_1 and angles ν, ϕ and ϕ_1 are defined in Fig. A2, and where J_m represents the m'th order Bessel function. Also, $k = \omega/c$ is the wavenumber and c represents the wave propagation speed, i.e. the speed of sound. The Green's function for a unit dipole in the ϕ_1-direction is similarly given by

$$G_{1\phi} = \frac{1}{r_1} \frac{e^{ikr}}{4\pi r} \sum_{m=-\infty}^{\infty} m i^m J_m(kr_1 \sin\nu)e^{im(\phi-\phi_1)}e^{-i\omega t} \qquad (4)$$

The foregoing forms of the Green's functions involve approximations which are valid only if the point of observation is in the geometric, as well as in the acoustic far-field of the source, — i.e., if the observation distance is much greater than both the physical dimensions of propeller disk and the acoustic wavelength in the fluid medium.

The sound pressure due to the thrust force then may be determined from

$$p_z(r,\phi,\nu,t) = \iint F_z(t;r_1,\phi_1)G_{1z}(r_1,\phi_1;r,\phi,\nu)r_1 dr_1 d\phi_1 \qquad (5)$$

and that due to the drag force from

$$p_\phi(r,\phi,\nu,t) = \iint F_\phi(t;r_1,\phi_1)G_{1\phi}(r_1,\phi_1;r,\phi,\nu)r_1 dr_1 d\phi_1 \qquad (6)$$

By substituting Eqs. (1) and (3) into (5) and noting that the frequency in the Green's function must be the same as that of the source component ($\omega = sB\Omega$, $k = \frac{sB\Omega}{c} = sk_1$), one obtains

$$p_z(r,\phi,\nu,t) = \iint \left[-\frac{ik_1\cos\nu}{4\pi r}\sum_s\sum_m si^m J_m(sk_1 r_1\sin\nu)e^{isk_1 r} \right.$$

$$\left. e^{im(\phi-\phi_1)}e^{-isB\Omega t}e^{isB\phi_1}F_z^o\alpha_s 2\pi r_1 dr_1 d\phi_1 \right] \qquad (7)$$

Because of the factors $e^{im(\phi-\phi_1)}$ and $e^{isB\phi_1}$, the integration over ϕ_1 results in zero terms, except for $m = sB$, and where the integration introduces a factor of 2π. (Since the radiation function G_{1z} is built up of components periodic in ϕ_1, as measured from some reference angle, and since the source distribution is also composed of terms periodic in ϕ_1, only those radiation function harmonics which are spatially in phase with the source distribution terms contribute to the sound pressure disturbance arriving at the point of observation.) The summation with respect to m and the integration over the angle ϕ_1 can thus be handled quite simply, and Eq. (7) may be reduced to

$$p_z(r,\phi,\nu,t) = \frac{-ik_1\cos\nu}{4\pi r}\sum_s\left[si^{sB}e^{isk_1 r}e^{isB\phi}e^{-isB\Omega t} \right.$$

$$\left. \int F_z^o\alpha_s J_{sB}(sk_1 r_1\sin\nu)2\pi r_1 dr_1 \right] \qquad (8)$$

Similarly, the sound pressure due to the torque-related forces is found to be

$$p_\phi(r,\phi,\nu,t) = \frac{Bi}{4\pi r}\sum_s\left\{ si^{sB}e^{isk_1 r}e^{isB\phi}e^{-isB\Omega t}\int\left[\frac{1}{r_1}F_\phi^o\alpha_s J_{sB}\right.\right.$$

$$\left.\left. (sk_1 r_1\sin\nu)2\pi r_1 dr_1 \right] \right\} . \qquad (9)$$

18

This elementary theory based on the rotating forces exerted on the fluid medium by the propeller blades predicts two series of discrete-frequency pressure disturbances; each series is composed of multiples of the blade passage frequency, and each pressure term varies inversely with the first power of the distance from the propeller hub to the observation point. Each series term involves a directivity factor, and the source level of each term is related to the aerodynamic harmonic forcing function which produces the dipole source. From the exponential factors in each series representation, one may note that at a fixed value of r, the angular position ϕ of constant phase rotates with the shaft velocity Ω.

Since the factors F_z^o, F_ϕ^o, and α_s in general are functions of radial position r_1, evaluation of the integrals in Eqs. (8) and (9) presents some difficulties. Some approximations are possible, as presented below. By use of the mean-value theorem, one may write

$$\int_0^a F_z^o \alpha_s J_{sB}(sk_1 r_1 \sin\nu) 2\pi r_1 dr_1 =$$

$$\left[\alpha_s J_{sB}(sk_1 r_1 \sin\nu)\right]_{r_1=a_z} \cdot \int_0^a F_z^o 2\pi r_1 dr_1 = \left[\alpha_s J_{sB}(sk_1 r_1 \sin\nu)\right]_{r_1=a_z} \cdot F_t$$

where a denotes the propeller radius, a_z is an "effective radius" at which $\alpha_s J_{sB}$ is to be evaluated in order to produce the correct value of the integral, and F_t represents the total thrust force exerted on the propeller. Equation (8) then may be reduced to

$$p_z(r,\phi,\nu,t) = -F_t \frac{ik_1 \cos\nu}{4\pi r} \sum_s \left\{ s e^{isB\pi/2} e^{isk_1 r} e^{isB\phi} e^{-isB\Omega t} \right.$$

$$\left. \left[\alpha_s J_{sB}(sk_1 r_1 \sin\nu)\right]_{r_1=a_z} \right\} \tag{10}$$

and, similarly, Eq. (9) may be rewritten as

$$p_\phi(r,\phi,\nu,t) = \frac{iT}{4\pi r}\left(\frac{1}{r_1}\right)^2_{r_1=a_\phi} \sum_s \left\{ sB\ e^{isB\pi/2} e^{isk_1 r} e^{isB\phi} e^{-isB\Omega t} \cdot \right.$$

$$\left. \left[\alpha_s J_{sB}(sk_1 r_1 \sin\nu)\right]_{r_1=a_\phi} \right\} \tag{11}$$

where a_ϕ is the effective radius for drag, analogous to a_z for thrust, and T represents the total drag torque. The values of a_z and a_ϕ depend upon both the radial variation in loading represented by F_z^0 and F_ϕ^0 and the angular variation of blade forces represented by the factor α_s; since the value of α_s is different for each frequency contribution, the effective radii a_z and a_ϕ generally also depend on the harmonic index s.

Morse and Ingard (Ref. 2) introduce the approximation that $a_z \approx a_\phi = a_d$ so that the total sound pressure due to the two dipole source mechanisms is given by the sum

$$p = p_z + p_\phi = \frac{1}{4\pi r} \sum_s \left[sk_1 F_t \cos\nu + \frac{T_{sB}}{(a_d)^2} \right] \left[\alpha_s J_{sB}(sk_1 r_1 \sin\nu) \right]_{r_1 = a_d} \cdot$$

$$e^{isB\left(\phi + \frac{\pi}{2}\right)} e^{-is(B\Omega t - k_1 r)} . \tag{12}$$

From this result one finds that the amplitude of the sth harmonic frequency component is given by

$$p_s = - \frac{(\alpha_s) sB\Omega}{4\pi rc} \left(-F_t \cos\nu + \frac{F_d}{M_d} \right) J_{sB}(sBM_d \sin\nu) \tag{13}$$

where M_d represents the rotational Mach number at the effective radius a_d,

$$M_d = \frac{a_d \Omega}{c}$$

and where $F_d = T/a_d$ represents the drag force.

Equation (13) gives the amplitude of propeller noise due to dipole source mechanisms associated with the aerodynamic force loadings on the propeller blades which give rise to thrust and rotational drag. By virtue of the $\cos\nu$ term, the thrust contribution vanishes in the plane of the propeller; the *sum* of the two contributions vanishes on the propeller axis, in view of the Bessel function directivity factor. [Equation (13) may be seen to be a generalization of Gutin's formulation.]

MONOPOLE SOUND

In addition to providing net lift and drag, a propeller blade element displaces some fluid by virtue of its thickness, and thus acts as a monopole sound source. In order to analyze this sound contribution, one may describe the propeller in terms of a blade thickness function $S_1(r_1', \phi_1')$, which defines the blade thickness distribution in polar coordinates r_1', ϕ_1' rotating with the propeller For a fixed radial distance r_1' in the propeller plane, the thickness function may be expressed as

$$S_1(r_1', \phi_1') = D_1(r_1')S_1(\phi_1') = D_1(r_1') \sum_{\ell=-\infty}^{+\infty} \beta_\ell e^{i\ell B\phi_1'} \tag{14}$$

where $D_1(r_1')$ gives the maximum blade thickness as a function of radial distance, and $S_1(\phi_1')$ and its Fourier expansion describes the blade cross-section profile. In terms of the nonrotating coordinates $r_1 = r_1'$ and $\phi_1 = \phi_1' + \Omega t$, the thickness function becomes $S(r_1, \phi_1 - \Omega t)$ and has the form sketched in Fig. A3.

The monopole source term in the general wave equation is the time derivative of the rate Q at which mass is displaced per unit area of the propeller plane. Here one finds that Q is given by

$$Q(r_1, \phi_1) = \rho\left(\frac{\partial S}{\partial t}\right) = -\rho\Omega S' = -\rho\Omega\left(\frac{\partial S_1}{\partial \phi_1'}\right) \tag{15}$$

where ρ denotes the density of air, so that the acoustic source term is

$$\frac{\partial Q}{\partial t}(r_1, \phi_1) = -\rho\Omega^2 S'' = \rho\Omega^2 \frac{\partial^2 S_1}{\partial \phi_1'^2} . \tag{16}$$

Using Eq. (14), one may rewrite this term as

$$\frac{\partial Q}{\partial t}(r_1, \phi_1) = -\rho\Omega^2 D_1(r_1) \sum_{\ell=-\infty}^{+\infty} \ell^2 B^2 \beta_\ell e^{i\ell B\phi_1'} . \tag{17}$$

To obtain the acoustic pressure at the observation point (r, ϕ, ν), one may form the product of the source function and

Green's function for a monopole source, and integrate this product over the source plane. After some manipulation, one arrives at

$$p(r,\phi,\nu,t) = - \frac{\rho\Omega^2 B^2}{4\pi r} \sum_{\ell=-\infty}^{+\infty} \left[\ell^2 e^{i\ell B(\pi/2+\phi)} e^{-i\ell(B\Omega t - k_1 r)} \right.$$

$$\left. \int D_1(r_1)\beta_\ell J_{\ell B}(\ell k_1 r_1 \sin\nu)2\pi r_1 dr_1 \right] \qquad (18)$$

As before, one is faced with evaluating an integral containing the product of a Bessel function and of two possibly complicated functions of the variable of integration. One may again apply the mean-value theorem and express the integral as

$$\int D_1(r_1)\beta_\ell J_{\ell B}(\ell k_1 r_1 \sin\nu)2\pi r_1 dr_1$$

$$= [\beta_\ell J_{\ell B}(\ell k_1 r_1 \sin\nu)]_{r_1=a_m} \cdot \int_0^a D_1(r_1)2\pi r_1 dr_1$$

$$= [\beta_\ell J_{\ell B}(\ell k_1 r_1 \sin\nu)]_{r_1=a_m} \cdot V_D , \qquad (19)$$

where V_D denotes the volume of a solid disk having the radius a of the propeller and the same radially-varying thickness as a propeller blade, and a_m represents an appropriate mean radius.

Thus, the sound pressure amplitude of the sth harmonic component due to the blade thickness (monopole source effect) is given by

$$P_s = - \frac{\rho\Omega^2 B^2}{4\pi r} s^2 V_D [\beta_s J_{sB}(s k_1 r_1 \sin\nu)]_{r_1=a_m} \qquad (20)$$

One may observe that here the directivity (the dependence on ν) is the same as for combined dipole sources, see Eq. (13). Also, the monopole term of Eq. (20) varies inversely with distance, just like the dipole term of Eq. (13). Comparing the monopole and dipole source terms further, one finds that the monopole term varies as the square of $sB\Omega$, whereas the thrust-dipole term involves the first power of $sB\Omega$ and the drag-dipole term involves the first

power of $sB\Omega$, modified by the rotational Mach number M_d. Also, one may observe that the dipole and monopole terms are 90° out of phase.

Effects of Disturbed Inflow and Forward Motion

The previous analysis has dealt only with the simple case of a rotating propeller with no forward motion and no nonuniformities in the inflow.

The effects of nonuniform flow are considered, for example, in the theoretical analysis of Morse and Ingard (Ref. 2) and have been given extensive attention in studies of compressor noise, (e.g., Refs. 4,5,6) where the presence of struts, stators, etc. ahead of the rotating blades serves to disturb inflow and thus produces perturbations of the aerodynamic loadings on the propeller blades. For small propeller-driven aircraft designed for quiet operation, this source of noise is likely to be unimportant and is not discussed here.

The effects of motion of the acoustic source(s) — that is, of forward motion of the aircraft — have also been studied (Refs. 2,7,8). Primarily, there result the well-known Doppler shift of observed frequencies and changes in the directivity. Both of these phenomena are amenable to straightforward analysis, but are of little interest here, and therefore are not treated further.

Comparison of Theoretical Predictions with Measured Data

Comparison of theory with experiment is made difficult by the complexity of the calculations (particularly for the higher harmonics), by the approximations involved in the derivations, by uncertainties in the experimental conditions, and by lack of sufficiently detailed data. Since the concern here is with discrete frequency noise, one needs narrow-band data for comparison, or at least an assessment that the data in specific bands are due predominantly to pure-tone propeller contributions. Because of the significant directivity effects, one also needs to know the source-receiver orientation rather precisely. Nearly all of the useful data presently available is from stationary operation (ground run-up), with measurements taken at several azimuthal positions around the airplane. (Comparison between theory and measurements usually is most convenient for positions in the plane of the propeller; however, the thrust-related dipole term vanishes here, and its contribution can then not be determined.)

Figures A4 and A5 compare the results of calculations with experimental measurements for the three-bladed OV-1 propeller.

Both figures pertain to the same observation position given from the propeller axis, in the plane of the propeller, but the former figure corresponds to a lower rotational speed and shaft horsepower than the latter. Dipole sound prediction calculations were carried out on the basis of Eq. (13), taking $2\alpha_s = 1$, which corresponds to a uniform distribution of aerodynamic forces over the blade width. Results are shown for two values of a_d: 70% and 80% of the propeller radius a; one notes that these two results agree well for the fundamental, but diverge increasingly for the higher harmonics — indicating that the choice of a_d affects the higher harmonics more strongly.

Also indicated in Figs. A4 and A5 are the sound pressure levels predicted for this same propeller due to monopole radiation. For the prediction calculations corresponding to Fig. A4 the disk volume V_D was approximated from a graph of blade thickness versus radius. For the lowest two harmonics, the calculation was carried out on the basis of Eq. (18), and by accomplishing the integration by means of a series expansion, with only the largest terms retained. For these harmonics, the effective radius a_m was found to be 0.57a and 0.64a, respectively. The third harmonic contribution was estimated by use of Eq. (20), with an effective radius $a_m = 0.75a$. The values plotted in the figure are based on the assumption of a rectangular blade cross-section profile (which assumption affects the Fourier coefficients β_s).* Since the effective radius and the Fourier coefficients to be used in the approximate Eq. (20) are related to the propeller geometry, and not the operating conditions, it seems valid to use values of these parameters which yield acceptable results at one set of operating conditions to predict noise levels at other operating conditions of the same propeller by use of the simpler Eq. (20). Figure 5 shows the monopole sound pressure levels calculated in that manner, assuming a rectangular blade profile and $a_m = 0.55a$ for s = 1,2, and 0.75a for s = 3.

---

*Levels for the first two harmonics were also calculated on the basis of a triangular variation of blade thickness with angle ϕ_i'. At the fundamental, the triangular thickness gave nearly the same result as the rectangular thickness, but at twice that frequency, the triangular distribution gave a level which was lower by nearly 10 dB. By the nature of the Fourier series representations, one would expect the difference between levels to increase rapidly with higher harmonics. As another example of the sensitivity of the theoretical model to small variations in the assumptions necessary for numerical evaluation, the level of the third harmonic was calculated using a rectangular thickness profile, but at an effective radius of 0.60a. This result was found to be about 13 dB lower than the value obtained with $a_m = 0.75a$.

Combination of sound levels due to monopole and diple sources is accomplished by the usual method of adding uncorrelated sound levels, since the pressures due to the two sources are 90° out of phase. Results of combination of the monopole terms with the dipole terms for $a_d - 0.8a$ are shown in Figs. A4 and A5 as well as corresponding measured data.* [It should be noted that the measured levels of Fig. A5 are obtained from octave-band, not narrow-band data; however, narrow-band data suggest that the octave-band levels are predominantly due to the discrete frequency contributions.] The agreement between predicted and measured levels is quite good. One notes that although the dipole term alone predicts the first harmonic quite accurately and approximates the second harmonic reasonably, inclusion of the monopole contribution greatly improves the prediction for the third harmonic.

Figure A6 presents a comparison between predictions and data for another propeller, and also indicates predictions computed by methods from Hubbard (Ref. 9) and Dodd (Ref. 10) for the dipole and dipole-plus monopole sources. Insufficient information regarding the propeller geometry is available to allow prediction of the blade thickness pressure term by the method of Eq. (20). The measured data shown in Fig. A6 are seen to agree reasonably well with the levels predicted here by use of only the dipole term based on $a_d = 0.8a$. Estimates of the monopole source contribution shown in Fig. A6 have been prepared on the basis of the assumption that the propeller of Fig. A6 is geometrically similar to that of Figs. A4 and A5.

In order to assess how well one may predict the thrust dipole contribution, calculations have been carried out for observer positions out of the planes of the two previously discussed propellers. Calculated levels and measured data are compared in Figs. A7 and A8. For the U-10 propeller (Fig 8) agreement between estimated and measured values is seen to be quite acceptable for positions 30° ahead and behind the propeller plane, but very poor for 60° behind the plane of the propeller, particularly in the second and third harmonics. The agreement for the OV-1 propeller (Fig. A7 is generally poor. Brief further study shows that the high-frequency predictions are even worse for angles closer to the axis of rotation; in particular, the data suggests the presence of strong tonal contributions in the axial direction, which the theory predicts to vanish.

---

*In order to make the "free-field" predictions correspond to the measurements made near the ground, 6 dB has been added to all predicted values, in order to account for ground reflection.

What physical arguments can one advance regarding the difference between the predicted and actual behaviors? (1) Nonuniform flow: It seems unlikely that parts of the aircraft upstream from the propeller could disturb the inflow seriously. It *is* of interest, however, that the aircraft for which best agreement was obtained at 30° out of the propeller plane has a single engine, whereas the other craft has two wing-mounted engines. Conceivably, the forebody of the airplane might disturb the inflow in the latter case, but it seems doubtful that the effect would be as strong as observed. (2) Reflection and radiation from the ground, and from wings, fuselage, etc.: Again, these effects appear incapable of producing the large observed difference between calculated and measured levels;* radiation of sound from airplane surfaces (e.g., due to structureborne vibration) cannot be evaluated from the available data. (3) Approximations in analytical evaluation: The thrust and drag forces on the propeller blades have been approximated by uniform loading distributions, and in the evaluation of the resulting Fourier coefficients the propeller solidity was taken to be sufficiently small so that essentially point loadings result. These approximations assure relatively large high-frequency content in the excitation due to dipole-related forces. Similarly, expansion of the blade thickness distribution on the basis of a uniform cross-section probably overemphasizes the actual high-frequency spectral content. Since the disagreement between theory and measurements becomes greater with increasing frequency at positions out of the propeller plane, it appears that the above approximations are not the source of any discrepancies.

None of the above possibilities presents themselves as obvious sources of discrepancies between theory and data; deeper investigation of these and other conceivable mechanisms is required, but is beyond the scope of the present work.

ESTIMATION OF TOTAL ACOUSTIC POWER

One may determine the acoustic power radiated by the dipole and monopole sources by integrating acoustic intensities obtained from Eqs. (13) and (20) over a sphere of radius r (i.e., over all angles ν) and adding the results. However, this computation may be somewhat complicated, and one may do just as well for general

---

*However, ground reflection may cause the directivities measured with the aircraft on the ground to differ from those produced by the aircraft in flight.

estimation purposes by evaluating the pressures at an "average" angle $\nu = 45°$ and multiplying the resulting average intensity by the area of the sphere.

Thus, one may estimate the acoustic power W_s of the sth harmonic due to both dipole and monopole sources from

$$W_s = \frac{2\pi r^2}{\rho c} [p_{s2}^2 + p_{s1}^2] \tag{21}$$

where p_{s2} represents the value of the dipole-related pressure, as found from Eq. (13) for $\nu = 45°$ and p_{s1} represents the monopole-related pressure, as obtained from Eq. (20) with $\nu = 45°$.

ESTIMATION SCHEME

The acoustic power W_s for each harmonic component must be calculated separately. Generally only the lowest few components ($s = 1,2,3$) are of interest.

1. Calculate rp_{s2} from the modified* Eq. (13),

$$rp_{s2} \approx \frac{sB\Omega}{4\pi c} \left| \frac{T}{a_d M_d} - \frac{F_t}{\sqrt{2}} \right| J_{sB}(sBM_d/\sqrt{2}) \tag{13a}$$

where $M_d = a_d \Omega/c$

$\qquad a_d = 0.8a$

The propeller thrust F_t and drag torque T usually are available from propulsion system characteristics. Otherwise, for a propeller with radius a, constant section lift and drag coefficients C_L and C_D, and with a small pitch angle, one may use

---

*Obtained by taking $\nu = 45°$ and $2\alpha_s \approx 1$. This approximation for α_s applies for uniform distribution of the aerodynamic forces over the blade width.
Note that values of $J_m(x)$ are available in standard tables of Bessel functions and that (see Ref. 2)

$$J_m(x) \approx \begin{cases} \frac{1}{m!}\left(\frac{x}{2}\right)^m & \text{for } x \ll 1 \\ \sqrt{\frac{2}{\pi x}} \cos\left(x - \frac{2m+1}{4}\pi\right) & \text{for } x \gg 1 \end{cases}$$

$$F_t \approx 0.17 C_L \rho U_{tip}^2 A_b$$

$$T \approx 0.13 C_D \rho U_{tip}^2 A_b a$$

where U_{tip} is the blade tip speed and A_b the total blade area (for B blades, projected onto plane of rotation).

2. Find rp_{s1} from the modified Eq. (20),

$$rp_{s1} \approx \frac{(sB\Omega)^2}{4\pi} V_D \beta_s \ J_{sB}\left(\frac{sB\Omega}{c\sqrt{2}} a_m\right) \tag{20a}$$

where one may find the propeller disc volume V_D by integrating the radial thickness distribution, or approximately from

$$V_D \approx \pi a^2 d$$

where d is the average blade thickness. The Fourier coefficient β_s of the circumferential blade thickness distribution may be calculated from a known thickness function $S(\phi)$ for the propeller, from

$$\beta_s = \frac{1}{\pi} \int_0^{2\pi} S(\phi) \cos(mB\phi) d\phi$$

or may be approximated for a low solidity-ratio propeller by

$$\beta_s \approx \frac{B}{\pi} \left(\frac{b}{a}\right)_{avg}$$

where $(b/a)_{avg}$ represents the average propeller chord to radius/ratio. Unless better information is available, one may take $a_m = 0.55a$ for $s = 1$, $a_m = 0.65a$ for $s = 2$, $a_m = 0.75a$ for $s = 3$.

3. Calculate the total acoustic power W_s produced at frequency $\omega = sB\Omega$ from

$$W_s = \frac{2\pi}{\rho c} \left[(rp_{s2})^2 + (rp_{s1})^2\right] \tag{21a}$$

and then find the corresponding power level from

$$L_W = 10 \log(W_s/W_{ref})$$

4. Determine the frequency ω_s at which the sth component occurs from

$$\omega_s (\text{radians/sec}) = sB\Omega$$

or

$$f_s(\text{Hz}) = \omega_s/2\pi = sB\Omega/2\pi$$

Illustrative Calculation

Consider a three-bladed propeller of 4 ft radius, rotating at 2100 rpm and producing a thrust of 340 lb at a torque of 350 ft/lb, at 1000 ft altitude (where the air density is 0.070 lb/ft^3 and the speed of sound is 1100 ft/sec).

To use Eq. (13a), find

$\Omega = 2100$ rev/min $= 2100(2\pi/60)$rad/sec $= 220$ rad/sec

$a_d = 0.8a = 0.8(4 \text{ ft}) = 3.2 \text{ ft}$

$M_d = a_d\Omega/c = (3.2 \text{ ft})(220 \text{ rad/sec})/(1100 \text{ ft/sec}) = 0.64$

$BM_d/\sqrt{2} = 3(0.64)/\sqrt{2} = 1.35$

$$\frac{B\Omega}{4\pi c}\left| \frac{T}{a_d M_d} - \frac{F_t}{\sqrt{2}} \right| = \frac{3(220 \text{ rad/sec})}{4\pi(1100 \text{ ft/sec})} \left| \frac{350 \text{ ft-lb}}{(3.2 \text{ ft})(0.64)} - \frac{340 \text{ lb}}{\sqrt{2}} \right|$$

$$= 0.0525 \left| 170 - 240 \right| = 3.7 \text{ lb/ft.}$$

Then,

for[*] $s = 1$, $rp_{s_2} = 3.7 \ J_3(1.35) \quad = 3.7(4.5\times10^{-2}) = 0.17 \quad$ lb/ft

for $s = 2$, $rp_{s_2} = 2(3.7) \ J_6(2.70) = 7.4(6.5\times10^{-3}) = 0.048$ lb/ft

for $s = 3$, $rp_{s_2} = 3(3.7) \ J_9(4.05) =11.1(1.05\times10^{-3})= 0.011$ lb/ft

---

[*]Values of Bessel functions J_3, J_6, J_9 found from *Handbook of Mathematical Functions*, Ed. by M. Abramowitz and I.A. Stegun, National Bureau of Standards, Washington, D. C. 1964, p. 398.

To use Eq. (20a), one needs to know also the average blade thickness d and the average ratio of the blade chord to the blade radius. These values, which may be obtained from a drawing of the propeller, here are taken as $d = 0.2$ ft, $(b/a)_{avg} = 0.25$.

Then find

$$V_D \approx \pi a^2 d = \pi (4 \text{ ft})^2 (0.2 \text{ ft}) = 10.1 \text{ ft}^3$$

$$\beta_s \approx \frac{B}{\pi} \left(\frac{b}{a}\right)_{avg} = \frac{3}{\pi} (0.25) \approx 0.24$$

$$\frac{\rho (B\Omega)^2}{4\pi} V_D \beta_s = \frac{0.07 \text{ lb}_m/\text{ft}^3}{32.2 \text{ lb}_m \text{ ft}/\text{sec}^2 \text{lb}} \frac{[(3)(220 \text{ rad/sec})]^2}{4\pi} (10.1 \text{ ft}^3)(0.24)$$

$$= 180 \text{ lb/ft}$$

$$\frac{B\Omega a}{c\sqrt{2}} = \frac{3(220 \text{ rad/sec})(4 \text{ ft})}{\sqrt{2}(1100 \text{ ft/sec})} = 1.70$$

and

for $s = 1$, $rp_{s_1} = 180 \, J_3[1.70(0.55)] = 180 \, J_3(0.93)$
$$= 180(.015) = 2.7 \text{ lb/ft}$$

for $s = 2$, $rp_{s_1} = 4(180) \, J_6[2(1.70)(0.65)] = 720 \, J_6(2.2)$
$$= 720(2.1\times10^{-3}) = 1.5 \text{ lb/ft}$$

for $s = 3$, $rp_{s_1} = 9(180) \, J_9[3(1.70)(0.75)] = 1620 \, J_9(3.8)$
$$= 1620(6.1\times10^{-4}) = 1.0 \text{ lb/ft}$$

Since $\rho c = \left(\frac{.07}{32.2}\right) (1100) = 2.4 \text{ lb sec/ft}^3$, so that $2\pi/\rho c = 2.8 \text{ ft}^3/\text{lb sec}$, one finds from Eq. (21a) that

for $s = 1$, $W_s = 2.8[(0.17)^2 + (2.7)^2] = 20.4 \text{ ft lb/sec}$

for $s = 2$, $W_s = 2.8[(0.048)^2 + (1.5)^2] = 6.3 \text{ ft lb/sec}$

for $s = 3$, $W_s = 2.8[(0.011)^2 + (1.0)^2] = 2.8 \text{ ft lb/sec}$

Then since $W_{ref} \approx 0.74 \times 10^{-12}$ ft lb/sec,

for s = 1, L_W = 10 log $[20.4/(0.74 \times 10^{-12})]$ = 135 dB, re 10^{-12} watt

for s = 2, L_W = 10 log $[6.3/(0.74 \times 10^{-12})]$ = 129 dB, re 10^{-12} watt

for s = 3, L_W = 10 log $[2.8/(0.74 \times 10^{-12})]$ = 126 dB, re 10^{-12} watt

Since $B\Omega$ = 3(220 rad/sec) = 660 rad/sec, the frequencies associated with the foregoing "pure tone" sound levels are ω_1 = 660, ω_2 = 2(660), ω_3 = 3(660) rad/sec or f_1 = 105, f_2 = 210, f_3 = 315 Hz.

REFERENCES FOR APPENDIX A

1. Gutin, L., "On the Sound Field of a Rotating Propeller", Translation, NACA TM 1195, October 1948.

2. Morse, P.M. and K.U. Ingard, *Theoretical Acoustics,* McGraw Hill Book Co., New York, 1968.

3. Lamb, Sir H., *Hydrodynamics,* Dover Press, 1945.

4. Lowson, M.V., "Theoretical Studies of Compressor Noise", NASA CR 1287, 1969.

5. Morfey, C.C., "Sound Generation in Subsonic Turbomachinery", ASME Paper No. 69-WA/FE-4, 1969.

6. Sharland, I., "Sources of Noise in Axial Flow Fans", *J. Sound & Vib.,* I (3), 1964.

7. Garrick, I.E., and C.E. Watkins, "A Theoretical Study of the Effect of Forward Speed on the Free-Space Sound-Pressure Field Around Propellers", NACA TN 3081, 1953.

8. Lowson, M.V., "The Sound Field for Singularities in Motion", *Proc. Roy. Soc.* (London) Vol. 286, Series A, 1965, pp. 559–572.

9. Hubbard, H. H., "Propeller Noise Charts for Transport Airplanes", NACA TN 2968, 1953.

10. Dodd, K. N. and Roper, G. M., "A Deuce Programme for Propeller Noise Calculations", Royal Aircraft Establishment Technical Note No. M.S. 45, January 1958.
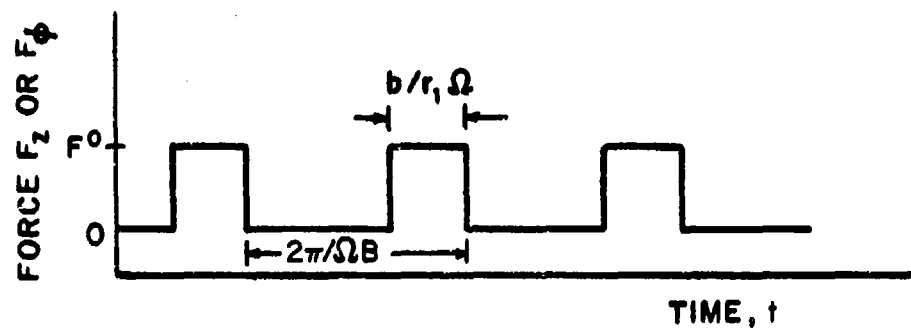
FIGURE A1   FORCE VARIATION AT TYPICAL LOCATION IN PROPELLER
             PLANE.   b = PROPELLER WIDTH IN PLANE, AT RADIUS r

FIGURE A2   COORDINATES

33

THICKNESS
FUNCTION
$S(r_1, \phi_1)$

$b/r_1 \, \Omega$

$2\pi/\Omega B$

TIME, t
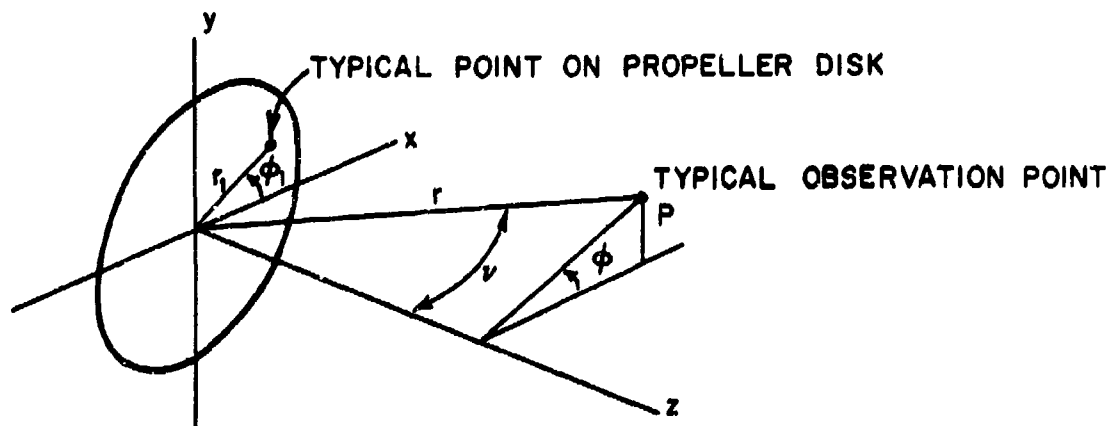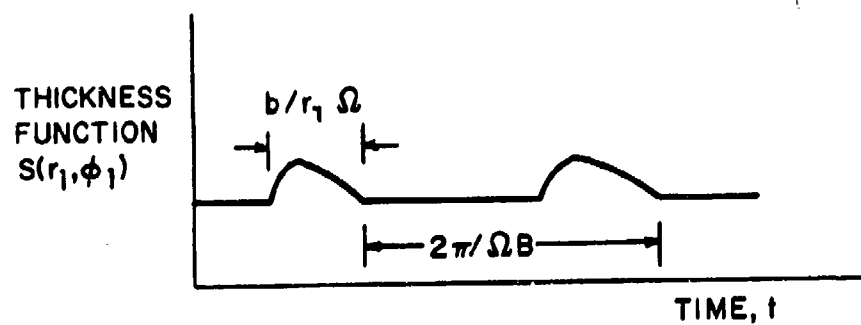
FIGURE A3   THICKNESS FUNCTION $S(r_1, \phi_1)$ IN NON-ROTATING
COORDINATES

SOUND PRESSURE LEVEL, (dB RE 0.0002 MICROBAR)

110

100

90

80

70

60

(a) MEASURED
(b) DIPOLE CALCULATION, EQ (13), $a_d/a = 0.7$
(c) DIPOLE CALCULATION, EQ (13), $a_d/a = 0.8$
(d) MONOPOLE CALCULATION, EQS (18) & (20)
(e) DIPOLE PLUS MONOPOLE CALCULATION, (c) + (d)

6 dB ADDED TO ALL CALCULATED
VALUES TO ACCOUNT FOR
GROUND REFLECTION

HARMONIC NUMBER s
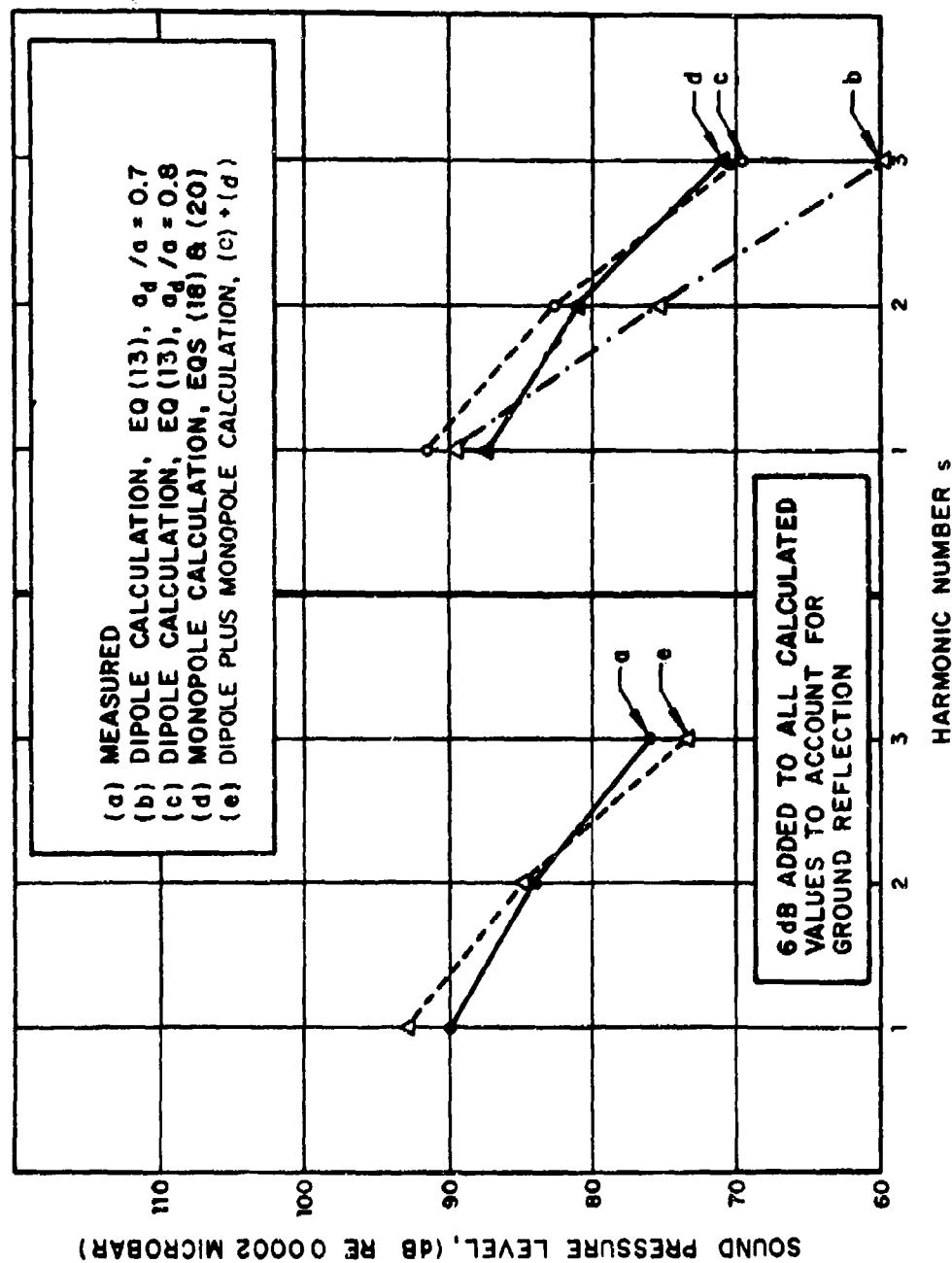
FIGURE A4   NARROW-BAND SOUND PRESSURE IN PLANE OF OV-1 PROPELLER
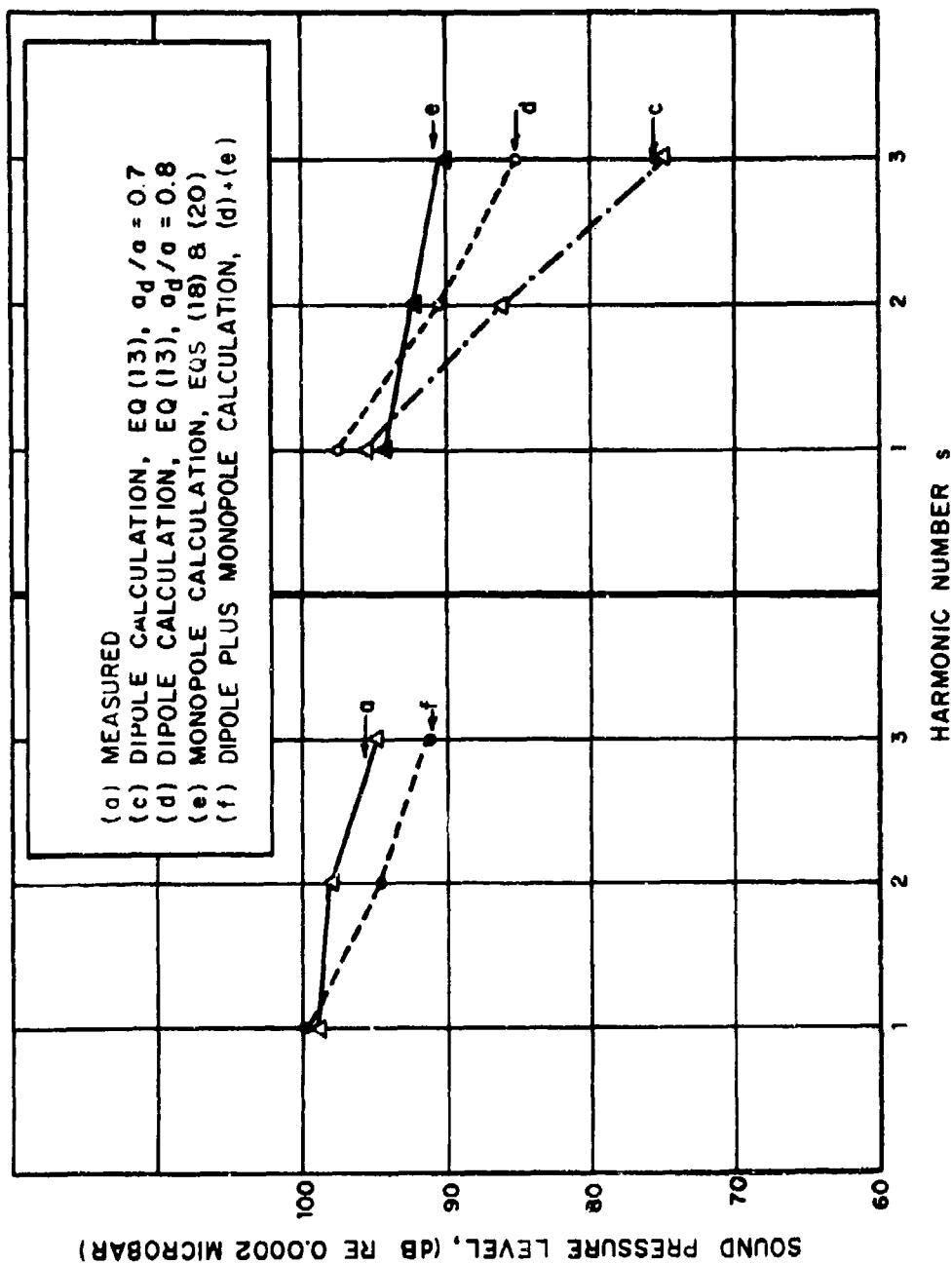
FIGURE A5   NARROW-BAND SOUND PRESSURE IN PLANE OF OV-1 PROPELLER

Legend (as shown on figure):
(a) MEASURED
(c) DIPOLE CALCULATION, EQ (13), $a_d/a = 0.7$
(d) DIPOLE CALCULATION, EQ (13), $a_d/a = 0.8$
(e) MONOPOLE CALCULATION, EQS (18) & (20)
(f) DIPOLE PLUS MONOPOLE CALCULATION, (d)+(e)

HARMONIC NUMBER s

SOUND PRESSURE LEVEL, (dB RE 0.0002 MICROBAR)

36

(a) MEASURED
(b) DIPOLE CALCULATION, REF. 9
(c) DIPOLE CALCULATION, EQ (13); $a_d/a = 0.7$
(d) DIPOLE CALCULATION, EQ (13); $a_d/a = 0.8$
(e) MONOPOLE CALCULATION, EQS (18) 8 (20)
(f) MONOPOLE PLUS DIPOLE CALCULATION, REF. 10
(g) DIPOLE PLUS MONOPOLE CALCULATION, (d)+(e)

6 dB ADDED TO ALL CALCULATED
VALUES TO ACCOUNT FOR
GROUND REFLECTION

HARMONIC NUMBER s

SOUND PRESSURE LEVEL, (dB RE 0.0002 MICROBAR)

FIGURE A6   NARROW-BAND SOUND PRESSURE IN PLANE OF U-10 PROPELLER
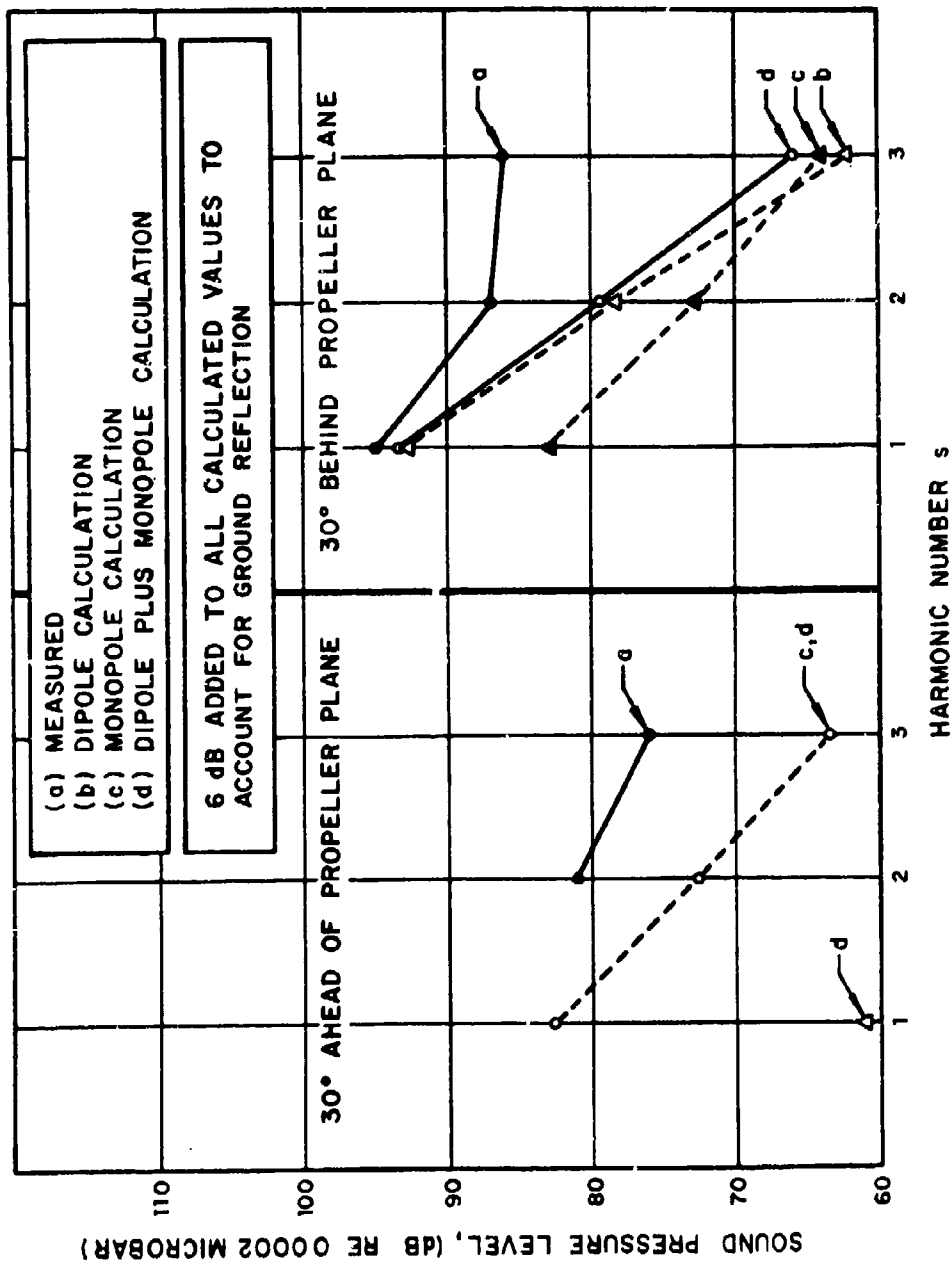
FIGURE A7   NARROW-BAND SOUND PRESSURE OUT OF PLANE OF OV-1 PROPELLER
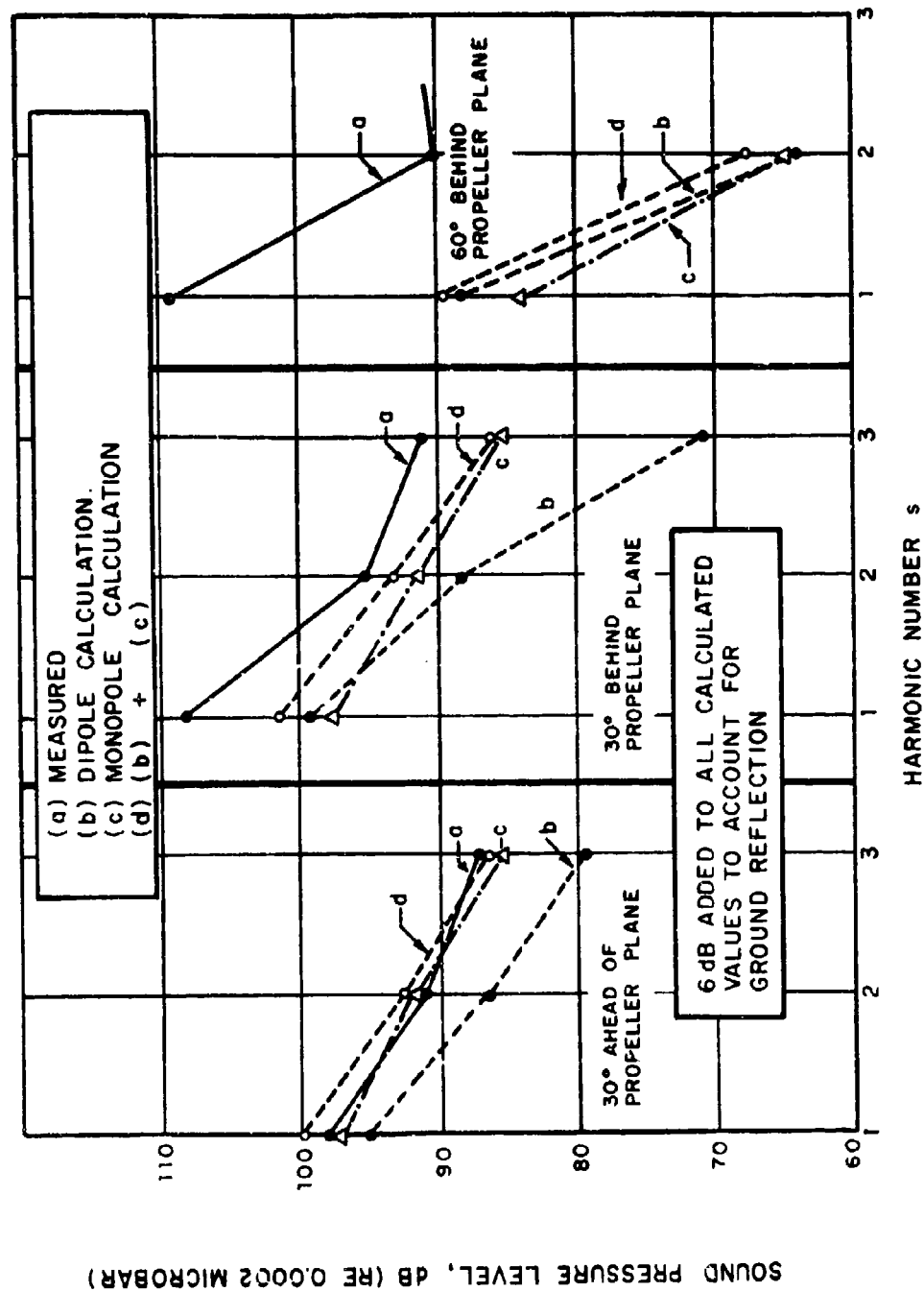
FIGURE A8   NARROW-BAND SOUND PRESSURE OUT OF PLANE OF U-10 PROPELLER

APPENDIX B

VORTEX NOISE OF PROPELLERS

VORTEX NOISE LEVEL

For low-speed quiet propellers, the broadband noise associated with vortex shedding becomes an important contributor to the acoustic power generated (Ref. 1). E.Y. Yudin (Ref. 2) originally developed a theory for the noise generated by rotating rods. H.H. Hubbard (Ref. 1) extended Yudin's work to the case of rotating airfoils, postulating that propeller-generated vortex noise is proportional to the first power of the blade area and the sixth power of the flow speed. Schlegel *et al.* (Ref. 3) have developed an empirical prediction scheme for the vortex noise obtained at fifteen degrees behind the propeller plane.

Schlegel's prediction for the overall vortex-noise sound pressure level L_p may be expressed as

$$L_{p(\theta=15°)} = -62 - 10 \log A_b + 60 \log U_{0.7}$$

$$- 20 \log (R/3) + 20 \log (C_L/0.4) \tag{1}$$

where A_b is the area of the propeller blade (in ft^2) projected onto the propeller plane; $U_{0.7}$ is the air velocity relative to the airfoil at the seven tenths radius (in ft/sec), R is the distance to the propeller hub (in ft), and C_L is the blade lift coefficient. This prediction was based on data obtained at $C_L = 0.4$, and implies that there is not vortex noise for $C_L = 0$; this is clearly not the case — rotating rods provide zero lift but do make vortex noise.

D. Ross (Ref. 4) developed a scheme for dealing with vortex noise involving an "acoustic conversion efficiency" η, which relates the acoustic power W to the mechanical drag power (i.e., to the blade section drag power) W_m. For cylindrical bodies of all shapes, Ross gives the conversion efficiency as

$$\eta = W/W_m = 9.0 \times 10^{-3}M^3 , \tag{2}$$

where M is the Mach number. For a two-dimensional airfoil, the mechanical power per unit length is given by

$$W_m = \frac{1}{2} \rho b U^3 C_D \tag{3}$$

where b is the foil's chord length, U the local flow speed and C_D the drag coefficient. The acoustic power radiated by a propeller blade of radius a thus may be written as

$$W = \frac{9 \times 10^{-3}}{c^3} \frac{\rho}{2} \int_0^a U^6(r)b(r)C_D(r)dr \tag{4}$$

where   c = sound speed

U(r) = flow speed at radius r

b(r) = chord length at radius r

$C_D(r)$ = drag coefficient at radius r.

For a propeller with B blades and a constant section drag coefficient $C_D = 0.01$, operating in air at sea level, one finds the acoustic power to be given by

$$W(\text{ft lb/sec}) = 8 \times 10^{-17} B \int_0^a U^6(r)\ell(r)dr \tag{5}$$

for U in ft/sec and b, r, a in ft. If the chord length is constant, the blade area A_b = Bab may be introduced, and the previous expression may be rewritten as

$$W = 8 \times 10^{-17} A_b \int_0^{1.0} U^6(r/a)d(r/a) \quad . \tag{6}$$

For a propeller with a small pitch angle, U(r) is very nearly proportional to r, and

$$\int_0^{1.0} U^6\left(\frac{r}{a}\right) d\left(\frac{r}{a}\right) = U^6_{tip} \int_0^{1.0} \left(\frac{r}{a}\right)^6 d\left(\frac{r}{a}\right) \cong U^6_{0.7} \tag{7}$$

where $U_{0.7}$ is the blade speed at the seven tenths radius.

41

By substituting Eq. (7) into (6) and taking the logarithms, one obtains

$$10 \log W = -160 + 10 \log A_b + 60 \log U_{0.7} , \qquad (8)$$

which, when converted to watts and referred to 10^{-12} watts, yields the acoustic power level as

$$L_W(\text{dB, re } 10^{-12} \text{ watts}) = -40 + 10 \log A_b + 60 \log U_{0.7} \qquad (9)$$

where A_b is in units of ft^2 and $U_{0.7}$ in ft/sec.

If the vortex noise were generated by a family of dipoles, all aligned in the plane of the propeller, then the sound pressure would vary as $\sin^2\theta$, where θ is the angle which a line from the observation point to the propeller hub makes with the propeller plane. One would then write the overall sound pressure level at the observation point as

$$L_p(\text{dB, re } 0.0002 \text{ microbar}) = L_W(\text{re } 10^{-12} \text{ watts}) - 8$$

$$+ 20 \log \sin\theta - 20 \log \frac{R}{3}$$

$$= -48 + 10 \log A_b + 60 \log U_{0.7}$$

$$+ 20 \log \sin\theta - 20 \log \frac{R}{3} . \qquad (10)$$

The value $C_D \approx 0.01$, for which the foregoing expressions have been derived, is estimated to be typical for a standard propeller section at $C_L = 0.4$. A comparison on this basis between Eq. (10) for $\theta = 15°$ and Schlegel's prediction at $C_L = 0.4$ [Eq. (1)] shows that Eq. (10) predicts a level that is 2 dB greater than that given by Eq. (1); thus, the agreement between the theoretically and experimentally derived prediction schemes is seen to be good.

SPECTRUM SHAPE

Schlegel (Ref. 3) gives an empirical spectrum shape for the vortex noise. The peak frequency f_{pk} of this spectrum depends on

the Strouhal number at the seven tenths radius, based on the projected blade thickness

$$d_p = d \cos\alpha + b \sin\alpha \qquad (11)$$

and is given by

$$f_{pk} = 0.28\, U_{0.7}/d_p \,, \qquad (12)$$

where d is the actual blade thickness, b is the chord and α the blade's angle of attack. The shape of the spectrum about this peak frequency is given in the Table below.

OCTAVE BAND SPECTRUM OF PROPELLER VORTEX NOISE

f_{OB}/f_{pk}	$\frac{1}{2}$	1	2	4	8	16
$L_{OA}-L_{OB}$	8	4	8	9	13	14

f_{OB} = center frequency of octave band

f_{pk} = peak frequency of vortex noise spectrum

L_{OA} = overall level

L_{OB} = level in octave band

DIRECTIVITY

If all of the dipole sources on the propeller blades were aligned parallel to the shaft axis, the vortex noise field would be that of a dipole along the propeller axis. However, in fact the dipoles on the propeller blades are not aligned from blade to blade, due to the pitch; this causes a smearing of the directivity pattern. An aligned dipole field would radiate nothing in the plane of the propeller, but a highly pitched propeller can generate considerable noise in its plane of rotation.

At an angle θ out of the plane of rotation, the angle between the line from the observer to the propeller hub and the normal to the axis of a dipole on a blade with pitch angle β is

$$\alpha = \beta \cos\psi - \theta \ , \qquad\qquad (13)$$

where ψ is the angle the propeller blade makes with a plane passing through the shaft axis and the observation point (see Fig. B1). The sound pressure level at the observation point (in the farfield) varies as $\sin^2\alpha$; the average level for a rotating pitched propeller blade may be written as

$$L_p(\theta,\beta) = L_p(\pi/2,0) \ \frac{1}{2\pi} \int_0^{2\pi} \sin^2(\beta \cos\psi - \theta) d\psi \ , \qquad (14)$$

in terms of the on-axis sound pressure level $L_p(\pi/2,0)$ of an unpitched propeller (at the same distance from the hub).

By expanding the integrand, one may rewrite the integral of Eq. (14) as

$$\int_0^{2\pi} \sin^2(-\theta + \beta \cos\psi) d\psi = (\sin^2\theta) \int_0^{2\pi} \cos^2[\beta \cos\psi] \ d\psi$$

$$+ (\cos^2\theta) \int_0^{2\pi} \sin^2[\beta \cos\psi] d\psi$$

$$- \frac{1}{2} (\sin 2\theta) \int_0^{2\pi} \sin[2\beta \cos\psi] \ d\psi \ . \quad (15)$$

The first integral on the right-hand side then can be expressed in terms of the zero order Bessel function, J_0:

$$\int_0^{2\pi} \cos^2[\beta \cos\psi] \ d\psi = \int_0^{2\pi} \frac{1}{2} [1 + \cos(2\beta \cos\psi)] d\psi$$

$$= \pi [1 + J_0(2\beta)] \ , \qquad\qquad (16)$$

from which it follows that the second integral obeys

$$\int_0^{2\pi} \sin^2[\beta \cos\psi] d\psi = \pi [1 - J_0(2\beta)] \ . \qquad (17)$$

The last integral vanishes because $\sin[2\beta \cos\psi]$ is an odd function of ψ.

By use of the foregoing results one may now rewrite Eq. (14) as

$$L_p(\theta,\beta) = L_p(\pi/2,0) \; \frac{1}{2} \; [1-J_0(2\beta) \cos 2\theta] \; . \tag{18}$$

The modification of the directivity pattern due to pitch is particularly significant for propellers designed to operate at very low rotation speeds, because propellers with low tangential to axial velocity ratios must have high pitch. The flattened directivity pattern associated with high pitch results in a lessening of the rise and fall of the vortex noise recorded on the ground as a propeller driven craft flies over at constant altitude. For the zero pitch case, the vortex noise level is greatest when the angle with the propeller plane is 45° (peaking once as the aircraft approaches and once as it flies away). For a slow speed propeller with a 45° pitch angle, the sound level at 45° out of the propeller plane is about the same as for the unpitched propeller, but continues to increase slowly as the aircraft approaches until a peak is reached (only a few dB higher than that at 45°) at 26° out of the propeller plane; the sound level then remains constant, within 0.5 dB, until the 26° peak is passed as the aircraft leaves.

COMPARISON OF PREDICTIONS WITH EXPERIMENTAL DATA

By combining Eq. (10) with (18) and including a drag coefficient proportionality relation, one obtains

$$L_p = -48 + 10 \log A_b + 60 \log U_{0.7} + 10 \log \left(\frac{C_D}{.01}\right)$$

$$+ \; 10 \log \left\{\frac{1}{2} \; [1-J_0(2\beta) \cos 2\theta]\right\} - 20 \log \left(\frac{R}{3}\right) \; . \tag{19}$$

In order to test this prediction relation, a search of the literature was made for well-documented propeller noise data. Enough must be given so that one can evaluate all of the parameters which appear in the foregoing relation. In addition, in order to check a vortex noise prediction against measured data, one needs a narrow-band spectrum, so that one can separate the broad-band vortex noise from rotational and engine harmonic noise (unless the vortex noise center frequency is in a region where vortex noise clearly dominates the one-third or octave band levels). Of noise measurements made on subsonic propellers and helicopter rotors, few have been made with an eye toward determining the

vortex noise. Consequently, most reported measurements do not give sufficient data; only three have been found which give detail to permit checking the vortex noise prediction scheme: one set of measurements is for a helicopter rotor (Ref. 5), one for a hovercraft pusher propeller (Ref. 6), and one for the low-speed propeller of a "quiet" aircraft.

In an investigation of helicopter rotor noise by Stuckey and Goddard (Ref. 5), a 3-bladed NACA 0012 section helicopter rotor was spun on a whirl tower at various speeds and pitch settings. The rotor thrust and sound pressure levels were recorded. Tests were conducted at rotational speeds between 180 and 250 revolutions per minute. The vortex noise levels were obtained by taking overall levels of the noise between 100 and 2500 Hz, which had been corrected for ground reflection. This procedure is justified, because this frequency range extends over the region of major vortex noise and is above the range of frequencies where blade rate harmonics contribute significantly to the noise level. Figure B2 shows the sound level measured at 7.5° behind the rotation plane and 151 ft away from the rotor hub (and corrected by Stuckey and Goddard for ground reflection) as a function of the mean lift coefficient C_{Lm},

$$C_{Lm} = L \bigg/ \left[A_b \, \frac{c}{2} \int_0^a U^2(r)\,dr \right] \approx L \bigg/ \left[A_b \, \frac{\rho}{2} U^2(0.58\ a) \right] \ , \qquad (20)$$

which relations are based on the assumption of a constant lift coefficient over the constant chord blade. The rotor pitch angle is also noted in the figure. The dotted curve of the figure represents the data, modified by use of Eq. (18) to correspond to a zero pitch propeller. For the rotor blade area $A_b = 114.8\ \text{ft}^2$ and for $U_{0.7} = 451$ ft/sec at 220 rpm, the zero-pitch sound pressure level at the measurement location is

$$L_p(7.5°,\ 151\ \text{ft}) = 80 + 10 \log \left(\frac{C_D}{.01} \right) \qquad (21)$$

Figure B3 shows the reported drag characteristics of the NACA 0012 section (Ref. 7), together with the section drag coefficient which is required to make the L_p calculated from Eq. (21) match the zero-pitch level of Fig. B2. Since the mean Reynolds number for drag calculations (at 0.58 a) is 3.6×10^6, and since the rotor is likely to have a standard roughness finish, this calculated drag curve seems to be not an unreasonable one.

In a series of noise measurements on a low performance light aircraft, vortex noise data was obtained for two propeller conditions and at two different angles to the propeller rotation plane. The tests included noise measurements in the propeller plane and on the rotation axis during ground run-up tests, and an additional measurement as the aircraft flew past a microphone. (Microphones were mounted over woodchip-filled boxes, which should have eliminated ground reflections when the aircraft was at a relatively high angle, as during the flyby. The woodchip boxes were too small to affect the ground reflection path from the aircraft when tied down.)

For a highly pitched propeller, the axial component of $U_{0.7}$ is appreciable and cannot be neglected. The axial velocity for the ground run-up test was estimated from the given shaft horsepower and the reasonable efficiency of 55%; the induced axial velocity was computed from energy considerations. In ground run-up, the blades of this propeller are under-pitched at the tips, leading to an increase in the mean lift coefficient by an estimated 15%. Figure B4 shows a comparison of the measured vortex noise with that predicted by use of Eq. (19) and Schlegel's spectrum shape. (The measured noise for the tie-down test has been corrected for 3 dB ground reflection.) The prediction for the ground run-up is probably too low because the propeller blade section drag was underestimated for this heavily loaded condition.

Narrow-band sound pressure level data have been reported for the pusher propeller of a Hovercraft Development Ltd. HD1 hovercraft (ref. 6). The measurements were conducted with the craft tied down on a concrete runway. Measurements were made at an angle of 15° behind propeller plane, at a distance of 100 ft from the hub, with the microphone 3.5 ft above the ground surface. The propeller is a two-bladed one, with a 7 ft diameter, a total blade area of 2.9 ft^2, a blade pitch angle at 0.75a of 8° 10', and a thickness at 0.7a of 0.445 in. Runs were made at 1500 rpm (23 SHP and 240 lb thrust) and at 2500 rpm (112 SHP and 670 lb thrust).

The blade section lift coefficient, based on the foregoing information and on the assumption of constant lift coefficient over the length of the blade is $C_{\ell} \approx 0.61$ at both rotation speeds. Since the propeller pitch angle $\beta' = 8° 10'$ is small compared with the out-of-plane angle $\theta = 15°$, the directivity function can be evaluated as

$$10\{\log \tfrac{1}{2} [1-J_0(2\beta) \cos 2\theta]\} \approx 20 \log (\sin\theta) = -11.8 \ . \quad (22)$$

Because of the hard surface over which the microphone was located, the predicted sound pressure level should be increased by 3 dB, to account for ground reflection. With this correction and an estimate of $C_D = 0.016$ for the drag coefficient at $C_L = 0.61$, the predicted sound pressure levels are,

$$L_p \text{ (dB, re 0.002 microbar)} = \begin{cases} 95, \text{ at 1500 rpm} \\ 82, \text{ at 2500 rpm .} \end{cases}$$

For an assumed 4° blade angle of attack of a 7% cambered section operating at $C_L = 0.61$ (Ref. 7), the projected blade thickness is found from Eq. (11) to be 0.073 ft. With this value Eq. (11) gives the center frequencies for the vortex noise to be 1420 and 2360 Hz for 1500 and 2500 rpm, respectively. Figure B5 shows a comparison of the prediction with the measured data; the agreement is seen to be acceptable.

ESTIMATION SCHEME

To determine the spectrum of the (broad-band) noise power generated by a given propeller, one may proceed as follows:

1. Find the overall acoustic power level from

$$L_w (\text{dB,re } 10^{-12} \text{ watts}) = -40 + 10 \log A_b (\text{ft}^2) + 60 \log U_{0.7} (\text{ft/sec}). \quad (9a)$$

Here A_b is the total blade area and $U_{0.7} \approx 0.7a\Omega$.

2. Find the projected blade thickness d_p from

$$d_r = d \cos\alpha + b \sin\alpha \quad (11)$$

where d is the blade thickness and b the blade's chord length (at the 0.7a radial location), and α its angle of attack. Then calculate the spectrum peak frequency from

$$f_{pk} = 0.28 \, U_{0.7}/d_p \quad (12)$$

3. Use the table below to develop the octave band spectrum of power.

OCTAVE BAND SPECTRUM OF PROPELLER VORTEX NOISE

f_{OB}/f_{pk}	$\frac{1}{2}$	1	2	4	8	16
$L_{OA}-L_{OB}$	8	4	8	9	13	14

f_{OB} = center frequency of octave band

f_{pk} = peak frequency of vortex noise spectrum

L_{OA} = overall level

L_{OB} = level in octave band

Illustrative Calculation

Consider the three-bladed propeller described at the end of Appendix A, again rotating at 2100 rpm. The total blade area is $A_b = 4$ ft^2, the blade thickness is $d = 0.2$ ft, the blade chord length is 0.8 ft, and the propeller's angle of attack is 15°. Then

$$U_{0.7} = 0.7a\Omega = 0.7(4\text{ft})(220\text{ rad/sec}) = 615 \text{ ft/sec}$$

$$L_W = -40 + 10 \log A_b + 60 \log U_{0.7}$$

$$= -40 + 10 \log(4.0) + 60 \log(615) = -40 + 10(0.6) + 60(2.8)$$

$$= 134 \text{ dB,re } 10^{-12}\text{watts};$$

$$d_p = d \cos\alpha + b \sin\alpha = 0.2 \cos 15° + 0.8 \sin 15° = 0.40 \text{ ft}$$

$$f_{pk} = 0.28\, U_{0.7}/d_p = 0.28(615)/0.40 = 430 \text{ Hz};$$

and from the table,

f_{OB}(Hz)	215	430	860	1720	3440	6900
$L_{W(OB)}$(dB,re 10^{-12}watts)	126	130	126	125	121	120

REFERENCES FOR APPENDIX B

1. Hubbard, H.H., "Propeller-Noise Charts for Transport Air-planes", NACA TN 2968, Washington, D.C., June 1953.

2. Yudin, E.Y., "On the Vortex Sound from Rotating Rods", NACA TM No. 1136, Washington, D.C., March 1947.

3. Schlegel, R., R. King, H. Mull, "Helicopter Rotor Noise Generation and Propagation", USAVLABS T.R. 66-4, Ft. Eustis, Virginia, October 1966.

4. Ross, D., "Vortex Shedding Sounds of Propellers", BBN Report No. 1115, Cambridge, Massachusetts, March 1964.

5. Stuckey, T.J. and J.O. Goddard, "Investigation and Prediction of Helicopter Rotor Noise", *J. Sound Vib.*, **5** (1), pp. 50–80 (1967).

6. Trillo, R.L., "An Empirical Study of Hovercraft Propeller Noise", *J. Sound Vib.*, **3** (3), pp. 476–509 (1966).

7. Abbott, I.H. and A.E. VonDoenhoff, *Theory of Wing Sections*, Dover Press, New York, 1949.

8. Widnall, S.E., "A Correlation of Vortex Noise Data from Helicopter Main Rotors", *Engineering Notes*, **6**, No. 3 (May 1969).
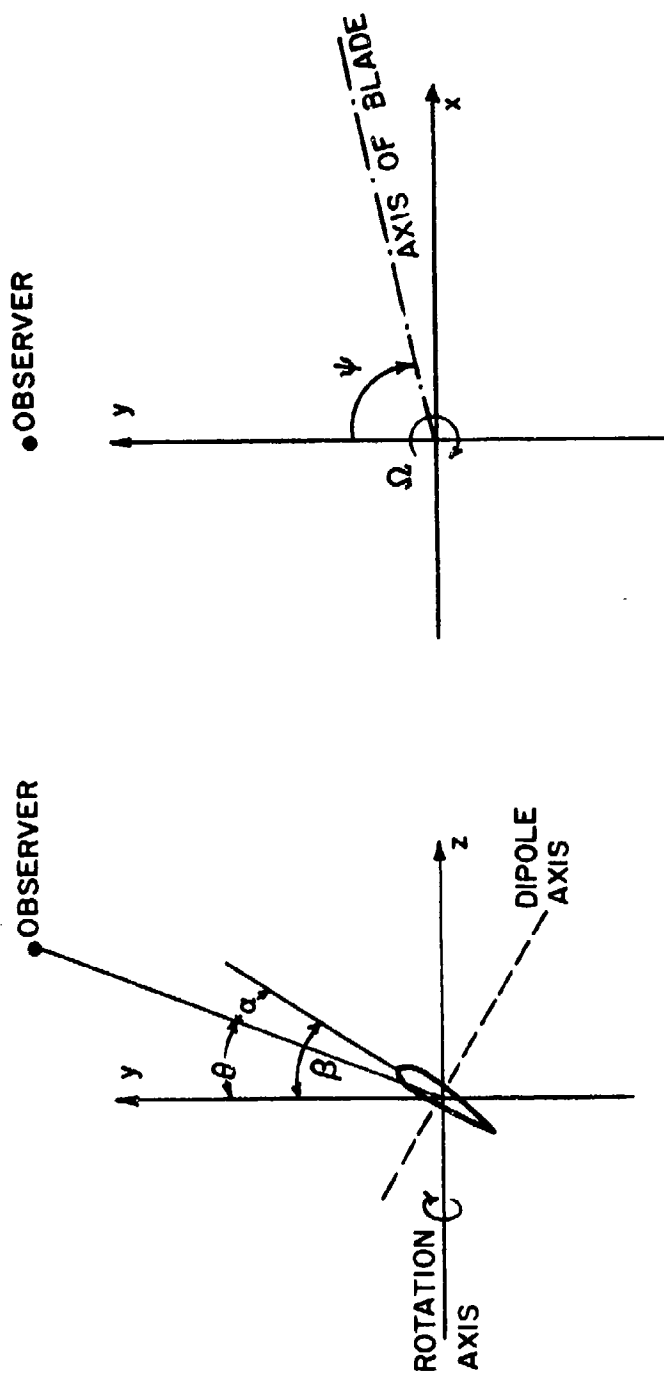
FIGURE B1   DEFINITIONS OF ANGLES FOR DIRECTIVITY ANALYSIS
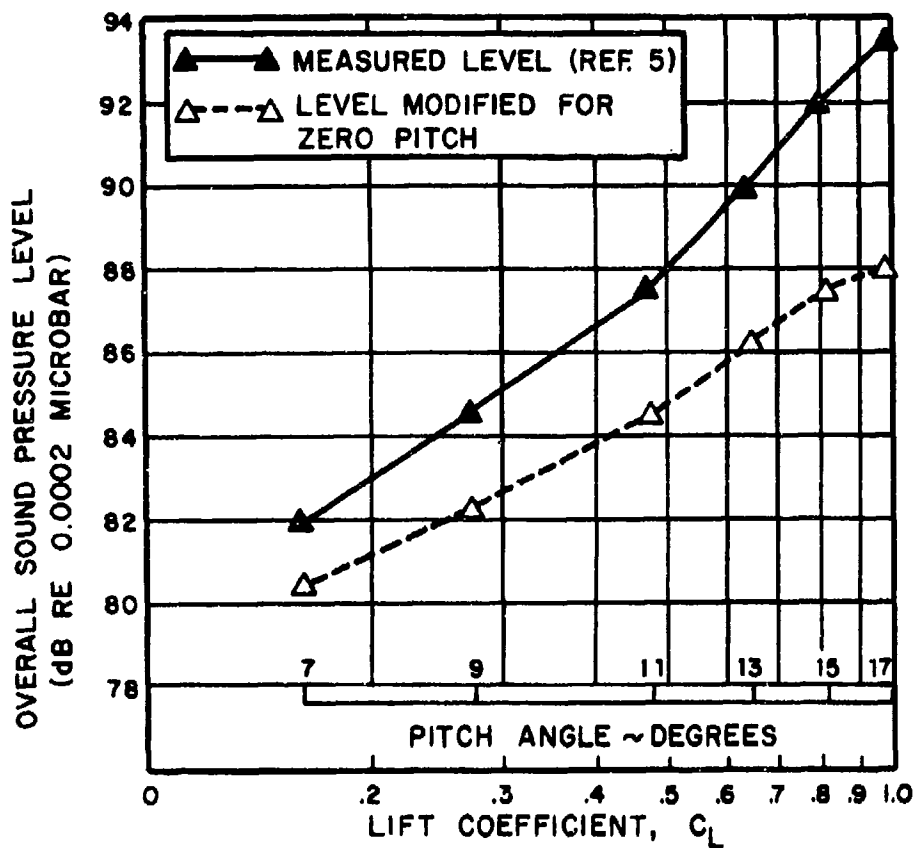
FIGURE B2   VORTEX NOISE AS A FUNCTION OF LIFT COEFFICIENT AND
ANGLE OF ATTACK, FOR HELICOPTER ROTOR OF REFERENCE
5, (AT 7.5° BEHIND ROTATION PLANE)
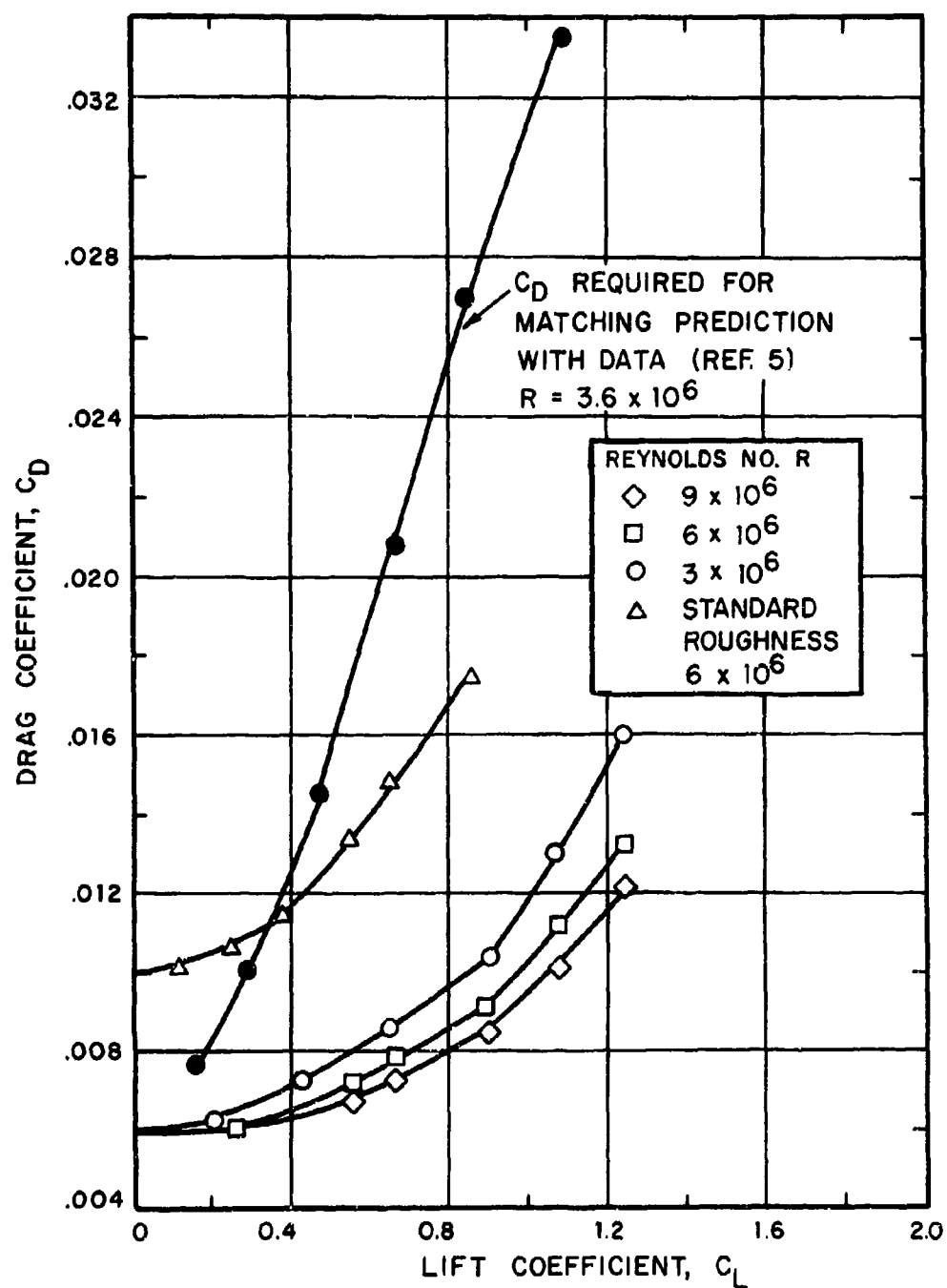
FIGURE B3   LIFT-DRAG CHARACTERISTICS OF NACA 0012 AIRFOIL SECTION
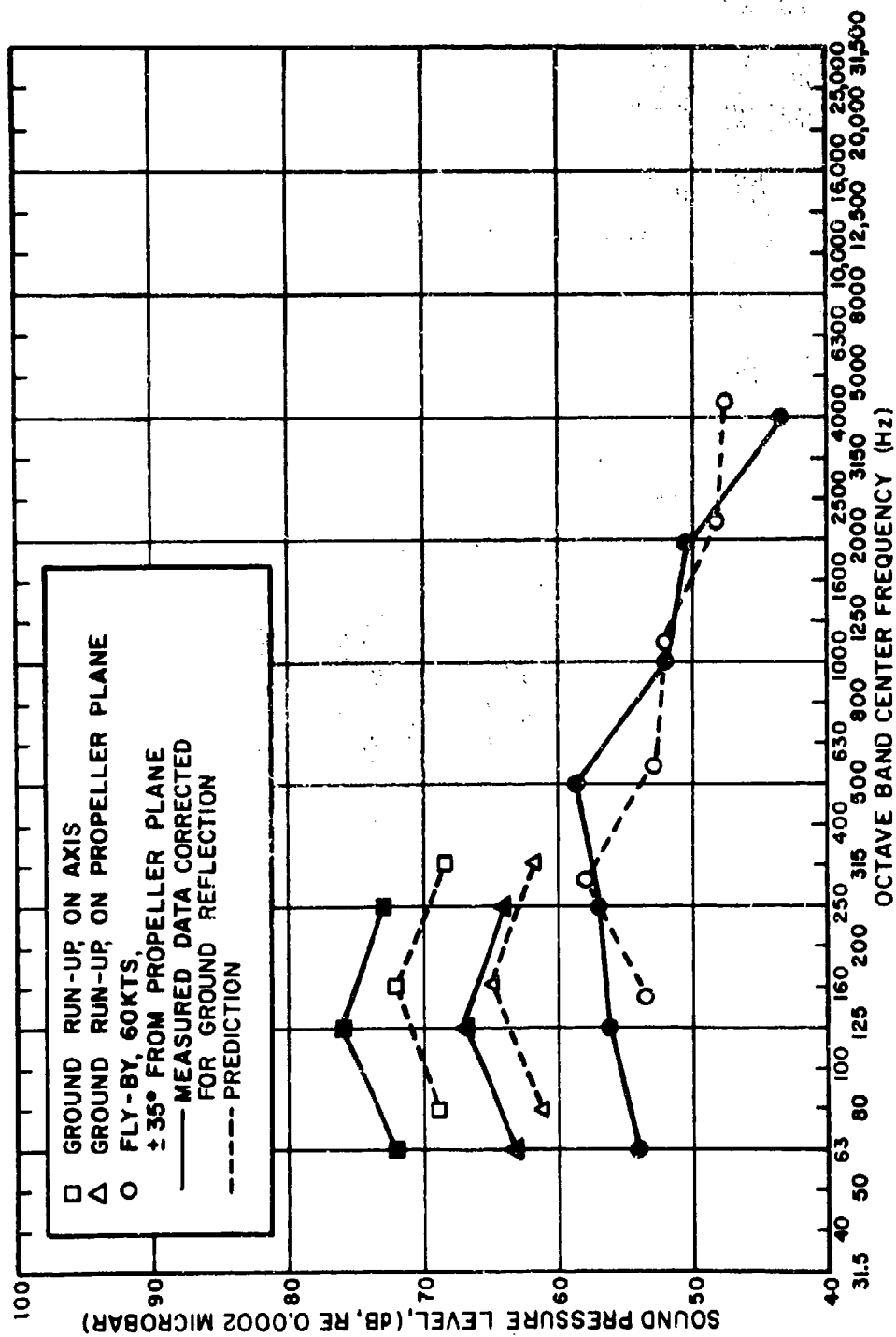
COMPARISON OF MEASURED AND PREDICTED VORTEX NOISE

FIGURE B4

OCTAVE BAND CENTER FREQUENCY (Hz)

SOUND PRESSURE LEVEL, (dB, RE 0.0002 MICROBAR)

□ GROUND RUN-UP, ON AXIS
△ GROUND RUN-UP, ON PROPELLER PLANE
○ FLY-BY, 60KTS,
±35° FROM PROPELLER PLANE
—— MEASURED DATA CORRECTED
FOR GROUND REFLECTION
----- PREDICTION

31.5 40 50 63 80 100 125 160 200 250 315 400 500 630 800 1000 1250 1600 2000 2500 3150 4000 5000 6300 8000 10,000 12,500 16,000 20,000 25,000 31,500

100 90 80 70 60 50 40
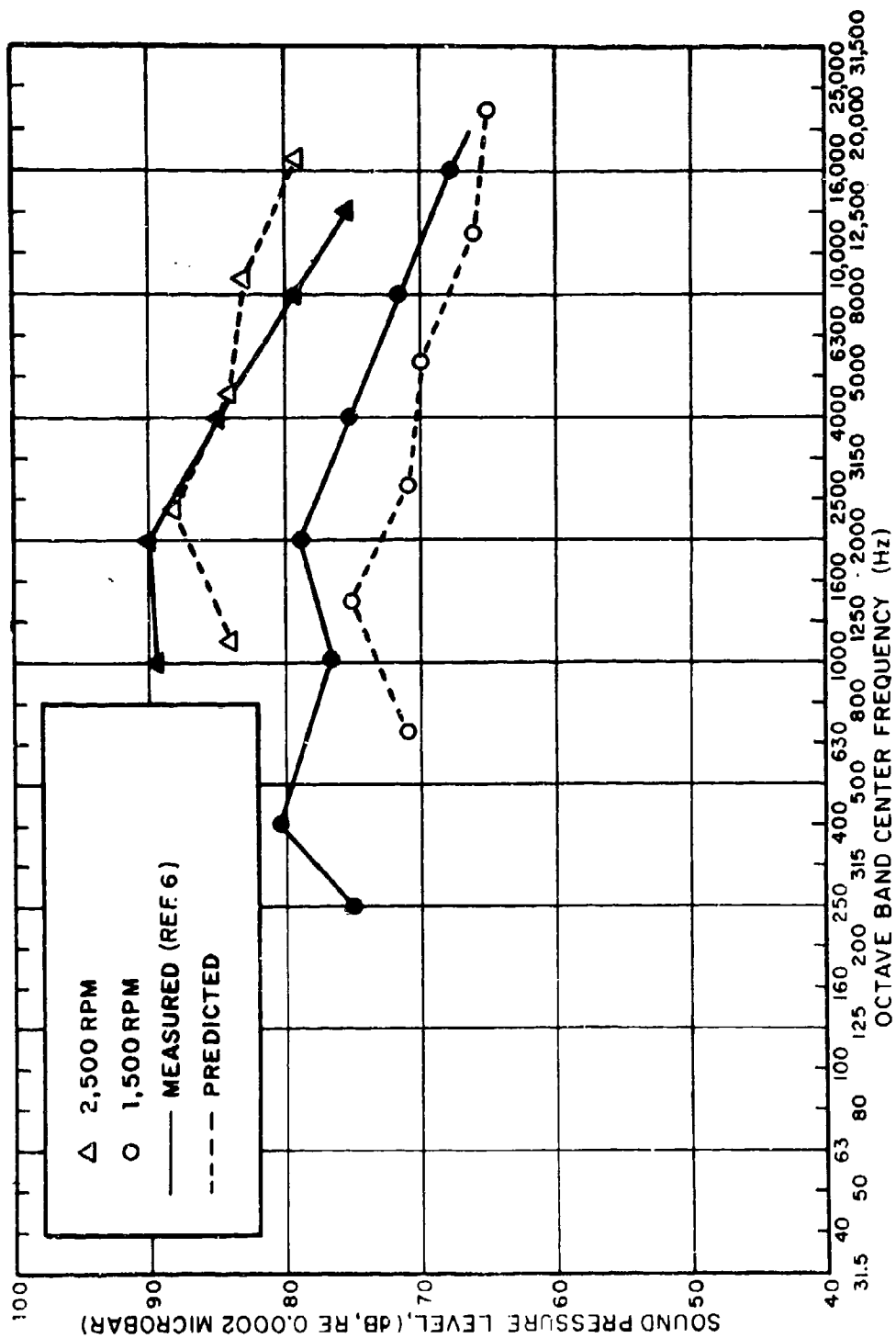
FIGURE B5   COMPARISON OF MEASURED AND PREDICTED VORTEX NOISE FOR H.D. 1
HOVERCRAFT, AT 15° OUT OF PROPELLER PLANE, 100 FT FROM HUB

APPENDIX C

NOISE OF PISTON ENGINES

NOISE SOURCES

The noise of piston engines, like that of any air-breathing internal combustion engine, may be considered in terms of three components: (1) intake, (2) exhaust, and (3) casing noise. In un-muffled engines, exhaust noise typically predominates. Casing noise - defined as the noise of an engine with "completely" muffled* exhaust and intake - is important only if the exhaust (and possibly the intake) indeed is well muffled.

The exhaust systems of internal combustion engines essentially release puffs of gas (possibly at considerable pressure) to the atmosphere as the exhaust valves open - and these pressure pulses constitute the primary components of exhaust noise. Clearly, exhaust ducting (such as manifolds, pipes, by-pass valves) can have very significant effects on the intensity and shape of these pressure pulses - and thus on the exhaust noise - in addition to adding noise (e.g., of a rushing or whistling nature) due to the flow in this ducting. (Ref. 1)

The foregoing remarks concerning exhaust noise also apply to intake noise, except that the intake ingests puffs of air, rather than emitting them. Acoustically, ingested puffs have the same effect as emitted ones; however, the exhaust pressure pulses have greater pressure differences associated with them than do intake pressure pulses. For this reason, and also because high-pressure pulses tend to change into shock-waves as they propagate along a duct, unmuffled exhausts usually are much more noisy than unmuffled intakes.

Casing noise may be ascribed to (1) the nearly explosion-like pressure pulses obtained from ignition of the fuel, (2) internal mechanisms, such as "piston slap" (lateral impacts of pistons against the cylinder walls) and impacts associated with valves and valve-lifters, (3) accessories, such as fuel pumps and fuel injectors, and (4) power transmission components, such as gears and bearings. (Ref. 2)

---

*The exhaust and intake of an engine may be considered as completely muffled if the addition of further attenuation for these sources does not reduce the observed noise of the engines.

DATA

Availability of Data on Spark-Ignition and Diesel Engines

The available data on the noise of spark-ignition (SI) engines is extremely limited and so inadequately documented that it is inadequate to serve as the basis for development of a noise prediction scheme. On the other hand, there does exist a useful body of information on the noise of diesel engines (Refs. 3, 4). Therefore, it appears sensible to use this diesel engine data as a basis for estimation, although aircraft are more likely to use SI engines than diesel engines.

Similarity of Spark-Ignition and Diesel Engine Noise

One may indeed argue that the noise of SI engines should be very much like that of a similar diesel engine. Clearly, the intake process does not depend on whether the fuel-air mixture is ignited by a spark or by compression later in the cycle, so that one would expect the intake noise of a given engine to be the same, whether that engine uses spark or diesel ignition. However, the intakes of SI engines may be designed somewhat differently than those of diesels (because SI engines may have carburators, for example), and thus may sound somewhat different.

The same sort of remarks as were made above concerning intake noise also apply to exhaust noise. Again, the exhaust puff does not depend on the ignition process - but rather on the exhaust valve timing, on the cylinder pressure at the instant the valve opens, and on the cylinder pressure-time characteristics during the time the valve is open. Although "indicator diagrams" (plots of cylinder pressure versus piston displacement or crank angle) for diesels differ considerably from those of SI engines for the compression and combustion parts of the cycle, the portions of these diagrams corresponding to the exhaust process tend to be very similar. (Ref. 1)

On the other hand, one might expect the casing noise of SI and diesel engines to differ more significantly. Diesel engines typically are designed for higher compression ratios than SI engines, and the (internal) combustion pressure pulses in diesels tend to be more sharply explosive than those in SI engines. The cylinder pressure spectra of diesels thus generally are higher than those of SI engines, and tend to have much more high-frequency content (Refs. 5-8). However, diesels usually are built much more

massively (to contain the higher pressures), so that less combustion noise tends to get through the structure (Refs. 9,10). The severity of piston-slap impacts depends on the cylinder pressure to some extent, so that these impacts are more severe in diesels (Refs. 4,11). Again, the more massive structures of diesels tend to reduce the noise radiated as a result of these impacts. Piston-slap is likely to make no significant contribution to the casing noise of any relatively small high-speed engines with tight-cylinder/piston clearances, which one might use in aircraft (Refs. 4,11).

Comparatively little is known about the accessory noise of the various types of engines (Ref. 12). There appears to be no reason that would lead one to believe that the noise of a power transmission component should be much different from that of a similar component in a different engine. (Also, these components usually do not contribute very significantly to the total casing noise.) Because of these considerations, and in the light of the foregoing discussion, it appears logical to base a noise prediction scheme for SI engines on diesel engine data. Such a scheme will at least provide a first approximation, which should prove useful until adequate SI engine data become available.

Available Data

An extensive field measurement and literature review program (Ref. 3) has yielded noise data on a large variety of diesel and natural-gas engines in electrical power plants and similar stationary installations. More than 50 engines (about half with 4-stroke and half with 2-stroke cycles), with power ratings between 12.5 and 5150 kw (9.5 to 3850 Hp), were studied at actual power outputs between 0 and 5150 kw and at speeds between 225 and 1800 rpm.

The "casing noise" of these engines was deduced from measurements in engine rooms, with the engine intakes and exhausts either outside the rooms or well-muffled. Measured acoustic characteristics of the rooms were used to interpret the engine noise data in terms of acoustic power spectra of the sources.

For some of these engines, the air intake or engine exhaust noise was measured out of doors, at some convenient distance from the intake or exhaust opening. Where no muffler was present, these measurements were directly interpreted in terms of acoustic power; where exhaust mufflers were present, the measured data were corrected by means of estimated attenuation characteristics of the muffler and exhaust piping to yield the approximate acoustic power of the unmuffled exhaust.

The data of Ref. 3 were re-analyzed in order to provide an improved method for predicting the engine noise spectra of interest here. This re-analysis involved discarding all data on gas engines (because these are inherently quieter than diesels), all data on engines with nonstandard structures (e.g., with thermal insulation), and all data on engines with Roots blowers (because these blowers add to the noise and are not likely to be used in aircraft); in addition, it involved re-examining the data in terms of a reduced frequency based on the "firing frequency". The results of this analysis are shown in the attached figures.

DATA ANALYSIS; ESTIMATION SCHEME

Exhaust Noise

Figure C1 summarizes octave-band exhaust noise data obtained from measurements on nine diesel engines with widely differing operating characteristics. In addition to points corresponding to individual measurements, this figure (as well as all the other figures of this section) also shows "average" and "average plus standard deviation" spectra, which were obtained by carrying out the appropriate arithmetic operations on the data corresponding to the points indicated at each frequency.* Because the acoustic power of engine noise sources has been found to be proportional to the engine power, the sound power levels in Fig. 1 and in the rest of the figures of this section have been reduced with respect to the engine power.

Because the exhaust valve of an engine cylinder opens once per cycle (i.e., once per power stroke or once per firing), the exhaust of an engine emits one puff per firing per cylinder. One would thus expect the exhaust noise spectrum to have a major peak at the firing frequency f_F, which for an N-cylinder engine may be found from

$$f_F(Hz) = \text{engine speed (rev/sec)} \cdot n \cdot N,$$

---

*The averaging, etc., computations were carried out not on the decibel values which correspond to the data points, but on the mean-square pressures they represent. The "energy" averages obtained in this way are likely to be most meaningful for estimation purposes. (Ref. 13)

where n is the number of power strokes per revolution. For a four-stroke cycle engine, $n = 1/2$; for a two-stroke cycle engine, $n = 1$.

The data of Fig. C1 are shown in Fig. C2, replotted against the ratio of octave band center frequency to firing frequency. Better collapse of the data is evident. Also shown in Fig. C2 is a curve which was suggested by Franken and Beranek (Ref. 14) for estimating the average exhaust noise levels one may expect from unmuffled piston engines; this curve may be seen to encompass most of the peaks of the average data curve, but to over-estimate the high-frequency noise considerably. An improved estimation curve, which follows all of the data peaks of Fig. C2, is presented in Fig. C7.

Intake Noise

Intake noise data obtained from measurements on six engines with unmuffled intakes are summarized in Fig. C3. The same data are shown in Fig. C4 as a function of firing frequency. Unlike for exhaust noise, this replotting does not improve the collapse of the data materially. However, since it does bring out the existance of a physically meaningful spectrum peak near the firing frequency, it appears advantageous to base an estimation scheme on Fig. C4, rather than on Fig. C3. The corresponding curve of Fig. C7 represents a smoothed envelope of the peaks of the "average" spectrum of Fig. C4.

Casing Noise

Figure C5 shows octave-band data on casing noise for 27 diesel engines with widely varying engine parameters, as indicated in the figure heading. The sound power levels indicated again are normalized with respect to engine output horsepower (Hp) and include A and C correction terms, which were found useful in Ref. 3 for improving the estimates of the overall levels. An "average curve", which is expected to be useful for general prediction purposes, (calculated on the basis of energy averaging, after discarding the most extreme points) is also given in the figure.

Figure C6 differs from Fig. C5 only in that the data are plotted against the ratio of octave band center frequency to engine firing frequency. A somewhat better collapse of the data is evident, so that use of Fig. C6 for estimation purposes appears preferable. The casing noise estimation curve given in Fig. C7 is a smoothed envelope of the peaks of the "average" curve of Fig. C6.

ESTIMATION SCHEME

Fig. C7 summarizes an estimation scheme for all three noise components; how the various estimation curves were developed was indicated above. As evident from Fig. C7, the noise of unmuffled exhausts always predominates. With a well-muffled exhaust, casing noise becomes most important. Silencing of the intake cannot reduce the total noise of an engine unless the exhaust and casing noise components have been reduced drastically.

In order to predict the noise of a given engine, one may proceed as follows:

1. First calculate the firing frequency from

    $$f_F(Hz) = \text{engine speed (rev/sec)} \cdot n \cdot N$$

    where N is the number of cylinders and
    $$n = \begin{cases} \frac{1}{2} \text{ for four-stroke cycle engines} \\ 1 \text{ for two-stroke cycle engines.} \end{cases}$$

    Then determine what actual frequencies f correspond to the reduced frequencies f/f_F of Fig. C7.

2. Find 10 log(Hp), A, C, using the relations given in Fig. C7. For each of the three noise components represented in the figure, use the values of L_W - 10 log(Hp) + A + C read from the figure to determine the corresponding octave band spectra.

    Note that one may obtain these spectra simply by relabeling the frequency and L_W scales, and by shifting the casing noise curve downward by the amount A + C with respect to the other two curves.

Illustrative Calculation

Consider an unmuffled "V-6" 6-cylinder four-stroke-cycle engine producing 90 Hp at 2100 rpm. Here

$$f_F = \text{rps} \cdot n \cdot N = \left(\frac{2100}{60}\right)\left(\frac{1}{2}\right) (6) = 105 \text{ Hz.}$$

Thus $f/f_F = 1$ corresponds to f = 105 Hz, $f/f_F = \frac{1}{2}$ to f = 52 Hz, $f/f_F = 4$ to 420 Hz, etc.

Since 2100 rpm > 1500 rpm, one finds A = 0, and for a "V" engine, C = 1; and

$$10 \log(Hp) = 10 \log(90) = 19.5 \text{ dB}$$

Therefore one obtains the engine noise spectra by relabeling the vertical coordinate scale of Fig. C7 as simply L_w(dB, re 10^{-12}watts), increasing all numbers indicated along this scale by 19.5 dB, and shifting the casing noise curve downward by 1 dB.

One thus finds, for example, that the peak exhaust noise power level is 131.5 dB (at 52 and 105 Hz), that the peak intake noise power level is 91.5 dB(re 10^{-12}watts) at 105 Hz, and that the highest casing noise level of 108.5 dB occurs between 840 and 1680 Hz.

REFERENCES FOR APPENDIX C

1. Kern, F. R., Jr., "Simulation of Exhaust Pressures of Air-craft Piston Engines," BBN Report No. 2072, prepared for NASA Langley Research Center under Contract NAS1-9559-4 (November 1970). To appear as a NASA Contractor Report.

2. Austen, A. E. W. and T. Priede, "Noise of Automotive Diesel Engines; Its Causes and Reduction," SAE International Automotive Engineering Congress Paper 1000A (Jan. 1965).

3. Miller, L. N., "Acquisition and Study of the Noise Data of Diesel and Gas Engines," BBN Report No. 1476, prepared for the Dept. of the Army, Office of the Chief of Engineers under Contract DA-49-129-ENG-565 (April 1967).

4. Ross, D. and E. E. Ungar, "On Piston-Slap as a Source of Engine Noise," ASME Paper 65-OGP-10 (1965).

5. Priede, T., "Noise due to Combustion in Reciprocating I. C. Engines," pp. 93-128 in *Advances in Automobile Engineering, Part III*, Ed. by G. H. Tidbury, Cranfield International Symposium Series Vol. 7, Pergamon Press (1965).

6. Priede, T., E. L. Grover and D. Anderton, "Combustion Induced Noise in Diesel Engines," Preprint 317, presented at the General Meeting of Institute of Marine Engineers, (16 Nov. 1967).

7. Anderton, D., M. Lalor, E. C. Grover, and T. Priede, "Assessment and Control of Combustion Induced Noise in I. C. Engines," *Combustion Engine Progress*, pp. 48-53 (1969).

8. Priede, T., "Relation Between Form of Cylinder Pressure Diagram in Diesel Engines," *Proceedings of the Institute of Mechanical Engineers*, (AD) No. 1 (1960-1961).

9. Priede, T., E. C. Grover and M. Lalor, "Relation Between Noise and Basic Structural Vibrations of Diesel Engines," SAE Paper No. 690450 (May 1969).

10. Priede, T., A. E. W. Austen and E. C. Grover, "Effect of Engine Structure on Noise of Structural Engines," *Proceedings of the Institute of Mechanical Engineers*, pp. 113-136 (1964-1965).

11. Ungar, E. E. and D. Ross, "Vibrations and Noise due to Piston-Slap in Reciprocating Machinery," *Journal of Sound and Vibration*, 2(2), pp. 132-146 (1965).

12. Priede, T., "Noise of Diesel Engine Injection Equipment," *Journal of Sound and Vibration*, 6, pp. 443 (1967).

13. Kerwin, E. M., Jr., "Decibels and Levels," Chapter 3 of *Noise Reduction*, Ed. by L. L. Beranek, McGraw-Hill Book Co., Inc., New York, 1960.

14. Franken, P. A., p. 693 in *Noise Reduction*, Ed. by L. L. Beranek, McGraw-Hill Book Co., Inc., New York, 1960.
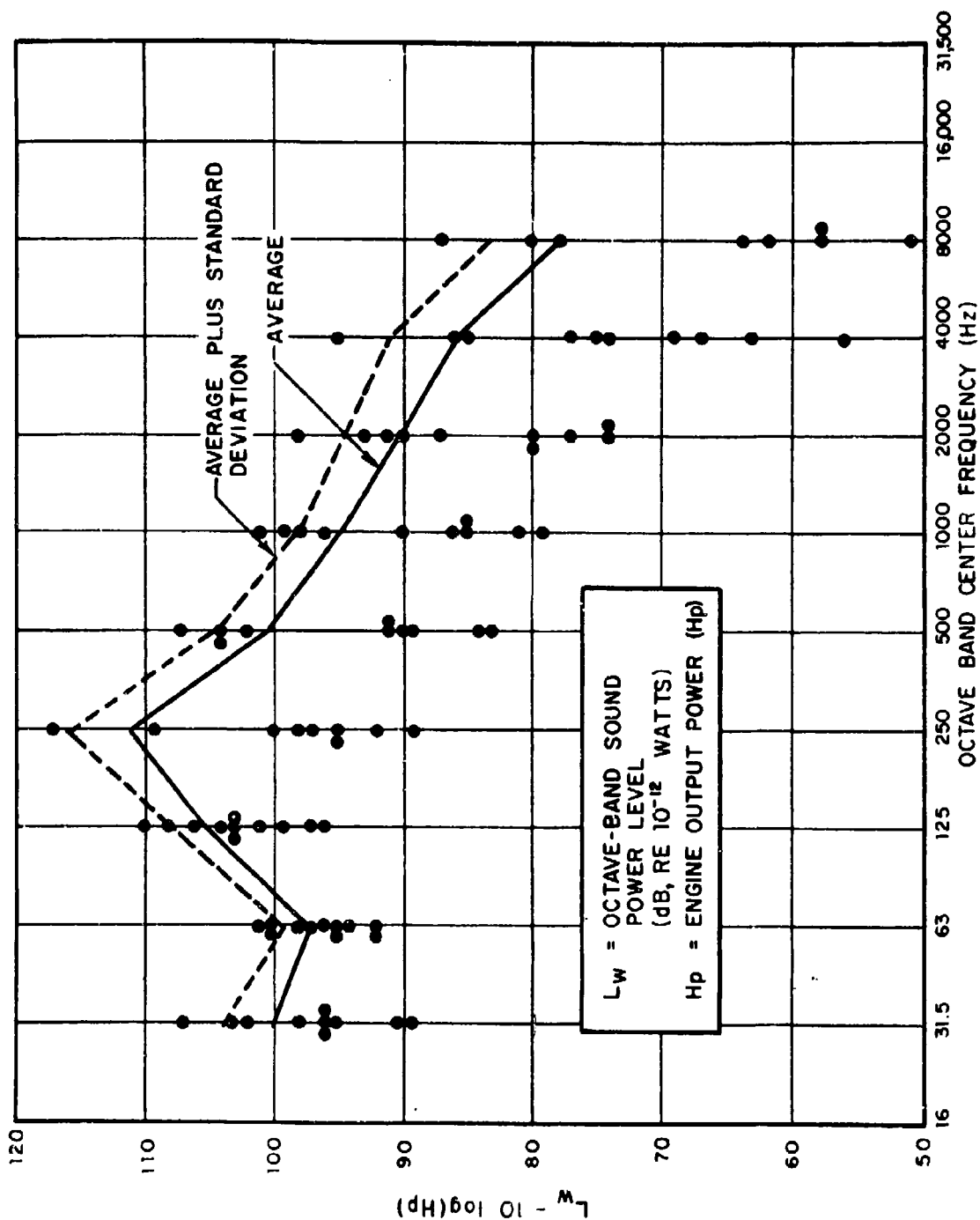
FIGURE C1   EXHAUST NOISE OF NINE UNMUFFLED DIESEL ENGINES (160 TO 7000 HP, 240
TO 1800 RPM, 2 & 4 STROKE CYCLES, 30 TO 480/SEC FIRING FREQUENCY)
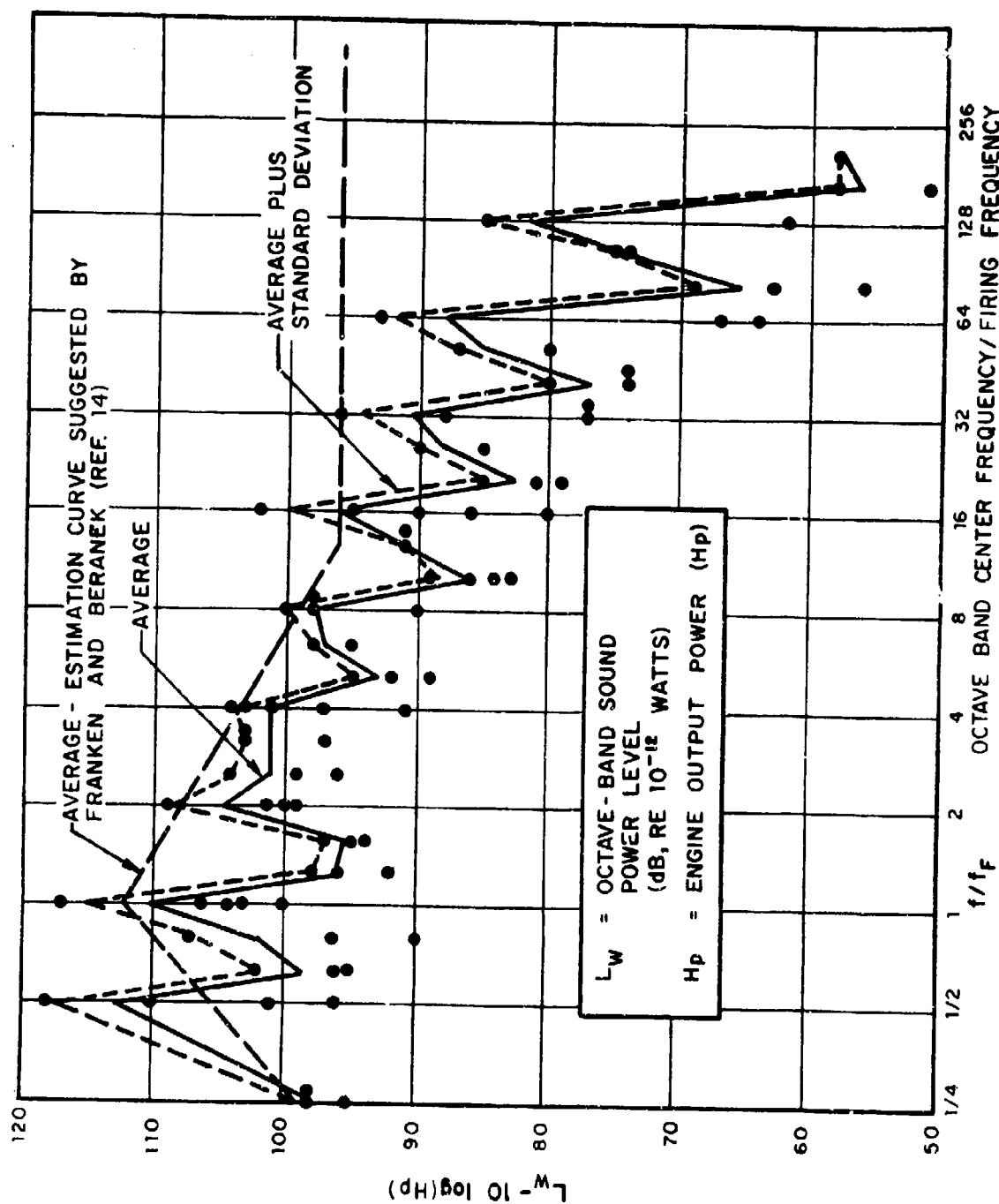
FIGURE C2   EXHAUST NOISE OF UNMUFFLED DIESEL ENGINES, AS FUNCTION OF
FREQUENCY/FIRING FREQUENCY
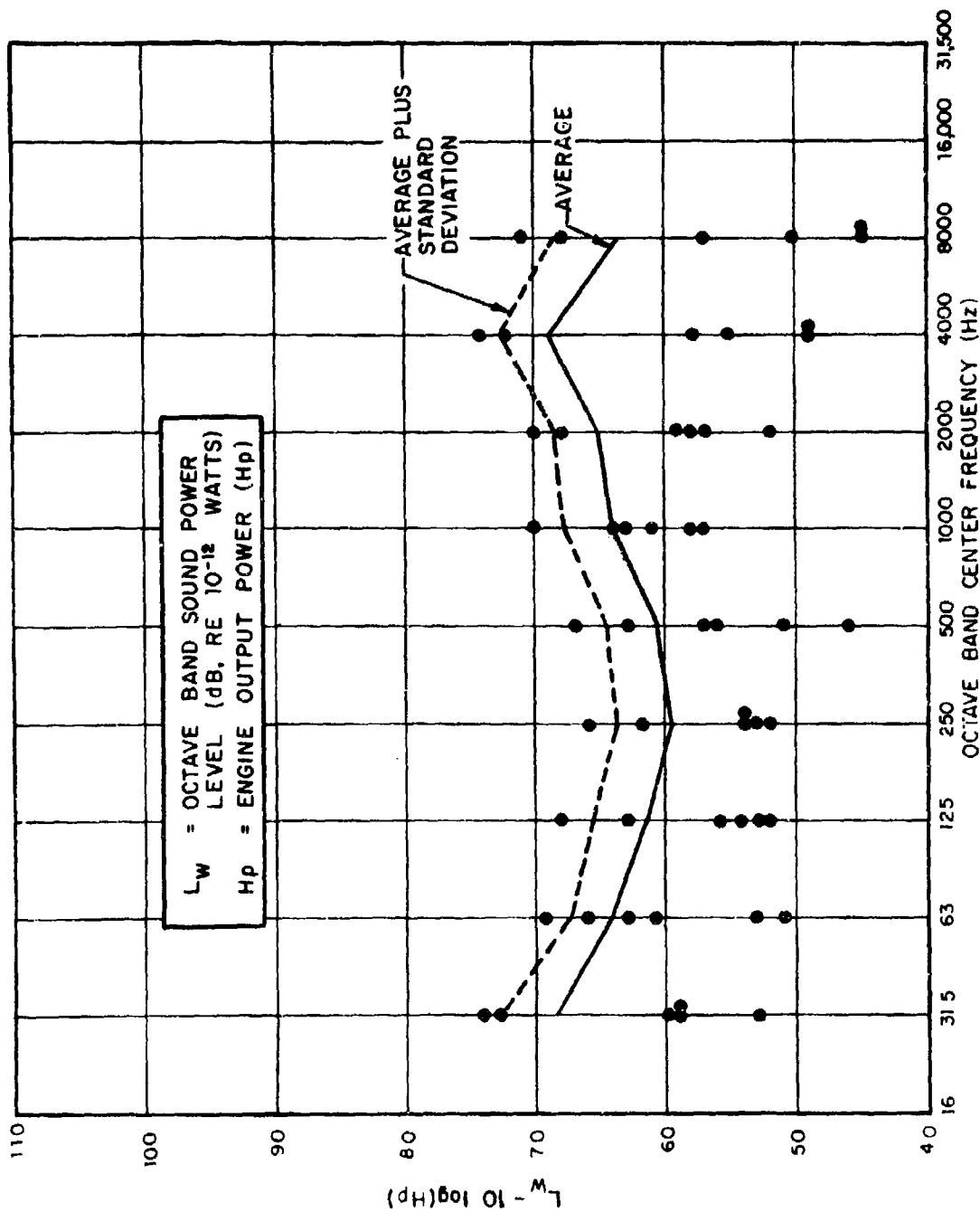
FIGURE C3   INTAKE NOISE OF SIX UNMUFFLED DIESEL ENGINES (300 TO 4000 HP, 260 TO 1200 RPM, 2 AND 4 STROKE CYCLES, 22 TO 60/SEC FIRING FREQUENCY)
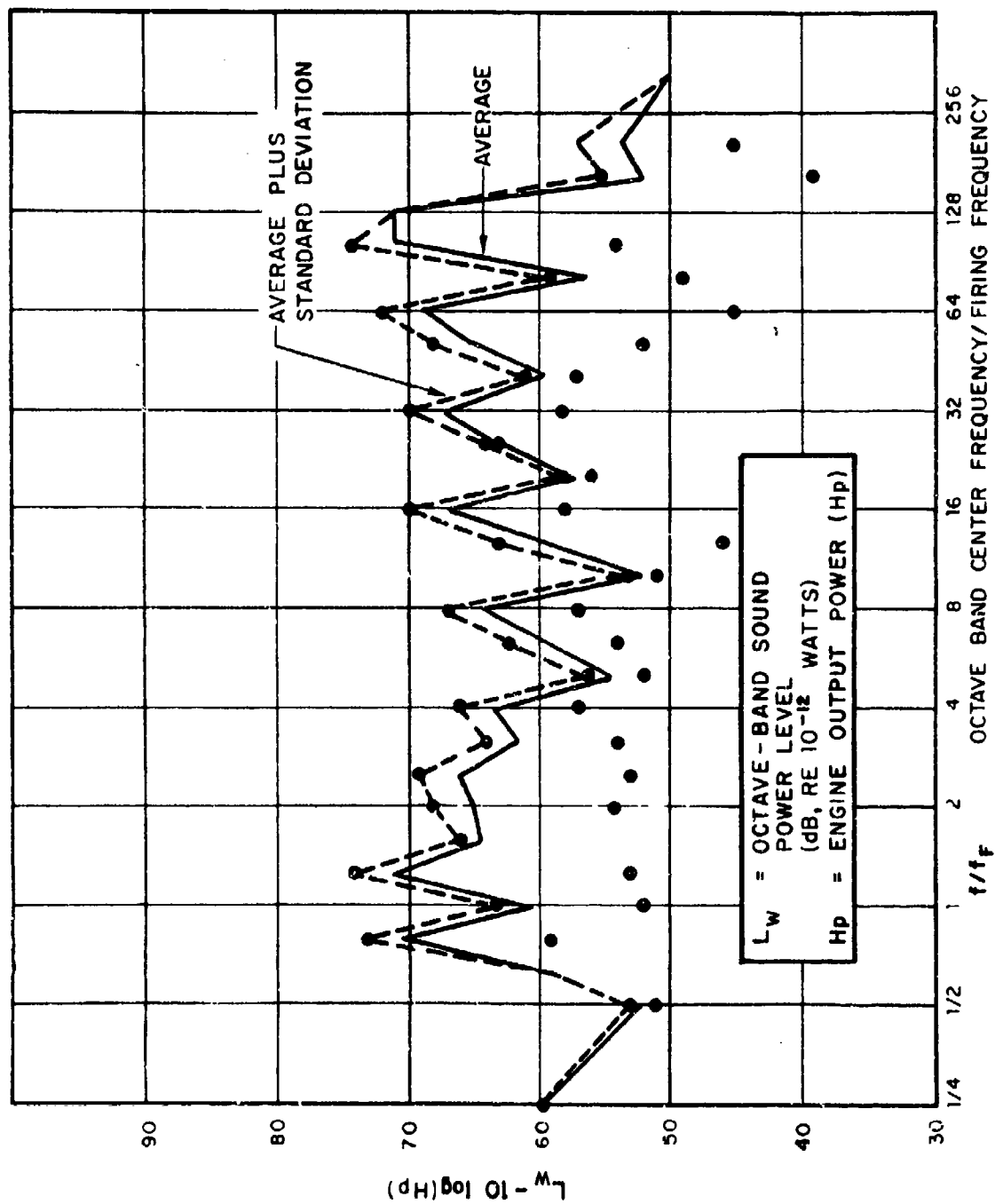
FIGURE C4   INTAKE NOISE OF DIESEL ENGINES AS FUNCTION OF FREQUENCY/FIRING
FREQUENCY
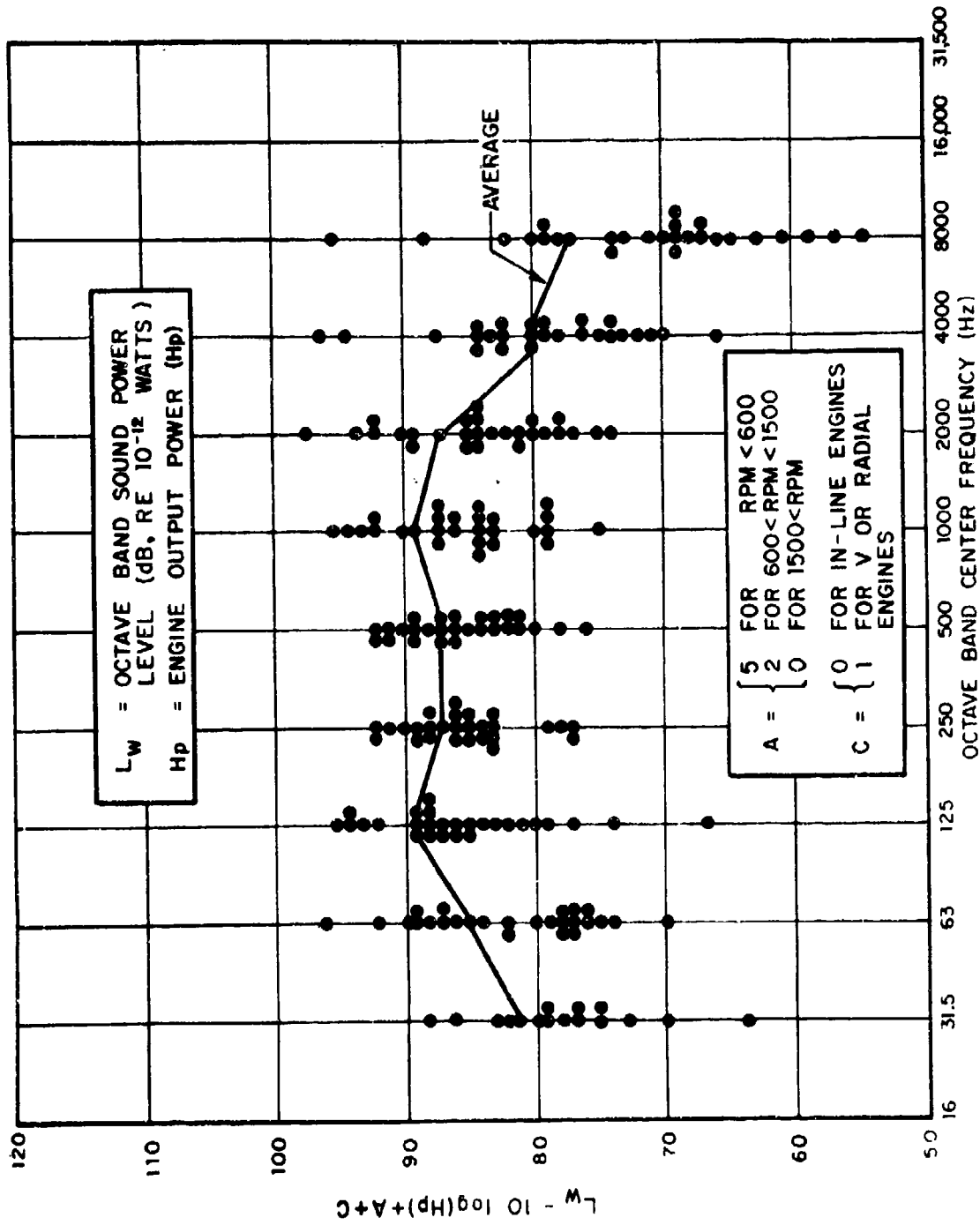
FIGURE C5   CASING NOISE OF 27 DIESEL ENGINES [12.5 TO 2900 KW (9 TO 2200 HP) 2 TO 4 STROKE CYCLES, 240 TO 1800 RPM, 30 TO 480 SEC FIRING RATES TURBOCHARGED AND NATURALLY ASPIRATED 4,5,8,10 CYLINDERS, IN-LINE AND V]

FIGURE C6   CASING NOISE OF 27 DIESEL ENGINES AS FUNCTION OF FREQUENCY/
FIRING FREQUENCY

AVERAGE

L_W = OCTAVE BAND SOUND POWER
LEVEL (dB RE 10^{-12} WATTS)

H_p = ENGINE OUTPUT POWER (Hp)

$A = \begin{cases} 5 & \text{FOR RPM} < 600 \\ 2 & \text{FOR } 600 < \text{RPM} < 1500 \\ 0 & \text{FOR } 1500 < \text{RPM} \end{cases}$

$C = \begin{cases} 0 & \text{FOR IN-LINE ENGINE} \\ 1 & \text{FOR V OR RADIAL ENGINE} \end{cases}$

• 4 - STROKE CYCLE ENGINES
o 2 - STROKE CYCLE ENGINES

OCTAVE BAND CENTER FREQUENCY/ FIRING FREQUENCY

f/f_F

1/4   1/2   1   2   4   8   16   32   64   128   256

L_W - 10 log(Hp)+A+C

50   60   70   80   90   100   110   120

Y-axis label: $L_W - 10 \log(H_p) + A + C$

Y-axis values: 120, 110, 100, 90, 80, 70, 60, 50

X-axis values: 1/8, 1/4, 1/2, 1, 2, 4, 8, 16, 32, 64, 128, 256

X-axis labels: f/f_F OCTAVE BAND CENTER FREQUENCY/FIRING FREQUENCY

Legend insert:

L_W = OCTAVE-BAND SOUND POWER LEVEL (dB, RE 10^{-12} WATTS)

H_p = ENGINE OUTPUT POWER (Hp)

$A = \begin{cases} 5 \text{ FOR RPM} < 600 \\ 2 \text{ FOR } 600 < \text{RPM} < 1500 \\ 0 \text{ FOR } 1500 < \text{RPM} \end{cases}$

$C = \begin{cases} 0 \text{ FOR IN-LINE ENGINE} \\ 1 \text{ FOR V OR RADIAL ENGINE} \end{cases}$

Curve labels:

UNMUFFLED EXHAUST (USE A=C=0)

CASING (USE VALUES OF A AND C GIVEN IN INSERT)

UNMUFFLED INTAKE (USE A = C = 0)

• INDICATES ESSENTIALLY PURE-TONE COMPONENT; LEVELS NOT SO MARKED CORRESPOND TO BROAD-BAND COMPONENTS FOR PREDICTION PURPOSES.

FIGURE C7   ESTIMATION OF NOISE OF PISTON ENGINES

APPENDIX D

NOISE OF ROTATING COMBUSTION ENGINES

DATA

Data on the noise of Curtiss-Wright Corp. rotating combustion (Wankel) engines are presented in Ref. 1. These data, adjusted for engine speed and horsepower output (so as to make the data collapse into a form best suited for prediction purposes), are summarized in the figures which follow this text.

As in virtually all engines, intake and exhaust noise tends to dominate over noise from all other sources. This noise from "all other sources", which one observes if the intake and exhaust are effectively muffled, is called casing noise and is labeled as such in the figures. (Also see corresponding discussion under the heading of "Noise of Piston Engines".)

AIR-COOLED AND WATER-COOLED ENGINES

The data points indicated in the figures correspond to measurements carried out on two RC-2-60 water-cooled engines*, operating at between 2500 and 5000 rpm while producing between 30 and 103 Hp. The two engines to which these data points apply differ only in their intake port configurations; one has side-ports, the other, peripheral ports. The peripheral port configuration tends to result in noise levels which are slightly higher (by at most 0.5 db for casing noise, 1.5 db for exhaust noise, and 2.5 db for intake noise) than those for side-ports.

Although detailed data on the noise of air-cooled engines are not given in Ref. 1, that document does present comparisons between the noise levels of an air-cooled RC-2-90 engine and those of water-cooled RC-2-60 engines. The curves for air-cooled engines in the attached figures were obtained from the differences between typical air-cooled and water-cooled engine data.

---

*Curtiss-Wright uses the first number after the RC to designate the number of rotors, and the second to give the displacement (in cubic inches) per rotor.

DISCUSSION

The data available were measured on only three different types of engines, all having two rotors, with about the same displacement. The effects of adding more rotors are not known, but one might expect the noise spectrum to shift with the firing frequency.

No data on the effects of engine size (rotor displacement) are available at all. The number of Wankel engine types in operation is very limited; some small engines of lawn-mower size are in production, as are some engines for small automobiles, but no engines rated significantly above 100 Hp appear to be available as yet.

ESTIMATION SCHEME

Clearly, an average of the measured spectra should serve for prediction purposes. Probably the most meaningful average is that which corresponds to the mean-square value computed for all of the data points at each frequency. Correspondingly, the "average" and "average plus standard deviation" curves indicated in the figure have been obtained, not by performing the appropriate arithmetic operations on the decibel numbers represented by the various data points, but by performing those operations on the corresponding mean-square values. (See Ref. 2.) Because of the relatively large standard deviations calculated for most of the data, "average minus standard deviation" values generally turn out to be too low to fit on the plots and therefore do not appear in the figures.

Average curves for all three types of noise from rotating combustion engines are summarized in Fig. D4.

In order to estimate the acoustic power produced by a given rotary combustion engine, calculate $15 \log(\text{rpm}/1000) + 10 \log(\text{Hp})$, add this value to the numbers given on the vertical scale of Fig. D4, and relabel that scale simply $L_W(\text{dB}, \text{re } 10^{-12}\text{watts})$.

Illustrative Calculation

For an air-cooled rotating combustion engine producing 90 Hp at 2100 rpm,

$$15 \log(\text{rpm}/1000) + 10 \log(\text{Hp}) = 15 \log(2.1) + 10 \log(90) \approx 24.5 \text{ dB}.$$

Thus, for example, the 110 dB value of Fig. D4, at which the exhaust noise peak occurs (at 1000 Hz), corresponds to 134.5 dB.

REFERENCES FOR APPENDIX D

1. Berkowitz, M., W. Hermes and H. Lamping, "Rotating Combustion Engine Evaluation for Low Noise Level Aircraft Applications," Curtiss-Wright Corp. Report CW-WR-69-078.F; prepared for Naval Air Systems Command under Contract N000019-69-C-0460, January 1970.

2. Kerwin, E. M., Jr., "Decibels and Levels," Chapter 3 of *Noise Reduction*, Ed. by L. L. Beranek, McGraw-Hill Book Co., Inc., New York, 1960.
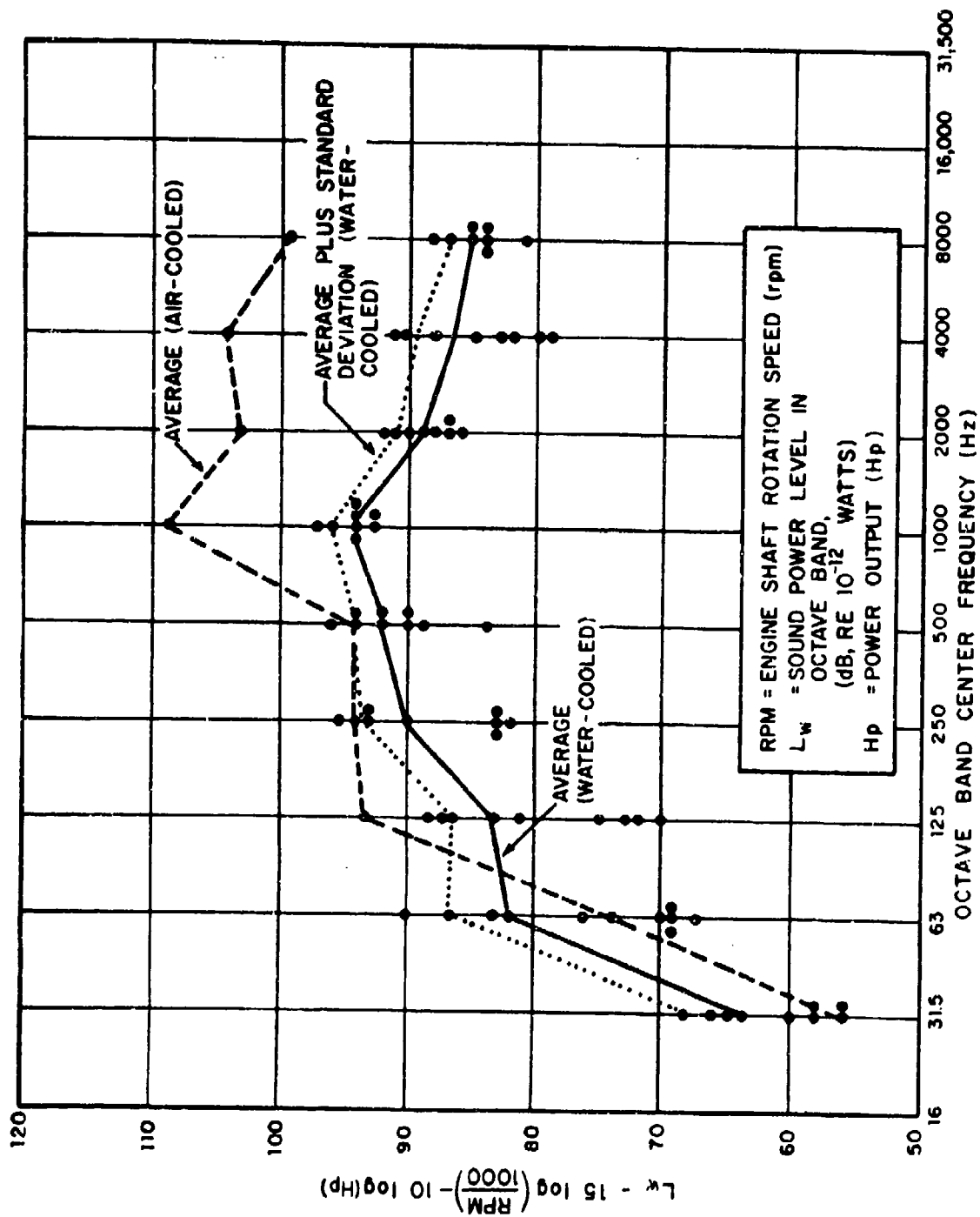
FIGURE D1   INTAKE NOISE OF ROTATING COMBUSTION ENGINES

RPM = ENGINE SHAFT ROTATION SPEED (rpm)
L_w = SOUND POWER LEVEL IN OCTAVE BAND, (dB, RE 10^{-12} WATTS)
Hp = POWER OUTPUT (Hp)

AVERAGE (AIR-COOLED)

AVERAGE PLUS STANDARD DEVIATION (WATER-COOLED)

AVERAGE (WATER-COOLED)

OCTAVE BAND CENTER FREQUENCY (Hz)

$L_w - 15 \log\left(\frac{RPM}{1000}\right) - 10 \log(Hp)$

75
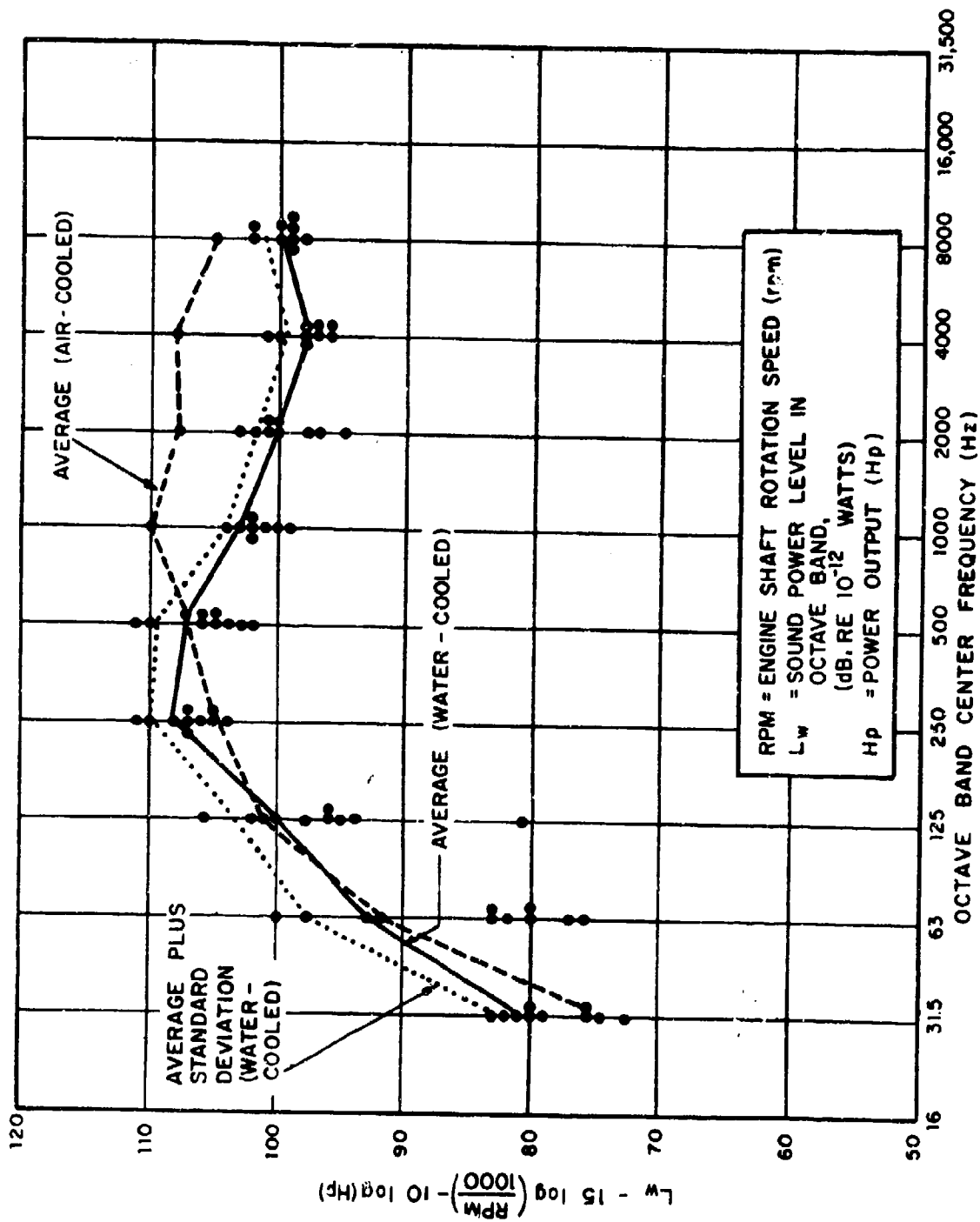
FIGURE D2   EXHAUST NOISE OF ROTATING COMBUSTION ENGINES

76

AVERAGE (AIR-COOLED)

AVERAGE PLUS STANDARD DEVIATION (WATER COOLED)

AVERAGE (WATER-COOLED)

RPM = ENGINE SHAFT ROTATION SPEED (rpm)

L_W = SOUND POWER LEVEL IN OCTAVE BAND, (dB, RE 10^{-12} WATTS)

Hp = POWER OUTPUT (Hp)

OCTAVE BAND CENTER FREQUENCY (Hz)

16   31.5   63   125   250   500   1000   2000   4000   8000   16,000   31,500

40   50   6()   70   80   90   10()

$$L_W - 15 \log\left(\frac{RPM}{1000}\right) - 10 \log(Hp)$$
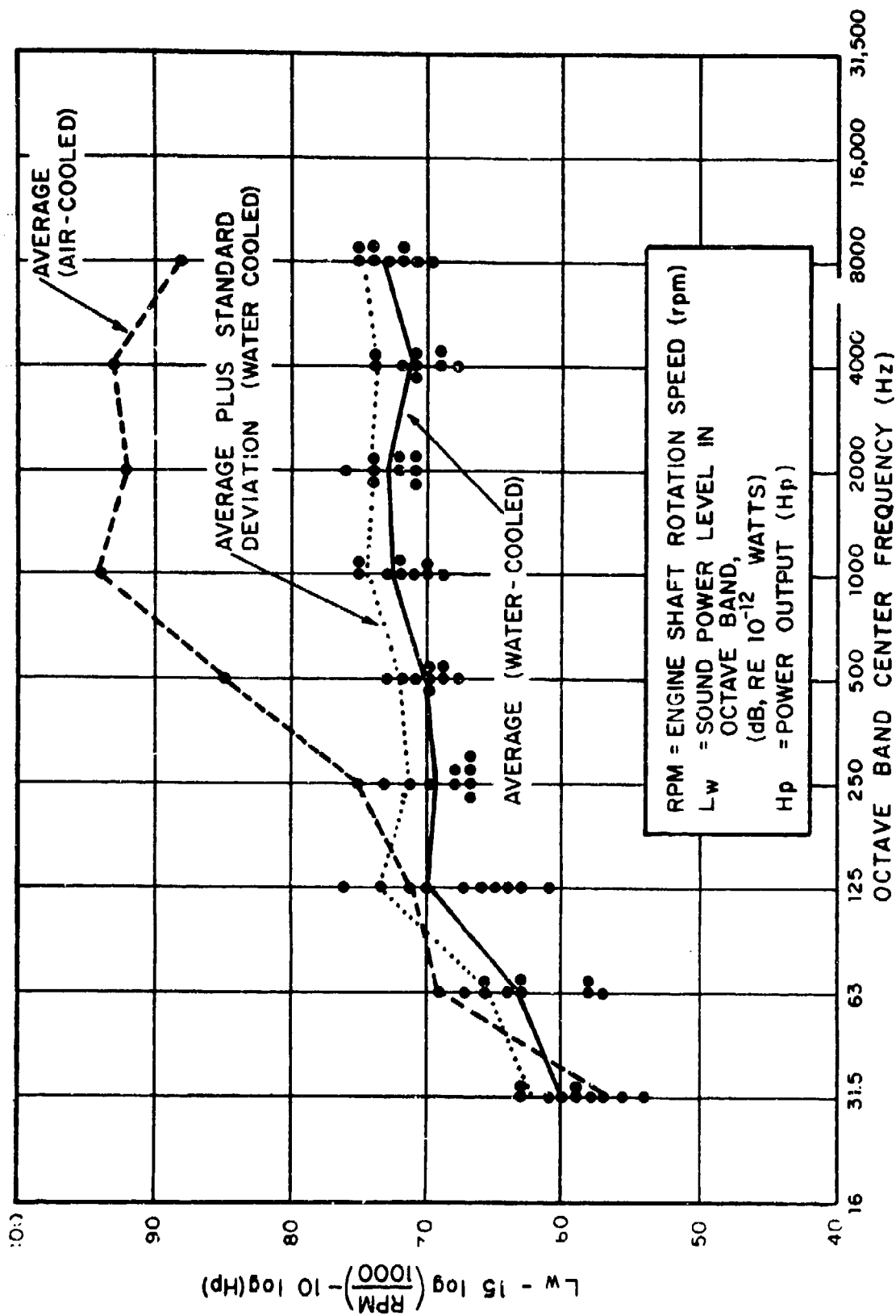
FIGURE D3   CASING NOISE OF ROTATING COMBUSTION ENGINES

77
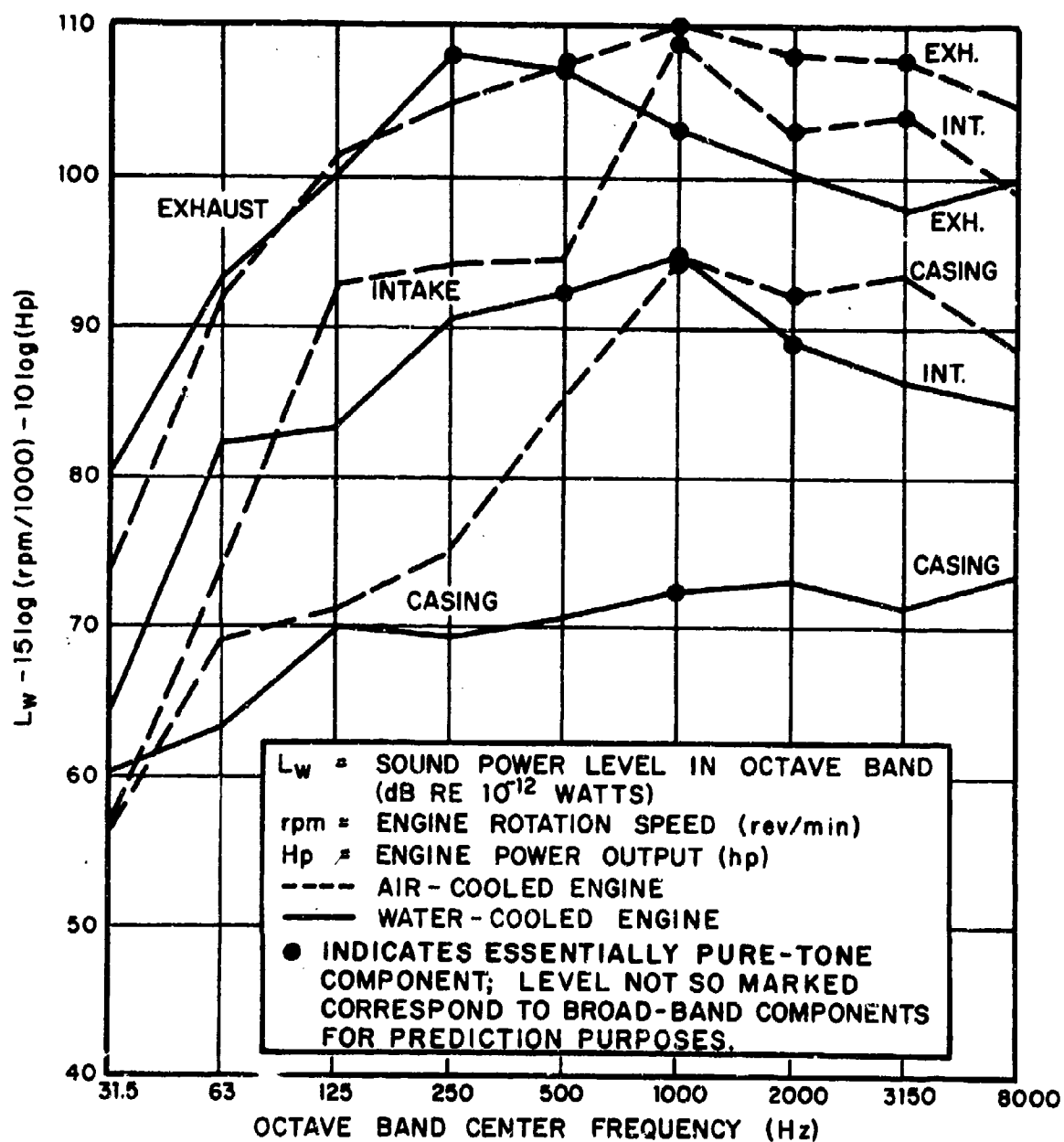
FIGURE D4 AVERAGE SOUND POWER OF ROTARY COMBUSTION ENGINES

APPENDIX E

NOISE FROM TURBOSHAFT ENGINES

AVAILABLE DATA

Although no broadly useful collection of data pertaining to the noise of aircraft turboshaft (turbo-prop) engines appears to be available, such a collection of data has been assembled for stationary gas turbine installations (Ref. 1). Accordingly, it appears useful to develop a noise prediction method on the basis of this collected stationary engine data, until more directly relevant data become available. The data reported in Ref. 1 were obtained largely from measurements carried out on operating installations rated between 240 and 1500 Hp and rotating at between 1,200 and 43,000 rpm.

NOISE SOURCES

The noise from turbine inlets and exhaust tends to be most prominent. If these sources are well-muffled, one is left with the "casing noise" of the turbine.

As air flows through the turbine inlet into the compressor, the compressor blades "chop" the flow; the compressor acts like a siren and produces a rather pure-tone noise component. This component typically results in a peak in the noise at the "blade-passage frequency" of the rotating blades in the first compressor stage. The blade-passage frequency f_B(Hz) is given by the product of the number of blades in that stage and the compressor speed in revolutions/sec. Another pure-tone component, which often results in a minor spectrum peak, usually occurs at the shaft rotation frequency. This frequency f_S(Hz) is equal to the shaft rotation speed in revolutions/sec.

The flow within a turbine also produces noise by siren-action to some extent. But there the corresponding pure-tone components tend to be masked by broader-band noise components associated with turbulence and turbulence-related fluctuations in lift and drag of the turbine blades. Accordingly, casing noise and exhaust noise tends to be more nearly of a broad-band character, although spectrum peaks at the blade-passage and shaft-rotation frequencies tend to be present.

COLLAPSE OF DATA

Figure E1 summarizes all of the intake noise data available from Ref. 1, in terms of octave-band power level, reduced with respect to rated power, plotted against actual frequency. (An attempt at referring the noise to the actual power produced by the turbines resulted in much greater scattering of the data; turbines make considerable noise even when operating at zero power output, and the noise of a turbine often increases relatively little as its power output increases. Although other parameters, such as intake flow rate, possibly may affect the noise, insufficient data is available for the assessment of their importance.)

In addition to all of the data points, Fig. E1 also shows three sample spectra which illustrate the typical double-peaked character of inlet noise, with peaks at the blade-passage and shaft-rotation frequencies.

Figures E2 and E3 show the same data as Fig. E1, but plotted against the ratio of frequency to blade-passage and to shaft-rotation frequency, respectively. In the construction of Fig. E2, only data near the high-frequency peak of spectra like those shown in Fig. E1 were retained; low-frequency data were omitted. In cases where not enough information was available to permit determination of the blade-passage frequency, it was assumed for purposes of constructing Fig. E2 that this frequency corresponds to the aforementioned high-frequency peak.

Figure E3 similarly shows only data near the low-frequency peak of the original un-reduced spectra. Here, however, the shaft rotation frequency was known in all cases.

Figure E4 presents exhaust noise data in terms of actual frequency, and Figs. E5 and E6 present the same data, but in terms of ratios of frequency to blade-passage and shaft-rotation frequencies. Figures E7, E8, and E9 are similar plots for casing noise.

The spread of the inlet noise data is seen to be considerably less in the reduced frequency plots of Figs. E2 and E3 than in the actual frequency plot of Fig. E1. Similarly, the exhaust noise data cluster somewhat better in Figs. E5 and E6 than in Fig. E4, and the casing noise data collapse better in Figs. E8 and E9 than in Fig. E7.

ESTIMATION CURVES

The "average" and "average plus standard deviation" spectra shown in the figures have been calculated by performing the appropriate arithmetic operations on the mean-square values which correspond to the data points at each frequency. Such energy averages (Ref. 2) are expected to be most meaningful for estimation purposes. (Note that no "average minus standard deviation" spectra are given in the figures. Because of the relatively large standard deviations found here, such spectra would fall off the bottom of the graphs.)

The various "average" spectra are most applicable for general estimation purposes, whereas the "average plus standard deviation" spectra are useful for estimating the highest noise levels one is likely to obtain.

Because the average inlet noise spectrum has pronounced peaks at the blade-passage and shaft-rotation frequencies, one may base an estimation scheme on Figures E2 and E3. Such a scheme is presented in Fig. E10, which suggests estimating the inlet noise spectrum of any turbine engine in two parts - a low-frequency part centered at the shaft-rotation frequency, and a high-frequency part centered at the blade-passage frequency* - and interpolating between these two parts as needed. Comparison of Fig. E10 with Fig. E1 shows that the scheme of Fig. E10 preserves the essential character of the unreduced-frequency spectra.

If one attempts to construct a prediction scheme for exhaust noise like that which was developed for inlet noise, than one finds that either the two partial spectra must coalesce, or one cannot reproduce the essential character of the average spectrum of Fig. E4. Because the shaft-rotation frequency is physically more meaningful for exhaust noise than is the blade-passage frequency, a prediction scheme based on the shaft-rotation frequency is suggested. This scheme is presented in Fig. E11, which is based on averaging and smoothing of the spectra of Figs. E5 and E6 (aligned so that the peak-frequencies coincide). Again, Fig. E11 may be seen to be very similar to the average spectrum of Fig. E4, which is plotted in terms of actual (non-reduced) frequency.

---

*The partial spectra of Fig. E10 were obtained by smoothing the average spectra of Figs. E2 and E3 and by omitting those portions of these spectra which are so far from the peak-frequencies that the estimation is likely to be unreliable.

Finally, one finds that the two reduced casing noise spectra of Figs. E8 and E9 cannot be made to coalesce in any meaningful way to produce an estimation which resembles the average spectrum of Fig. E7. Also, it is likely that casing noise may be dom..nated by the effects of auxiliary components and casing structural parameters, rather than by the siren-like blade-passage effects. Thus, the average spectrum of Fig. E7, which spectrum is reproduced in somewhat smoothed form in Fig. E12, is likely to be best for estimation purposes.

ESTIMATION SCHEME

In order to predict the noise produced by a given turboshaft engine, one should deal with each of the three major noise components (inlet, exhaust, casing) separately.

1. Use Fig. E10 to estimate the inlet noise power. Calculate the shaft rotation frequency f_S from

$$f_S(Hz) = \text{compressor rotation speed (rev/sec).}$$

and the blade-passage frequency f_B from

$$f_B(Hz) = f_S \cdot \text{number of blades in first compressor rotor stage}$$

Determine the actual frequencies that correspond to the frequency ratios indicated in Fig. E10 and the power levels L_w that correspond to the reduced levels shown.

Plot the levels corresponding to each octave-band center frequency.

Re-plot the two partial spectra obtained by this process, and connect the point corresponding to $f/f_S = 4$ with that for $f/f_B = 1/4$ by a straight line (corresponding to the dotted line of Fig. E10). If the two partial spectra overlap, use a smoothed (upper bound) envelope for the total spectrum.

2. Use Fig. E11 to estimate the exhaust noise, by replacing the frequency ratios in that figure with the corresponding frequencies and the reduced power level by the actual power level.

3. Use Fig. E12 to estimate the casing noise, by replacing the reduced power levels indicated by the corresponding actual power level.

Illustrative Calculation

Consider a turboshaft engine rated at 90 Hp, with a compressor which has 22 blades in its first (rotating) stage, and which rotates at 27,000 rpm.

Since here 10 log(Hp) = 19.5 dB and f_S = 27,000/60 = 450 Hz, f_B = (450)(22) = 9,900 Hz, one finds the following power levels corresponding to Fig. E10:

f/f_S	1/4	1/2	1	2	4					
f/f_B						1/4	1/2	1	2	4
f(Hz)	112	225	450	900	1,800	2,500	5,000	10,000	20,000	40,000
L_W(dB)	95	103	105	102.5	101	103	111	118	116	113

By shifting the computed values to the nearest standard octave-band frequency and connecting those two partial spectra, one obtains the curve shown in Fig. E13.

Using the same values of f_S and 10 log(Hp) in conjunction with Figs. E11 and E12, one similarly obtains the exhaust and casing noise curves also shown in Fig. E13.

REFERENCES FOR APPENDIX E

1. Miller, L. N., "Acquisition and Study of the Noise Data of Gas Turbine Engines". BBN Report No. 1477, prepared for Dept. of the Army, Office of the Chief of Engineers, under Contract DA-49-129-ENG-656 (August 1967).

2. Kerwin, E. M., Jr., "Decibels and Levels", Chapter 3 of *Noise Reduction*, Ed. by L. L. Beranek, McGraw-Hill Book Co., Inc., New York, 1960.

84
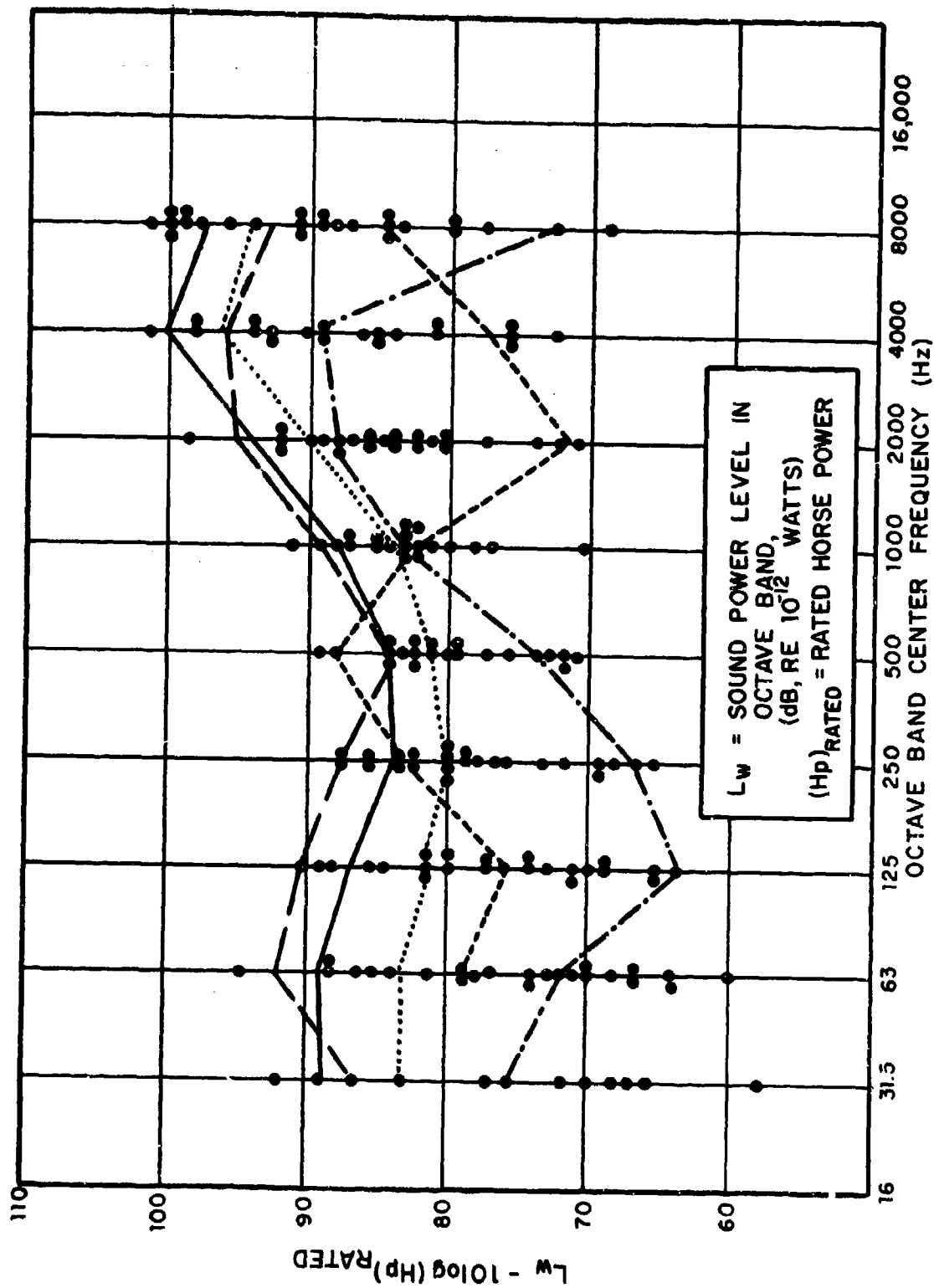
FIGURE E1   INLET NOISE OF 26 GAS TURBINES (RATED BETWEEN 240 and 1350 Hp)

Legend (on chart):

L_W = SOUND POWER LEVEL IN OCTAVE BAND, (dB, RE 10^{-12} WATTS)

$(Hp)_{RATED}$ = RATED HORSE POWER

X-axis: OCTAVE BAND CENTER FREQUENCY (Hz)

Y-axis: $L_W - 10 \log (Hp)_{RATED}$

85
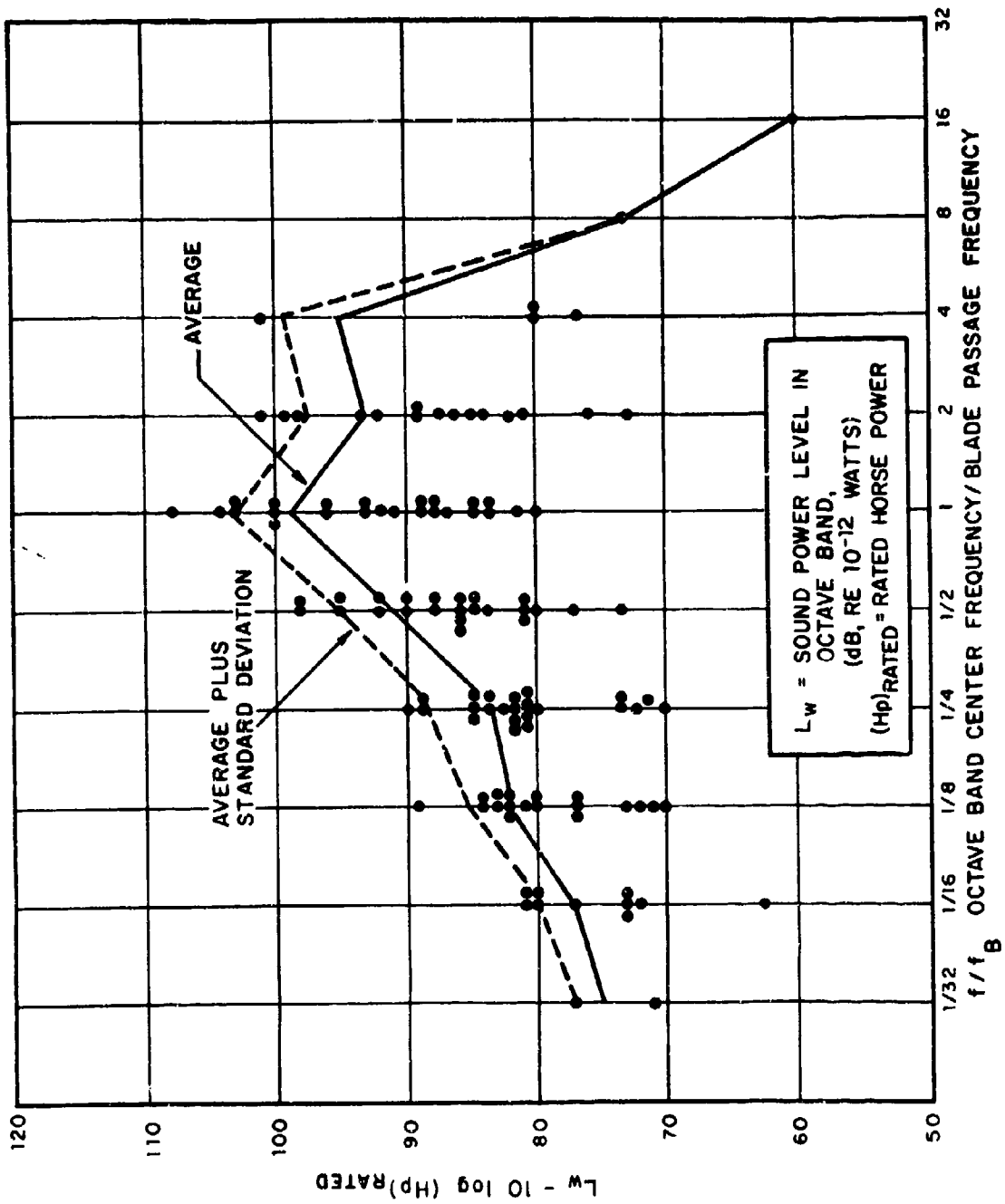
FIGURE E2   GAS TURBINE INLET NOISE AS FUNCTION OF BLADE PASSAGE FREQUENCY f_B

L_W = SOUND POWER LEVEL IN OCTAVE BAND, (dB, RE 10^{-12} WATTS)

$(Hp)_{RATED}$ = RATED HORSE POWER

AVERAGE

AVERAGE PLUS STANDARD DEVIATION

f / f_B OCTAVE BAND CENTER FREQUENCY/BLADE PASSAGE FREQUENCY

$L_W - 10 \log (Hp)_{RATED}$

86
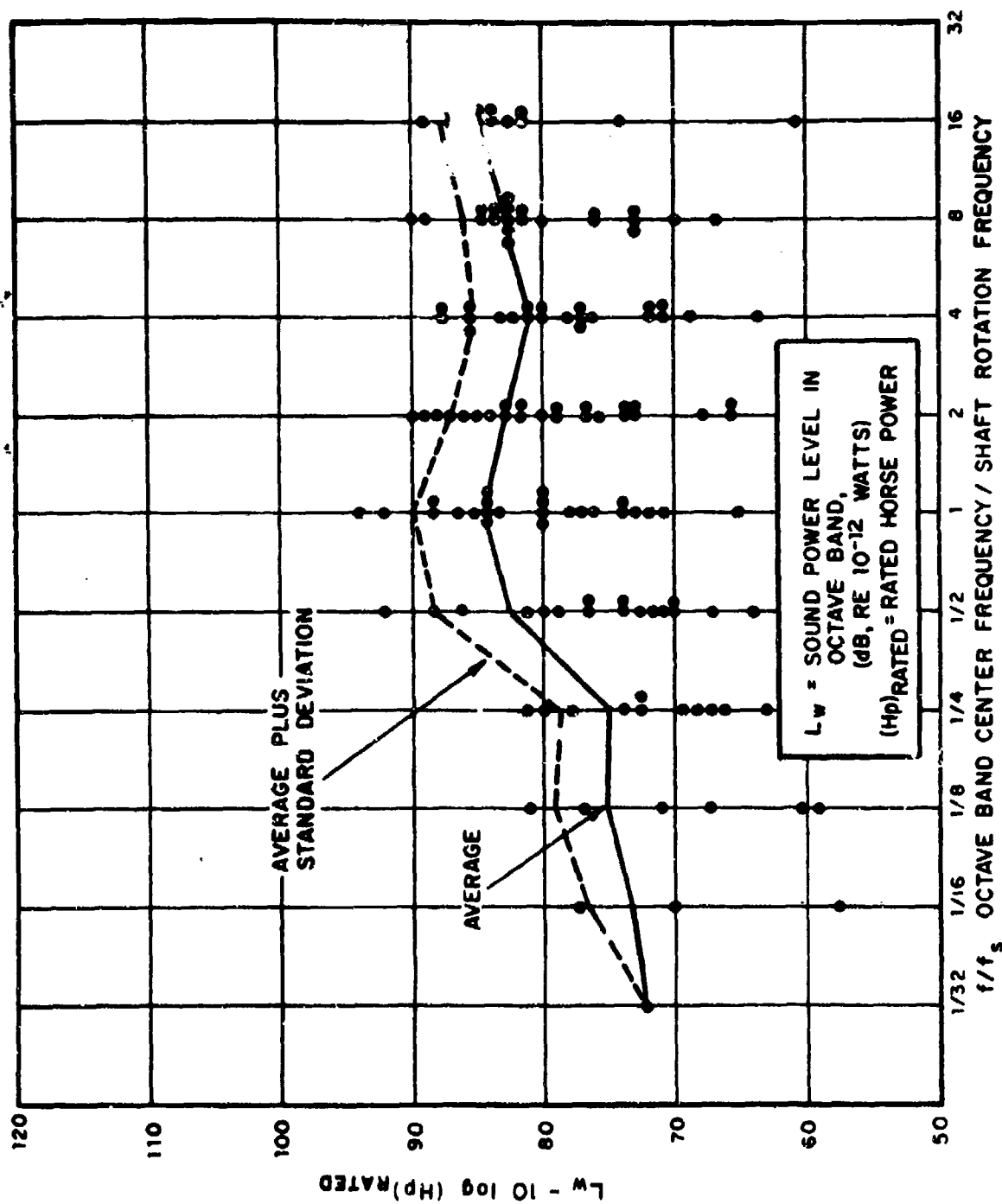
FIGURE E3   GAS TURBINE INLET NOISE AS A FUNCTION OF SHAFT ROTATION FREQUENCY f_S

87
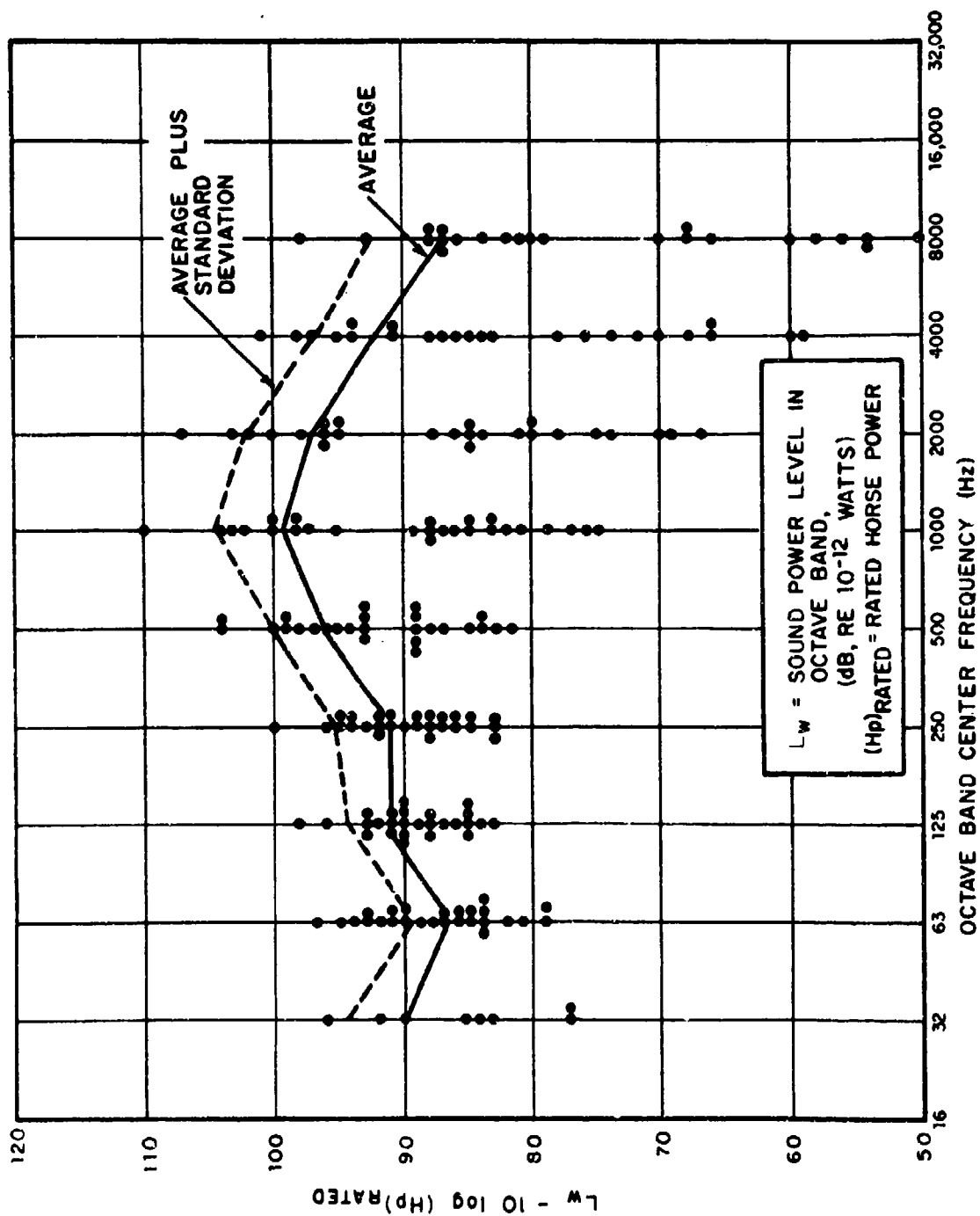
FIGURE E4   EXHAUST NOISE OF 30 GAS TURBINES (RATED BETWEEN 240 AND 1350 HP)

88
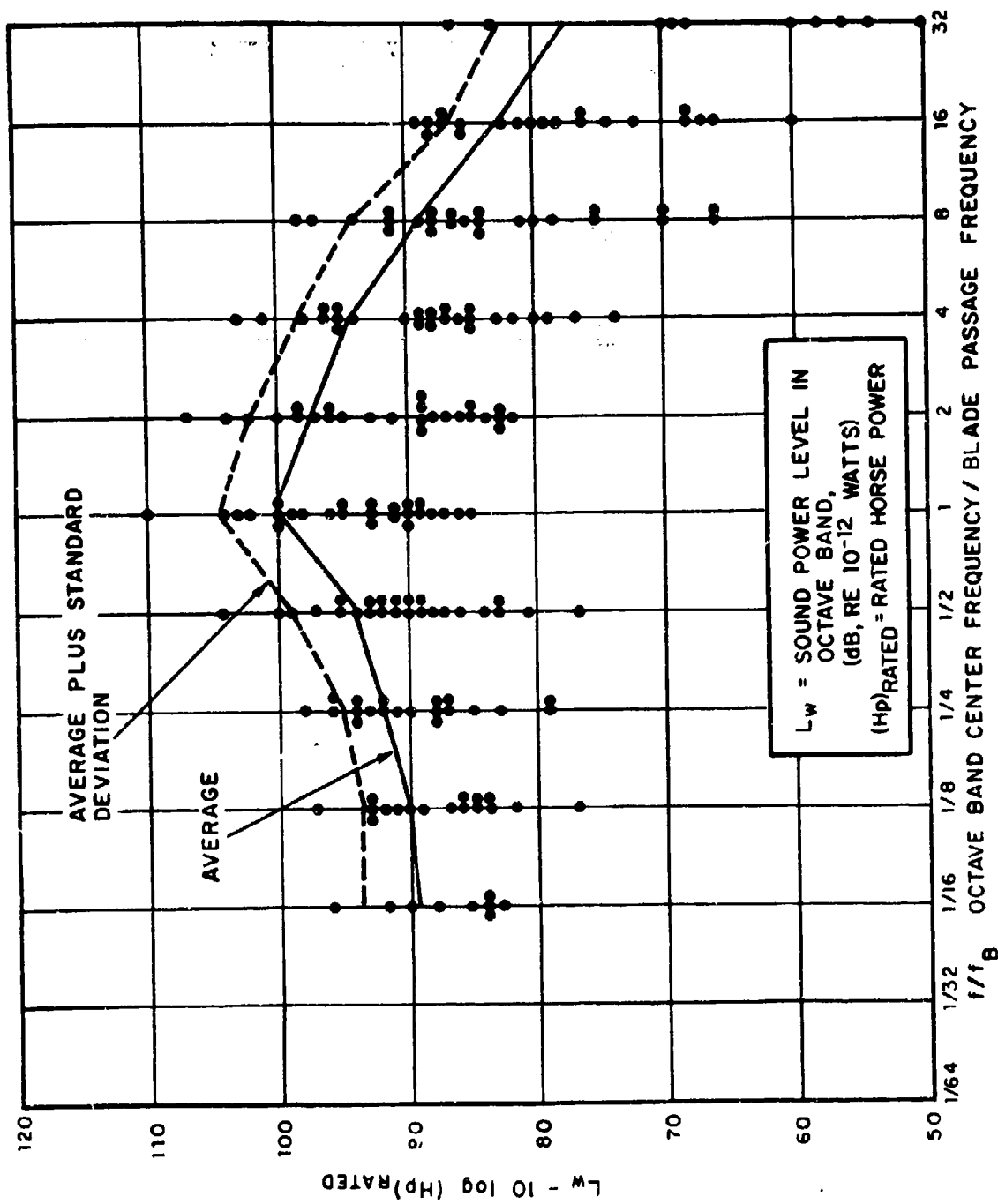
FIGURE E5   GAS TURBINE EXHAUST NOISE AS FUNCTION OF BLADE PASSAGE FREQUENCY f_B

89
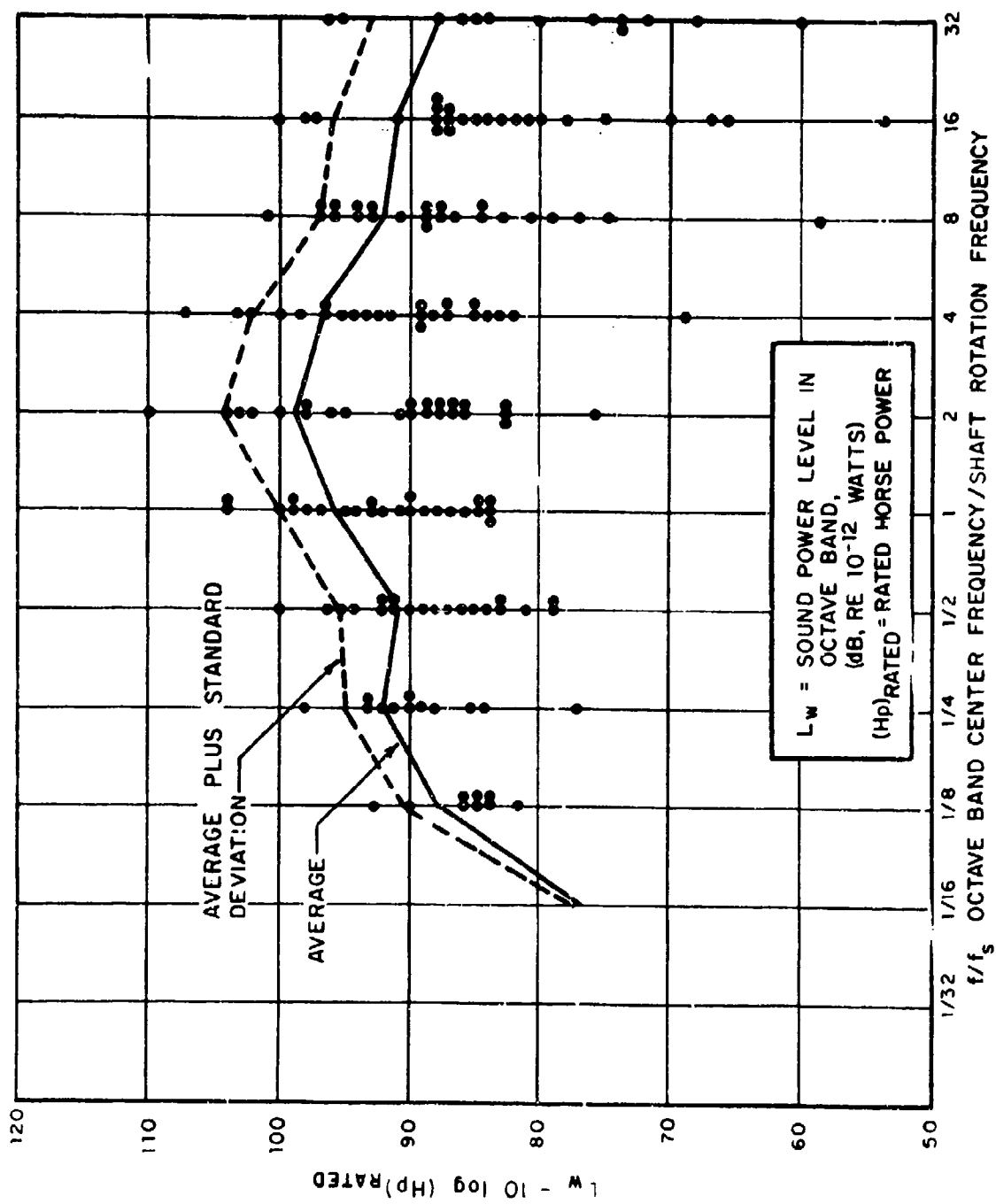
FIGURE E6   GAS TURBINE EXHAUST NOISE AS FUNCTION OF SHAFT ROTATION FREQUENCY f_S
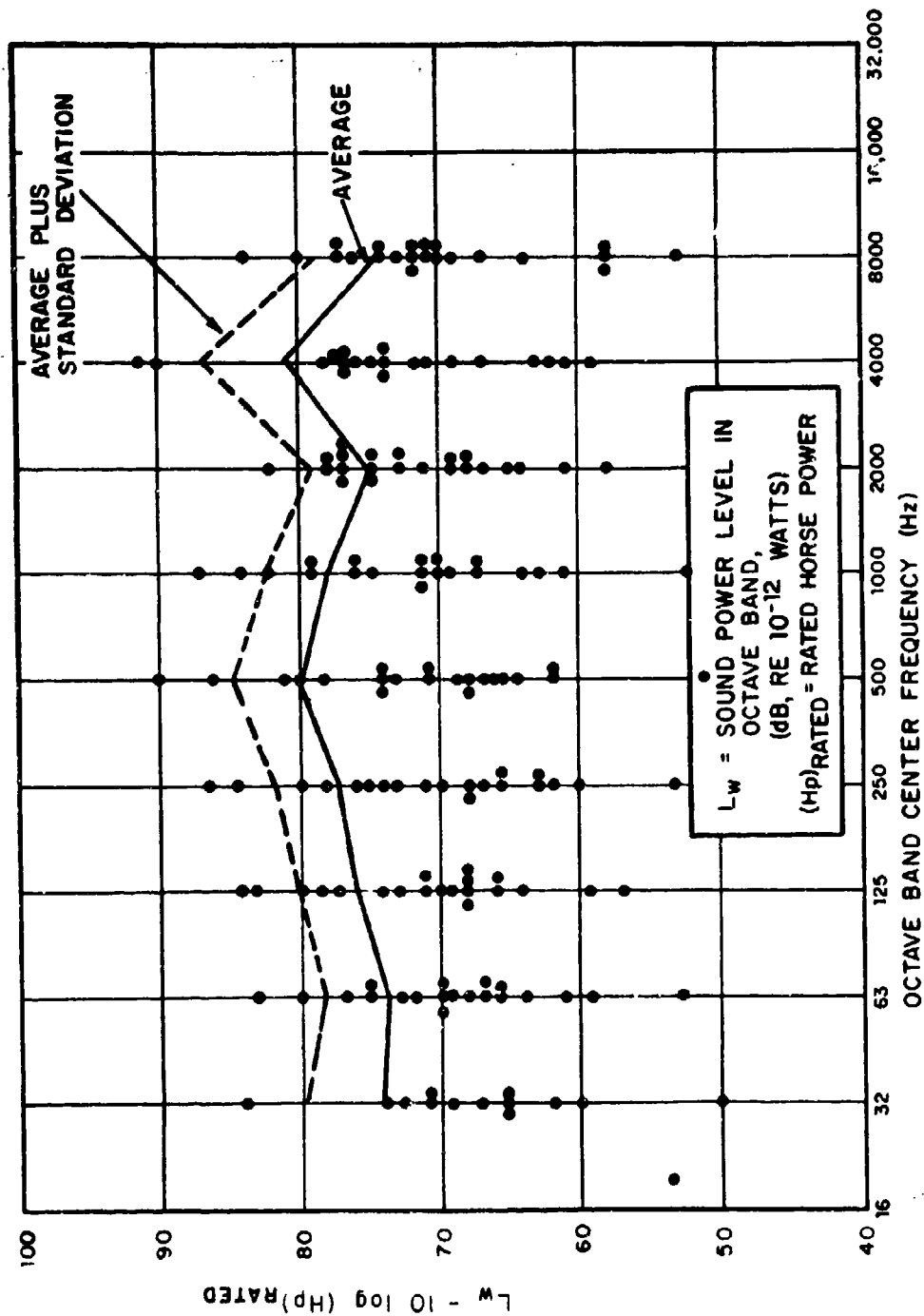
FIGURE E7   CASING NOISE OF 18 GAS TURBINES (RATED AT 240 TO 1500 HP)
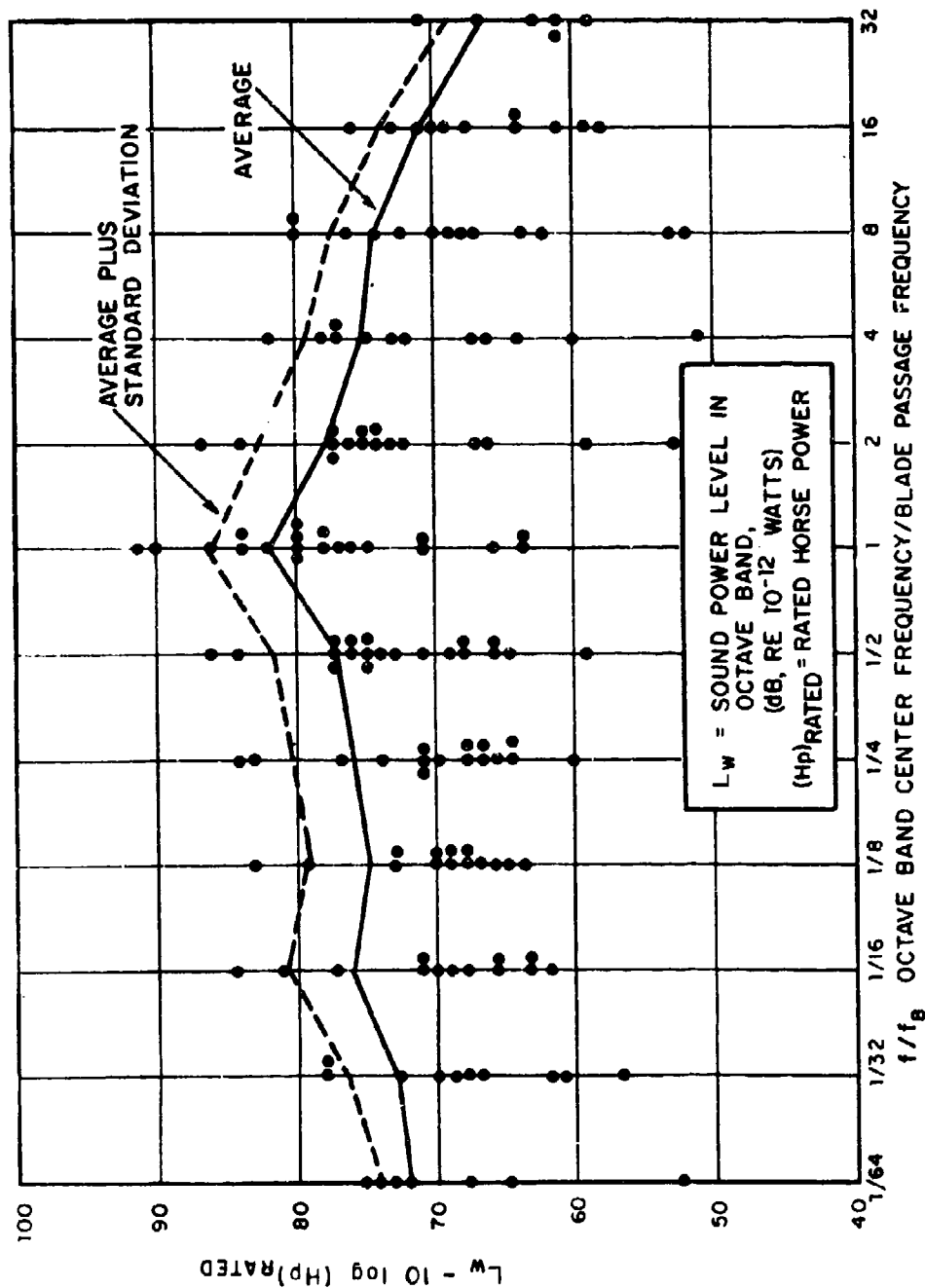
FIGURE E8   CASING NOISE OF 18 GAS TURBINES AS FUNCTION OF BLADE-PASSAGE FREQUENCY f_B

92
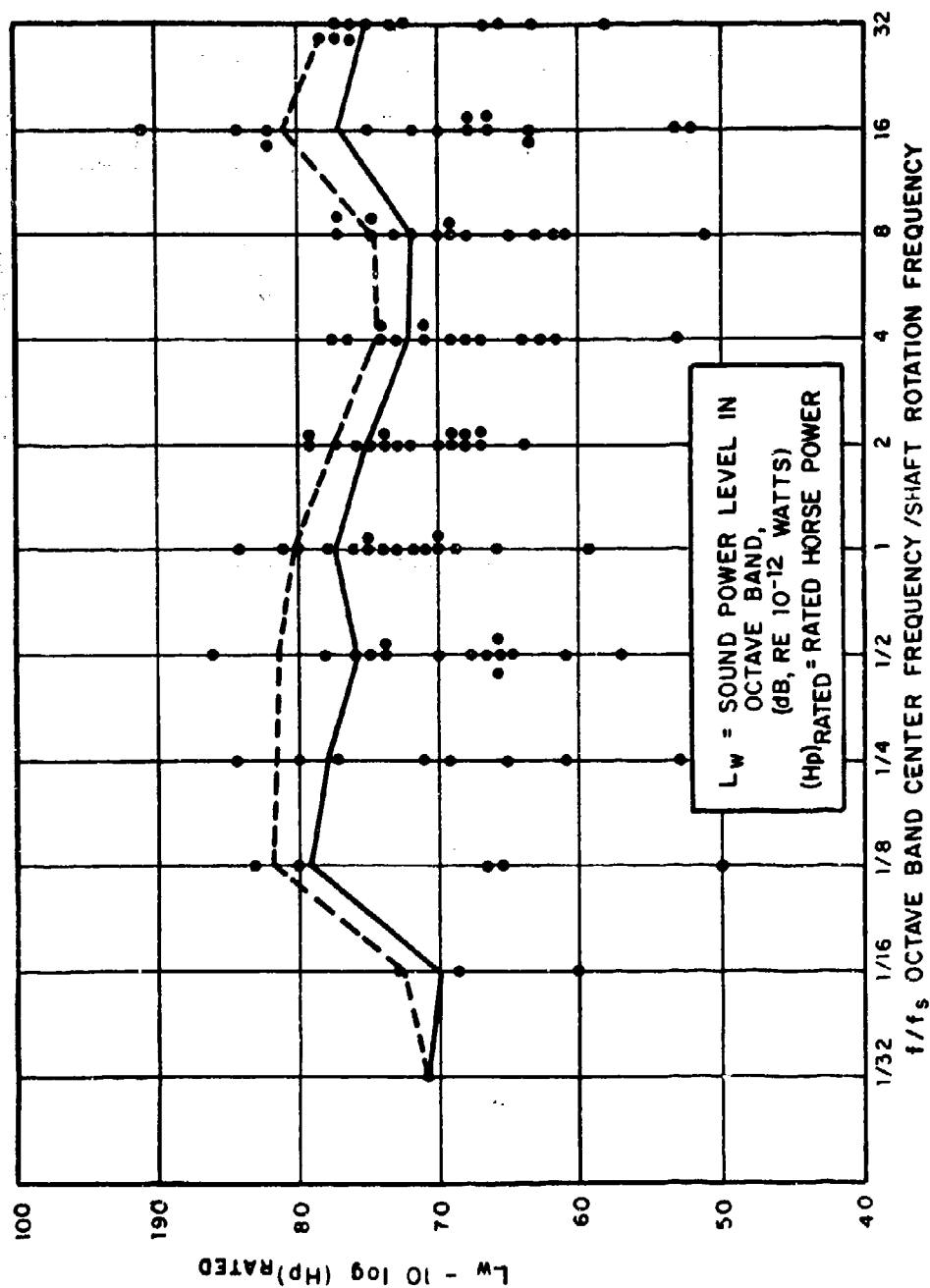
FIGURE E9   CASING NOISE OF 18 GAS TURBINES AS FUNCTION OF COMPRESSOR-SHAFT
ROTATION FREQUENCY f_S

93

INDICATES ESSENTIALLY PURE-TONE COMPONENT; LEVELS NOT SO MARKED CORRESPOND TO BROAD-BAND COMPONENTS FOR PREDICTION PURPOSES.

f_B = BLADE PASSAGE FREQUENCY (Hz)
f_S = SHAFT ROTATION FREQUENCY (Hz)
f = OCTAVE BAND CENTER FREQUENCY (Hz)
L_W = SOUND POWER LEVEL IN OCTAVE BAND, (dB, RE 10^{-12} WATTS)
$(Hp)_{RATED}$ = RATED TURBINE OUTPUT POWER

f/f_B

f/f_S

$L_W - 10 \log (Hp)_{RATED}$
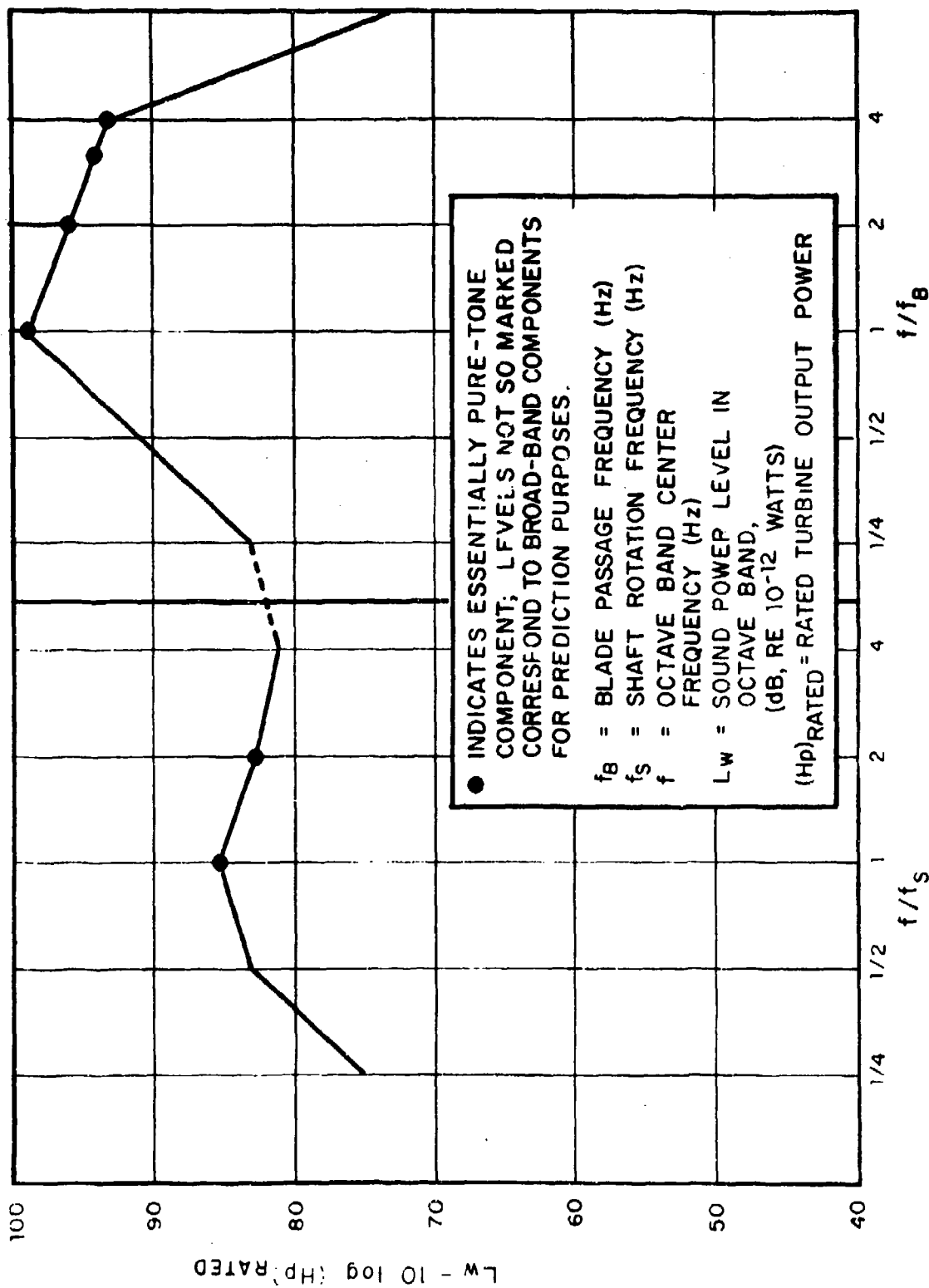
FIGURE E10   ESTIMATION OF TURBINE INLET NOISE

94
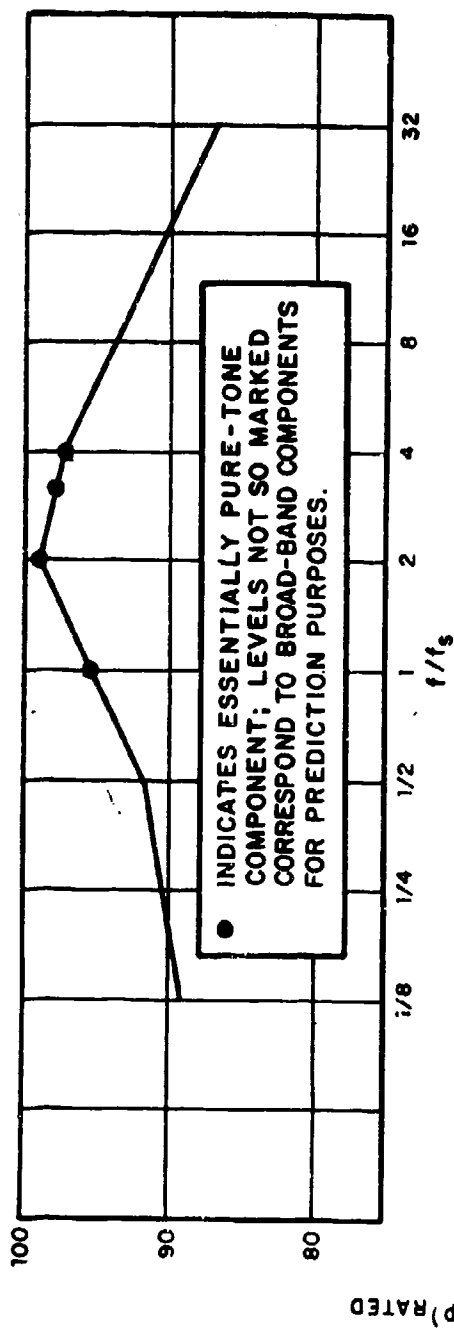
FIGURE E11   ESTIMATION OF TURBINE EXHAUST NOISE

● INDICATES ESSENTIALLY PURE-TONE COMPONENT; LEVELS NOT SO MARKED CORRESPOND TO BROAD-BAND COMPONENTS FOR PREDICTION PURPOSES.

f/f_s

$L_W - 10 \log (Hp)_{RATED}$
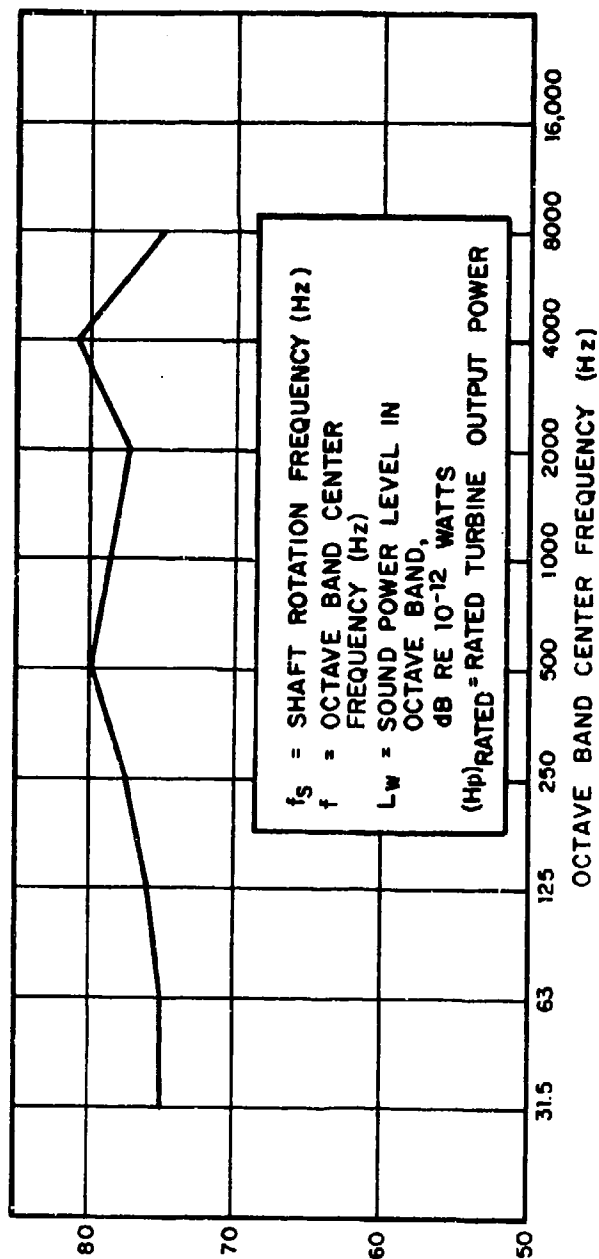
FIGURE E12   ESTIMATION OF TURBINE CASING NOISE

OCTAVE BAND CENTER FREQUENCY (Hz)

f_s = SHAFT ROTATION FREQUENCY (Hz)

f = OCTAVE BAND CENTER FREQUENCY (Hz)

L_W = SOUND POWER LEVEL IN OCTAVE BAND, dB RE 10^{-12} WATTS

$(Hp)_{RATED}$ = RATED TURBINE OUTPUT POWER

95
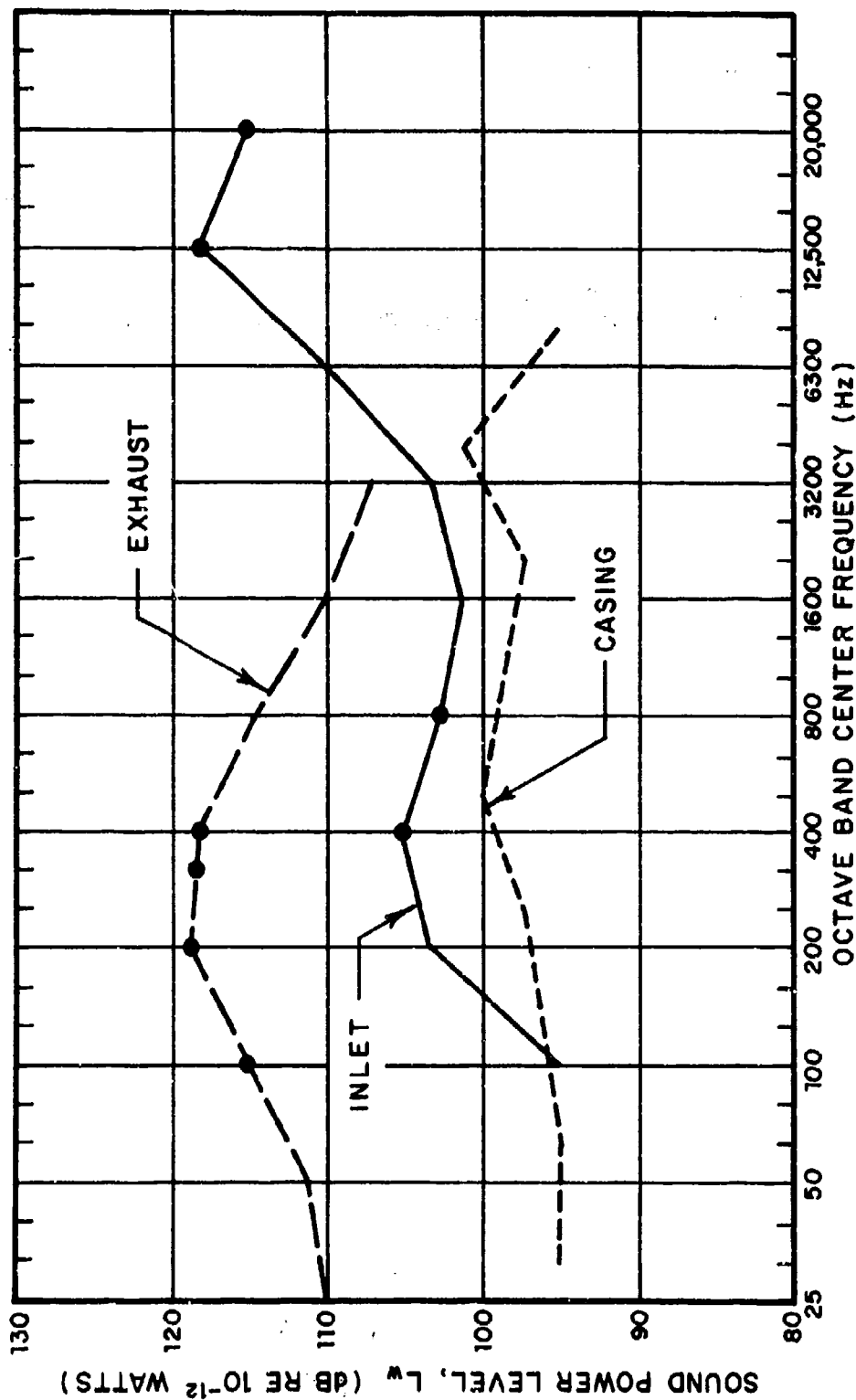
FIGURE E13   ESTIMATED NOISE FROM 90 Hp TURBOSHAFT ENGINE WITH 22 BLADES IN FIRST
STAGE, OPERATING AT 27,000 RPM

APPENDIX F

DISCRETE-TONE NOISE PRODUCED BY TURBOJET FANS

INTRODUCTION

Fans and compressors of turbojet engines typically produce high-pitched whining sounds, which consist primarily of one or more pure-tone components. Axial-flow fans resemble multi-bladed propellers, and the basic mechanisms responsible for fan noise are in part the same as those which cause propeller noise. Also, in both cases, the pure-tone components are associated with pressure fields that spin about the axis of rotation.

However, propeller noise theory is inapplicable to fans (and its use can lead to gross underestimates of fan noise). The ducts in which fans are housed affect the aerodynamics, as well as the propagation of sound, and the dominant sources of fan noise are associated with the interactions of successive rows of (rotor and stator) blades.

SOURCE MECHANISMS (Ref. 1 - 3)

Two sources of pure-tone noise are of primary importance for subsonic rotors — i.e., for rotors which move subsonically relative to the air flow: (1) The fluctuating lift generated on a downstream blade row as it interacts with the wakes formed by the upstream blade row produces an effective acoustic force field in the plane of the blades. (2) A siren-like volume source effect is produced as successive blade rows present a periodic obstruction to the flow; the obstruction is minimum when the wakes are in line, and maximum when they are alternately spaced.

The mechanisms present in subsonic fans also are present in supersonic fans, but in supersonic fans there occur also other mechanism, which may be of greater importance. These mechanism are associated with the rotor shock-wave field, which radiates directly, and which also produces lift fluctuations on the stator blades. Because of the greater noise from supersonic rotors, such rotors should be avoided in "quiet aircraft" applications, and will not be discussed further here.

PREDICTION

Much theoretical work has been done on the various noise mechanisms (e.g., Refs. 2-4). However, most of the relations that have been developed are not very useful for prediction of noise because they require information on various aerodynamic details which is generally not available until a prototype has been built. And by then, of course, one may obtain much better data on the noise simply by measuring it.

Perhaps the best means for predicting the level of the fundamental pure-tone component generated by a fan consists of a relation derived in Ref. 3, which gives the sound pressure level $L_{p(200')}$ produced at 200 ft to the side of fan engines, at the blade-passage frequency, as

$$L_{p(200')}(dB, re\ 0.0002\mu bar) = 50\ log\ U_{tip}(ft/sec) + 20\ log\ D(in) - 75 \tag{1}$$

in terms of the tip speed U_{tip} of the fan blade and the fan diameter D.

If one assumes the directivity to be uniform — an assumption that is not strictly valid, but that is justified for the simplified scheme for estimation of aural detection suggested in this report — then one may easily determine the sound power level that corresponds to Eq. (1). Noting that $U_{tip} = \Omega D = D\pi\Omega_r/30$, where Ω represents the fan rotational speed in radians/sec and Ω_r that same speed in rpm, and by changing the dimensions of D to ft, one may obtain

$$L_W(dB, re\ 10^{-12}\ watts) = 50\ log\ \Omega_r(rpm) + 70\ log\ D(ft) - 56 \tag{2}$$

In Ref. 3 there is also presented a comparison of Eq. (1) with experimental data obtained on 6 different fans. For tip speeds up to about 700 ft/sec, Eq. (1) is very nearly an upper bound to the data; the data in this region fall largely within + 1 dB and - 7 dB of the values given by Eq. (1). For transonic tip speeds, i.e. between 700 and 1500 ft/sec, the data are more widely scattered and fall essentially between + 5 dB and - 10 dB of Eq. (1).

Although it is well known that fan noise in general also contains several significant harmonics of the fundamental blade-passage frequency, no adequate means are available for predicting the sound levels associated with these harmonics. Experimental

data (Ref. 2) also indicate wide fluctuations in the relative levels of the first few harmonics, even in successive runs of the same engine. On the basis of the very limited amount of data available, it may suffice for aural detectability estimation purposes to consider only the first three harmonics of the fundamental, and to take the levels of successive harmonics to decrease by 3 dB.

ESTIMATION SCHEME

To estimate the discrete-tone sound levels produced by a turbojet fan, proceed as follows:

1. Calculate the blade-passage frequency

$$f_B = B\Omega$$

where B represents the number of rotor blades in the fan's last stage, and Ω the fan's rotational speed (in radians/sec). Then use Eq. (2) to determine the acoustic power L_W produced at that frequency.

2. Then take L_W - 3 dB at 2 f_B
    L_W - 6 dB at 3 f_B
    and L_W - 9 dB at 4 f_B

    as the remaining significant pure-tone components for detectability estimation purposes.

3. Repeat steps 1 and 2 for the fan's next-to-last stage, but reduce all levels by 3 dB (Ref. 1).

Illustrative Calculation

Consider a 1.65 ft diameter fan with 22 blades in its first and 29 blades in its second (and last) stage rotor, operating at 5,800 rpm (= 610 rad/sec).

For the last stage, then, f_B = BΩ = 29(610) $\approx$ 17,500 Hz and
L_W = 50 log Ω_r + 70 log D - 56
     = 50 log(23,300) + 70 log(1.65) - 56 = 171 dB, re 10^{-12} watts.

Thus one obtains 171 dB at 17.5 kHz, 168 dB at 35 kHz, 165 dB at 52.5 kHz, and 162 dB at 70 kHz.

Then for the first stage, one finds that at $f_B = 22(610) \approx$ 13.5 kHz, $L_w = 171 - 3 = 168$ dB, and at 27 kHz one obtains 165 dB, etc.

Note, however, that frequencies above 30 kHz are of no concern in relation to aural detection. Also see illustrative calculation at end of Appendix H.

REFERENCES FOR APPENDIX F

1. H.S. Ribner, "The Noise of Aircraft", Trans. Fourth Congress on Aeronautical Sciences, pp. 13-71.

2. Anon., "Investigation of Discrete-Frequency Noise Generation by Aero-Engine Compressors and Fans", Bolt Beranek and Newman Inc., Report No. 1617 (Feb. 1968). Submitted to General Electric Co., Aircraft Engine Group, Evansdale, Ohio.

3. M.V. Lowson, "Theoretical Studies of Compressor Noise", Wyle Laboratories Research Staff Report WR68-15 (Aug. 1968). Prepared under Contract NAS1-6885.

4. "Fan Noise Research". Sec. II of *Basic Aerodynamic Noise Research*, ed. I.A. Schwartz, NASA SP-207 (1969). (A collection of papers by several contributors.)

5. S.L. Bragg and R. Bridge, "Noise From Turbojet Compressors", *J. Roy. Aero. Soc.* 68, pp. 1-10 (Jan. 1964).

APPENDIX G

NOISE OF GAS JETS

The primary source of noise from any well-muffled and acoustically enclosed aircraft propulsion system (e.g., from a turbofan engine "buried" in the fuselage of an aircraft and provided with appropriate inlet and exhaust ducts) is due to the thrust-producing jet efflux from the system.

Much work has been done on the noise of jets, and well-validated prediction methods are available, particularly for jets with relatively small velocities (Refs. 1-3), which are likely to be of greatest interest in relation to small quiet aircraft.

ACOUSTIC EFFICIENCY AND MECHANICAL POWER

Perhaps the best and simplest estimation method may be obtained on the basis of the summary study undertaken by Heckl (Ref. 4). It has often been observed that similar rockets or jets have very nearly the same "acoustic efficiency" σ_{ac} which is defined as

$$\sigma_{ac} = W/W_m \quad , \tag{1}$$

where W represents the total (overall) acoustic power radiated and W_m the mechanical power of the flow. This mechanical power is given by

$$W_m = F_t U_j \tag{2}$$

where F_t denotes the thrust and U_j the jet velocity. The thrust F_t of air-breathing propulsion systems obeys* (Ref. 5)

$$F_t = m_a(U_j - U_o) + m_f U_j + A_j(P_j - P_o) \tag{3}$$

---

*Note that this relation applies for any type of system that produces thrust by accelerating air; it thus applies equally well for propeller and jet-engine systems.

where m_a represents the mass-flow rate of air through the propulsion system, which flow enters the system with a relative velocity U_0 (typically the vehicle air-speed) and leaves with velocity U. Similarly, m_f represents the mass-flow rate of fuel, which enters the propulsion system with essentially zero velocity and exits with velocity U_j. In addition, A_j represents the area of the jet, P_j the pressure in the jet, and P_0 the ambient (intake air) pressure. In most propulsion systems, $m_a/m_f > 50$, and $P_0 \approx P_j$, so that

$$F_t \approx m_a(U_j - U_0) \approx m_a U_j \approx \rho U_j^2 A , \qquad (4)$$

where ρ represents the density of air in the jet and the usual condition $U_j \gg U_0$ has been assumed. Thus, the mechanical power may be approximated by

$$W_m \approx \rho A_j U_j^3 . \qquad (5)$$

Figure G1 summarizes the observed dependences of the acoustic efficiency on jet velocity, taken from Ref. 4. The band indicated for low velocities represents the scatter of data in this region; higher-turbulence jet flows here have significantly higher acoustic efficiencies. Also indicated in the figure are expressions which give the dependences of σ_{ac} on Mach number corresponding to the various straight lines shown in the figure. The dotted line within the low-frequency band represents an approximate energy average between the upper and lower bounds of that band, and may be used for general estimation purposes.

SPECTRUM SHAPE AND DIRECTIVITY

The jet noise spectrum may be estimated by use of Fig. G2, which shows how the octave-band levels differ from the overall level. The spectrum has the typical haystack shape, with its peak at the dimensionless frequency (Strouhal number) $fU_j/D = 0.2$, where f represents the actual frequency and D the jet (nozzle) diameter.

A curve for the estimation of directivity effects is given in Fig. G3. It shows that the highest sound levels occur at about 30° from the jet efflux axis, and that the sound levels ahead of the jet (at 180° from the efflux axis) are nearly 10 dB lower than the spatial average value.

ESTIMATION SCHEME

In order to estimate the noise produced by a given jet at a given location, one may proceed as follows:

1. Use the mechanical power W_m and the diameter D of the jet to calculate the jet velocity U_{je} of an equivalent jet at room temperature and zero altitude from

$$U_{je} = [W_m/\rho A_j]^{1/3} , \qquad (5a)$$

taking $\rho \approx 0.07$ lb/ft^3 .

2. Use Fig. G1 to find σ_{ac}, and from σ_{ac} find the overall acoustic power of the equivalent jet from

$$W = \sigma_{ac} W_m \qquad (1a)$$

Then calculate the corresponding power level from

$$L_w(dB, re\ 10^{-12} watts) = 10\ log(W/10^{-12} watts)$$

3. Add to this overall power level the correction ΔL_w for atmospheric pressure and temperature

$$\Delta L_w = 10\ log\ (P_{at}/P_{at,o}) + 40\ log\ (T_j/T_o) - 35(T_a/T_o)$$

where P_{at} = actual atmospheric pressure

$P_{at,o}$ = standard atmospheric pressure

T_j = absolute temperature of jet

T_a = absolute temperature of ambient air

T_o = absolute reference (room) temperature

4. Apply the directivity correction from Fig. G3, if directivity information is of interest.)*

5. Calculate the jet diameter from

$$D^2 = 4F_t/\pi\rho U_j^2 \qquad (4a)$$

or

$$D^2 = 4W_m/\pi\rho U_j^3 \qquad (5b)$$

and use Fig. G2 to obtain the octave band noise spectrum.

---

*Directivity effects are not used in the estimation method for aural detection suggested in this report. Directivity estimation is included here only for the sake of completeness.

Illustrative Calculation

Consider a propulsion system which generates a thrust of 155 lb by producing an air jet that emanates from a 1.65 ft diameter duct at 300 ft/sec and 250°F. The mechanical power of this jet is

$$W_m = F_t U_j = (155 \text{ lb})(300 \text{ ft/sec}) = 46,500 \text{ ft lb/sec}$$

and its area is $A_j = \pi D^2/4 = 2.44 \text{ ft}^2$. Hence

$$U_{je}^3 = \frac{W_m}{\rho A_j} = \frac{(4.65 \times 10^4 \text{ft lb}_f/\text{sec})}{(0.07 \text{lb}_m/\text{ft}^3)(2.44 \text{ft}^2)} \left(\frac{32.2 \text{lb}_m \text{ft}}{\text{lb}_f \text{sec}^2}\right) = 8.80 \times 10^6 \left(\frac{\text{ft}}{\text{sec}}\right)^3 ;$$

$$U_{je} = 206 \text{ ft/sec.}$$

From Fig. G1, $\sigma_{ac} \approx 2 \times 10^{-7}$;

$$W = \sigma_{ac} W_m = (2 \times 10^{-7})(4.65 \times 10^4 \text{ft lb/sec})(1.36 \text{ watt sec/ft lb})$$

$$= 1.26 \times 10^{-2} \text{ watts}$$

$$L_W = 10 \log(1.26 \times 10^{-2}/10^{-12}) = 10 \log(1.26 \times 10^{10}) = 101 \text{dB}, \text{re} 10^{-12} \text{watts}$$

If the ambient air is at $T_a = 40°F = 500°R$ and $P_{at,o} = 0.9 \text{atm}$, whereas the reference air temperature is $T_o = 70°F = 530°R$, the correction required is

$$\Delta L_W = 10 \log\left(\frac{P_{at}}{P_{at,o}}\right) + 40 \log\left(\frac{T_j}{T_o}\right) = 35 \log\left(\frac{T_a}{T_o}\right)$$

$$= 10 \log\left(\frac{0.9 \text{atm}}{1.0 \text{atm}}\right) + 40 \log\left(\frac{250 + 460°R}{530°R}\right) - 35 \log\left(\frac{500°R}{530°R}\right) = -0.4 + 5.0 + 0.8$$

$$\approx 5.5 \text{ dB}$$

Therefore the overall sound power level is $L_W + \Delta L_W = 106.5 \text{ dB, re } 10^{-12} \text{watts.}$

Since $U_j/D = (300 \text{ ft/sec})/(1.65 \text{ ft}) \approx 180/\text{sec}$, $fD/U_j = 1$ corresponds to $f = 180$ Hz. One may thus assign frequencies to the Strouhal numbers shown in Fig. G2. Some octave-band power levels found from the previously determined overall level of 106.5 dB, as obtained from Fig. G2, then are as follows:

f_{OB}(Hz)	18	36	72	180	360	720
L_{OB}(dB, re 10^- watts)	96	100	90	94	91	87

REFERENCES FOR APPENDIX G

1. *"Sonic and Vibration Environments for Ground Facilities - A Design Manual"*. Ed. by L. C. Sutherland, Wyle Laboratories, Research Staff Report No. WR68-2, prepared under Contract NAS8-11217 (March 1968).

2. Eldred, K., W. Roberts, and R. White, "Structural Vibrations in Space Vehicles," WADD Technical Report 61-62 (Dec. 1961).

3. Franken, P.A., "Jet Noise," Chapter 24 of *Noise Reduction*, Ed. by L.L. Beranek, McGraw-Hill Book Co., Inc., New York, 1960.

4. Heckl, M., "Strömungsgeräusche," *VDI-Zeitschrift*, Fortschritt Berichte, Reihe 7, No. 20, (Oct. 1969).

5. Boden, R.H., "Propulsion," Chapter 20 of *System Engineering Handbook*, Ed. by R.E. Machol, McGraw-Hill Book Co., Inc., New York, 1965.
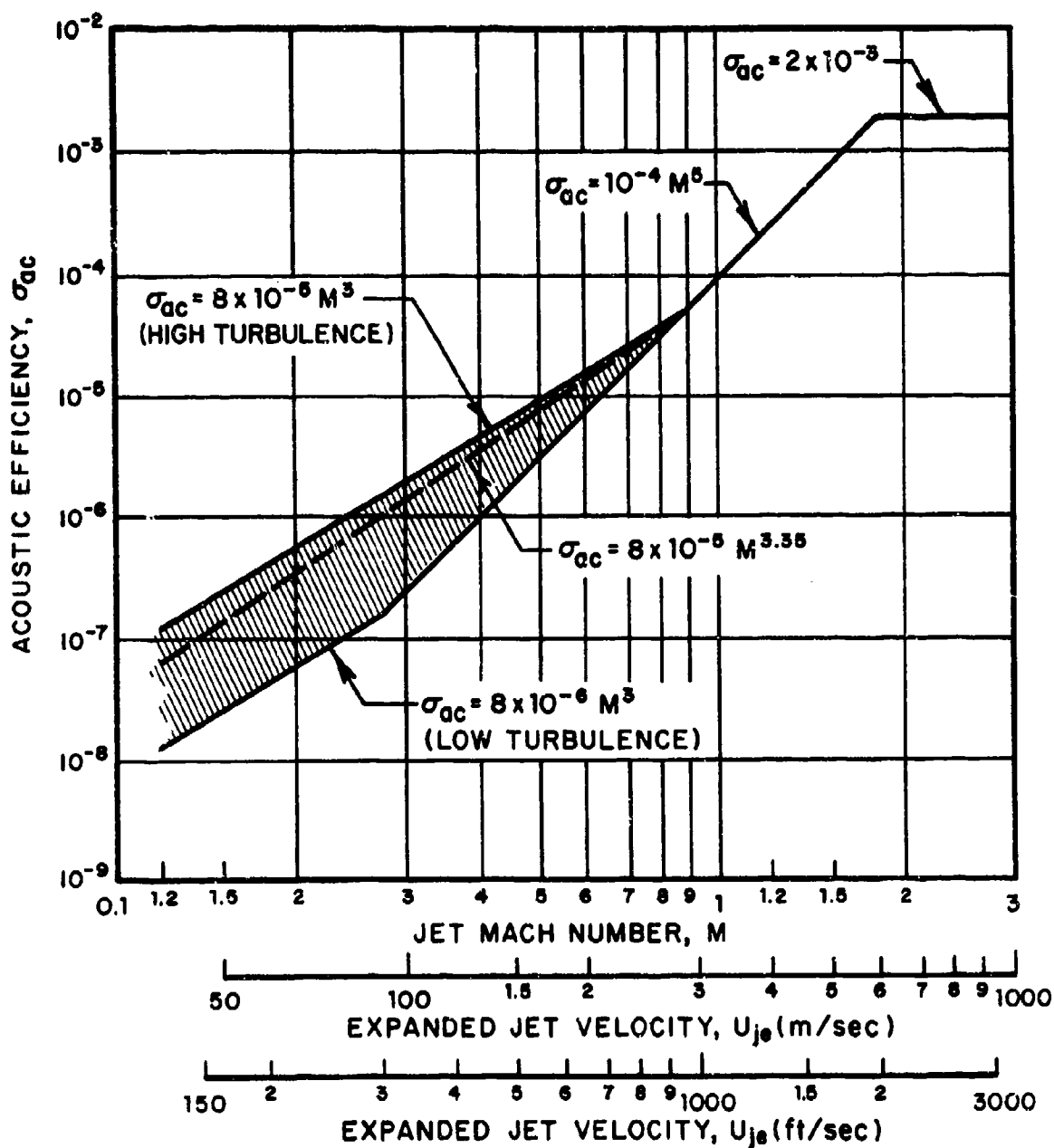
FIGURE G1   ACOUSTIC EFFICIENCY OF AIR JETS AT ZERO ALTITUDE AND
ROOM TEMPERATURE
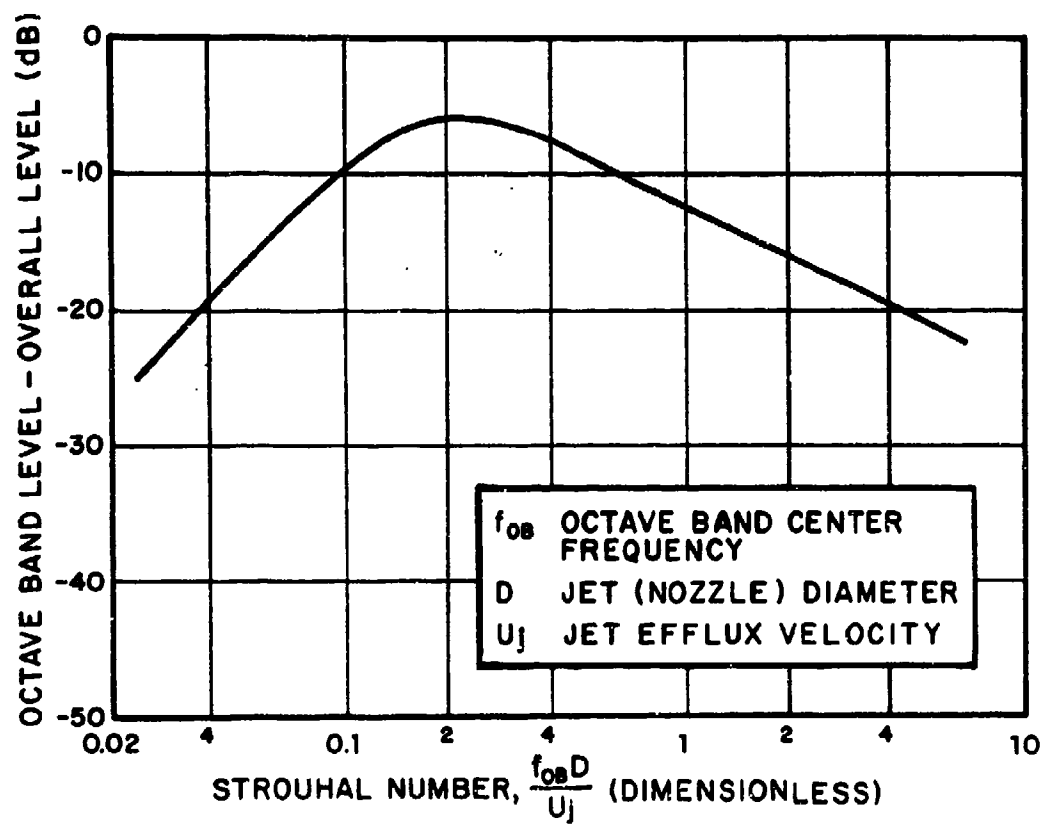
FIGURE G2   NORMALIZED OCTAVE-BAND SPECTRUM OF JET NOISE
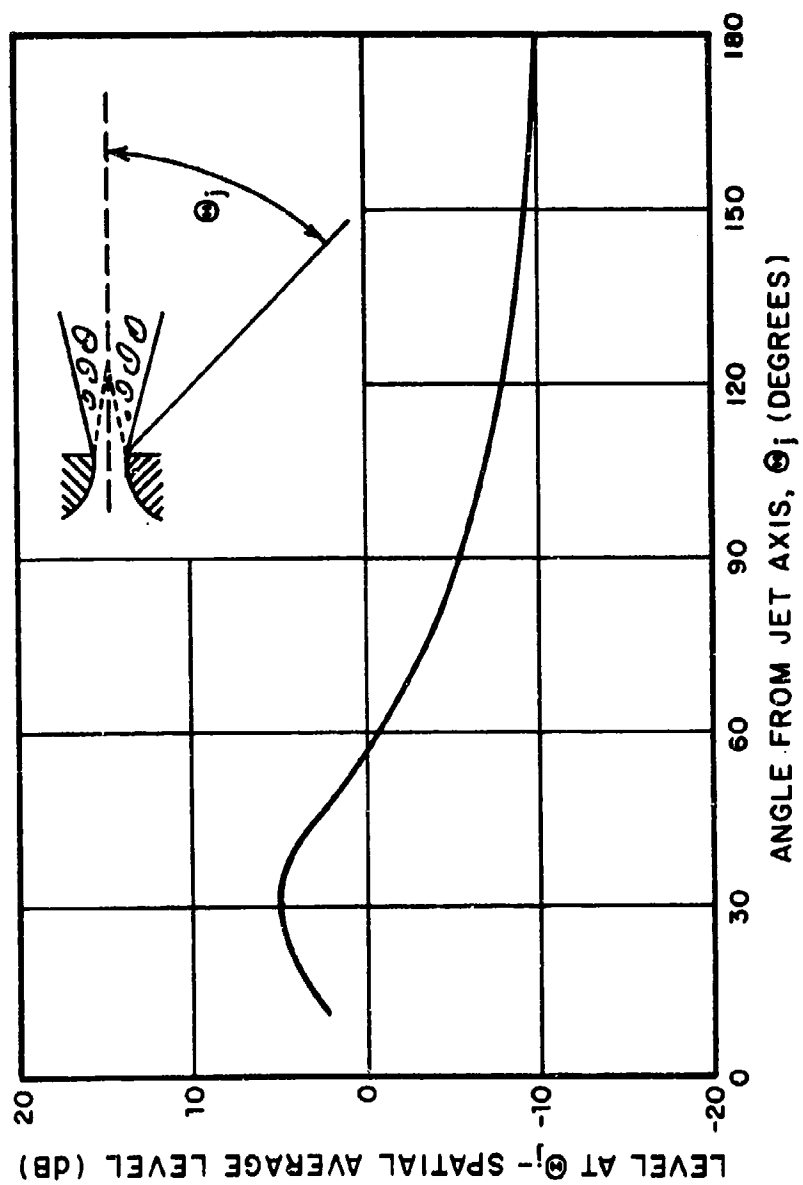
FIGURE G3   DIRECTIVITY OF JET NOISE

APPENDIX H

SOUND ATTENUATION IN CIRCULAR DUCTS

INTRODUCTION

The attenuation of sound propagating in ducts is a function of the sound source and of the geometrical and acoustical parameters of the duct.

The source may be described in terms of the spatial distribution of the sound-producing elements, and is usually expressed in terms of wave number parameters or modes. This source description also involves frequency-dependent impedance terms, which can be related to the various individual modes. Although flow can affect the source characteristics, it is convenient to consider this effect separately.

The geometry of a duct can be described in terms of the ratios of length to diameter of the lined duct, the ratio of lining thickness to duct width (or diameter), and the ratio of the length of the lined section to that of the unlined section of the duct. One then needs only one absolute length to describe the geometry, and one may compare this length to the acoustic wavelength.

The acoustical properties of a duct are commonly described in terms of the propagation constants τ_n and σ_n of modes, which constants are defined by the axial pressure function

$$p(z) = \sum_n p_{n+} e^{-ikz(\tau_n - i\sigma_n)} + \sum_n p_{n-} e^{ikz(\tau_n - i\sigma_n)} \qquad (1)$$

where k denotes the acoustic wavenumber (in free space). The propagation constants are related to characteristic modal impedances Z_n by

$$Z_n = \rho c / (\tau_n - i\sigma_n). \qquad (2)$$

In designing a duct, the one variable over which one has control, in addition to the geometry, is the wall impedance Z. For a rectangular duct without flow, the impedance of a homogeneous, locally reacting wall is related to the propagation constants as (Refs. 1-4)

$$\frac{i\rho c}{Z} = \sqrt{1 - (\tau_n - i\sigma_n)^2} \, \tan\left(kH\sqrt{1 - (\tau_n - i\sigma_n)^2}\right) \qquad (3)$$

where H denotes the width of the rectangular duct (assumed lined on one side). For a circular duct of diameter D, one may determine that

$$\frac{i\rho c}{Z} = \sqrt{1 - (\tau_n - i\sigma_n)^2} \; \frac{J_1\left[\frac{kD}{2}\sqrt{1 - (\tau_n - i\sigma_n)^2}\right]}{J_0\left[\frac{kD}{2}\sqrt{1 - (\tau_n - i\sigma_n)^2}\right]} \qquad (4)$$

where J_0, J_1 denote the Bessel functions of order 0 and 1. (This result is derived in the last part of this section.)

Air flow through the duct and/or high-intensity sound, leads to changes in the effective wall impedance and in the relation between the wall impedances and the axial sound propagation (Ref. 5). The changes are small, however, for centerline flow speeds that correspond to Mach numbers below 0.1 and for sound pressure levels below 140 dB (re 0.0002 microbar). Because high flow speeds and sound pressure levels are of limited interest here, their effects are neglected in the subsequent discussion.

Sound absorption at the duct walls and turbulent air flow cause the modes to interact. Therefore, the concept of modes, which is a mathematical device introduced to describe sound fields in rigid enclosures in terms of orthogonal functions, is not a useful one here. In particular, it makes no sense to consider modal distributions in a duct which are not compatible with any source configuration. Because of these problems with modes concept, and also because of the mathematical difficulties arising from the complex transcendental equations which describe the relation between wall impedances and modal parameters [Eqs. (3) and (4)], the analysis of sound attenuation presented here is based on approximations, which approach the idea of modes only insofar as a stabilized cross-distribution of sound pressure (with minimum attenuation along the duct) can be identified with a fundamental mode.

HIGH FREQUENCY ATTENUATION

It is convenient to consider two limiting frequency regions; a high-frequency region in which the acoustic wavelength λ is small compared to the duct diameter D, and a low-frequency region in which $\lambda > D$.

For high frequencies, the sound propagation in ducts may be analyzed in terms of rays. Figure H1 shows a cylindrical duct of length L and diameter D with incoherent point sources assumed located at one end, in the z = 0 plane. The source density is taken to be a function q(r) of the radius r, but not of the angular position φ.

Directly Emitted Rays

If the duct is lined with an absorbing material, most of the sound radiated out of the duct is due to rays which propagate through the duct without being reflected from the walls. Such unreflected rays which emanate from an element rdrdφ of the source region are confined to a spherical angle Ω_0. If no duct were present, the same source element would radiate into the spherical angle 2π. Therefore, the acoustic intensity due to rays emitted from the element rdrdφ and propagating without reflections is

$$dI = dI_0 \; \frac{\Omega_0}{2\pi} = dI_0 \; \sin \frac{\theta_0}{2} \; , \tag{5}$$

where dI denotes the intensity obtained with a very short or completely rigid duct. The intensity emitted from the entire source region is a function of the source distribution q(r) and obeys

$$I = I_0 \; \frac{\displaystyle\int_0^{D/2} q(r)dr}{\displaystyle\int_0^{D/2} \left[q(r)/\sin\frac{\theta_0}{2} \right] dr} \tag{6}$$

The duct geometry affects the angle θ_0;

$$\sin \frac{\theta_0}{2} = \left\{ 1 + \left[\frac{2L}{D} + \frac{r}{L}\left(\frac{2r}{D} - 1 \right) \right]^2 \right\}^{-1/2} \tag{7}$$

Considerable reduction of the sound intensity can be obtained only if θ_0 is small; then

$$\sin \frac{\theta_0}{2} \approx \frac{\theta_0}{2} \approx \frac{D}{2L} \; , \tag{8}$$

113

and

$$I = I_0 \frac{D}{2L} \tag{9}$$

for any source distribution.

Reflected Rays; Attenuation of Short Ducts

In order to take account of the imperfect absorptivity of the duct lining, one must consider the rays that are reflected from the walls before they leave the duct. The rays which suffer one reflection are confined to the spherical angle $\Omega_1 - \Omega_0$, where $\Omega_1 = 2\pi \sin\theta_1/2$ corresponds to rays that are emitted from a duct with a diameter of 3D, as shown in Fig. H2. If one again limits oneself to a relatively long duct for which Eq. (8) holds, then one finds that the contribution from rays which are reflected before they leave the duct is given by

$$I = I_0 (1-\alpha)\frac{D}{L} \tag{10}$$

where α represents the absorption coefficient of the duct wall. From Eqs. (9) and (10), one may then determine the attenuation (in decibels) to obey

$$\Delta L = - 10 \log \frac{D}{L} \left(\frac{3}{2} - \alpha\right); \tag{11}$$

this relation provides one with an estimate of the performance of short ducts lined with an absorbing material. Because the absorption coefficient α usually increases with increasing angle of incidence or, equivalently, because rays which suffer more reflections are attenuated more highly, one usually may neglect the contributions from multiply reflected rays.

Attenuation of Long Ducts

One may analyze the multiple reflections of rays in long ducts by considering the mean free path ℓ of a ray between successive reflections at the walls. The intensity in the duct then decays according to

$$I = I_0 e^{-\alpha z/\ell} \tag{12}$$

For weakly attenuated rays, which propagate almost axially, the mean free path length ℓ is found to vary directly as the duct diameter D and inversely as the (small) angle ϵ between the wall and the initial direction of propagation

$$\ell = \frac{D}{\epsilon} \ . \tag{13}$$

The set of rays which results in a pressure minimum at the wall suffers the least attenuation. For this set of rays, the angle ϵ is determined by the ratio of the radial to the axial wavenumbers,

$$\epsilon \approx \tan \epsilon = \frac{k_r}{k_z} \approx \frac{k_r}{2\pi} \lambda \ . \tag{14}$$

For circular ducts, the pressure minimum at the wall is determined by the first zero of the Bessel function $J_0(k_r r)$; this zero occurs for $k_r r \approx 2.4$, corresponding to which

$$k_r \approx 4.8/D \tag{15}$$

Accounting only for rays which emanate from the source nearly axially ($\epsilon \ll 1$), one obtains the attenuation ΔL (in decibels), as

$$\Delta L = 4.35 \ \frac{\alpha L}{D} \ \frac{\lambda}{2\pi} \ \frac{4.8}{D} = 3.3\alpha_z \ \frac{L}{D} \ \frac{\lambda}{D} \ . \tag{16}$$

The absorption coefficient α_z for such rays usually is small, and can be approximated by

$$\alpha_z \approx 4\epsilon \ \text{Re}\left\{\frac{Z}{\rho c}\right\} , \tag{17}$$

where $\text{Re}\{Z/\rho c\}$ is the real part of the wall impedance for normally incident sound, divided by the characteristic impedance ρc of the gas in the duct.

Since the attenuation in a longer duct turns out to be proportional to the square of λ/D — which is small in the region of high frequencies — no great improvement can be obtained by extending a short duct. The initial section, for which the attenuation is approximately given by Eq. (11), contributes almost all

of the attenuation. If one desires to increase the attenuation substantially, one needs to curve the duct or add obstructions to interact with the axial rays.

LOW-FREQUENCY ATTENUATION

Analysis of the performance of lined ducts at frequencies at which the ducts are not very long compared to the wavelength involves three problems. They are associated with the source region, with transitions from a rigid duct to a lined duct (and vice versa), and with the duct termination.

Source Distribution

As previously mentioned, the spatial distribution of sources can be described only inadequately by modes. At low frequencies, at which the acoustic wavelength is greater than the duct diameter, the spatial distribution becomes stable in a very short distance along the duct. The stabilized radial distribution suffers the least attenuation with distance; one may therefore obtain a conservative estimate of the attenuation performance of lined ducts by considering only the stabilized distribution. This approach, which does not account for the actual source characteristics, is employed below.

Duct Terminations and Lining Discontinuities

The exact calculation of reflection and transmission coefficients at the transition from a rigid duct to a lined duct is extremely difficult. Heins and Feshbach (Ref. 6) applied a Wiener-Hopf technique to develop series approximations. The first term of their series agrees with results obtained from the simplest considerations, using the basic modal impedances $Z_R = \rho c$ for rigid ducts and $Z_S = \rho c/(\tau - i\sigma)$ for lined ducts. Such approximations are appropriate in the case of moderate attenuation, and will be employed in the present analysis. Effects of duct terminations have been studied by Levine and Schwinger (Ref. 7), who have calculated the radiation from an unflanged pipe. One finds that one may obtain an adequate approximation by considering only the mass reactance in parallel with the plane wave impedance at the open end of a rigid duct (Ref. 8). Results for the radiation from lined ducts generally show somewhat higher values than obtained from this approximation; this difference can be ascribed in part to the curvature of the wavefront in the duct.

The geometry of discontinuities in the duct lining and of unflanged open tailpipes to be studied is shown in Fig. H3, which indicates a lined duct of length L_s, connected to a tailpipe of length L_R with rigid walls; the duct and tailpipe are taken to have the same diameter D.

The transmission of sound through individual homogeneous parts of the duct may conveniently be described by means of transfer matrices, which involve the propagation constant and the characteristic impedance of the stabilized radial distribution (or fundamental mode). The effects of series-arrangements of different parts may then be determined by multiplication of these transfer matrices. Thus, the sound pressure and velocity at the inlet of the absorbing duct are related to those quantities at the open end of the rigid tailpipe, to the first order of approximation, by

$$
\begin{pmatrix} p_1 \\ v_1 \rho c \end{pmatrix} \approx \begin{pmatrix} \cos[kL_S(\tau-i\sigma)] & i\,\dfrac{\sin[kL_S(\tau-i\sigma)]}{\tau-i\sigma} \\ i(\tau-i\sigma)\,\sin[kL_S(\tau-i\sigma)] & \cos[kL_S(\tau-i\sigma)] \end{pmatrix}
$$

$$
\cdot \begin{pmatrix} \cos kL_R & i\,\sin kL_R \\ i\,\sin kL_R & \cos kL_R \end{pmatrix} \begin{pmatrix} p_2 \\ \rho c v_2 \end{pmatrix} \qquad . \qquad (18)
$$

At the open end of an unflanged pipe of diameter D, the pressure and velocity are related by

$$
\frac{v_2 \rho c}{p_2} \approx 1 + \frac{4}{i\,kD} \quad . \qquad (19)
$$

One may then calculate the attenuation of the duct in terms of the ratio of the pressure at the inlet of the absorbing duct to that at the open end of the tailpipe, as

$$
\Delta L = 20 \, \log \left| \frac{p_{(1)}}{p_2} \right| \; dB \quad . \qquad (20)
$$

The inlet pressure $p_{(1)}$ depends on the source conditions, as discussed below.

Source Connected to Absorbing Duct via Unlined Duct

Here the pressure p_1 results from the complex amplitudes p_{1+} and p_{1-} of an incident wave and of the wave reflected at the wave-impedance discontinuity at the inlet of the absorbing duct;

117

$$p_1 = p_{1+} + p_{1-} \tag{21}$$

For the plane wave in the rigid inlet duct, there applies the relation

$$v_1 \rho c = p_{1+} - p_{1-} . \tag{22}$$

If the source is not specified otherwise, one may assume that its internal impedance is equal to the characteristic impedance ρc. Then the pressure $p_{(1)}$ is equal to the pressure p_{1+} of the incident wave, and from Eqs. (18) to (22) one obtains the attenuation (in decibels) as

$$\Delta L = 8.7 k \sigma L_s + 10 \log \left(1 + \frac{4}{(kD)^2} \right) \tag{23}$$

$$+ 20 \log \left| 1 + \frac{1 - e^{-2ikL_s(\tau - i\sigma)}}{4(\tau - i\sigma)} (1 - \tau + i\sigma) \left[1 - \tau + i\sigma + \frac{e^{-2ikL_R}}{1 + ikD/2}(1 + \tau - i\sigma) \right] \right| .$$

The first term represents the attenuation of a homogeneous lined duct. The second term gives the reflection loss at the end of an unflanged pipe. The part of the third term which involves $1 - e^{-2ikL_s(\tau - i\sigma)}$ accounts for waves propagating back and forth in the lined duct, which result from reflections at the discontinuities in the duct lining; the part of the third term with the coefficient e^{-2ikL_R} accounts for waves reflected between the end of the lined duct and the open end. (Note that the latter reflected waves disappear for $kD \to \infty$, which corresponds to an anechoic termination of the rigid tailpipe).

For strong reflections from the open end of the tailpipe ($kD \to 0$), and weak interaction between the two ends of the absorbing duct, the third term of Eq. (23) reduces to

$$20 \log \left| 1 + \frac{1 - \tau + i\sigma}{4(\tau - i\sigma)} \left[1 - \tau + i\sigma + e^{-2ikL_R}(1 + \tau - i\sigma) \right] \right|$$

which for $\tau > 1 \gg \sigma$ becomes

$$20 \log \left| 1 - \frac{\tau-1}{2\tau} e^{-2ikL_R} \right|$$

Thus, quarter wavelength resonances in the tailpipe ($kL_R = \pi/2$) result in positive values and half wavelength resonances ($kL_R = \pi$) in negative values of the third term of Eq. (23), as long as $\tau > 1$, which is the case below the first resonance in the duct lining.

For very short absorbing ducts ($kL_S \to 0$), the third term of Eq. (23) becomes

$$20 \log \left| 1 + \frac{ikL_S}{2}(1-\tau+i\sigma)\left[1 - \tau + i\sigma + \frac{e^{-2ikL_R}}{1+ikD/2}(1+ -i\sigma) \right] \right|$$

Sound Source Located Directly at the Inlet of the Absorbing Duct

For a low-impedance source (pressure source), the pressure $p_{(1)}$ which characterizes the attenuation performance of the duct is equal to the pressure p_1. Equations (18) and (19) here yield

$$\Delta L = 8.7k\sigma L_S + 10 \log \left(1 + \frac{4}{(kD)^2} \right)$$

$$+ 20 \log \left| 1 - \frac{e^{-2ikL_R}}{1+ikD/2} + \frac{1-e^{-2ikL_S(\tau-i\sigma)}}{2(\tau-i\sigma)} \beta \right| \quad (24)$$

$$\beta = \left[1 - \tau + i\sigma + \frac{e^{-2ikL_R}}{1+ikD/2}\left(1 + \tau - i\sigma \right) \right] \quad (24a)$$

Within the approximation valid for $\tau \approx 1$, the third term here accounts for reflections from the discontinuity of the duct lining and from the end of the tailpipe, in agreement with Eq. (23).

For a high-impedance source (velocity source) at the inlet of the absorbing duct, the reference pressure $p_{(1)}$ results from the velocity v_1 multiplied by the characteristic impedance $\rho c/(\tau-i\sigma)$, and one obtains

$$\Delta L = 8.7k\sigma L_s + 10 \log \left(1 + \frac{4}{(kD)^2}\right)$$

$$+ 20 \log \left| 1 - \frac{e^{-2ikL_R}}{1+ikD/2} + \frac{1-e^{-2ikL_s(\tau-i\sigma)}}{2(\tau-i\sigma)} \beta_1 \right| \qquad (25)$$

$$\beta_1 = \left[1 - \tau + i\sigma + \frac{e^{-2ikL_R}}{1+ikD/2} \left(1 + \tau - i\sigma\right) \right] \qquad (25a)$$

This result differs from Eq. (24) only in the algebraic sign relating to the phases of reflected waves in the lined duct.

The source impedance does not affect the attenuation performance of the duct, if the reflected wave from the discontinuity of the duct lining can be neglected ($e^{-2kL_s\sigma} \ll 1$).

PROPAGATION CONSTANTS FOR CIRCULAR DUCTS

The linearized wave equation in cylindrical coordinates r,z is

$$\frac{\partial^2 p}{\partial z^2} + \frac{1}{r}\frac{\partial}{\partial r}\left(r \frac{\partial p}{\partial r}\right) + k^2 p = 0 \qquad (26)$$

With the axial dependence

$$p(z) \sim e^{-ikz(\tau-i\sigma)}, \qquad (27)$$

one obtains Bessel's differential equation for the radial dependence,

$$\frac{\partial^2 p}{\partial r^2} + \frac{1}{r}\frac{\partial p}{\partial r} + k^2[1 - (\tau-i\sigma)^2]p = 0. \qquad (28)$$

The solution compatible with a finite axial pressure is

$$p(r) \sim J_0[kr\sqrt{1 - (\tau-i\sigma)^2}], \qquad (29)$$

where J_0 is the zero order Bessel function. Boundary conditions at a homogeneous, locally reacting wall at $r = D/2$

$$- \frac{1}{i\omega\rho} \frac{\partial p}{\partial r} = v_r = \frac{1}{i\rho c} \sqrt{1 - (\tau-i\sigma)^2} \frac{J_1[kr\sqrt{1 - (\tau-i\sigma)^2}]}{J_0[kr\sqrt{1 - (\tau-i\sigma)^2}]} p \qquad (30)$$

can be described by the wall impedance

$$Z = \left(\frac{p}{v_r}\right)_{r=D/2} \qquad (31)$$

Thus, the propagation constants τ, σ may be calculated from

$$\frac{i\rho c}{Z} = \sqrt{1 - (\tau-i\sigma)^2} \frac{J_1[k\frac{D}{2}\sqrt{1 - (\tau-i\sigma)^2}]}{J_0[k\frac{D}{2}\sqrt{1 - (\tau-i\sigma)^2}]} \qquad (32)$$

The various solutions of this transcendental equation are commonly attributed to various modes.

A reasonable approximation for the fundamental mode (which has the smallest attenuation constant σ) can be obtained by a finite-difference approximation:

$$\frac{\partial p}{\partial r}(r_n) \approx \frac{m}{D}\left[p\left(r_n+\frac{D}{2m}\right) - p\left(r_n-\frac{D}{2m}\right)\right] \qquad (33)$$

$$\frac{\partial^2 p}{\partial r^2}(r_n) \approx \left(\frac{2m}{D}\right)^2\left[p\left(r_n+\frac{D}{2m}\right) - 2p(r_n) + p\left(r_n-\frac{D}{2m}\right)\right] , \qquad (34)$$

where m denotes the number of elements considered in $0 \le r \le D/2$. The subscript n refers to a particular location.

Figure H7 shows the system considered for $m = 2$. The finite-difference approximations of Eq. (28) at the points 1 and 2 may be written

$$\frac{16}{D^2}(-p_1+p_2) + \frac{16}{D^2}(p_2-p_1) + k^2[1 - (\tau-i\sigma)^2]\, p_1 = 0 \qquad (35)$$

$$\frac{16}{D^2}(p_3-2p_2+p_1) + \frac{16}{D^2}(p_3-p_1) + k^2[1 - (\tau-i\sigma)^2]\, p_2 = 0 \qquad (36)$$

The boundary conditions Eqs. (30) and (31) can be approximated by

$$p_3 = 1 - \frac{2}{1 + \dfrac{8Z}{ikD\rho c}}\, p_2 \,. \qquad (37)$$

The coefficients of the homogeneous system of Eqs. (35) to (37) vanish for

$$\tau - i\sigma = \sqrt{1 - \frac{1}{3}\left(\frac{8}{kD}\right)^2\left[1 + \frac{1}{1+\frac{8Z}{ikD\rho c}} \overset{(+)}{\underset{(-)}{}} \sqrt{1 - \frac{1}{1+\frac{8Z}{ikD\rho c}} + \frac{1}{\left(1+\frac{8Z}{ikD\rho c}\right)^2}}\right]} \qquad (38)$$

For $|8Z/kD\rho c| \gg 1$, the result

$$\tau - i\sigma \approx \sqrt{1 - i\,\frac{4}{kD}\,\frac{\rho c}{Z}} \qquad (39)$$

agrees with the general approximation for propagation constants in ducts of arbitrary shape, with weak effects of the absorbing wall (Ref. 3)

$$\tau - i\sigma = \sqrt{1 - i\,\frac{U_a}{kS}\,\frac{\rho c}{Z}} \quad, \qquad (40)$$

where U_a denotes the absorptive part of the duct perimeter, S the area of the duct cross section.

For $|8Z/kD\rho c| \ll 1$, Eq. (38) yields

$$\tau - i\sigma = \sqrt{1 - \frac{1}{3}\left(\frac{8}{kD}\right)^2} \tag{41}$$

There is no wave propagation in a duct with soft walls below the cut-off frequency at which

$$\frac{kD}{2} = \frac{4}{\sqrt{3}} \tag{42}$$

This value closely approximates the first zero of the zero-order Bessel function.

As evident for the extreme cases of rigid and soft duct linings, Eq. (38) gives a good approximation for the propagation constant of the fundamental mode. In the vicinity of

$$\frac{Z}{kD\rho c} = \frac{1}{16}(\sqrt{3}-1), \tag{43}$$

a vanishing square-root in Eq. (38) indicates the highest attenuation.

ESTIMATION SCHEME

In order to estimate the attenuation provided by a given duct, one may proceed as described below.

1. Determine the frequency

$$f_D = c(T)/D$$

above which the duct may be considered as large compared to a wavelength (that is, $D > \lambda$). Here $c(T)$ denotes the speed of sound in the gas in the duct (which speed is proportional to the square-root of the absolute temperature).

2. Calculate the duct diameter/length ratio D/L.

3. For frequencies $f > f_D$ (where $\lambda < D$),

    (a) If $D/L < 1$, find the attenuation ΔL from

$$\Delta L = 10 \ \log \left(\frac{L/D}{1.5 - \alpha} \right) . \tag{11a}$$

    (b) If $D/L > 1$, find the attenuation from

$$\Delta L = 3.3 \ \alpha_z \ \frac{L}{D} \ \frac{\lambda}{D} \approx 10 \ \frac{L}{D} \left(\frac{\lambda}{D} \right)^2 \ \text{Re} \left\{ \frac{Z}{\rho c} \right\} \tag{16a}$$

4. For frequencies $f < f_D$ (where $\lambda > D$), the lengths L_S and L_R of the lined and unlined duct portions (if any), must be considered, in addition to the type of sound source.

    Consider a duct geometry as shown in Fig. H3, with a duct lining configuration as shown in Fig. H4. Radial partitions are used in order to obstruct axial sound propagation inside the lining. The absorptive material is assumed to have a rigid, open-pore structure; the acoustical properties required for its specification are the flow resistance $\Xi b/\rho c$, the structure factor χ and the porosity σ_p. For a layer of absorptive material that is thin compared to the wavelength, $\chi \approx \tau \approx 1$.

    (a) Calculate the wall impedance Z of the lined duct from

$$\frac{Z}{\rho c} = i \ \frac{k_w}{k} \ \frac{1 - \dfrac{\sigma_p k}{k_w} \cot(k_w b_L) \cot \left[kd \left(1 - \dfrac{b_L}{d} \right) \right]}{\cot(k_w b_L) + \dfrac{\sigma_p k}{k_w} \cot \left[kd \left(1 - \dfrac{b_L}{d} \right) \right]} \tag{44}$$

    where

$$\frac{k_w}{k} = \sqrt{\chi - i \ \frac{\Xi b}{\rho c} \ \frac{\sigma_p}{k b_L}} \ , \tag{45}$$

    and k denotes the wavenumber in free space.

    (b) Find the approximate propagation constants σ, τ of the duct by use of Eq. (38), (39), or (41), whichever is applicable, depending on the value of $8Z/kD\rho c$.

(c)   Calculate the attenuation that results over the length L_S of a lined duct from

$$\Delta L_L (dB) = 8.7 \ k\sigma L_S$$

(d)   Calculate the attenuation that results due to reflections at the end of the duct from

$$\Delta L_E (dB) = 10 \ log \ [1 + (2/kD)^2]$$

(e)   Determine the attenuation due to interaction between a lined section and an unlined tailpipe from

$$\Delta L_I (dB) = \begin{cases} 0, \text{ if entire duct is lined} \\ \text{third term* of Eq. (23), otherwise} \end{cases}$$

(f)   Determine the attenuation due to source effects from

$$\Delta L_S (dB) = \begin{cases} \text{third term of Eq.(24), for low-impedance source} \\ \text{third term of Eq.(25), for high-impedance source} \end{cases}$$

(g)   Find the total attenuation from

$$\Delta L = \Delta L_L + \Delta L_E + \Delta L_I + \Delta L_S$$

Sample Results

The results of some sample calculations are plotted in Figs. H5 and H6. Figure H5 pertains to a duct which is lined over a length $L_S = 3D$ and which has an unlined tailpipe of the same length; the lining thickness is (d = D/2) and the absorbing material is a thin layer of thickness b = d/10 with a flow resistance that is twice the characteristic impedance ρc of the gas. The attenuation $8.7 \ k\sigma L_S$ over a length L_S of a homogeneous lined duct and the reflection loss $10 \ log \ [1 + (kD/2)^2]$ of the tailpipe are plotted in Fig. H5. Figure H6 shows the excess attenuation $\Delta L - 8.7 \ k\sigma L_S$, which accounts for interactions in the case of a ρc-source impedance. The excess attenuation can be approximated by the reflection loss of the tailpipe in the frequency region where the total length $L_S + L_R$ exceeds a quarter wavelength.

---

*or approximations, see text

Illustrative Calculations

High-Frequency Effect

Evaluate the effect of placing a 13 ft long duct of 1.65 ft exit diameter at the outlet of a small turbofan engine, if the flow leaving the duct is at 250°. (This duct obviously will affect only the noise emanating from the engine outlet; a duct at the inlet will be required to reduce the noise emanating from that end of the engine.)

The speed of sound at 70°F is 1100 ft/sec; thus at 250°F,

$$c = 1100 \sqrt{\frac{460+250}{460+70}} = 1270 \text{ ft/sec.} \quad \text{Then}$$

$$f_D = c(t)/D = (1270 \text{ ft/sec})/(1.6 \text{ ft}) = 770 \text{ Hz}$$

At all frequencies above 770 Hz, the duct is large compared to the acoustic wavelength.

Since $D/L = 1.65/13 \approx 0.127$, Eq. (11a) applies. If the duct is unlined, $\alpha = 0$ and the attenuation provided by the duct is

$$\Delta L = 10 \log \frac{L/D}{1.5-\alpha} = 10 \log \frac{13/1.65}{1.5-0} = 7 \text{ dB}$$

at all frequencies above about 800 Hz. (If the duct contains a lining with an absorptive coefficient $\alpha = 0.4$, one obtains $\Delta L = 8.5$ dB. The value of α generally depends on frequency, however, so that one would need to carry out the foregoing calculation at several frequencies in the range of interest.)

Ducts Muffling only One of Two Like Sources

If an unmuffled (and unducted) fan produces 171 dB, re 10^{-12} watts at 17.5 kHz, one may assume 168 dB from the outlet and 168 dB from the inlet.* Adding a duct with $\Delta L = 7$ dB to the outlet would reduce the noise from that source to 161 dB, but would not affect the inlet noise — and thus would result in a level of 169 dB, re 10^{-12} watts (which corresponds to a decrease of only 2 dB). However, adding a duct with $\Delta L = 7$ dB to both inlet and outlet would reduce the 171 dB by 7 dB, i.e. to 164 dB.

---

*See Fig. 1 for combined acoustic levels.

Low-Frequency Effect

Consider now what effect the previously described duct would have on sound at 150 Hz, if half of the duct is lined with an acoustically absorptive system having a wall impedance $Z = 2.5\rho c$ (at 150 Hz), and half is unlined (see Fig. H5 for general configuration).

Since $f_D = 770$ Hz, one must use item 4 of the preceding estimation scheme. If Z is given (as obtained from experimental data, for example) one need not calculate it. Since

$$k = \omega/c = 2\pi f/c = 2\pi(150/\text{sec})/(1270 \text{ ft/sec}) = 0.743/\text{ft},$$

one finds

$$\frac{8Z/\rho c}{kD} = \frac{8(2.5)}{(0.743/\text{ft})(1.65 \text{ ft})} = \frac{20.0}{1.23} = 16.3$$

This value is much greater than unity; therefore Eq. (39) applies. With $(4/kD)(\rho c/Z) = (4/1.23)(1/2.5) = 1.30$ that equation becomes

$$\tau - i\sigma = [1-i(1.30)]^{1/2} = \left[\sqrt{1+(1.30)^2}\, e^{-i \text{ arc tan } 1.30}\right]^{1/2}$$

$$= \left[1.64 e^{-152.4°}\right]^{1/2} = 1.28 e^{-126.2°}$$

$$= 1.28(\cos 26.2° - i \sin 26.2°) = 1.15 - i0.565$$

Then, since the lined length is $L_S = 6.5$ ft,

$$\Delta L_L = 8.7 k \sigma L_S = 8.7(0.743/\text{ft})(0.565)(6.5 \text{ ft}) = 23.5 \text{ dB}$$

$$\Delta L_E = 10 \log[1+(2/kD)^2] = 10 \log[1+(2/1.23)^2] = 5.5 \text{ dB}$$

and from Eq. (23), letting $\xi = \tau - i\sigma$,

$$\Delta L_I = 20 \log \left| 1 + \frac{1 - e^{-2ikL_S\xi}}{4\xi/(1-\xi)}\, \beta_1 \right|$$

where $\beta_1 = 1 - \xi + \dfrac{e^{-2ikL_R}}{1+ikD/2}(1 + \xi)$

one finds after much arithmetic that $\beta_1 \approx -1.08 + i(2.18)$ and $\Delta L_I \approx 0$ dB.

For a high-impedance source (which produces essentially the same acoustic pressure with and without the added duct — probably a reasonable approximation for engine noise sources) one finds from Eq. (25) that

$$\Delta L_S = 20 \log \left| 1 - \frac{e^{-2ikL_R}}{1+ikD/2} + \frac{1 - e^{-2ikL_S\xi}}{2\xi}\beta_1 \right| \approx 4 \text{ dB}$$

The total attenuation at 150 Hz therefore is $23.5 + 5.5 - 0 + 4 = 33$ dB.

REFERENCES FOR APPENDIX H

1. Morse, P.M., "The Transmission of Sound Inside Pipes," *J. Acoust. Soc. Am.* 11, p. 205 (1939).

2. Cremer, L., "Nachhallzeit und Dämpfungsmass bei streifendem Einfall," *Akust. Z.* 5, p. 57 (1940).

3. Cremer, L., "Theorie der Luftschall-Dämpfung im Rechteckkanal mit schluckender Wand und das sich dabei ergebende höchste Dämpfungsmass," *Acustica* 3, p. 249 (1953).

4. Kurze, U., "Untersuchungen an Kammerdämpfern," *Acustica* 15, p. 139 (1965).

5. Kurze, U., "Influence of Flow and High Sound Levels on the Attenuation in a Lined Duct," (Abstr.), *J. Acoust. Soc. Am.* 47, p. 122 (1970). (To be published by U. Kurze and C. H. Allen).

6. Heins, E. and H. Feshbach, "The Coupling of Two Acoustical Ducts," *J. Math. and Physics* XXVI, p. 143 (1947).

7. Levine, H. and J. Schwinger, "On the Radiation of Sound from an Unflanged Circular Pipe," *Phys. Rev.* 73, p. 383 (1948).

8. Kurze, U., "Schallabstrahlung an der Austritts-öffnung von Kanälen," *Acustica* 20, p. 253 (1968).
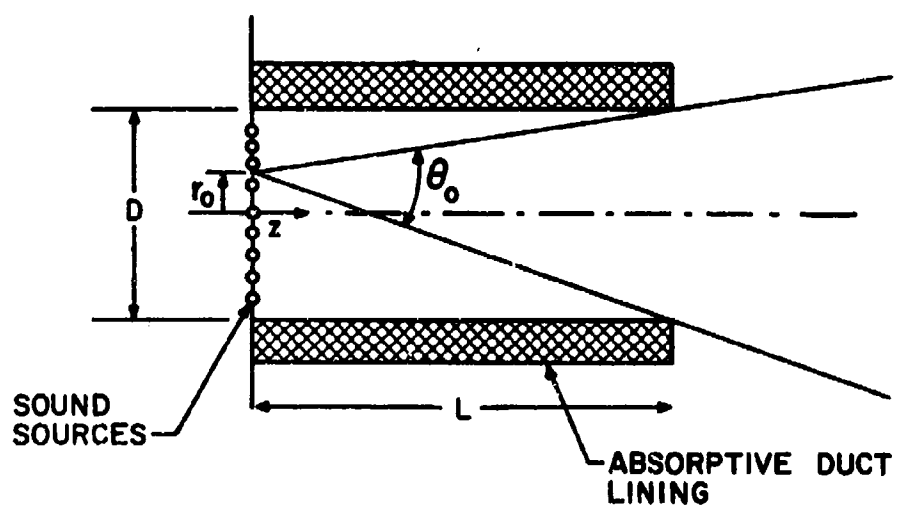
FIGURE H1   RAYS EMITTED FROM CIRCULAR DUCT WITHOUT REFLECTION
             FROM WALLS

130
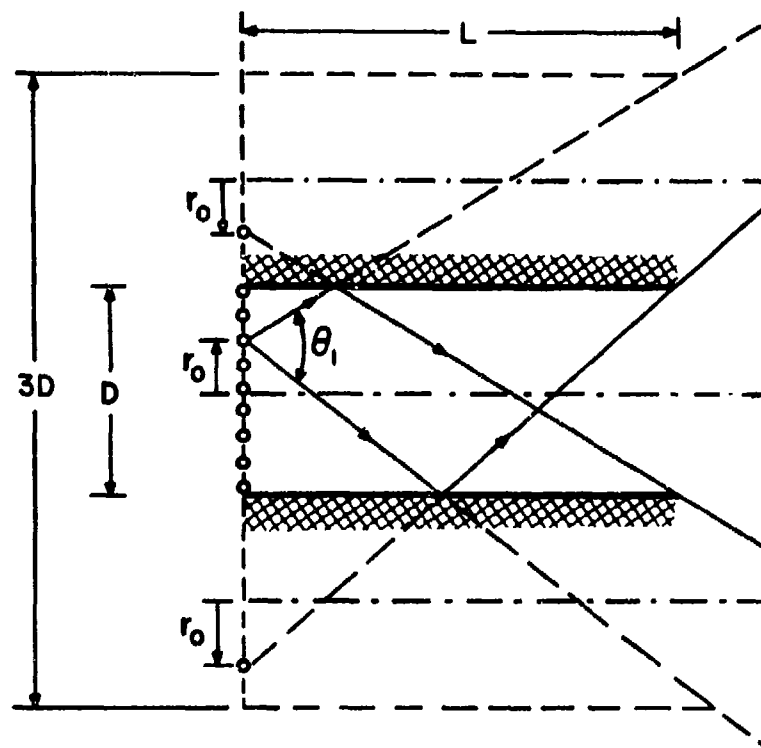
FIGURE H2   RAYS EMITTED FROM DUCT AFTER ONE REFLECTION
(CONSTRUCTED FROM IMAGE SOURCES)
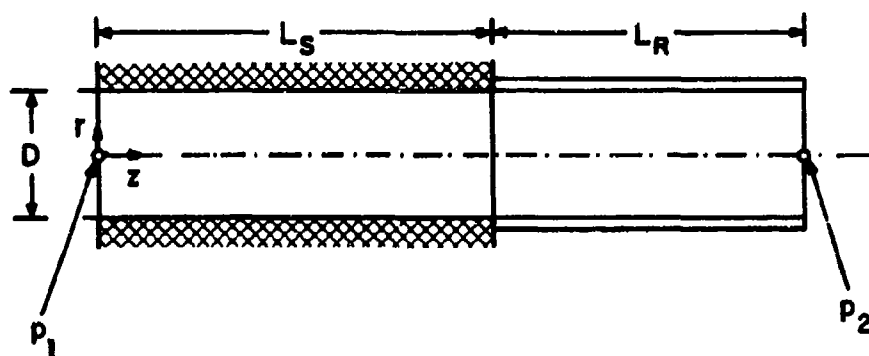
FIGURE H3   LINED DUCT WITH RIGID TAILPIPE
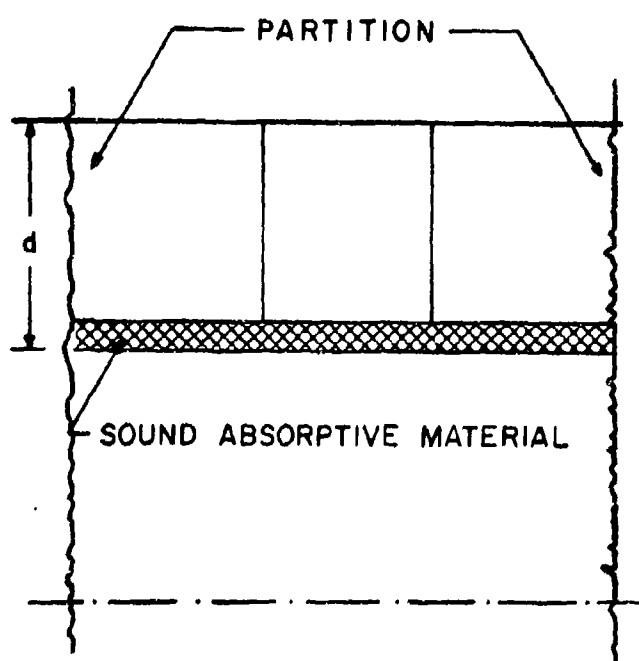
FIGURE H4   DUCT LINING GEOMETRY

ATTENUATION (dB)

LINED DUCT $\Delta L_L = 8.7\ k\sigma L_s$

REFLECTION LOSS OF TAILPIPE END $\Delta L_E = 10 \log \left[1 + \left(\frac{2}{kD}\right)^2 \right]$ dB

$d = \lambda/4$

$2\rho c$

$d = D/2$

SOURCE D

$L_S = 3D$

$L_R = 3D$

DIAMETER/WAVELENGTH, D/λ

0.01   0.1
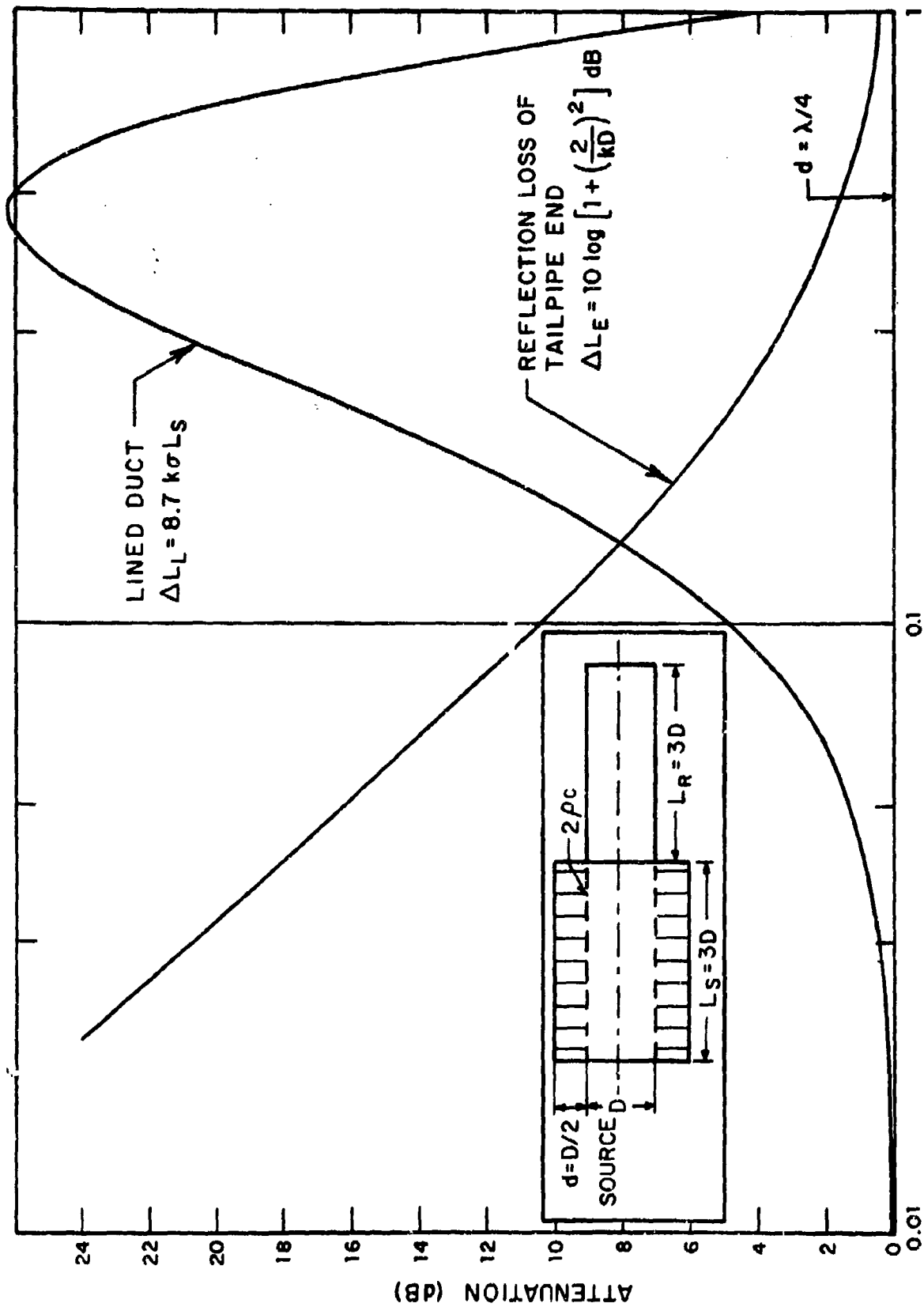
FIGURE H5   CALCULATED ATTENUATION OF THE LINED DUCT AND REFLECTION LOSS OF TAILPIPE
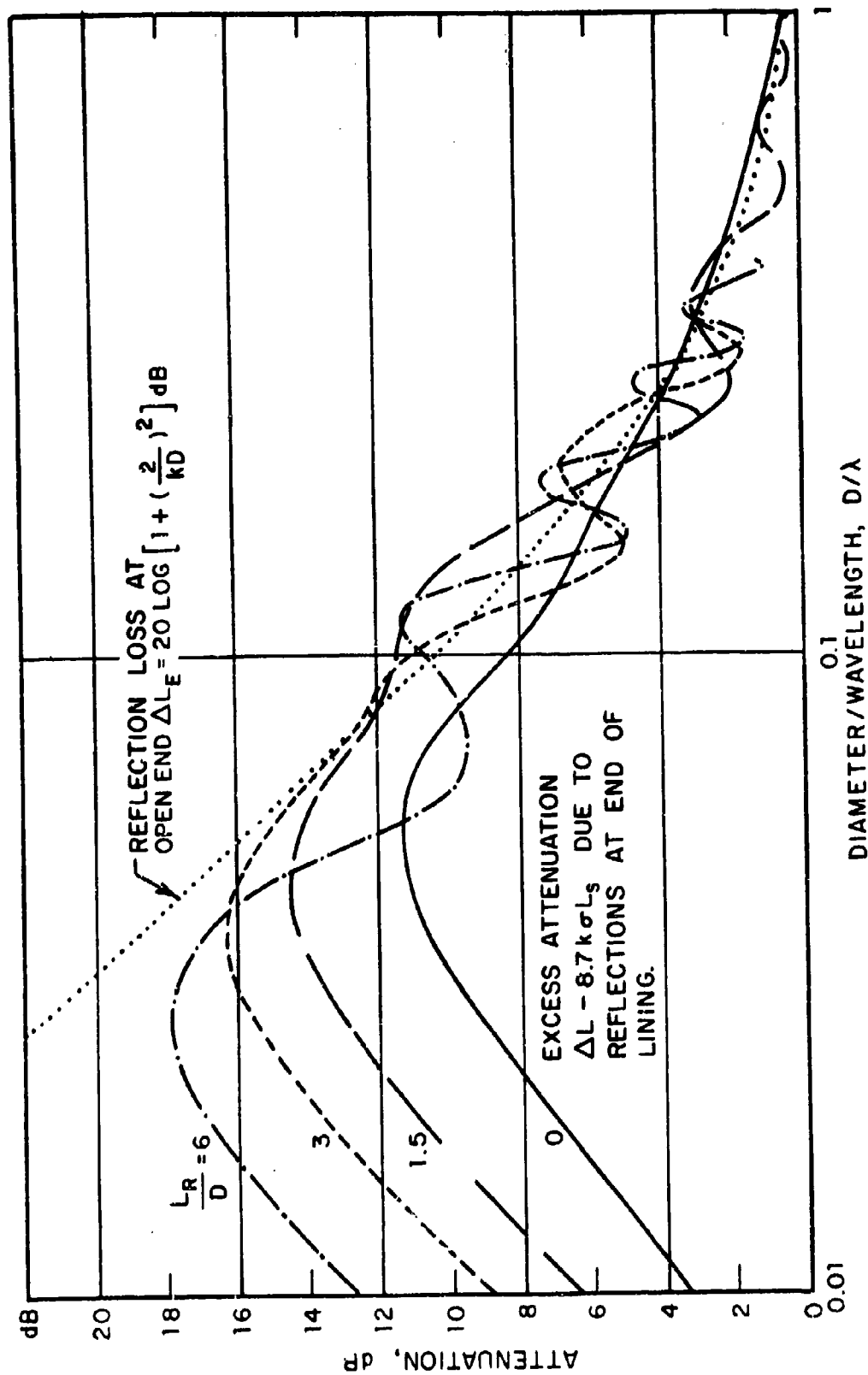
FIGURE H6 EXCESS ATTENUATION DUE TO REFLECTIONS AT TRANSITION FROM LINED DUCT TO THE RIGID TAILPIPE, AND REFLECTION LOSS AT THE OPEN END OF UNFLANGED TAILPIPE, FOR VARIOUS RATIOS OF LENGTH L_R OF IHE TAILPIPE IO THE DUCT DIAMETER D. (SAME DUCT LINING AS IN FIGURE H5)

135
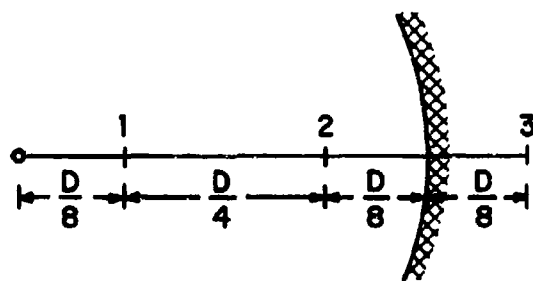
FIGURE H7   POINTS ALONG CROSS-SECTION OF LINED DUCT
USED FOR FINITE-DIFFERENCE APPROXIMATION
OF DIFFERENTIAL EQUATION (28)

APPENDIX J
GEAR NOISE

MECHANISM OF NOISE GENERATION

Tooth Contact Forces

Gear sets transmit torque and power by virtue of forces
transmitted via mating gear teeth. When a given tooth does not
make contact with a mating tooth, it is subject to zero force;
when contact is made, the inter-tooth force increases, reaches
a maximum, decreases, and again returns to zero when the tooth
disengages. These dynamic tooth forces, which are inherent in
the operation of gears (and which may be modified or aggravated
by inaccuracies in gear tooth profiles and gear alignment),
cause the gear to vibrate. These gear vibrations may radiate
sound directly, or they may cause vibrational energy to travel
via the shaft and bearings to the gearbox, which may then radiate
sound into the surrounding air.

Characteristics of Noise

One may deduce some qualitative properties of the gear noise
spectrum by considering the dynamic tooth interaction forces.
The force acting on a gear, and thus the gear noise, may be ex-
pected to have a periodic component associated with the tooth
contact frequency f_t. In addition, one would expect periodic
components at the shaft-rotation frequencies of the various inter-
acting gears, due to any asymmetries and other geometric inaccura-
cies of the gears.

For a geometrically perfect gear set, the force spectrum
(and therefore also the sound spectrum) would have components at
only the tooth contact frequency and its harmonics, with the am-
plitude of these spectral components depending on the shape of
the force-time curve corresponding to a single tooth contact.
The amplitudes of these components may be expected to be approxi-
mately constant up to the frequency which corresponds to the re-
ciprocal of the effective duration T_{eff} of a contact force pulse
(see Fig. J1); beyond this frequency, the amplitudes are expected
to decrease rapidly.

For an imperfect gear, or with unsteady driving moment, the shapes - as well as the amplitudes - of the tooth-force pulses may vary with a period that corresponds to the shaft-rotation frequency f_s, as sketched in Fig. J1. Because of this "amplitude modulation" of the tooth force pulses, the spectra here may be expected also to contain components at the shaft rotation frequency and at harmonics of that frequency. Measured spectra of gear noise (e.g., see Fig. 10 of Ref. 1) are in agreement with the foregoing qualitative considerations.

DATA

Available Data

Although much work has been done on gear noise, only quali-tative understanding of it rests on a relatively firm basis. The present state of the technology does not permit one to predict the noise of a gear set from the basic physical parameters of that set (except from correlations of empirical data), and generally also does not permit one to predict with much confidence the ef-fects of design changes on noise. A number of relevant recent publications are indicated in the appended reference list.

The only available collection of data on the noise of many different gears, measured under well-known conditions, appears to be that of Refs. 1 and 2. These references summarize the results of noise measurements on 76 sets of power gears (including spur and bevel gears and planetary sets) transmitting between 10 and 25,000 kw (7.5 and 18,500 Hp) at peripheral speeds between 3.6 and 160 m/sec (12 and 525 ft/sec) with gearing ratios up to 256.

Dependence of Overall Noise on Transmitted Power and Tooth Force

A careful statistical analysis of the measured gear noise data revealed a strong correlation (0.87 correlation coefficient) between the total acoustic power produced by a gear set and the mechanical power transmitted by that set. A similar correlation was found between noise and the average tooth force.

Figure J2 (taken from Ref. 2) shows how the measured overall sound power levels of gear sets vary with the transmitted power (which for these measurements was between 75% and 100% of the design power for the sets tested). Also indicated in that figure is a line which corresponds to the mean of the measured points, as well as dashed lines which correspond to one standard devia-tion from the mean. An equation for the mean line is also given in the figure.

Noise Spectra

Octave-band noise spectra, derived from Refs. 1 and 2, are presented in Figs. J3, J4 and J5 for the three classes of gears and speeds treated in the original references. Figures J3 and J4, which may be seen to be very similar, pertain to planetary and spur gear sets operating at relatively high speeds; Fig. J5 pertains to gears of various types operating at lower speeds.

The spectra in Figs. J3-5 are presented in terms of differences between overall levels and octave band levels. In addition to spectra corresponding to the means of the data, curves are given which correspond to the mean $\pm$ standard deviation.

PREDICTION CURVES

By combining the average dependence of overall acoustic power on transmitted mechanical power, as given in Fig. J2, with the spectra of Figs. J3-5 one may arrive at octave-band spectra of sound power referred to mechanical power.

Figure J6 shows mean spectra obtained in this manner, and is readily applicable for general noise estimation purposes. Because of the similarity of the mean-curves of Figs. J3 and J4, these two have been combined (averaged and smoothed) into a single "high-speed" gear noise curve; the "low-speed" curve is obtained directly from Fig. J5.

ESTIMATION SCHEME

In order to estimate the noise produced by a gear set (two mating gears), one may proceed as follows:

1. Select the curve of Fig. J6 that corresponds to the rotational speed (rpm) of the smaller (higher-speed) gear.

2. Calculate $10 \log(Hp)$, where Hp is the mechanical horsepower transmitted by the gear set, and add this value to the numbers shown along the vertical scale of Fig. J6. The resulting numbers then represent the octave-band sound power levels for the gear set.

3. Calculate the tooth contact frequency from

$$f_t(Hz) = N_t(rpm)/60$$

where N_t is the number of teeth on either gear and rpm is the rotational speed (in revolutions/min) of that same gear.

Then, for aural detection estimation, take the levels (obtained from the foregoing steps) at frequencies f_t, $2f_t$, $3f_t$ to correspond to pure tones, and the levels for octave bands above $3f_t$ to correspond to broad-band noise. Delete all parts of the spectrum of Fig. J6 below f_t. (No appreciable noise is produced at these low frequencies.)

Illustrative Calculation

Consider a gear set transmitting 100 Hp, with the smaller gear (which has 18 teeth) rotating at 3000 rpm. Here

$$10 \ \log(Hp) = 20$$

$$f_t = N_t(rpm)/60 = 18(3000)/60 = 900 \ Hz$$

This is a "high-speed" gear set (rpm > 1500); the dashed curve of Fig. J6 applies. For aural detection estimation, one thus obtains the following pure tone noise levels:

f(Hz)	200	1800	2700
L_w (dB, re 10^{-12} watts)	91	89	86

plus the following octave-band levels:

f(Hz)	4000	8000
L_w (dB, re 10^{-12} watts)	85	78

with no significant noise below 900 Hz.

REFERENCES FOR APPENDIX J

1. Zumbroich, J., "Untersuchungen des Gerauschverhaltens Moderner Hochlastgetriebe," PhD Thesis, Technische Hochschule Aachen, June 1964.

2. Opitz, H., J. Zumbroich and J. Timmers, "Serienunter-suchungen des Gerauschverhaltens Moderner Hochlastgetriebe," *Industrie-Anzeiger, Essen,* 87, No. 96, pp. 445-455 (1965).

3. Schlegel, R. C., R. J. King and H. R. Mull, "How to Reduce Gear Noise," *Machine Design,* 6, pp. 134-142 (27 Feb. 1964).

4. Michalec, G. W., "Vibration in Geared Systems," *Machine Design,* 37, pp. 164-173 (16 Sept. 1965).

5. Niemann, G. and M. Unterberger, "Reduction of Gear Noise," *VDI Zeitschrift* 101(6), pp. 201-212 (1959) German.

6. Klykin, I. V., "Controlling the Noise of Reduction Gearing and Marine Internal Combustion Engines," in "Control of Noise and Vibration in Ships," U. S. Dept. of Commerce, Office of Technical Services, Report No. DTS 63-21340, Chapt. 17, pp. 346-353 (1963).

7. Nakamura, K., "Experimental Studies about the Effects of Dynamic Tooth Loads upon Gear Noise," *Bull. Japan Soc. Mech. Eng.* 10(37), pp. 180-188 (1967).

8. Nakamura, K., "Tooth Separations and Abnormal Noise on Power Transmission Systems," *Bull. Japan Soc. Mech. Eng.,* 10(41), pp. 846-854 (1967).

9. Thomson, D. C., "Investigation of the Relationship between Gear Design and Tooth Noise," Marine Engg. Lab., Annapolis, Maryland, Report No. 178164 (Sept. 1964).

10. Ehrenreich, M. and M. Rubin, "Noise Analysis of a Vehicle Transfer Gearbox," *Proc. Inst. Mech. Engrs.* AD, 175, pp. 337-350 (1960-1961).

11. Rosen, M. W., "Acoustic Studies on Power Transmission," in *Underwater Missile Propulsion,* Ed. by L. Greiner, Compass Publications, Arlington, Va. (1967).

12. Rabek, E. E., "Airborne and Structure-Borne Noise of Small Gear Motors," *J. Sound and Vibration* 9, pp. 8-14 (June 1967).
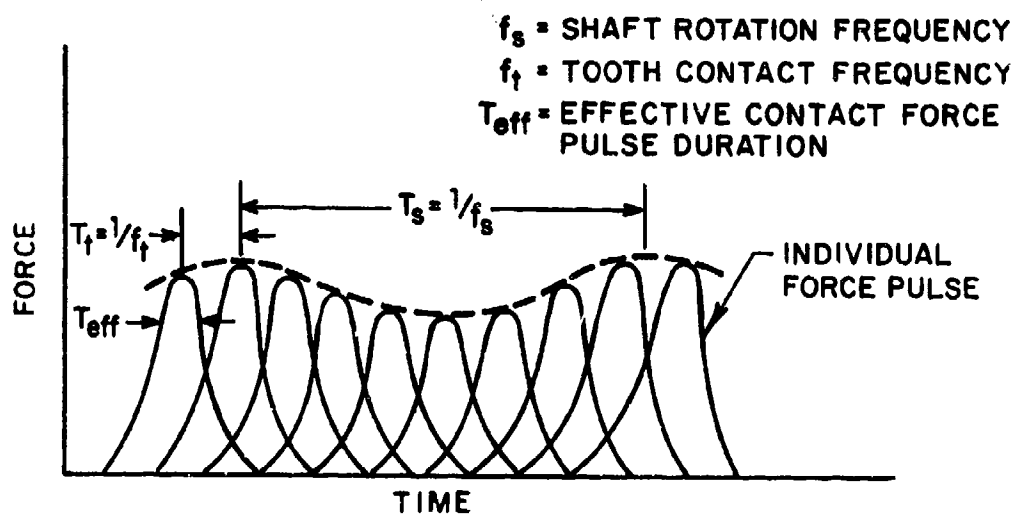
FIGURE J1   SCHEMATIC TIME-VARIATION OF GEAR INTERACTION FORCE
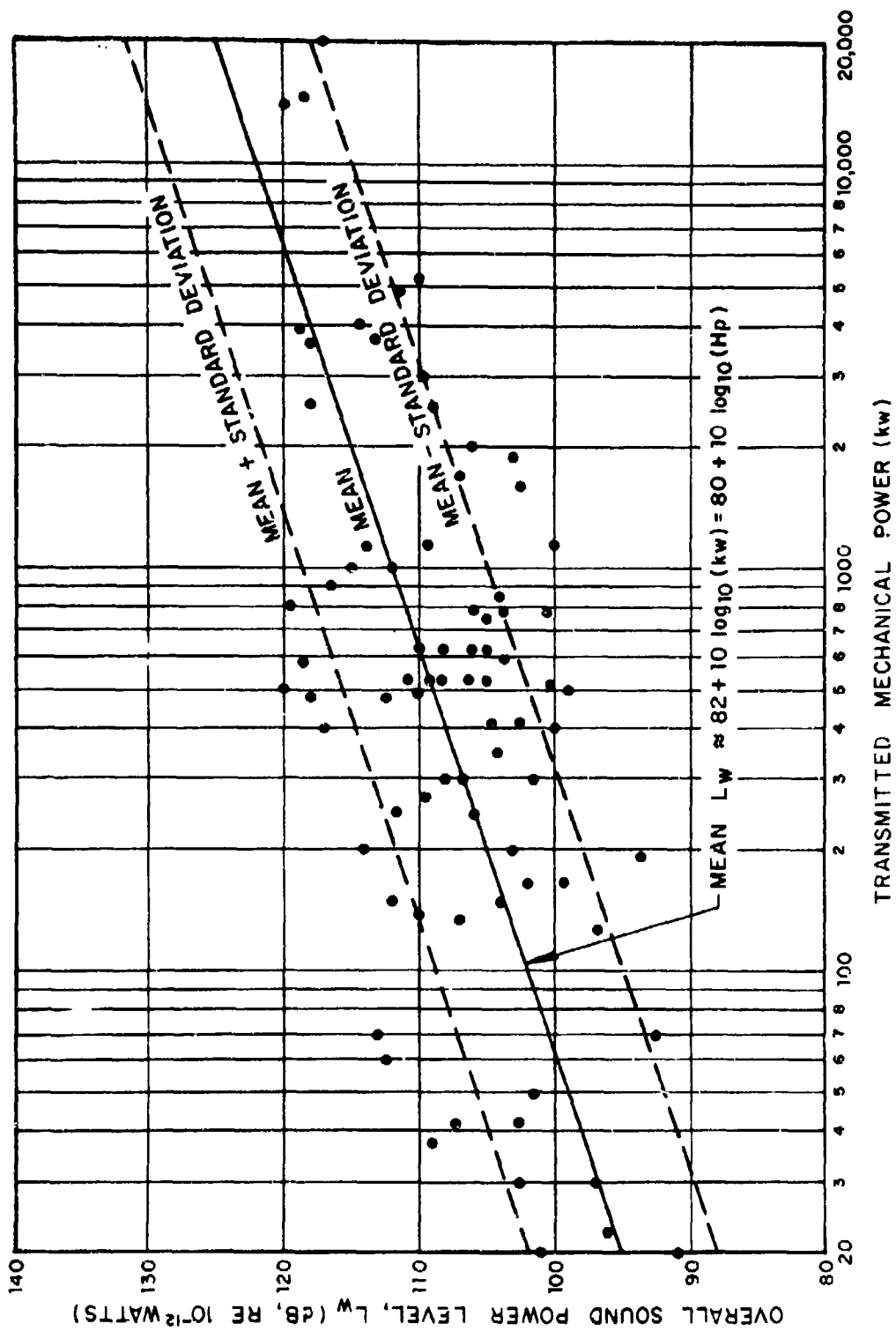
FIGURE J2   OVERALL SOUND POWER LEVEL OF GEARS AS A FUNCTION OF THE TRANSMITTED MECHANICAL POWER

MEAN $L_W \approx 82 + 10 \log_{10}$ (kw) = $80 + 10 \log_{10}$ (Hp)

TRANSMITTED MECHANICAL POWER (kw)

OVERALL SOUND POWER LEVEL, L_W (dB, RE 10^{-12} WATTS)
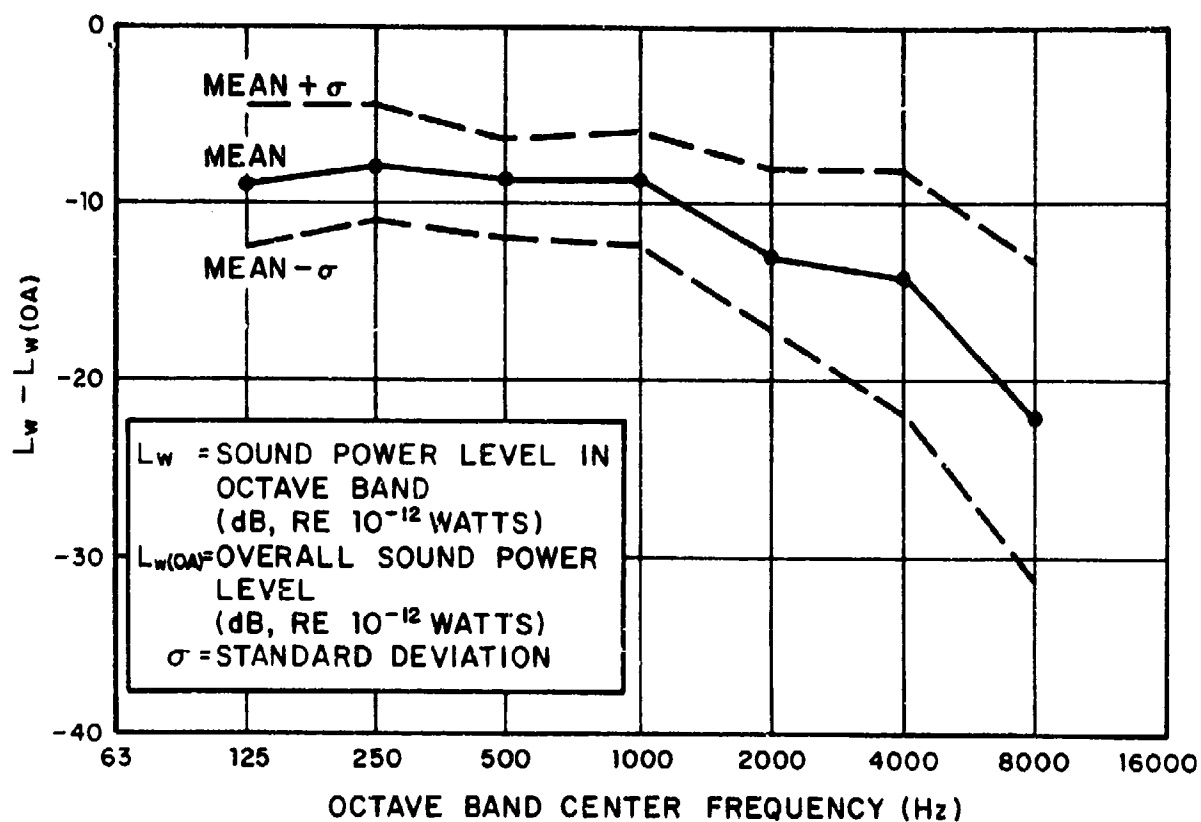
FIGURE J3   OCTAVE-BAND SOUND POWER SPECTRA FOR PLANETARY GEARS,
RPM $\geq$ 1500
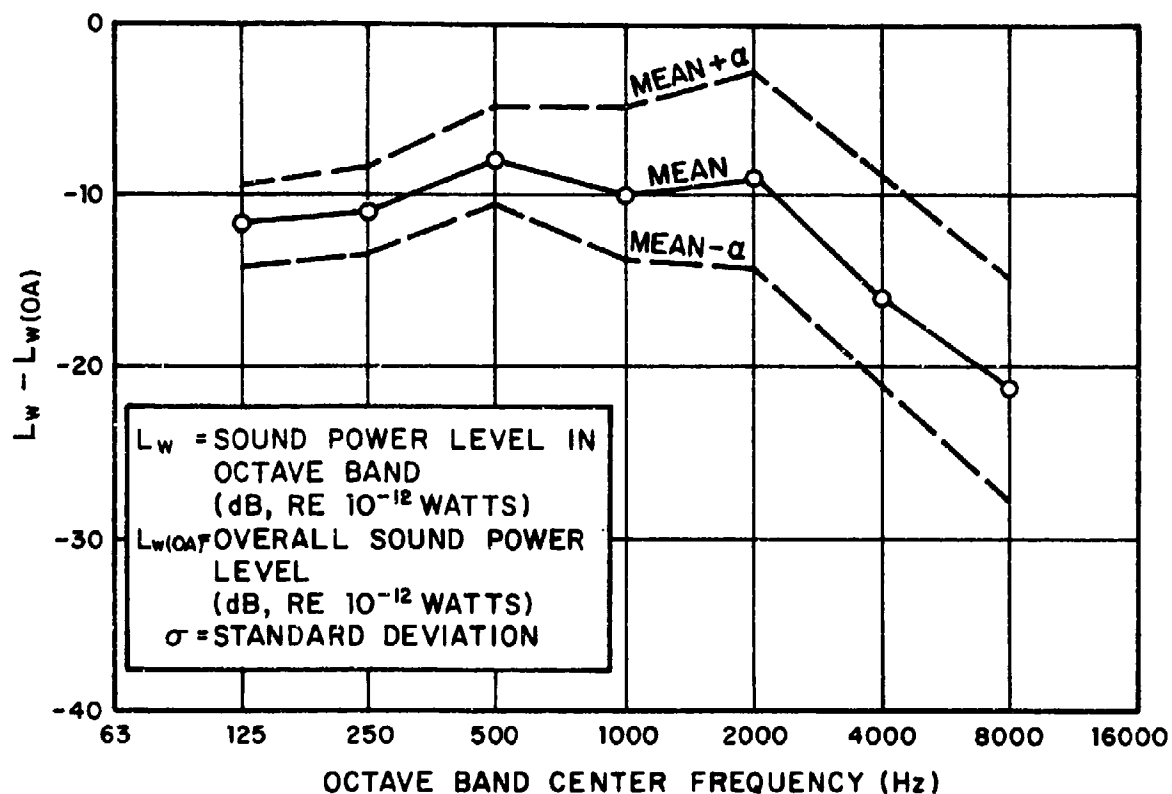
FIGURE J4   OCTAVE BAND SOUND POWER SPECTRA FOR SPUR GEARS,
RPM ≥ 3000

145
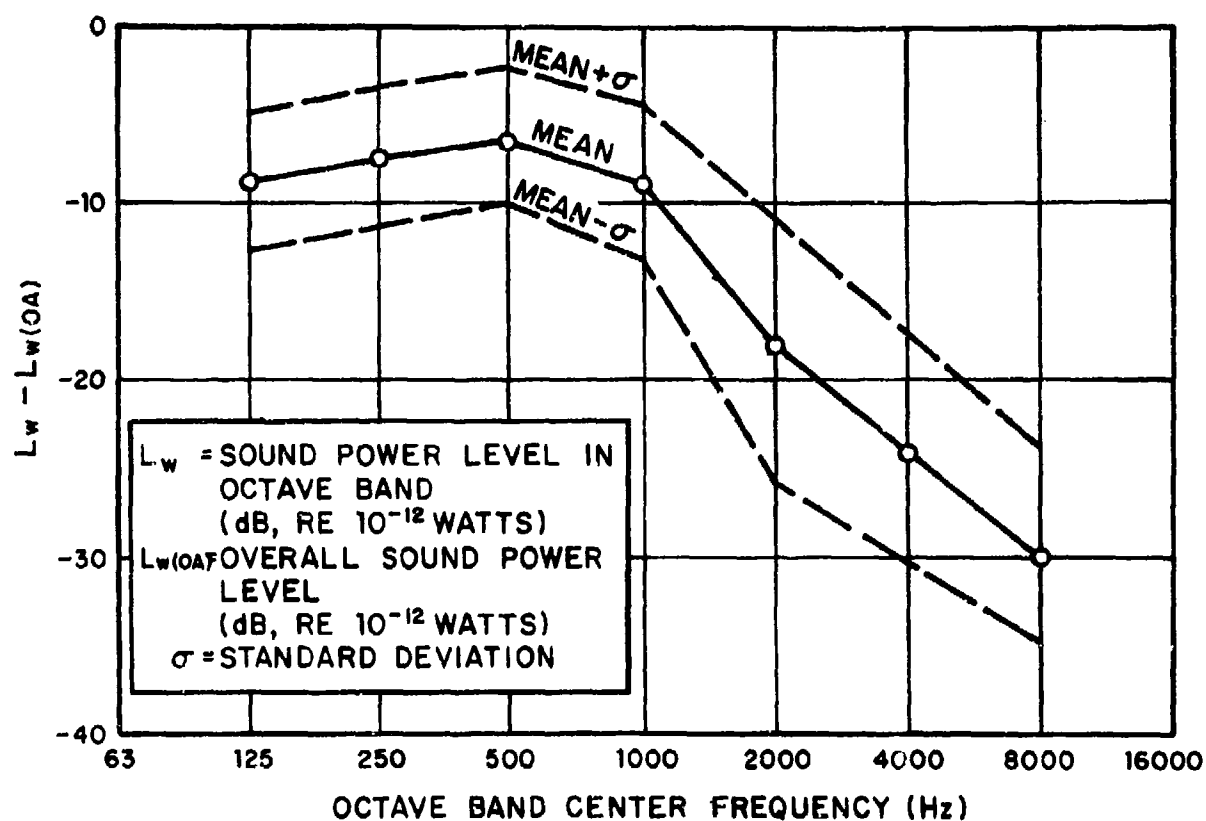
FIGURE J5   OCTAVE BAND SOUND POWER SPECTRA FOR SPUR, BEVEL, AND
             BEVELSPUR GEARS, RPM $\leq$ 1500

146
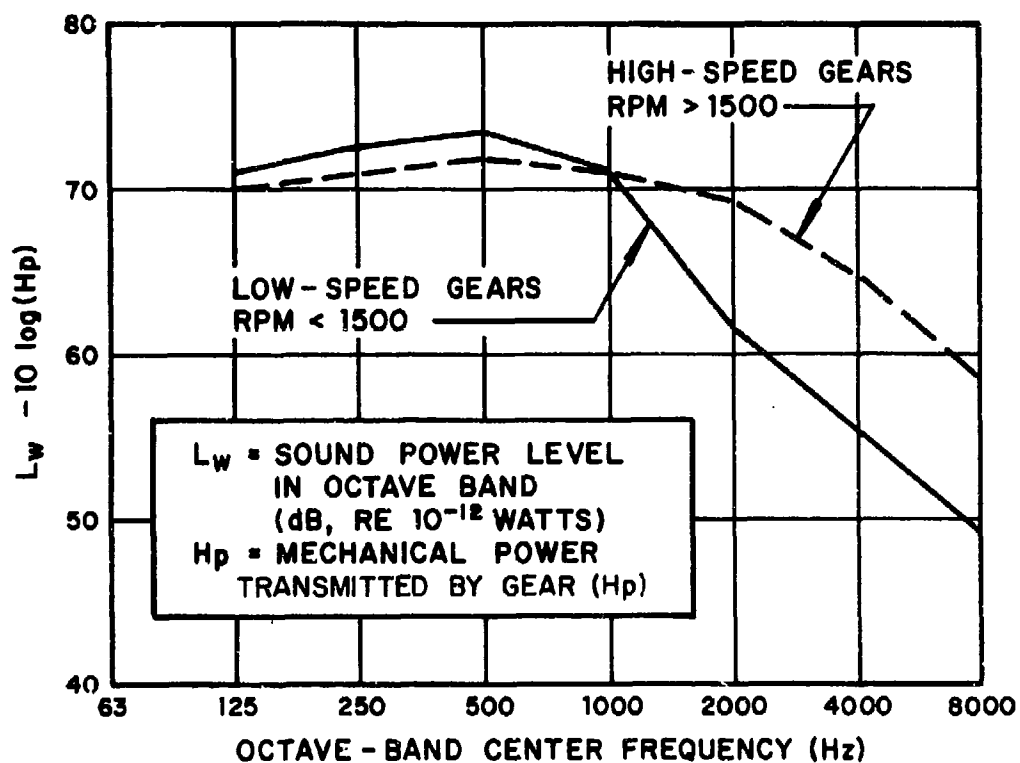
FIGURE J6   ESTIMATION OF GEAR NOISE

147

APPENDIX K

SOUND RADIATED FROM FLOW OVER RIGID SURFACES

SOUND FROM TURBULENT BOUNDARY LAYER

Infinite Surface

The sound power radiated to the atmosphere (per unit area) from an infinite turbulent boundary layer supported by a rigid flat surface provides a lower bound for the sound power radiated by a finite system. Because of this fact, and because analysis of the infinite case is relatively simple and exhibits the important parameters, presentation of a summary of the analysis is justified here.

Mathematical Model of Boundary Layer

Extensive experimental and theoretical work has been done to obtain descriptions of the pressures on surfaces under turbulent boundary layers (Refs. 1-6). These pressures usually are described in terms of space-time correlation functions

$$\phi_p(x_1, x_3, t) \equiv <p(x_{10}, x_{30}, t_0) p(x_{10}+x_1, x_{30}+x_3, t_0+t)> \tag{1}$$

where x_{10} and x_{30} represent coordinates on the surface, x_{10} in the direction of the flow and x_{30} perpendicular to the flow direction; x_1 and x_3 represent the separation between two observation points, the brackets $<...>$ indicate averaging over x_{10}, x_{30}, and time t_0. One may calculate the wavenumber-frequency spectrum of the pressure as:

$$\Phi_p(\underline{k}_p, \omega) = \frac{1}{(2\pi)^3} \iiint \phi_p(\underline{x}, t) e^{-i(\underline{k}_p \cdot \underline{x} - \omega t)} \, d\underline{x} \, dt \tag{2}$$

where $\underline{k}_p$ is the wavenumber vector, with the components k_1 and k_3, and $\underline{x}$ is the separation vector, with components x_1 and x_3, and ω represents the radian frequency.

It has been shown (Ref. 1) that the observed behavior of the wavenumber-frequency spectrum may be represented by

$$\Phi_p(\underline{k}_p, \omega) = \Phi_f(\omega) \, \Phi_d \left| k_1(\omega) - \frac{\omega}{U_c} \right| \Phi_3 \left| k_3(\omega) \right| \tag{3}$$

148

where $\Phi_f(\omega)$ represents the frequency spectrum one measures with a transducer that is fixed at one location on the surface, $\Phi_d(k_1)$ describes the decay of eddies in the flow direction, and $\Phi_3(k_3)$ is the wavenumber spectrum in the cross-stream direction.

The two wavenumber spectra typically obey

$$\Phi_d(k_1) = (L_d/\pi)(1 + k_1^2 L_d^2)^{-1} \tag{4}$$

$$\Phi_3(k_3) = (L_3/\pi)(1 + k_3^2 L_3^2)^{-1} \tag{5}$$

where L_d represents the eddy decay length, which may be approximated by

$$L_d \approx 9U_c/\omega \tag{6}$$

and L_3 is the transverse correlation length, which may be approximated as

$$L_3 \sim U_c/0.7\omega \tag{7}$$

in terms of the convection velocity U_c, which is approximately 0.7 times the free-stream velocity U.

The "fixed transducer" spectrum $\Phi_f(\omega)$ may be determined from the corresponding normalized spectrum, which is given in Fig. K1 and further discussed below.

Sound Radiation

Only those fluctuating pressure components for which the wavenumbers k_p are smaller than the acoustic wavenumber $k = \omega/c$ (where c represents the speed of sound) contribute to the sound radiation. Accordingly, the spectrum of the radiated acoustic pressure at the wall is given by

$$\Phi_{ac}(\omega) = \Phi_f(\omega) \iint_{(\overline{k}_1 + \overline{k}_3 < k)} \Phi_d\left(k_1 - \frac{\omega}{U_c}\right)\Phi_3(k_3)dk_1 dk_3 \ . \tag{8}$$

If one substitutes Eqs. (4), (5), (6) and (7) into Eq. (8), and limits oneself to the usual case of interest here where the convection velocity U_c is much smaller than the speed of sound ($U_c \ll c$), one obtains

$$\Phi_{ac}(\omega) \approx \Phi_f(\omega) \iint\limits_{(\overline{k}_1 + \overline{k}_3 < k)} \left[\frac{U_c}{9\pi\omega}\right] \left[\frac{U_c}{0.7\pi\omega}\right] dk_1 dk_3$$

(9)

$$\approx \Phi_f(\omega) \left[\frac{U_c^2}{6.3\pi^2\omega^2}\right] \pi k^2 .$$

With $U_c \approx 0.7U$, this result reduces to

$$\Phi_{ac}(\omega) \approx 2.5 \times 10^{-2} M^2 \Phi_f(\omega)$$

(10)

where $M = U/c$ represents the Mach number of the free-stream flow.

Equation (10) gives the acoustic pressure spectrum in terms of the boundary layer pressure spectrum. From this result one may readily obtain the relation

$$p^2/p_{bl}^2 \approx 2.5 \times 10^{-2} M^2$$

(11)

which holds between the mean-square acoustic pressure p^2 in a given frequency band $\Delta\omega$ and the mean-square pressure p_{bl}^2 in the boundary layer in the same band; these pressures are related to the spectra as

$$p^2 = \int_{\Delta\omega} \Phi_{ac}(\omega) d\omega , \qquad p_{bl}^2 = \int_{\Delta\omega} \Phi_f(\omega) d\omega .$$

(12)

The acoustic power W radiated from a surface of area A may be estimated from

$$W = Ap^2/4\rho c ,$$

(13)

where ρ represents the density of the air, as usual.

Frequency Distribution

The fixed-transducer spectrum of boundary layer pressure fluctuations, which also determines the spectrum of radiated sound in view of Eq. (10), may be determined from the normalized fixed-transducer spectrum $\Phi_f^1(\omega)U/\delta^*$ shown in Fig. K1 as a function of the dimensionless frequency (Strouhal number) $S = \omega\delta^*/U$, where δ^* represents the displacement thickness of the boundary layer.

The spectrum values are adjusted so that $\Phi_f^1(\omega)$ satisfies the relation

$$\int_{-\infty}^{\infty} \Phi^1(\omega)d\omega = 1 \; ; \tag{14}$$

then the actual spectrum $\Phi_f(\omega)$ is related to the normalized spectrum $\Phi_f^1(\omega)$ as

$$\Phi_f(\omega) = p_{OA}^2 \Phi_f^1(\omega) \tag{15}$$

in terms of the overall mean-square fluctuating pressure p_{OA}^2 in the boundary layer. From Fig. K1 and Eq. (15) one may deduce how the fluctuating pressure p_{b1}^2 in third-octave bands varies with frequency; the result is indicated in Fig. K2.

The boundary layer displacement thickness δ^* is a function of the Reynolds number and Mach number. For low Mach numbers, and for Reynolds numbers in the range between 10^6 and 10^7, which is of primary interest for small aircraft, one may estimate δ^* from

$$\delta^* \approx 0.0025 \ X \tag{16}$$

where X is the distance from the front (leading edge) of the body of concern (Ref. 7).

In order to estimate the actual levels, one still requires the mean-square overall boundary layer pressure p_{OA}^2. There exists much evidence (Ref. 8) that the corresponding root-mean-square pressure is proportional to the free-stream dynamic pressure q. The constant of proportionality depends on Reynolds number, Mach number, and surface roughness, but for most smooth aircraft surfaces one may take

$$p_{OA} \approx 0.006 \ q \ . \tag{17}$$

Effects of Surface Edges

Whereas pressures acting on a rigid surface can give rise to no appreciable acoustic particle velocities, pressures near an edge do not encounter the high impedance of the surface and thus cause greater velocities, and therefore more noise radiation. Thus, the noise associated with edges is likely to dominate over the noise from boundary layers on relatively rigid surfaces. The noise associated with edges is discussed in the following section.

SOUND FROM FLOW PAST FINITE BODIES

Airfoil in Large-Scale Turbulent Flow

A body moving through a turbulent fluid experiences unsteady lift and drag forces; the related reaction forces on the fluid are responsible for sound radiation. In most practical cases of interest, e.g., of an aircraft flying through atmospheric turbulence, the spatial scale of the pressure fluctuations is considerably larger than the airfoil dimensions. There then occur lift and drag fluctuations, which act essentially like acoustic point dipole sources. (The point source approximation is valid because the associated acoustic wavelengths are much greater than the characteristic surface dimensions.)

The acoustic power W radiated by a point dipole at frequency f is given by

$$W = \pi F^2 f^2 / 3\rho c^3 \qquad (18)$$

where F^2 represents the mean-square fluctuating force, ρ the density of the ambient air, and c the speed of sound in air.

One may express the root-mean-square fluctuating lift or drag force in terms of the corresponding lift or drag coefficient $C_{L(or\ D)}$ as

$$F_{L(or\ D)} \approx \frac{1}{2}\rho U^2 A C_{L(or\ D)} (u_{rms}/U) \qquad (19)$$

where U represents the free-stream (mean) velocity, A a reference area, and u_{rms} the root-mean-square fluctuating velocity. If one knows the turbulence spectrum $u_{rms}(f)/U$, one may then calculate the corresponding force spectra, and from these, the associated acoustic power.

Measurements by Clark and Ribner (Ref. 9) have verified the proportionality of sound radiated from an airfoil in large-scale turbulent flow to the mean-square fluctuating force on the airfoil, and Sharland (Ref. 10) has observed that the directivity pattern of the sound radiation from such an airfoil is like that of a classical dipole..

Small-Scale Turbulent Flow over Airfoil

If the disturbances on the airfoil and the associated acoustic wavelengths λ are small compared to the airfoil dimensions (e.g. the chord b), one no longer has the effect of point dipoles Instead, for $\lambda < b$, one has essentially arrays of unsteady forces acting at the various edges (Refs. 11, 12).

Chanaud and Hayden (Refs. 11-13) have considered two separate trailing-edge noise sources*: (1) interaction of turbulent boundary layer with the edge, and (2) forces due to wake vortices acting on the edge. By analysis of the problem in terms of dimensionless groups of parameters and application of empirical data, they have derived the following prediction expression for the overall acoustic power level:

$$L_{W(OA)} \approx \chi + 10 \log (\delta w U^6) - 5 \tag{20}$$

where $L_{W(OA)}$ = overall acoustic power level (dB, re 10^{-12} watts)

w = spanwise dimension of edge (ft)

U = free-stream velocity (ft/sec)

δ = boundary layer thickness or wake thickness (ft)

$\chi = \begin{cases} -27 \text{ dB for boundary layer/edge interaction} \\ -23 \text{ dB for wake vortex effect.} \end{cases}$

The corresponding octave band spectra (Ref. 13) may be obtained from Figs. K3 and K4.

The turbulent boundary layer thickness δ at the trailing edge of an airfoil depends on the angle of attack, the surface condition of the airfoil, and the smoothness of the inflow.

---

*No corresponding leading edge studies have been undertaken, but because the pressure fluctuations at the trailing edge generally exceed those at the leading edge when the inflow is undisturbed, trailing edge noise tends to dominate.

Unless one has better information, one may estimate δ from the corresponding value for a smooth flat plate, for which

$$\delta \approx 0.4 \, b^{4/5} \, (\nu/U)^{1/5} \tag{21}$$

where δ and the chord b are in units of ft, ν represents the kinematic viscosity of the air (ft^2/sec) and U is the free-stream velocity (ft/sec).

The wake thickness δ_W also depends strongly on the condition of the airfoil. For thin tapered-edge airfoils at small angles of attack one may estimate δ_W as the sum of the airfoil edge thickness and 2δ. For airfoils at considerable angles of attack (say, $|\alpha| > 5°$), one may estimate δ_W from

$$\delta_W \approx b \, \sin\alpha \tag{22}$$

where b is the chord length. Note that narrow-band wake noise seldom occurs for $|\alpha| > 5°$, and only boundary layer/edge inter-action noise is significant for such cases.

ESTIMATION SCHEME

Flow Over Fuselage

In order to estimate the broad-band noise produced by turbu-lent flow over a fuselage (or similar body), one may proceed as follows:

1. Divide the fuselage into a number of convenient regions over which the boundary layer is relatively uniform.

2. For each region,

    (a) Determine the boundary layer displacement thickness δ^* by using available aerodynamic data or estimating on the basis of

    $$\delta^* = 0.0025 \, X$$

    where X represents the distance from the aircraft nose to the middle of the region. Then calculate the actual frequencies f that correspond to the reduced frequen-cies $f\delta^*/U$ shown along the horizontal axis of Fig. K2.

(b) Determine the corresponding octave band sound power level $L_{w(OB)}$ by adding*

$$51 + 20 \log q \ (lb/ft^2) + 10 \log A \ (ft^2)$$

to the numbers shown along the vertical coordinate of Fig. K2.

4. Combine the octave-band levels for all regions (band by band), by the method discussed in the main text and Fig. 1 of the main text.

Flow Over Airfoils

In order to estimate the noise produced by flow over airfoils, proceed as follows:

1. Find the (broad-band) noise due to turbulent flow by

(a) Estimating the boundary layer thickness δ at the trailing edge, either from aerodynamic data or by use of Eq. (21)

(b) Calculating the overall acoustic power level from Eq. (20), with $\chi = -27$ dB

(c) Determining the octave-band spectrum by use of Fig. K3.

2. Find the (essentially pure-tone) noise associated with vortex shedding by

(a) Estimating the wake thickness, either from aerodynamic data or from

$$\delta_W = \begin{cases} \delta_{te} + 2\delta & \text{for } |\alpha| < 5° \\ b \sin\alpha & \text{for } |\alpha| > 5° \end{cases}$$

---

*By combining Eqs. (11), (13) and (17), taking $\rho = 0.07 \ lb/ft^3$ and $c = 1100 \ ft/sec$, and using the standard definitions and reference value for power level, one finds that

$$L_w = 10 \log [1.3 \times 10^5 \ q^2 \ (lb/ft^2) \ A \ (ft^2)] + 20 \log [p_{OB}/p_{OA}]$$

where δ_W represents the airfoil's trailing edge thickness. (Note that vortex noise occurs only very rarely for $|\alpha| > 5°$.)

(b) Calculating the overall acoustic power level from Eq. (20), with $\chi = -23$ dB.

(c) Determining the octave-band spectrum by use of Fig. K4. (For aural detection estimation, use the value at $f\delta_W/U \approx 0.2$ as a pure tone, and consider remainder of spectrum as broad-band noise.)

3. If the (predominantly low-frequency) noise due to flight through large-scale turbulence is of concern, estimate this noise for a specified turbulence spectrum $u_{rms}(f)/U$ by

(a) calculating the fluctuating lift and drag forces from Eq. (19)

(b) using Eq. (18) and $L_w = 10 \log (W/W_{ref})$ to determine the sound power level at each frequency.

REFERENCES FOR APPENDIX K

1. Chandiramani, K.L., "Fundamentals Regarding Spectral Representation of Random Fields--Application to Wall-Pressure Field Beneath a Turbulent Boundary Layer," BBN Report No. 1728, (15 September 1968).

2. Ffowcs-Williams, J.R. and R.H. Lyon, "The Sound Radiated from Turbulent Flows near Flexible Boundaries," BBN Report No. 1054, Contract Nonr 2321(00) (August 1963).

3. Corcos, G.M., "The Structure of the Turbulent Pressure Field in Boundary-Layer Flows," *J. Fluid Mech.*, **18**, pp. 353-353-378 (March 1964).

4. Corcos, G.M., "Resolution of Pressure in Turbulence," *JASA*, **35**, pp. 192-199 (1963).

5. Willmarth, W.W. and C.E. Wooldridge, "Measurement of the Fluctuating Pressure at the Wall beneath a Thick Turbulent Boundary Layer," *J. Fluid Mech.*, **14**, pp. 187-210 (1962).

6. Bull, M.K., *et al.*, "Wall Pressure Fluctuations in Boundary Layer Flow and Response of Simple Structures to Random Pressure Fields," University of Southampton AASU Report 243, (July 1963).

7. Bies, D.A., "A Review of Flight and Wind Tunnel Measurements of Boundary Layer Pressure Fluctuating and Induced Structural Response," NASA CR-626 (1966).

8. Chandiramani, K.L., S.E. Widnall, R.H. Lyon and P.A. Franken, "Structural Response to Inflight Acoustic and Aerodynamic Environments," BBN Report No. 1417 (July 1966). Prepared for NASA Marshall Space Flight Center.

9. Clark, F.J.F. and H.S. Ribner, "Direct Correlation of Fluctuating Lift and Radiated Sound for an Airfoil in Turbulent Flow," *J. Acoust. Soc. Am.*, **46**, 3 (Part 2), (1969).

10. Sharland, I.J., "Sources of Noise in Axial Flow Fans," *J. Sound and Vibration*, I(3), (1964).

11. Hayden, R.E., "Sound Generation by Turbulent Wall Jet Flow over a Trailing Edge," M.S. Thesis, Purdue University (1969).

12. Hayden, R.E., Paper FF-10 with R.C. Chanaud, 1970 Spring Meeting of the Acoustical Society of America, Atlantic City, New Jersey.

13. Chanaud, R.C. and R.E. Hayden, "Edge Sound Produced by Two Turbulent Wall Jets," Paper FF-11, 1970 Spring Meeting of the Acoustical Society of America, Atlantic City, New Jersey.

157
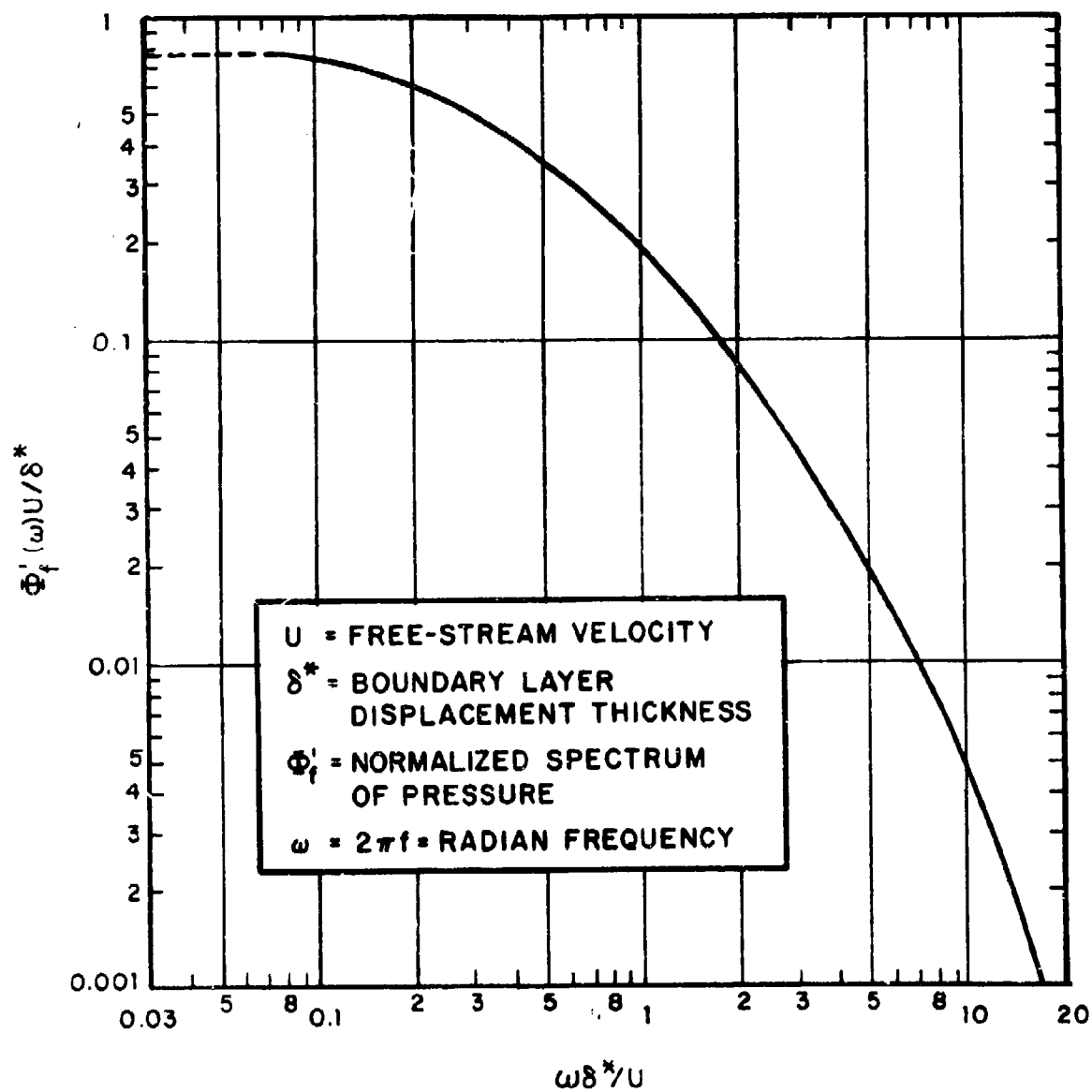
FIGURE K1   NORMALIZED FIXED-TRANSDUCER SPECTRUM OF PRESSURE
FIELD UNDER TURBULENT BOUNDARY LAYER
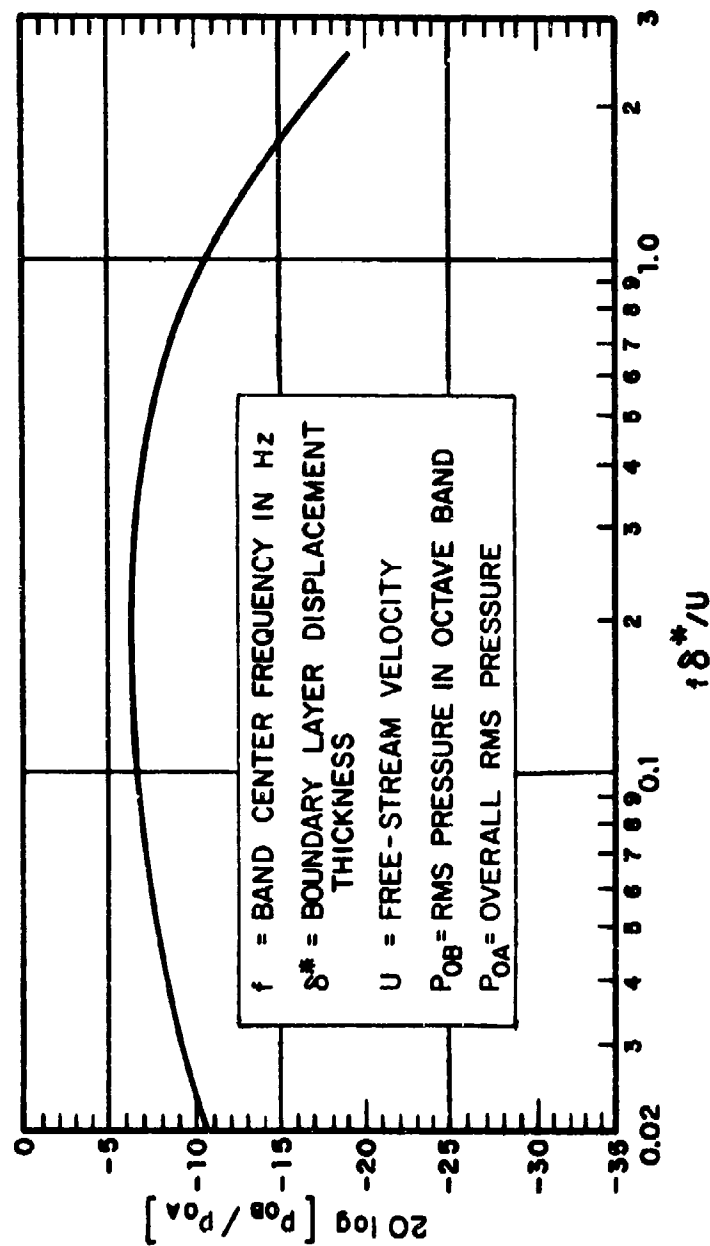
FIGURE K2   NORMALIZED OCTAVE AND THIRD-OCTAVE BAND SPECTRUM OF BOUNDARY
LAYER PRESSURE FLUCTUATIONS

f = BAND CENTER FREQUENCY IN Hz

δ^* = BOUNDARY LAYER DISPLACEMENT THICKNESS

U = FREE-STREAM VELOCITY

P_{OB} = RMS PRESSURE IN OCTAVE BAND

P_{OA} = OVERALL RMS PRESSURE

$f\delta^*/U$

$20 \log \left[P_{OB}/P_{OA} \right]$

FIGURE K3   EDGE NOISE SPECTRUM FOR TURBULENT BOUNDARY LAYERS
FLOWING OVER A TRAILING EDGE
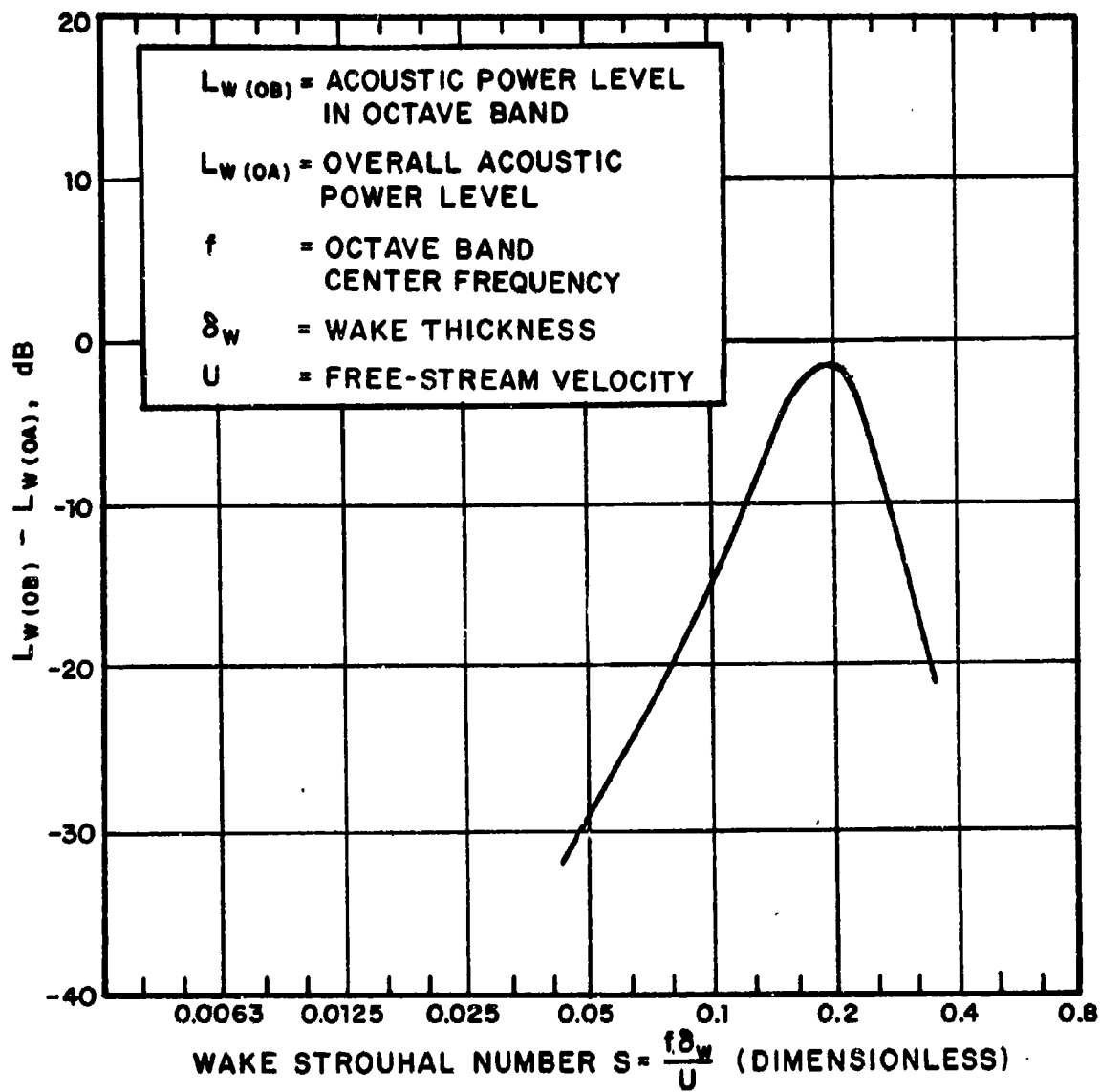
FIGURE K4   WAKE NOISE SPECTRUM FOR AIRFOILS AT SMALL ANGLES OF
ATTACK

161

APPENDIX L

SOUND RADIATION FROM BEAM-REINFORCED
PLATES EXCITED BY POINT FORCES

INTRODUCTION

An unsteady force applied to an aircraft structure (e.g., to a stringer or directly to the skin), sets this structure into motion, and such motions lead to the radiation of sound. This section presents an approach toward estimating the sound radiated from typical aircraft structures excited by a normal point force.

Aircraft surface structures typically consist of a thin skin, reinforced at intervals by stringers, rings, frames, etc. For the present approximate prediction purposes it suffices to consider all such structures as thin flat plates with straight reinforcing beams, and to address the two simplest and most significant corresponding sound radiation problems. Accordingly, the following paragraphs deal with sound radiation from beam-reinforced plates excited by oscillating localized (point) forces, which act normal to the plane of the plate, either on the skin or on a reinforcing beam.

POWER INPUT FROM POINT FORCE

Admittance of Beam-Plate System

The point input admittance Y_c of a system which consists of an infinitely long uniform reinforcing beam connected continuously all along its length to a uniform plate of infinite extent is given (Ref. 1) by

$$Y_c = Y_b - \frac{1}{\pi \beta_I \omega m_b} \left[1 + \frac{(3-r^2)\cos^{-1}r + (3+r^2)\sinh^{-1}r}{2r^3(1-r^2)^{1/2}} \right]. \quad (1)$$
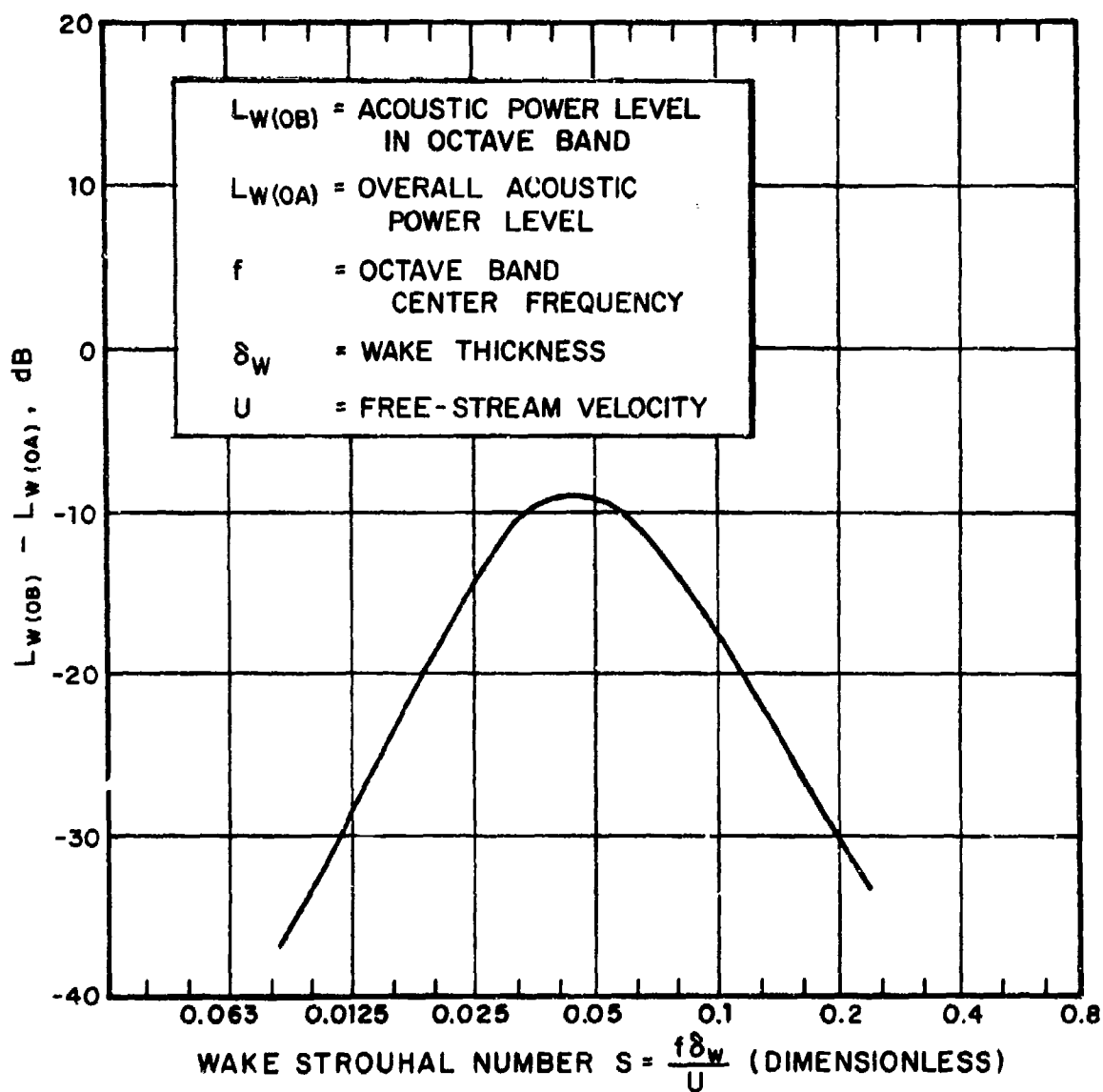
This expression applies for the simplest case in which the exciting force is so located and the beam section is of such a shape that the beam does not twist as it flexes. The first term,

$$Y_b = [2m_b c_b(1+i)]^{-1} \quad (2)$$

represents the point input admittance of the beam in absence of
the plate, whereas the rest represents the contribution due to
the plate. The symbols employed in the foregoing relations have
the following definitions:

$\omega = 2\pi f$ = radian frequency

m_b = mass per unit length of beam

$\beta_I = B/D \approx 12I/h^3$

$r = c_p/c_b = \sqrt{h/\alpha_I}$

$B = EI$ = bending stiffness of beam

$D \approx Eh^3/12$ = flexural rigidity of plate

E = Young's modulus

I = centroidal moment of inertia of beam cross-section

h = plate thickness

$c_p = [\omega h c_L/\sqrt{12}]^{1/2}$ speed of bending waves in plate

$c_b = \sqrt{\omega \alpha_I c_L}$ = speed of bending waves in beam

$c_L = \sqrt{E/\rho_s}$ = longitudinal wave velocity

ρ_s = density of material of beam and plate

α_I = radius of gyration of beam cross-section

Admittance of Plate

The point input admittance of an infinite plate is given
(Ref. 2) by

$$Y_p = \left[8\sqrt{Dm_p}\right]^{-1} \approx \left[\frac{4h^2}{\sqrt{3}}\sqrt{E\rho_s}\right]^{-1} = \left[\frac{4}{\sqrt{3}}h^2\rho c_L\right]^{-1} \tag{3}$$

where m_p is the mass per unit area of the plate. This expression
also represents the frequency-average of the admittance of a
finite plate, provided that the averaging interval encompasses
several resonances (Ref. 3).

Power Input

The power W_{in} supplied to a system by an oscillating force
of amplitude F depends only on the real part of the input admit-
tance Y,

$$W_{in} = \frac{1}{2}|F|^2 \text{Re}(Y) ; \tag{4}$$

hence one obtains

$$W_{in} = \begin{cases} |F|^2/8m_b c_b & \begin{array}{l}\text{for excitation on beams of} \\ \text{beam-plate systems}\end{array} \\ |F|^2/16\sqrt{Dm_p} & \text{for excitation plates}\end{cases} \qquad (5)$$

EXCITATION ACTING ON BEAM OF BEAM-PLATE SYSTEM

Components

The sound radiation here may be considered as composed of three parts:

(1) radiation from the vicinity of the excitation point (near-field radiation),

(2) radiation from waves propagating along the beam, and

(3) radiation from reverberant vibration field on the plate.

Near-Field Radiation

The acoustic power radiated by the near-field in the vicinity of the excitation point may be approximated (Ref. 7) by

$$W_1 \approx 0.34(\lambda_c + w)\rho c \lambda_b v^2 \qquad (6)$$

where $\lambda_c \approx \pi h c_L/\sqrt{3}$ c = flexural wavelength of plate at critical frequency

$\lambda_b = c_b/f$ = bending wavelength of beam

w = width of beam

ρ = density of ambient air

c = speed of sound in ambient air

v = velocity amplitude at excitation point.

With $v = F|Y_c|$ and Y_c as given by Eq. (1),one may then readily determine the power W_1.

Radiation from Waves Propagating along Beam

Because reinforcing beams typically are strongly coupled to the plate, energy in waves travelling along the beam tends to be transmitted into the plate within a relatively short distance. Therefore radiation from these propagating waves tends to be negligible.

Radiation from Plate; Estimation Scheme

The plate flexural wavenumber in the direction parallel to the beam is equal to the wavenumber $k_b = \omega/c_b$ for waves on the beam. This wavenumber component is small compared to the (total) wavenumber $k_p = \omega/c_p$ for free bending waves on the plate. Therefore, free plate flexural waves propagate in directions nearly perpendicular to the beam (Ref. 4).

If the plate is infinite and if $c_p < c$, the free flexural waves radiate no sound at all; if $c_p > c$, they radiate well. However, the plates in actual aircraft structures cannot be considered infinite, so that infinite-plate results here are relatively meaningless.

As plate waves propagate along a finite structure, they soon encounter beams, where they are partly reflected and partly transmitted. In any bay between reinforcing beams the initial and multiply-reflected waves build up a reverberant wave field, in which amplifications can occur as the result of resonance effects, and where sound is radiated because of interaction of the plate waves with the boundaries. In order to analyze this case most simply, one may make the very reasonable assumptions that all of the power supplied to the structure is transmitted to the plate, and that in the steady state the power input to the plate must equal the power lost by the plate.

The loss of power from a finite panel may be considered as consisting of two parts: acoustic radiation (W) and mechanical dissipation (W_d). Hence one may write an energy balance

$$W_{in} = 2W + W_d = A<v^2>(m_p \omega \eta + 2\rho c \sigma) \tag{7}$$

where A = area of plate (one side)

η = loss factor of plate

$<v^2>$ = mean-square velocity of plate

σ = acoustic radiation efficiency.

The factor 2 appears in the above equation, because acoustic energy generally is radiated from both sides of a plate. The acoustic power radiated from one side may then be written as

$$W = A<v^2>\rho c \sigma = \frac{W_{in}}{2 + \dfrac{m_p \omega \eta}{\rho c \sigma}} \tag{8}$$

where the second form was obtained by use of Eq. (7). W_{in} may be calculated from Eq. (5).

EXCITATION ACTING ON PLATE

If a force acts on a finite plate, there again results a reverberant flexural wave field on the plate, as previously discussed. Whereas the plate wave field due to excitation on a beam tends to consist primarily of wave components propagating perpendicular to the beam, that due to point excitation directly on the plate tends to be more homogeneous in direction.

However, the same energy balance considerations apply here as before, so that Eq. (8) applies for the present case as well; the only difference is that W_{in} and σ_{rad} are different for the two excitation conditions. W_{in} here is given by Eq. (5), and σ_{rad} here is computed on the basis of the entire plate perimeter (see Fig. L1).

ESTIMATION OF LOSS FACTOR AND RADIATION EFFICIENCY

Loss Factor

In spite of considerable effort that has been expended on the problem, there still exists no reliable general means for predicting the loss factor η of realistic aircraft structural panels. Some such prediction means are suggested in Ref. 5, but for structures which are as complex as those in actual aircraft, these prediction means are not much more reliable than simply assuming $\eta \approx 0.01$.

Radiation Efficiency

The acoustic radiation efficiency σ_{rad} of beam-reinforced plates has been analyzed in Refs. 3 and 6 and is also discussed in text books (Refs. 4, 7). Figure L1 summarizes the dependence of σ_{rad} of a finite panel on frequency and the various panel parameters and may be used to estimate σ_{rad}.

ESTIMATION SCHEME

In order to estimate the sound radiated from a panel excited by an oscillatory point force of amplitude $|F|$ acting either directly on the panel or on a reinforcing beam (or rib) at the panel's edge, one may proceed as follows:

1. Use Fig. L1 to estimate the radiation efficiency, as a function of frequency. This is best done by calculating the values of the various parameters indicated in the figure and plotting a graph like that in Fig. L1, based on those values.

2. Find the power input W_{in} from the appropriate form of Eq. (5).

3. Calculate the radiated power W (at each frequency) from Eq. (8) (using the structural loss factor value $\eta \approx 0.01$ unless better information is available) and determine the sound power level from $L_W = 10 \log (W/W_{ref})$.

REFERENCES FOR APPENDIX L

1. Lamb, G.I., Jr., "Input Impedance of a Beam Coupled to a Plate, *J. Acoust. Soc. Am.* **33**, 5, pp. 628-633 (1961).

2. Ungar, E.E., "Mechanical Vibrations," Chapt. 6 of *Mechanical Design and Systems Handbook*, Ed. by H.A. Rothbart, McGraw-Hill Book Co., Inc., New York (1964).

3. Smith, P.W., Jr., and R.H. Lyon, "Sound and Structural Vibration," NASA CR-160 (March 1965).

4. Cremer, L. and M. Heckl, *Körperschall*, Springer Verlag (1967).

5. Ungar, E.E., "Damping of Panels," Chapt. 14 of *Noise and Vibration Control*, Ed. by L.L. Beranek, McGraw-Hill Book Co., Inc., New York (1971).

6. Maidanik, G., "Response of Ribbed Panels to Reverberant Acoustic Fields," *J. Acoust. Soc. Am.* **34**, 6, pp. 809-826 (1962).

7. Ver, I.L. and C.H. Holmer, "Interaction of Sound Waves with Solid Structures," Chapt. 11 of *Noise and Vibration Control*, Ed. by L.L. Beranek, McGraw-Hill Book Co., Inc., New York (1971).
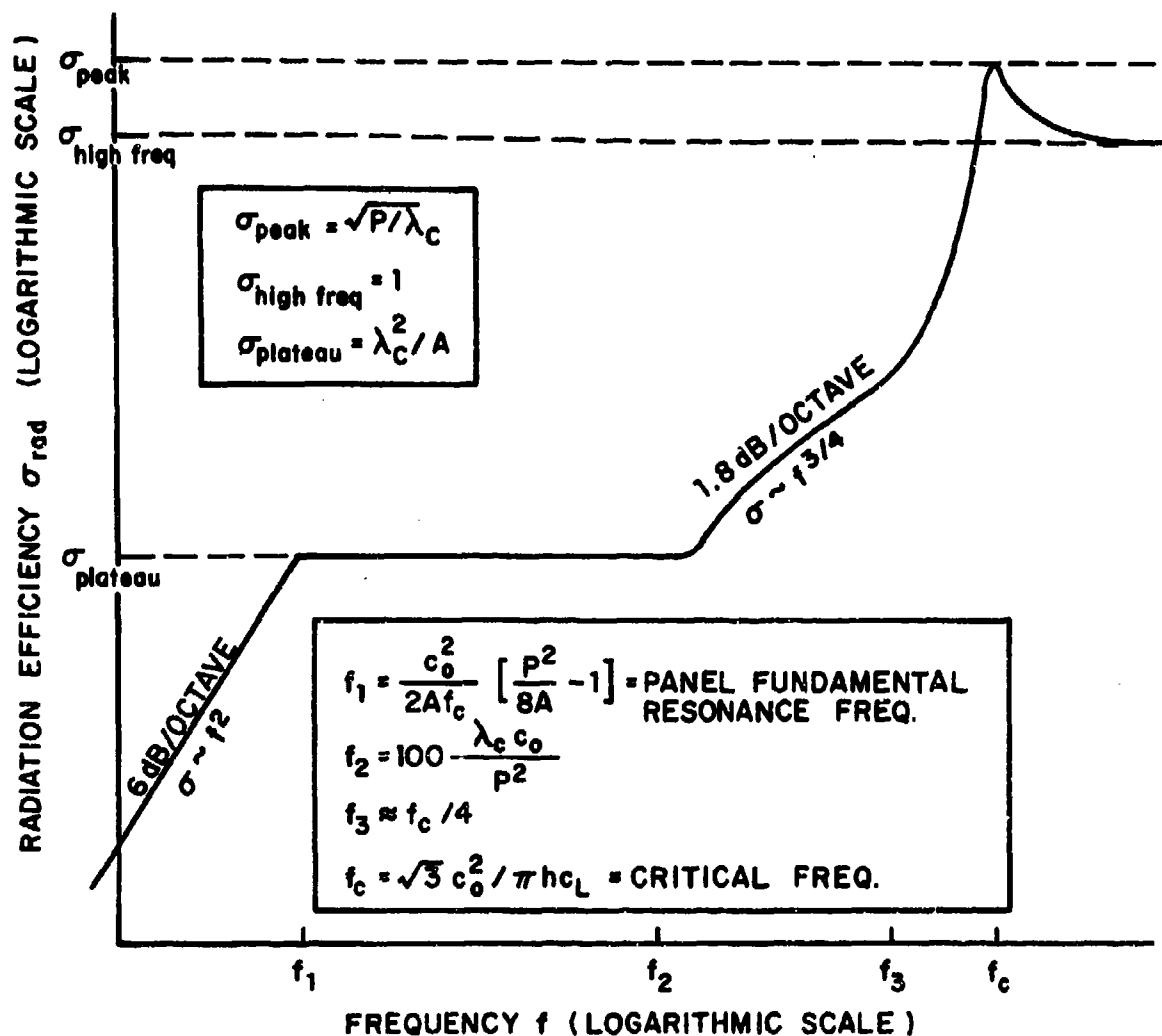
P = EFFECTIVE PERIMETER OF PANEL*

$\lambda_c = c_0/f_c$ = PANEL FLEXURAL WAVELENGTH AT CRITICAL FREQUENCY

A = PANEL AREA (ONE SIDE)

c_L = LONGITUDINAL WAVE VELOCITY IN PANEL MATERIAL

c_0 = SPEED OF SOUND IN AMBIENT AIR

h = PANEL THICKNESS

* FOR EXCITATION ON PANEL, P = ACTUAL PANEL PERIMETER
   FOR EXCITATION ON BEAM   P = 2·(LENGTH OF EXCITED EDGE BEAM)

FIGURE L1   ESTIMATION OF ACOUSTIC RADIATION EFFICIENCY OF PANELS

160

APPENDIX M

ATMOSPHERIC PROPAGATION EFFECTS

INTRODUCTION

The aural detectability of an aircraft is determined not only by the acoustic characteristics of the source and by the acoustic environment and sensitivity of the receiver, but also by the propagation characteristics of the intervening atmosphere. This section summarizes the propagation effects which may affect the detectability of a small "quiet" aircraft approaching a ground observer at an altitude of a few hundred feet. The slant ranges of interest here are of the order of a few thousand feet, and the angles of elevation θ_e typically are small (usually less than 20°).

Most of the available literature on sound propagation is concerned with either overhead flight ($\theta_e > 20°$) of aircraft or with ground-to-ground propagation ($\theta_e = 0°$). For the case of overhead flight, only the effects of spreading and atmospheric absorption are significant. For ground-to-ground propagation, the effects of ground absorption and atmospheric refraction must also be considered and may, in fact, make the principal contribution to attentuation.

One may consider two types of propagation factors: (1) "predictable" factors, which occur at all times and at all locations, and (2) "variable" factors, which vary with time and location. The predictable factors include spreading and atmospheric absorption; spreading is independent of all meteorological variables, and absorption can be predicted from given temperature and humidity profiles. The variable factors include terrain attenuation, attenuation due to turbulent scattering, attenuation by fog and rain, focusing and formation of shadow zones by refraction; all of these depend on the local terrain and/or prevailing meteorological conditions.

In addition to attenuating an acoustic signal, propagation effects may alter the acoustic "signature" (i.e. the waveform, spectrum, or time-variation of the spectrum) of a source. Although this consideration is of greater importance for helicopter audibility than for quiet aircraft, it will also be considered here briefly.

"PREDICTABLE" EFFECTS

Spreading Loss

The energy from an acoustic source spreads over an increasing area as it propagates away from the source. This spreading results in a decrease in the acoustic intensity with increasing distance from the source, or in "spreading loss" ΔL_s which obeys

$$\Delta L_s (dB) = 20 \log (R/R_0) \tag{1}$$

where R represents the range from the source to the observation point and R_0 represents the range to a reference point (usually at unit distance from the source). ΔL_s thus indicates how much reduction in the acoustic pressure one measures as the result of moving the observation point from R_0 to R.

Atmospheric Absorption

Atmospheric absorption is usually described in terms of an absorption coefficient α, which generally is measured in units like dB/1000 ft and accounts for "excess attenuation" beyond that due to spreading. The classical absorption coefficient α_{cl} accounts for losses due to viscosity, heat conduction, heat radiation and diffusion; it is negligible at frequencies below several kHz. The molecular absorption coefficient α_{mol} accounts for absorption of energy from the sound field by internal modes of the gas molecules, and is negligible at frequencies up to several hundred Hz.

The vast literature on this subject has been discussed in a recent review (Ref. 1) and empirically derived corrections have been added to the theoretical results, resulting in formulae which match the available data almost perfectly. The results are outlined below and are illustrated in Fig. M1.

The classical absorption coefficient at a temperature of 59°F obeys

$$\alpha_{cl}(dB/1000 \text{ ft}) = 5.3 \times 10^{-2}(f/1000)^2 \tag{2}$$

where f represents the frequency in Hz. This absorption coefficient is independent of humidity and increases by about 1% for each 20°F increase in temperature.

171

The molecular absorption coefficient is given by

$$\alpha_{mol}(\text{dB}/1000 \text{ ft}) = a_{max}\left\{\left[0.18\,\frac{f}{f_m}\right]^2 + \left[\frac{2(f/f_m)^2}{1+(f/f_m)^2}\right]^2\right\}^{1/2} \tag{3}$$

where $a_{max} = 0.0078\, f_m(T^*)^{-2.5}e^{7.77(1-1/T^*)}$

$f_m = (10 + 6600\, h + 44,400\, h^2)P^*/(T^*)^{0.8}$

$h_0 = \dfrac{h'}{7.57}\,\dfrac{T^*}{P^*} = $ Percent Mole Ratio

$h' = $ humidity (gm/m^3)

$P^* = P_0/P_{00}$

$T^* = T/T_o$

$P_0 = $ atmospheric pressure (psi)

$P_{00} = $ reference atmospheric pressure = 14.7 psi

$T = $ absolute temperature ($^\circ$R)

$T_o = $ reference temperature = 519°R

$f = $ frequency (Hz)

This relation is plotted in Fig. M1 for the particular temperatures 20°, 59° and 100°F. Examination of the curves reveals that for a tropical climate (temperature approaching 100°F., humidity greater than 40%) the coefficient may be approximated rather precisely by

$$\alpha_{mol}(\text{dB}/1000 \text{ ft}) = 2(f/1000) \tag{4}$$

where f again represents the frequency in Hz.

"VARIABLE" EFFECTS

Focusing

The possibility of anomalously high intensities over distant regions has been a subject of great interest in the study of ground-to-ground propagation of rocket launch noise. When wind and temperature profiles are favorable, propagation gains of around 15 dB at all frequencies may be observe. relative to normally observed levels. Such gains occur when the effective sound velocity decreases with height up to a certain altitude and then increases with height above that.

In general, the probability that focusing will decrease the aural detection range of small low-flying aircraft is small, for the following reasons:

1. Even for ground-to-ground propagation, the conditions for focusing occur rarely. (For example, in static firings of a rocket at NASA's Marshall Space Flight Center, focusing occurred only in about 13% of the cases. Ref. 2) As the source is raised, the probability of focus formation is decreased.

2. For ground-to-ground propagation, the distance to a focal region is rarely less than two or three miles (Ref. 2). Any air-to-ground focal regions would occur at even greater distances. If an aircraft is detected under non-focusing conditions at a distance of the order of a mile or less, then some signal enhancement at a distance of several miles will be of little concern, because it will largely be cancelled by the increased spreading and absorption losses.

If low-altitude flights are envisioned in areas where the meteorological conditions may present an appreciable probability of focusing, then it may be worthwhile to obtain meteorological data in order to minimize this probability. Often appropriate choices of aircraft approach azimuth may be available to minimize the probability of focusing in the target area. (See Ref. 2.)

Terrain Attenuation

For low angles of elevation, additional attenuation may be provided by ground cover. Reference 3, which reports measurements of ground-to-ground propagation through a jungle in Panama is the classical paper on this subject. The principal results are shown in Fig. M2.

The important question for aircraft detectability considerations is how these results are affected as the source elevation is increased. A number of studies indicate that terrain attenuation decreases monotonically with source height and becomes negligible at an elevation angle of around 6°. For example, Parkin and Scholes (Ref. 4) found that the attenuation of a helicopter at a range of 3000 ft began to increase rapidly as it descended below 300 ft height. Hubbard and Maglieri (Ref. 5) found that the detectability of a single-propeller aircraft decreased substantially with decreasing elevation angle and attributed this to the increased terrain attenuation; they also conducted a number of measurements to determine the functional dependence of the terrain loss coefficient on elevation angle (Fig. M3). Loewy (Ref. 6) has attempted to develop a general procedure to account for the effect of elevation angle, but his procedure appears to be based on insufficient information and has not been validated.

Although a great deal of work remains to be done before reliable quantitative predictions can be made, it is clear qualitatively that the aural detectability of an aircraft can be reduced by flying along a path along which the ground attenuation is high (e.g., where there is heavy foliage), and/or by flying at as low an altitude as possible. If a choice is available, detectability can be decreased by approaching the receiver on an azimuth along which the foliage is heaviest. For low-altitude flight over a forest or jungle, terrain attenuation may far outweigh the combined effects of spreading and atmospheric absorption.

Attenuation Due to Turbulent Scattering

At low frequencies, additional attenuation may be caused by scattering from turbulent fluctuations in the wind and temperature field. For isotropic turbulence, the scattering attenuation coefficient is proportional to frequency and to the gustiness (i.e., the root-mean-square wind speed fluctuation, divided by the mean wind speed).

For an rms wind fluctuation of one m/sec, Horiuchi (Ref. 7) has estimated the attenuation coefficient to be on the order of .002 f dB/1000 ft. Based on experiments conducted at the Marshal Space Flight Center, the following suggested *minimum* values were obtained for the average meteorological conditions prevailing there (Ref. 1):

$$\alpha_{scat}(dB/1000 \text{ ft}) = 0.03 \text{ for } f < 7 \text{ Hz}$$

$$= 0.0042f \text{ for } 7 < f < 60 \text{ Hz}$$

$$= 0.25 \text{ for } 60 < f < 200 \text{ Hz}$$

At these low frequencies, the attenuation due to turbulent scattering may be greater than that due to absorption; at higher frequencies, absorption effects tend to predominate.

Shadow Zones

Refraction by wind and temperature gradients can sometimes lead to "shadow zone" regions in which the sound levels are greatly reduced. The distance X_s to the beginning of the shadow zone is given approximately by

$$X_s = \left[\frac{2h_s c}{du/dz}\right]^{1/2} \tag{5}$$

where h_s is the mean height of source and receiver, c is the sound velocity and du/dz is the gradient of effective sound velocity (Ref. 8). For purposes of minimizing detectability, one wishes to decrease X_s as much as possible. This can be accomplished by flying at low altitude into the wind. However, even for a reasonably large gradient of 0.01 ft/sec per ft, one obtains a shadow zone at a distance as large as about two miles, for a source height of 400 ft.

An ideal shadow zone occurs only in the limiting case of geometric acoustics (high frequencies). In practice, appreciable energy is diffracted and scattered into a shadow zone. Wave acoustics predicts an attenuation coefficient inside the shadow which is proportional to $f^{1/3}$ (Ref. 9) so that high frequencies are attenuated most.

Attenuation Due to Fog and Rain

The presence of suspended water droplets may cause additional attenuation through the mechanisms of viscous dissipation and heat conduction. The theoretical and experimental facts have been reviewed in Ref. 10. Attenuations on the order of 0.5 dB/1000 ft (increasing with frequency) may be obtained for propagation through heavy natural fogs. Analysis of measurements reported in Ref. 10 indicates that the effect of light rain on sound propagation is very small.

EFFECTS OF PROPAGATION ON PRESSURE SIGNATURES

Aircraft detectability may be increased by the **existence** of easily recognizable regularities in the acoustic (pressure vs. time) "signature" of the source. These regularities are of primary importance for helicopter detection (Ref. 6), but may also play a significant role for other types of aircraft. Therefore, a brief description of the effect of the propagation channel on acoustic signatures is also included here.

Random inhomogeneities in the refractive index cause frequency-dependent fluctuations in the amplitude and phase of acoustic waves. Expressions for these fluctuations have been derived by Tatarski (Ref. 11). The effect on the signal form can be determined by introducing these expressions into the spectral representation of the signal and then calculating a statistical average. This procedure has been carried out by Shirkova (Ref. 12). For simple wave forms, such as a rectangular pulse, he obtained analytical formulas for the distortion. The distortion of an arbitrary waveform can be calculated by numerical methods.

A major criticism of Shirokova's work is that he assumes a normal distribution for the correlation coefficient of the refractive index fluctuations. However, Tatarski has shown that a correlation proportional to the 2/3 power of distance provides a more accurate description of the fluctuations. Therefore, Shirokova's formulae should be revised to account for this.

In general, one may expect larger distortion of signal shapes when the conditions near the ground are unstable. Instability is usually characterized by gusty winds and superadiabatic lapse rates, which result in turbulence near the ground. Experimental evidence of this effect has been obtained by observing the distortion of pressure wave forms from sonic booms (Ref. 13). Early in the morning when conditions near the ground are generally stable, the wave forms closely resembled the theoretical "N" shape. In the afternoon when superadiabatic conditions prevail,

wide variations ranging from spiked to rounded signatures were
noted. In fact, the magnitude of the correlation coefficient
to be used in the formula discussed above can be expressed di-
rectly in terms of the gradients of wind and temperature near
the ground (Ref. 11).

ATTENUATION CALCULATIONS

Sound Pressure at a Given Range

The reference quantities for sound power level L_W and sound
pressure level L_p are such that the sound pressure level
$L_p(R_o = 1 \text{ ft})$ at 1 ft from a point source is related to the power
level of that source as (e.g., Ref. 14)

$$L_p(R_o) = L_W - 0.5 \text{ dB} \tag{6}$$

The sound pressure level at any range R from the source may then
be calculated from

$$L_p(R) = L_p(R_o) - \Delta L_p \tag{7}$$

where the total attenuation ΔL_p is given by

$$\Delta L_p = \Delta L_s + \alpha_{tot} \cdot R. \tag{8}$$

Here, ΔL_s represents the loss due to spreading and α_{tot} the ab-
sorption coefficient (in dB/unit distance) resulting from all
other effects.

By combining Eqs. (1) and (6)-(9) and expressing R in feet,
one obtains the sound pressure level $L_p(R)$ at a range of R ft
from a source with acoustic power level L_W as

$$L_p(R) = L_W - 20 \log R - \alpha_{tot}(\text{dB/ft}) \cdot R - 0.5 \tag{9}$$

Range for Given Sound Pressure

By substitution into the foregoing equation one may readily
determine the sound pressure that results at a given distance
from a given source. However, determining the range at which a
prescribed sound pressure is obtained from a given source is

more difficult, because Eq. (9) cannot be solved algebraically for R. Figure M4 has been prepared to facilitate the numerical solution of this inverse problem; it permits one to obtain a "corrected" value* R_c which corresponds to a given value of α_{tot} from the easily calculated "uncorrected" value R_u that one obtains from Eq. (9) for $\alpha_{tot} = 0$.

---

*The corrected and uncorrected ranges are related by

$$20 \log R_u = 20 \log R_c + \alpha_{tot} R_c$$

and, of course,

$$20 \log R_u = L_W - L_p - 0.5$$

where both L_W and L_p are given.

REFERENCES FOR APPENDIX M

1. Wyle Labs., *Sonic and Vibration Environments for Ground Facilities - A Design Manual*, Chapter 7, 1968.

2. Essenwanger, O., "Profile Types of Sound Speed in the Lower Atmosphere and their Relationships to Acoustic Focusing", U.S. Army Missile Command, Redstone Arsenal, Alabama, Report RR-TR-66-6, 1966.

3. Eyring, C.F., "Jungle Acoustics", *J. Acoust. Soc. Amer.* 18, 257 (1946).

4. Parkin, P.H. and W.E. Scholes, "Oblique Air-to-Ground Sound Propagation Over Buildings", *Acustica*, **8**, 99 (1958).

5. Hubbard, H.H. and D.J. Maglieri, "An Investigation of Some Phenomena Relating to Aural Detection of Airplanes", NACA TN-4337 (1958).

6. Loewy, R.G., "Aural Detection of Helicopters in Tactical Situations", *Am. Helicopter So. J.* **8**, 36 (1963).

7. Horiuchi, I., "Effects of Atmospheric Turbulence on the Propagation of Sound", ONR Technical Report (1953).

8. Ingard, U., "The Physics of Outdoor Sound", Proc. of the Fourth Annual National Noise Abatement Symposium (1953).

9. Pridmore-Brown, D.C. and U. Ingard, "Sound Propagation into the Shadow Zone in a Temperature-Stratified Medium above a Plane Boundary", *J. Acoust. Soc. Amer.* **27**, 36 (1955).

10. Bolt Beranek and Newman Inc., "Investigation of Acoustic Signalling Over Water in Fog", BBN Report No. 674 (1960).

11. Tatarski, V.I., *Wave Propagation in a Turbulent Medium*, Dover Publications (1961).

12. Shirkova, T.A., "The Variation in the Form of a Pulse Caused by the Effect of Random Inhomogenieties in a Medium", *Soviet-Physics-Acoustics* 9, 78 (1963).

13. Maglieri, D.J. and T.L. Parrott, "Atmospheric Effects on Sonic-Boom Pressure Signature", *Sound* 2, 11 (1963).

14. Peterson, P.G. and E.E. Gross, Jr., *Handbook of Noise Measurement*, General Radio Co., West Concord, Mass., 6th Edition, Sec. 2.8, 1967.
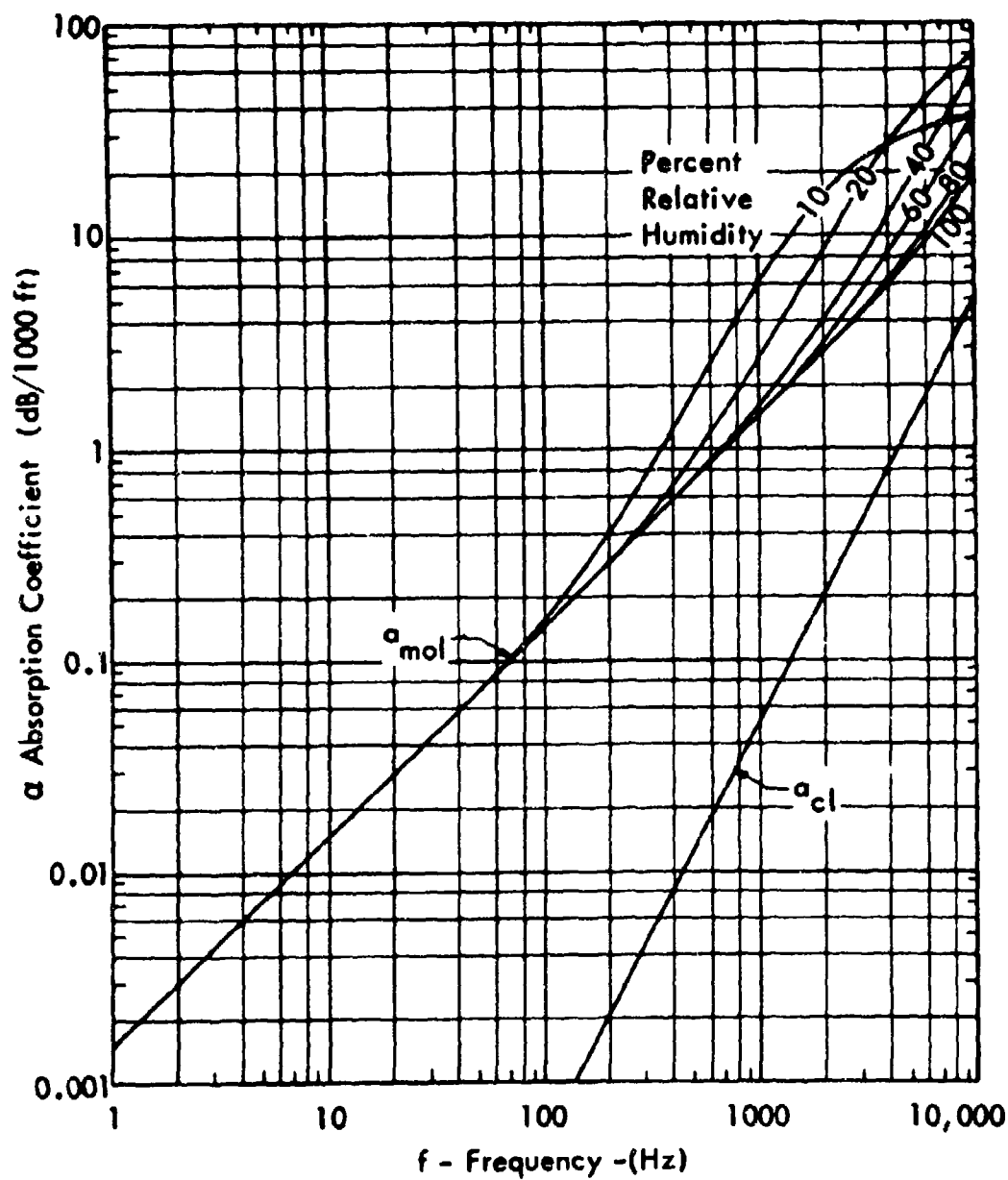
FIGURE M1a   VALUES OF AIR ABSORPTION COEFFICIENTS AT 59°F AND
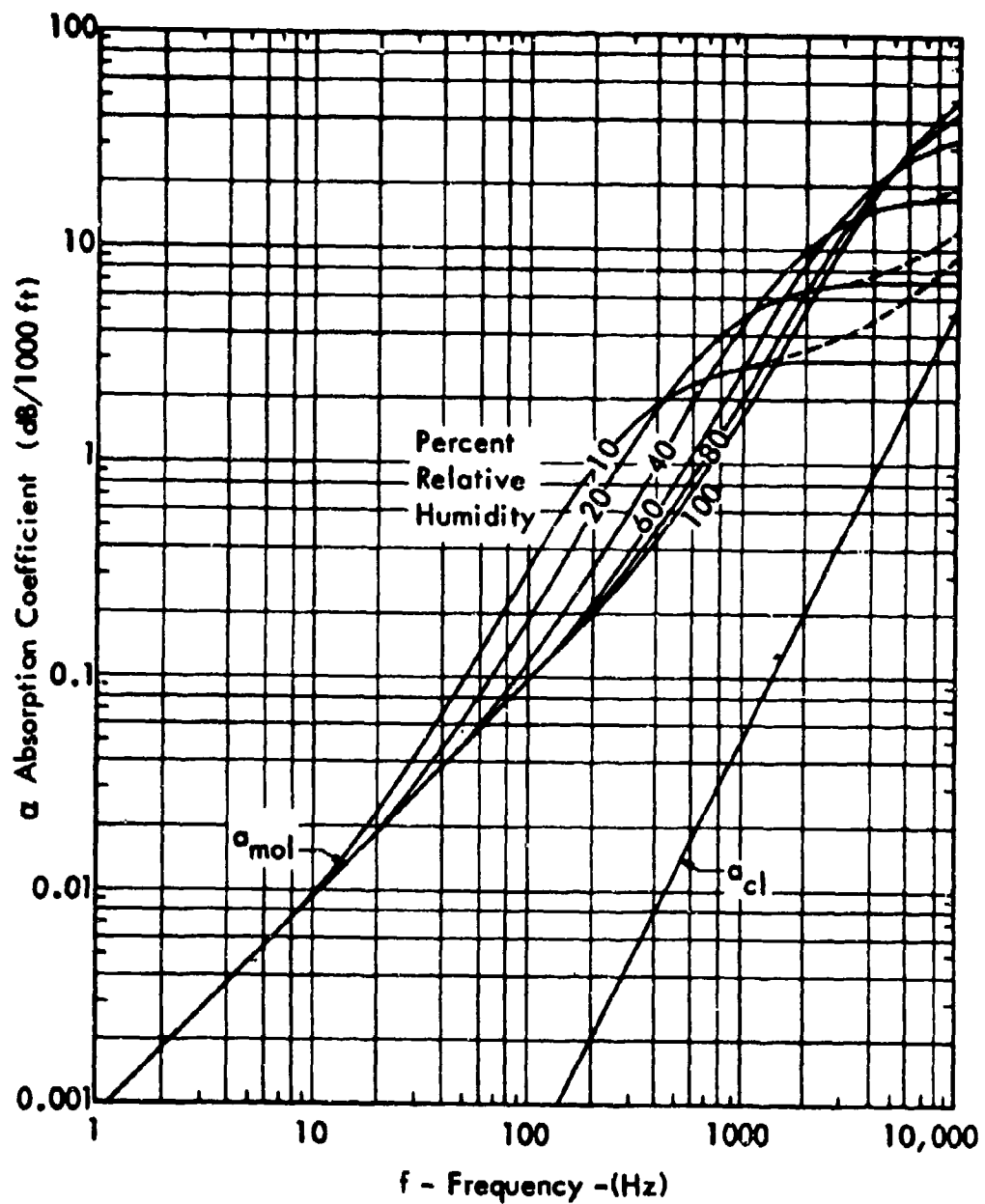VARIOUS RELATIVE HUMIDITIES (FROM REFERENCE 1)

FIGURE M1b   VALUES OF AIR ABSORPTION COEFFICIENTS AT 20°F AND
VARIOUS RELATIVE HUMIDITIES (FROM REFERENCE 1)
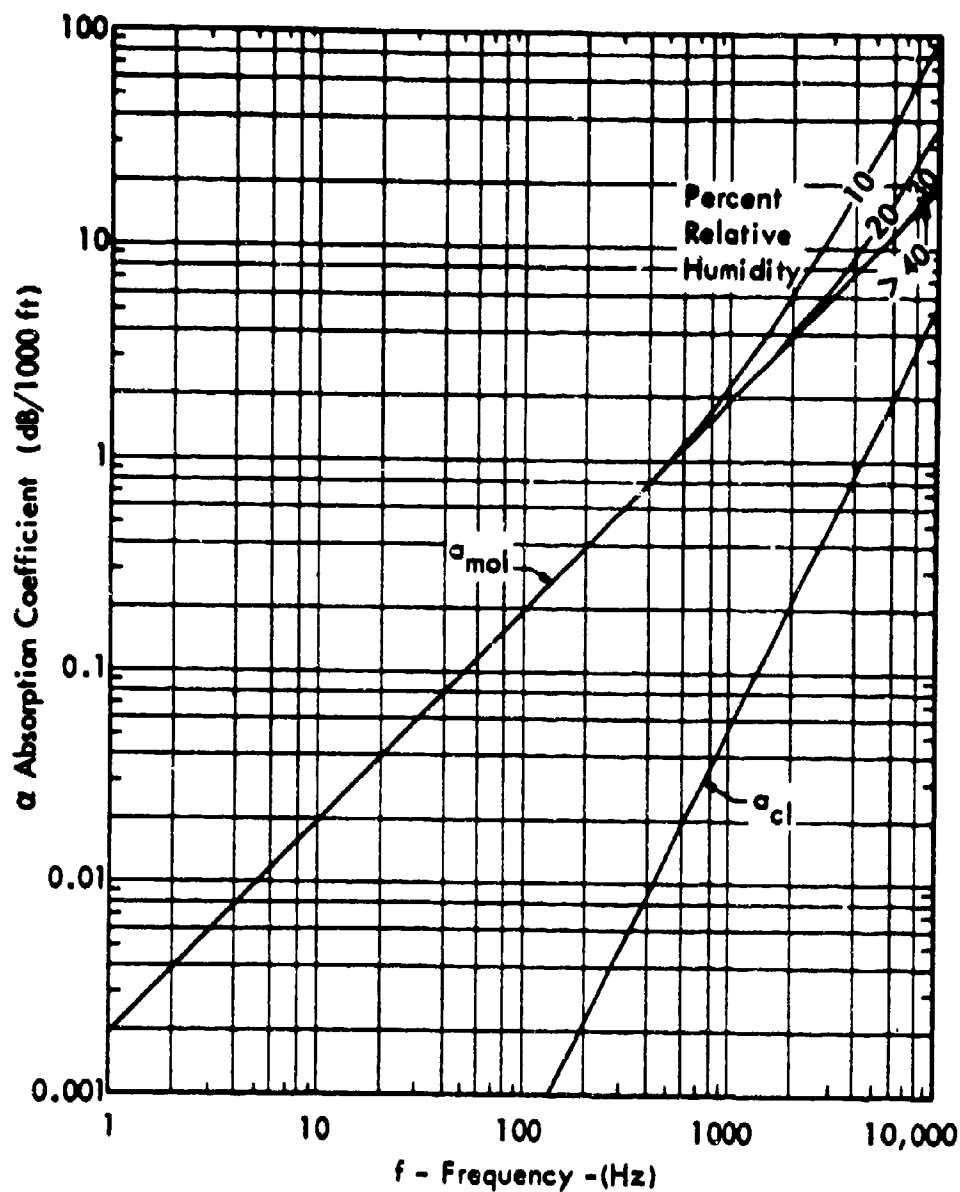
FIGURE M1c   VALUES OF AIR ABSORPTION COEFFICIENTS AT 100°F
AND VARIOUS RELATIVE HUMIDITIES (FROM REFERENCE 1)

FIGURE M2a   TERRAIN LOSS COEFFICIENTS FOR GRASS AREA. (A) OVER TERRAIN THINLY COVERED WITH SHORT (6-12IN.) GRASS; (B) OVER TERRAIN THICKLY COVERED WITH SHORT (18IN.) GRASS; (C) THROUGH A THICK STAND OF SHORT GRASS; (D) THROUGH SHRUBBERY AND OVER SHORT GRASS; (E) THROUGH THICK TALL (6FT.) GRASS (FROM REFERENCE 3)
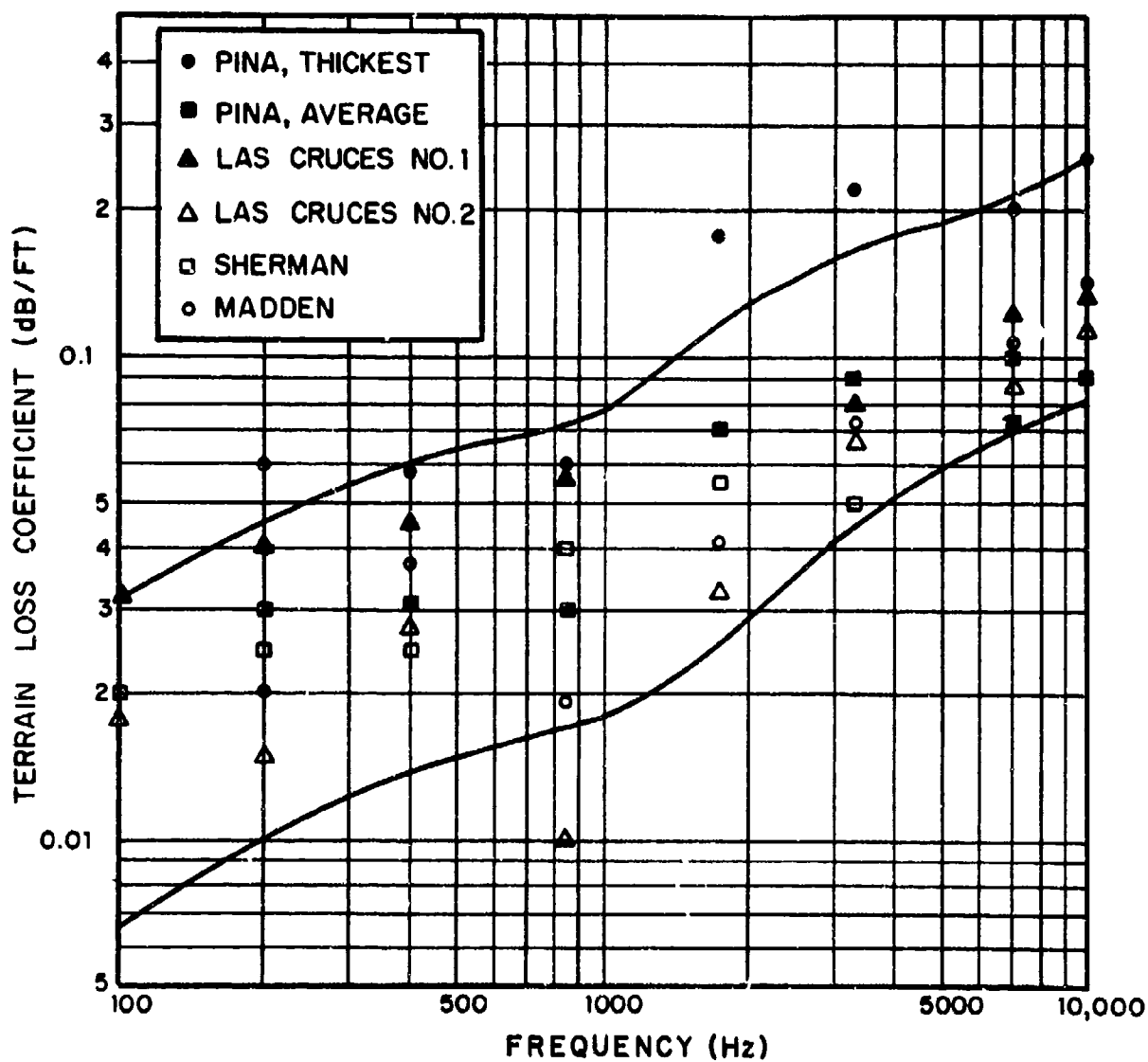
FIGURE M2b   TERRAIN LOSS FOR TROPICAL FOREST AREAS (FROM
REFERENCE 3)

184

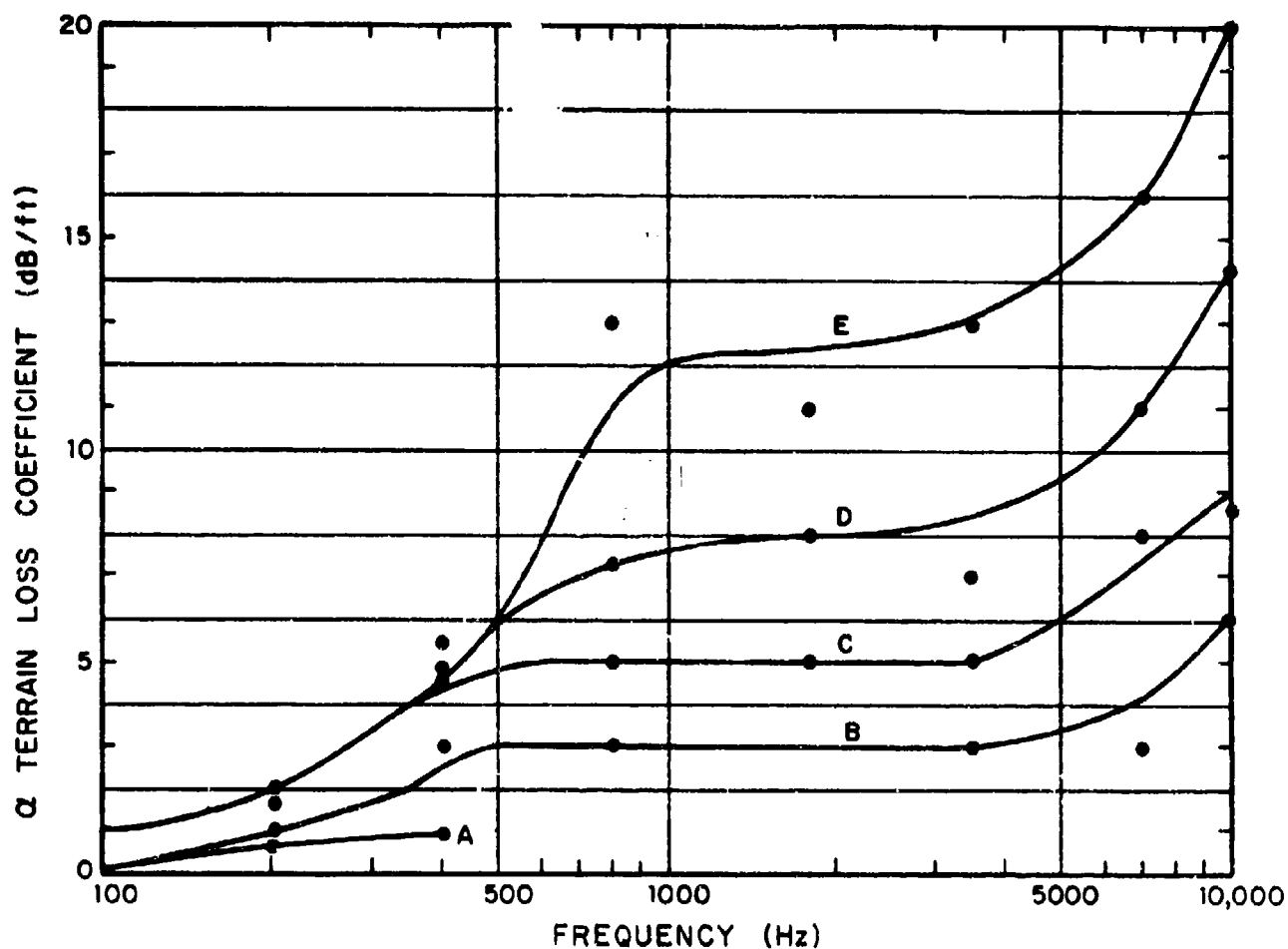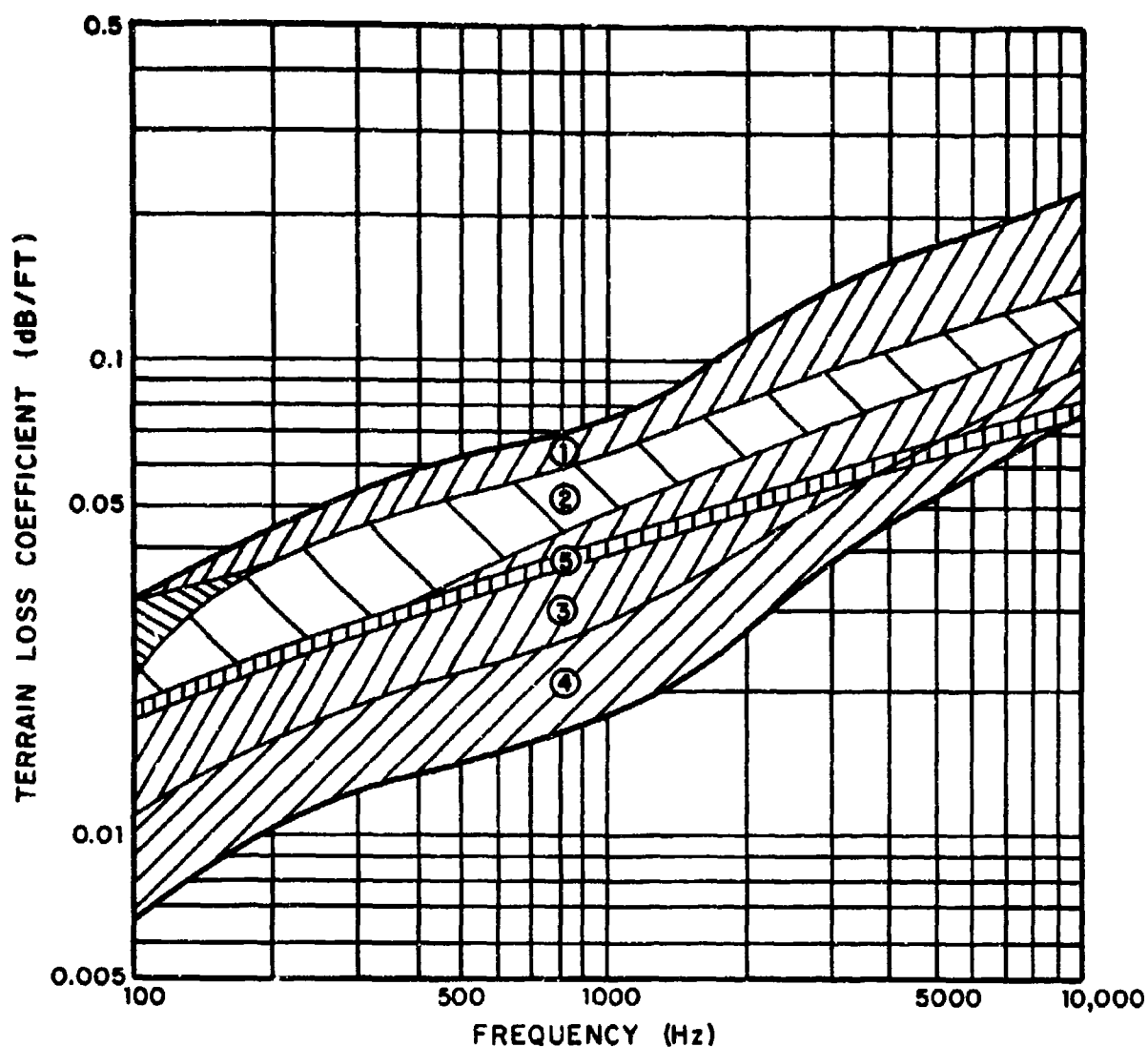FIGURE M2c   A CHART FROM WHICH TO ESTIMATE TERRAIN LOSS COEFFICIENTS FOR TROPICAL JUNGLES. ZONE 1, VERY LEAFY, ONE SEES A DISTANCE OF APPROXIMATELY 20 FT., PENETRATION BY CUTTING; ZONE 2, VERY LEAFY, ONE SEES APPROXIMATELY 50 FT., PENETRATED WITH DIFFICULTY BUT WITHOUT CUTTING; ZONE 3, LEAFY, ONE SEES A DISTANCE OF APPROXIMATELY 100 FT., FREE WALKING IF CARE IS TAKEN; ZONE 4, LEAFY, ONE SEES A DISTANCE OF APPROXIMATELY 200 FT., PENETRATION IS RATHER EASY; ZONE 5, LITTLE LEAFY UNDERGROWTH, LARGE BRACKETED TRUNKS, ONE SEES A DISTANCE OF APPROXIMATELY 300 FT., PENETRATION IS EASY (FROM REFERENCE 3).

FIGURE M3   EFFECT OF TERRAIN AND ELEVATION ANGLE ON THE TERRAIN LOSS
COEFFICIENT IN THE 150-300 Hz OCTAVE BAND (FROM REFERENCE 5)

FIGURE M4   EFFECT OF ABSORPTION ON RANGE FROM GIVEN SOURCE AT
WHICH PRESCRIBED SOUND PRESSURES ARE OBSERVED

187

APPENDIX N

AURAL DETECTABILITY

INTRODUCTION

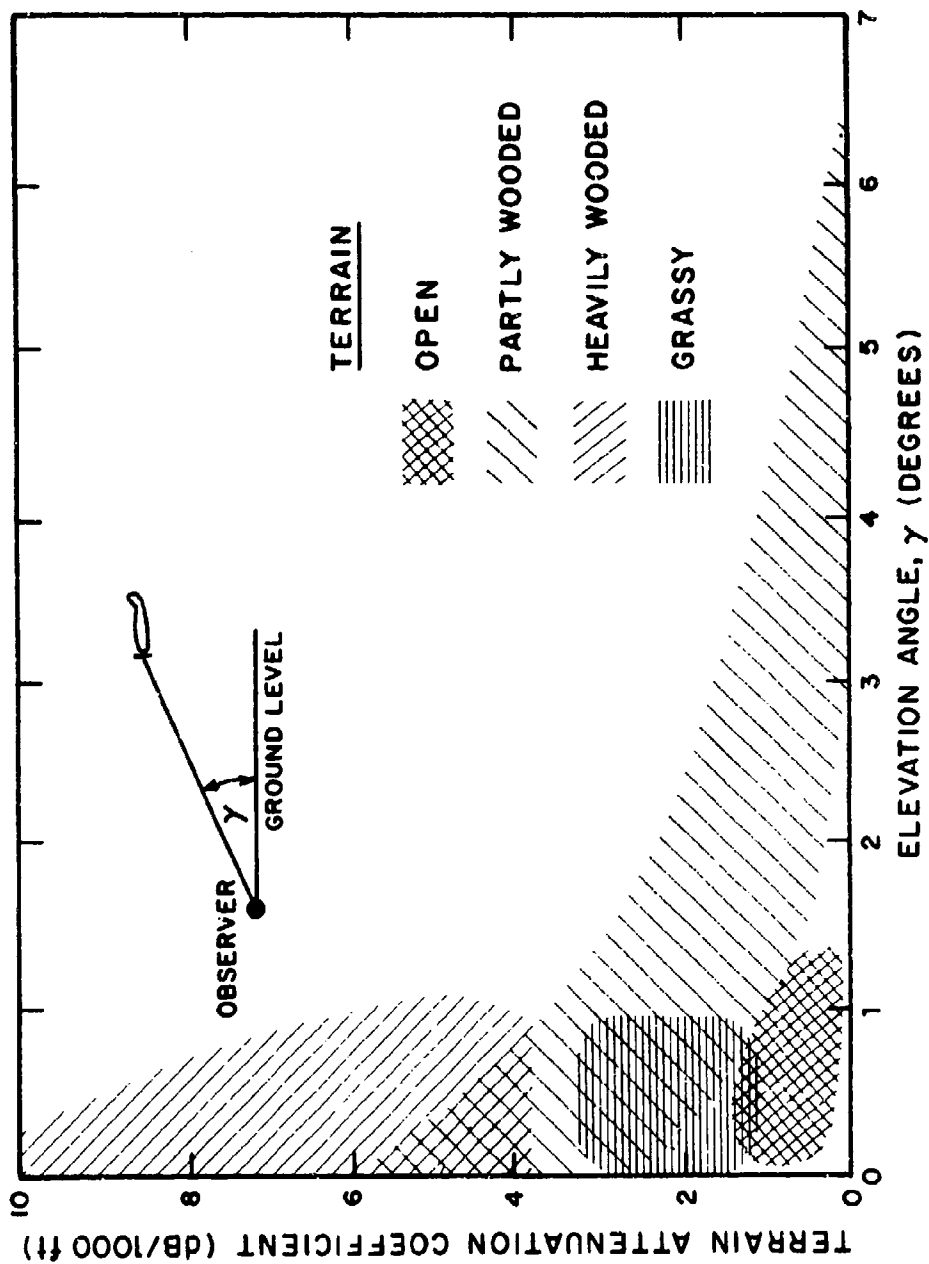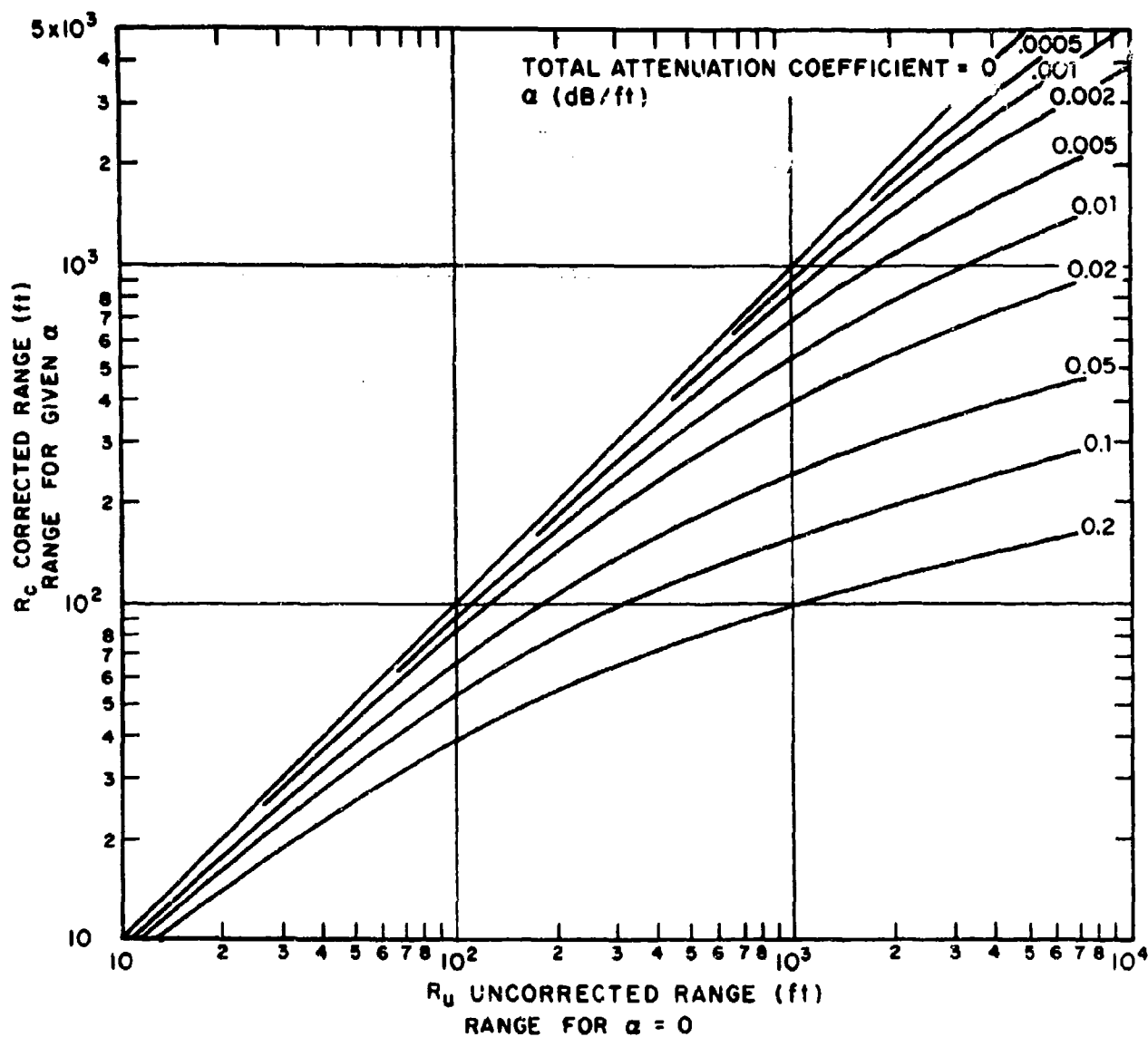In the absence of any ambient noise, an aircraft may be heard if the level of its noise at the location of the listener exceeds the threshold of hearing of the listener in any frequency range. The presence of the ambient noise tends to raise the threshold of detectability to a higher level, which may be called the "detection threshold". Increased intensity of the ambient noise in a given frequency band causes the detection threshold to exceed the threshold of hearing by increasing amounts.

Generally speaking, an aircraft is aurally detectable if its acoustical signal at the location of the listener exceeds both the threshold of hearing and the masking threshold. Consequently, a *necessary* condition for aural detection is that the signal exceeds the threshold of hearing of the observer in at least one frequency band; a *sufficient* condition is that the acoustical signal exceeds also the detection threshold corresponding to the ambient noise level present at the time of observation at the location of the listener.

Since the ambient noise varies from place to place – and also varies with the time of day at any given location – the aural detectability of a given aircraft differs for different situations.

In addition, aural detection is affected by such psychological factors as the observer's familiarity with the aircraft's acoustic signature (i.e., whether he knows what he is supposed to listen for), his other duties (which may interfere with his listening concentration), and the penalties associated with failure to hear an approaching aircraft as early as possible.

Because of the many variables involved in determination of detectability criteria for a complex signal in the presence of fluctuating ambient noise, the problem is a very complex one. In order to arrive at an engineering approximation of detectability described in this report, it was necessary to rely on laboratory data of the threshold of hearing for pure tones and bands of noise, and on the concept of critical bandwidth to evaluate the masking effect of the ambient noise. The approach suggested here is likely to lead to significant errors in predicting detectability in actual field situations, but is expected to be adequate for the purpose of comparing the detectabilities of alternate aircraft designs.

The acoustical signature of an aircraft generally consists of pure tones and broadband noise. Since either type of component can be responsible for aural detectability, both must be considered. They are discussed separately in the following paragraphs.

DETECTABILITY OF PURE TONES

Hearing Threshold

As has been mentioned, the level at which a signal becomes detectable depends on the threshold of hearing and on the masking level provided by the ambient noise. The threshold of hearing for pure tones has been investigated extensively in the laboratory. Figure N1 shows the threshold of hearing for pure tones, as a function of frequency, as recommended by the International Standard Organization (Ref. 1). This figure pertains to an "average" young listener, and indicates that the ear is most sensitive to frequencies between about 3000 Hz and 5000 Hz.

Masking By Noise

Hawkins and Stevens (Ref. 2) measured the masking effect of white noise on a pure tone signal by exposing test subjects simultaneously to the pure-tone signal and the masking noise and noting at which noise levels the subjects could just recognize the tone as having a definite pitch. Figure N2 shows the observed difference between the pure tone level and the masking white noise level (in 1 Hz bands).

There exists some evidence that the human auditory system senses separately the energies in certain "critical bands" (whose bandwidths are such that the energy in the masking noise in these bands matches the energy in the just audible pure tone at the band's center frequency). Accordingly, one may treat various pure-tone components separately and use Fig. N2 as the basis for an acceptable detectability prediction scheme.

One may calculate the detection level $L_d(f)$, which is the level of a pure tone which is just detectable in the presence of noise with a spectrum level $L_{N,1}(f)$, simply from

$$L_d(f) = L_{N,1}(f) + \theta_c(f) \tag{1}$$

where $\theta_c(f)$ is a correction factor which is plotted in Fig. N2 and which gives one the noise in critical bands. The spectrum (1 Hz bandwidth) level $L_{N,1}$ is related to the noise level $L_{N,\Delta f}$ measured in a frequency band Δf (with center frequency) as

$$L_{N,1} = L_{N,\Delta f} \qquad - 10 \log \Delta f$$

$$= L_{N,oct} \qquad - 10 \log f + 1.5 \text{ for octave bands}$$

$$= L_{N,1/3 \ oct} - 10 \log f + 6.5 \text{ for 1/3-octave bands.} \qquad (2)$$

Detectability

A pure-tone signal thus may be considered detectable in the presence of noise, if the signal exceeds both the detection level $L_d(f)$ given by Eq. (1) and the hearing threshold of Fig. N1.

DETECTABILITY OF BROADBAND NOISE

Hearing Threshold

The threshold of audibility of octave bands of white noise (constant spectral level within the pass band) was determined by Robinson and Whittle (Ref. 3). Their result is shown as the dotted curve of Fig. N1. Comparing the threshold curves for pure tones with that for octave bands, one finds that the two curves are almost identical. The difference between the two thresholds is less than the errors in estimation procedures, and also is much smaller than the variation in the threshold of hearing for individual listeners.* (It should be noted, however, that the octave band threshold curve was obtained for constant spectral level within the pass band of the octave filter. Accordingly, these results are strictly applicable only for similar conditions.)

Masking By Noise

Like a pure-tone signal, a broad-band signal also may be masked by noise. Unfortunately, there appears to be available no experimental data directly applicable to predicting the masking of a broad-band signal by broad-band noise. The addition of a broad-band signal in a given band to a similar noise in that band would be sensed by a listener merely as an increase in loudness, unless the signal has a spectrum which differs from that of the noise — in which case the listener would eventually notice a change in the frequency content of what he hears.

One may perhaps obtain the best estimate of masking effects by comparing the levels of the signal and noise in critical bands.

---

*Zwicker and Heinz (Ref. 4) give threshold variances of 5.5 dB at 50 Hz, 3.8 dB at 1 kHz, and 10 dB at 12 kHz.

In other words, if one has a signal spectrum $L_{S,\Delta f_s}(f)$ given in frequency bands Δf_s with center frequencies f, and a noise signal $L_{N,\Delta f_n}(f)$ in bands Δf_n, one may compute the corresponding sound pressure levels in critical bands from

$$L_{S,\theta}(f) = L_{S,\Delta f_s}(f) - 10 \log \Delta f_s + \theta_c(f)$$

$$(3)$$

$$L_{N,\theta}(f) = L_{N,\Delta f_n}(f) - 10 \log \Delta f_n + \theta_c(f)$$

Detectability

The signal $L_{S,\Delta f_s}(f)$ may be considered as audible if its octave band level

$$L_{S,oct} = L_{S,\Delta f_s}(f) + 10 \log (f/\Delta f_s) \qquad (4)$$

exceeds the threshold of hearing for octave bands, and if in addition the sound pressure level $L_{S,\theta}(f)$ of the signal in any critical band exceeds the level $L_{N,\theta}(f)$ in the same critical band.

Note that if the signal and noise are given in the same bands, so that $\Delta f_s = \Delta f_n = \Delta f$, then

$$L_{S,\theta}(f) - L_{N,\theta}(f) = L_{S,\Delta f}(f) - L_{N,\Delta f}(f). \qquad (5)$$

Therefore, if signal and noise are given in the same bands, the signal may be considered detectable if it exceeds in any band both the hearing threshold and the noise. In other words, here the band detection level is equal to the noise level in the same band;

$$L_{d,\Delta f}(f) = L_{N,\Delta f}(f) \qquad (6)$$

Complications

Superposition on ambient noise of a broadband signal which is not of completely random character, but which exhibits an amplitude modulation, results not only in an increase in intensity but also in a change of the character of the composite signal. This change in character may enable a listener to detect the signal at a lower level than for a completely random signal.

Feldkeller and Zwicker (Ref. 5) have measured the effect of modulation on the detection of amplitude-modulated pure tones and bands of random noise. For bands of random noise with sound pressure levels above 20 dB and center frequencies above 1 kHz, one can notice amplitude modulations with modulation indexes exceeding 0.06.

Since in these experiments only a single band of amplitude-modulated noise was presented to the listener, the results are not immediately applicable to the aural detection of aircraft, where ambient noise is present in all bands and may compete for the attention of the listener. However, the extreme sensitivity of the ear to amplitude-modulation should be taken into account in designing aircraft for minimum aural detectability.

BACKGROUND NOISE LEVELS

Data on the ambient noise levels in jungles and forested areas are presented in the papers of Eyring (Ref. 6), McLaughlin and Hand (Ref. 7) and Saby and Thorpe (Ref. 8). The data given in these papers excludes transitory sounds, such as wind, rain and animal calls and may thus be used to obtain conservative estimates of aural detectability.

Eyring presents detection levels (Fig. N3) at various times of day for a dense, leafy jungle and for a forested area in Panama. The frequency range covered is from 100 to 6000 Hz. His detection levels were calculated essentially according to Eqs. (1) and (2), and thus apply to the detection of pure tones. In view of Eqs. (1), (2), and (6), the corresponding detection levels for bands of width f are higher than those shown in Fig. N3 by an amount $L_{d,\Delta f} - L_d = 10 \log \Delta f - \theta_c(f)$. [Values of the correction $(L_{d,oct} - L_d)$ from pure-tone to octave-band masking levels are shown in Fig. N2.]

McLaughlin and Hand present one-third octave band background levels at various locations and times in a Thailand jungle, for a frequency range from 100 to 1000 Hz. Although this paper is not readily available, some representative data for average day and night conditions have been reproduced in Ref. 9. Saby and Thorpe present spectrum levels of background noise in a Panama jungle, for high frequencies, from 8,000 to 25,000 Hz.

In Fig. N4 are shown the combined results derived from the aforementioned sources, all in terms of detection levels for pure tones. The two figures apply to average daytime and nighttime conditions, respectively. (For purposes of comparison, Fig. N4 also includes a curve for the minimum nighttime detection levels for a residential area, as derived from the background noise data of Ref. 10.)

The various sets of data are quite consistent and indicate that (a) detection levels increase with increasing density of vegatation, at all frequencies; (b) nighttime detection levels are lower than daytime levels at low frequencies, but are much higher at high frequencies. The latter effect is attributable to the nearly continuous presence of high-pitched inset sounds during the night. Over most of the frequency range, the detection levels are highest during early evening hours and lowest around midday. The variation of detection level with time of year was not investigated, but would be expected to be small relative to the diurnal variations.

An interesting question concerns the effect of the human listener on these detection levels, since the reported measurements were all made with a microphone placed a large distance from human observers, whereas the aural detection problem involves the detection level in the immediate vicinity of an observer. According to Ref. 8, however, the quieting of nearby insects in the presence of an observer does not measurably alter the detection levels.

REFERENCES FOR APPENDIX N

1. International Standards Organization, Document ISO, R226, (1961).

2. Hawkins, J.E., Jr. and S.S. Stevens, "The Masking of Pure Tones and Speech by White Noise," *J. Acoust. Soc. Amer.* **22**, pp. 6-13 (1950).

3. Robinson, D.W. and L.S. Whittle, "The Loudness of Octave-Bands of Noise," *Acustica* **14**, p. 33 (1964).

4. Zwicker, E. and W. Heinz, "Häufigkeitsverteilung der Hörschwelle," *Acustica,* **5**, Beiheft 1, p. 75 (1955).

5. Feldkeller, R. and E. Zwicker, *Das Ohr als Nachrichtenempfänger,* S. Hirzel Verlag, Stuttgart, 1956.

6. Eyring, C.F., "Jungle Acoustics," *J. Acoust. Soc. Amer.* **18**, p. 257 (1946).

7. McLaughlin and Hand, "Analysis of Background Sound from Data Recorded in Thailand," Report No. 8743-1-F, prepared for the Advanced Research Projects Agency, (1967).

8. Saby, J.S. and H.A. Thorpe, "Ultrasonic Ambient Noise in Tropical Jungles," *J. Acoust. Soc. Amer.* **18**, p. 271 (1946).

9. Smith, D.L. and R.P. Paxson, "The Aural Detection of Aircraft," Air Force Flight Dynamics Laboratory Report No. TM-69-1-FDDA (1969).

10. Bonvallet, G.L., "Levels and Spectra of Traffic, Industrial, and Residential Area Noise," *J. Acoust. Soc. Amer.* **23**, p. 435 (1951).
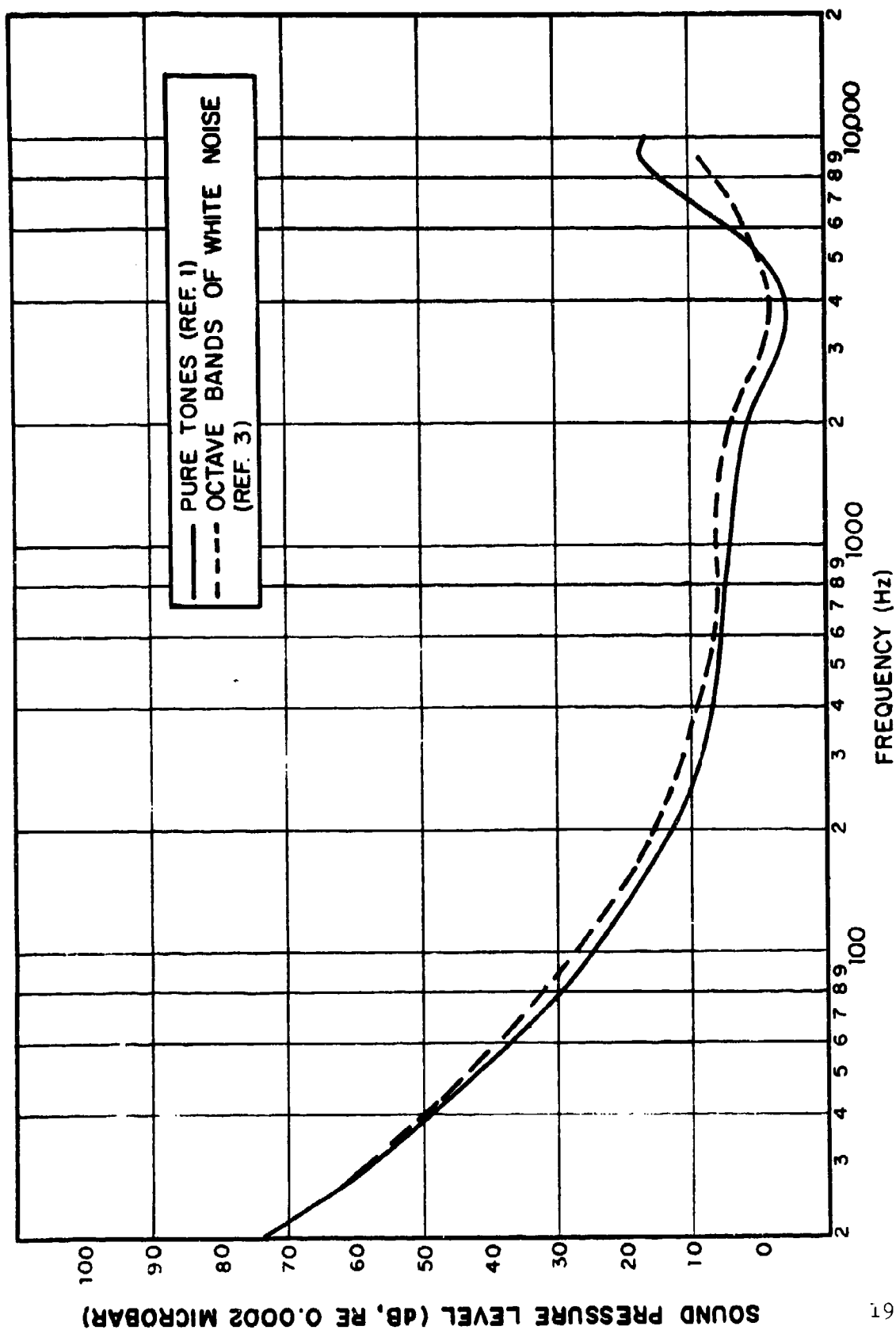
FIGURE N1   THRESHOLD OF HEARING

195
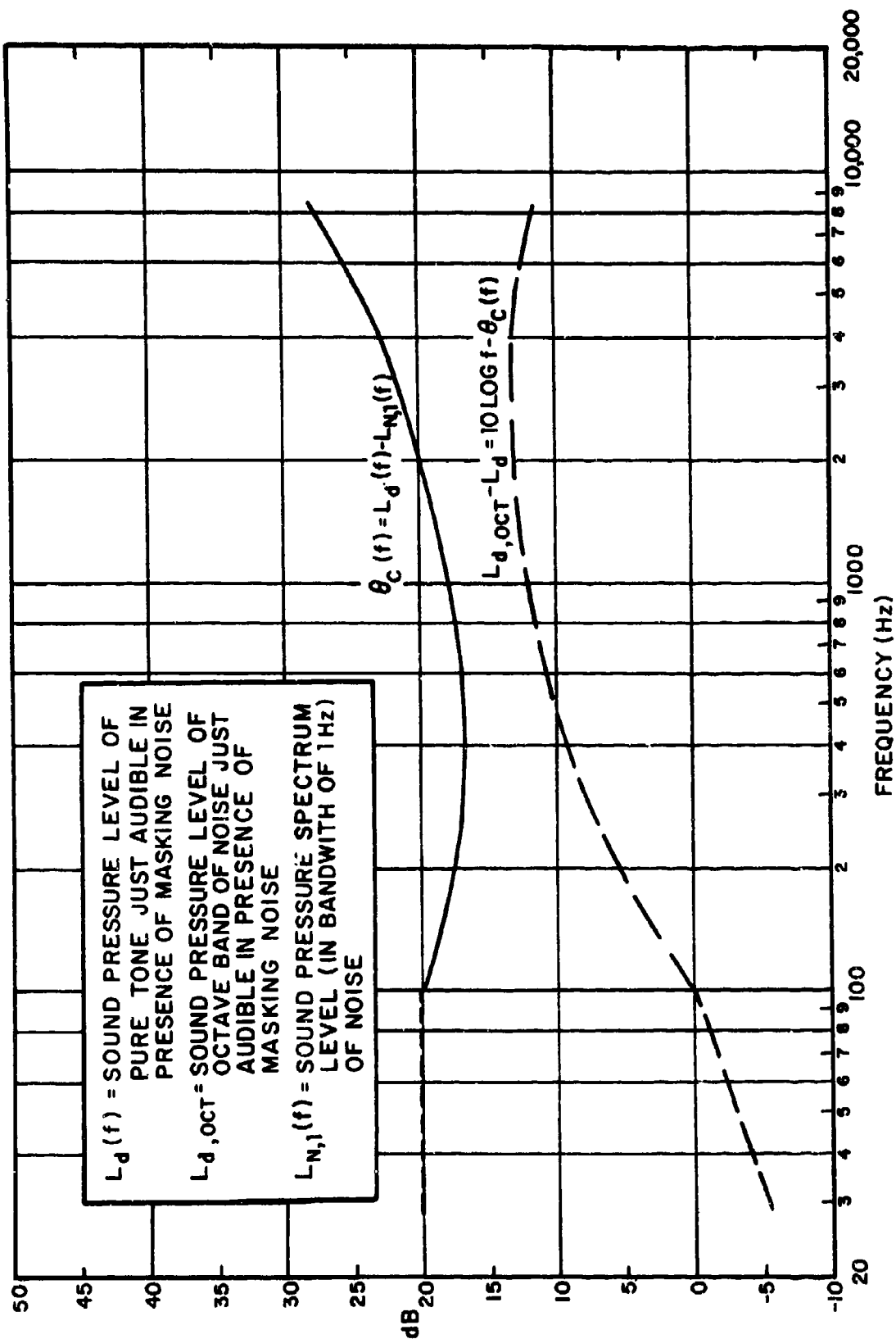
FIGURE N2   MASKING OF PURE TONES BY NOISE (REFERENCE 2), AND CORRECTION FOR OBTAINING OCTAVE-BAND DETECTION LEVELS $L_{d,OCT}$ FROM PURE-TONE DETECTION LEVELS L_d

$L_d(f)$ = SOUND PRESSURE LEVEL OF PURE TONE JUST AUDIBLE IN PRESENCE OF MASKING NOISE

$L_{d,OCT}$ = SOUND PRESSURE LEVEL OF OCTAVE BAND OF NOISE JUST AUDIBLE IN PRESENCE OF MASKING NOISE

$L_{N,1}(f)$ = SOUND PRESSURE SPECTRUM LEVEL (IN BANDWITH OF 1 Hz) OF NOISE

$\theta_c(f) = L_d(f) - L_{N,1}(f)$

$L_{d,OCT} - L_d = 10 \log f - \theta_c(f)$

FREQUENCY (Hz)

196
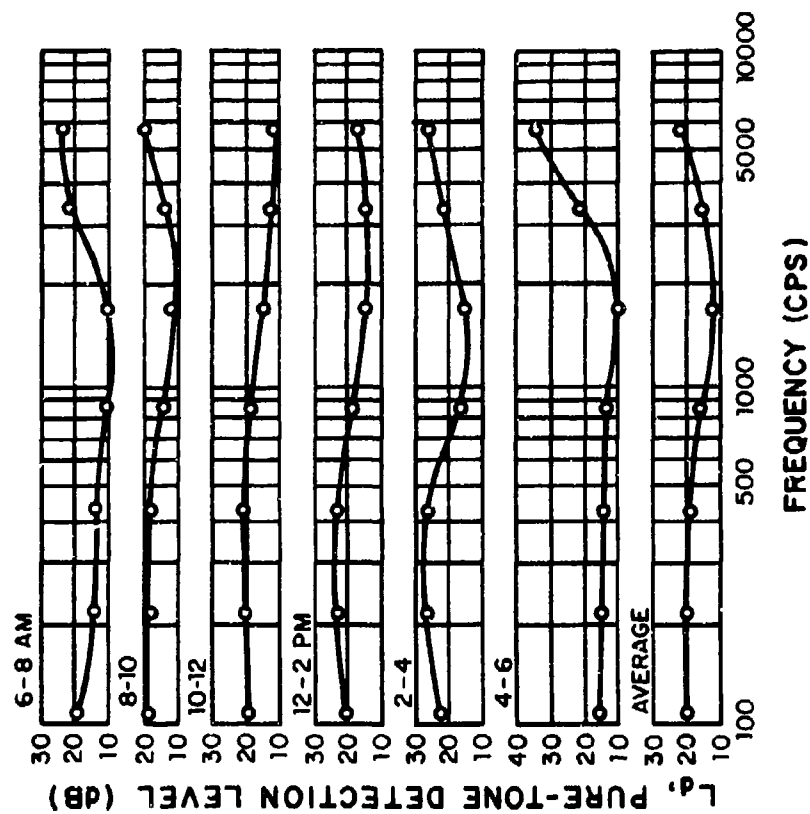
FIGURE N3a   DAYTIME VARIATION OF DETECTION LEVELS IN PANAMA FOREST AND JUNGLE
(FROM REFERENCE 6)

FIGURE N3b   NIGHTTIME VARIATION OF DETECTION LEVELS IN PANAMA FOREST AND JUNGLE
(FROM REFERENCE 6)

FIGURE N4   REPRESENTATIVE DETECTION LEVELS IN JUNGLES AND FORESTS
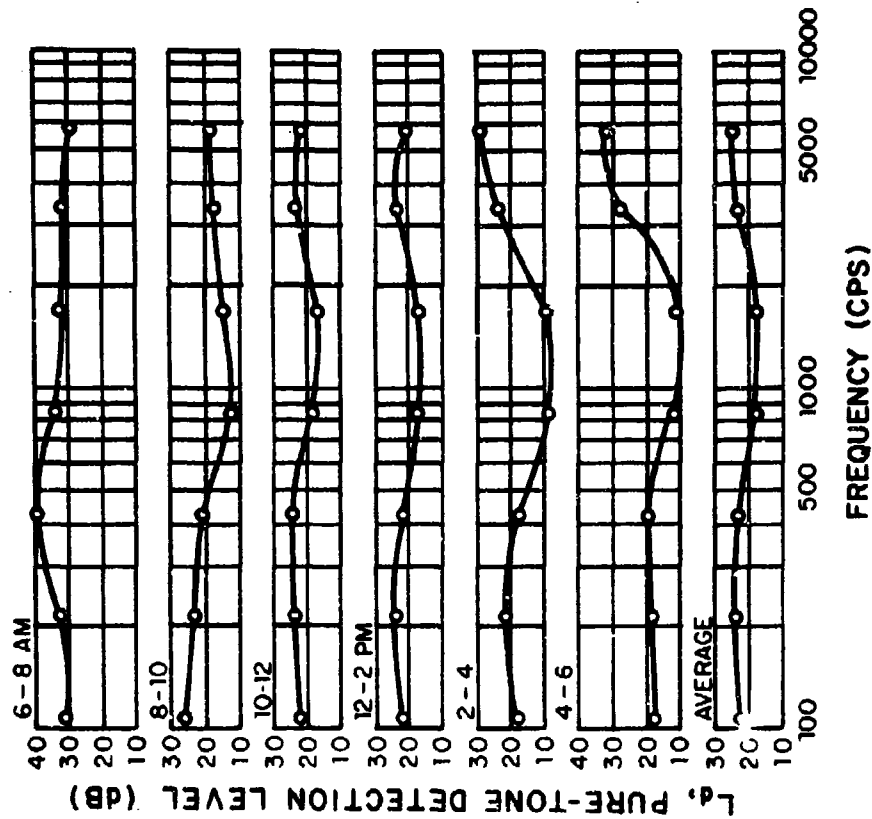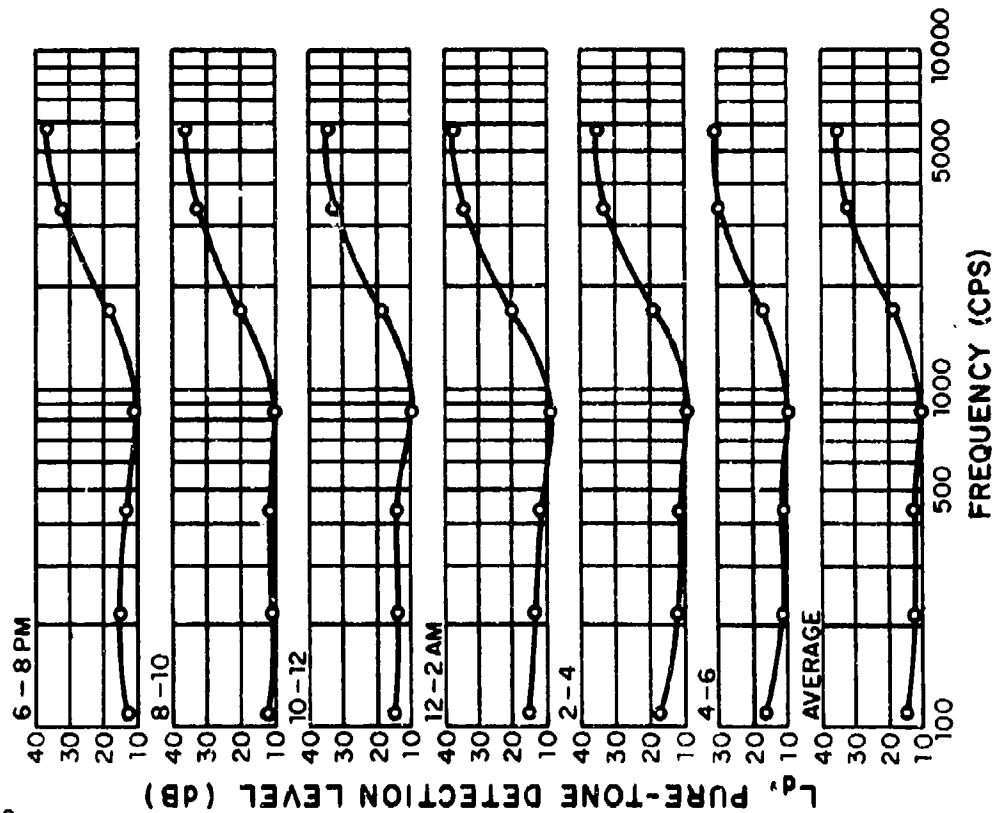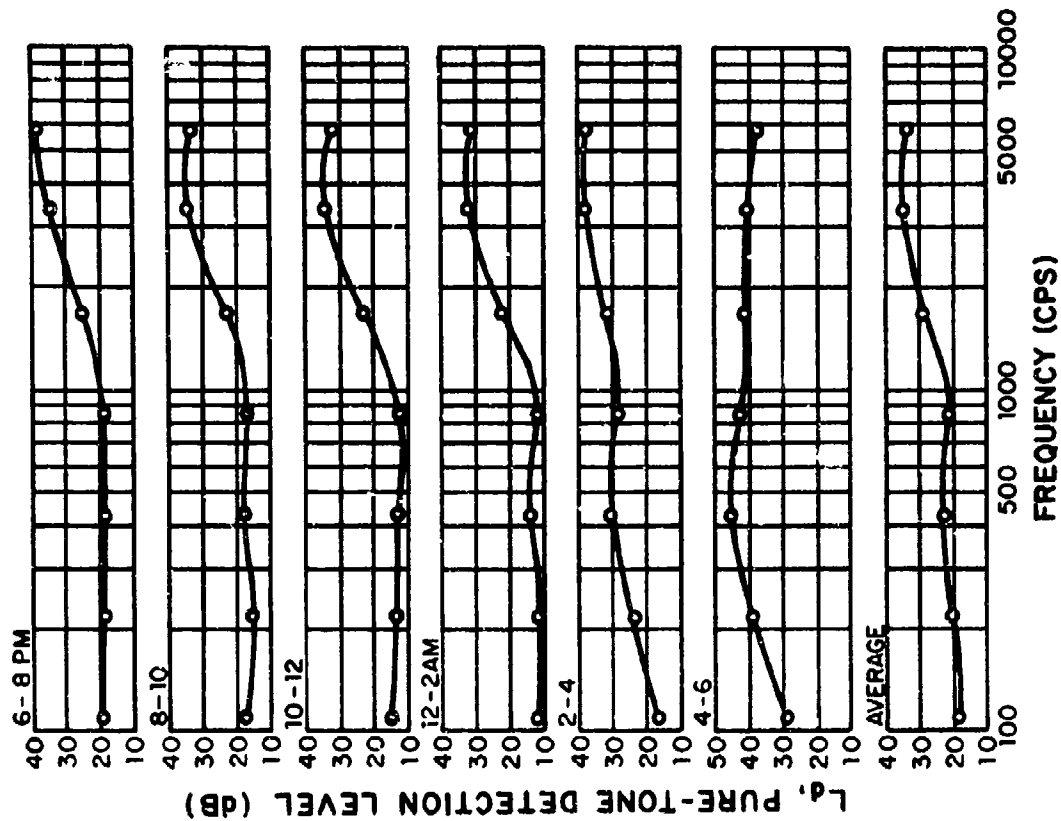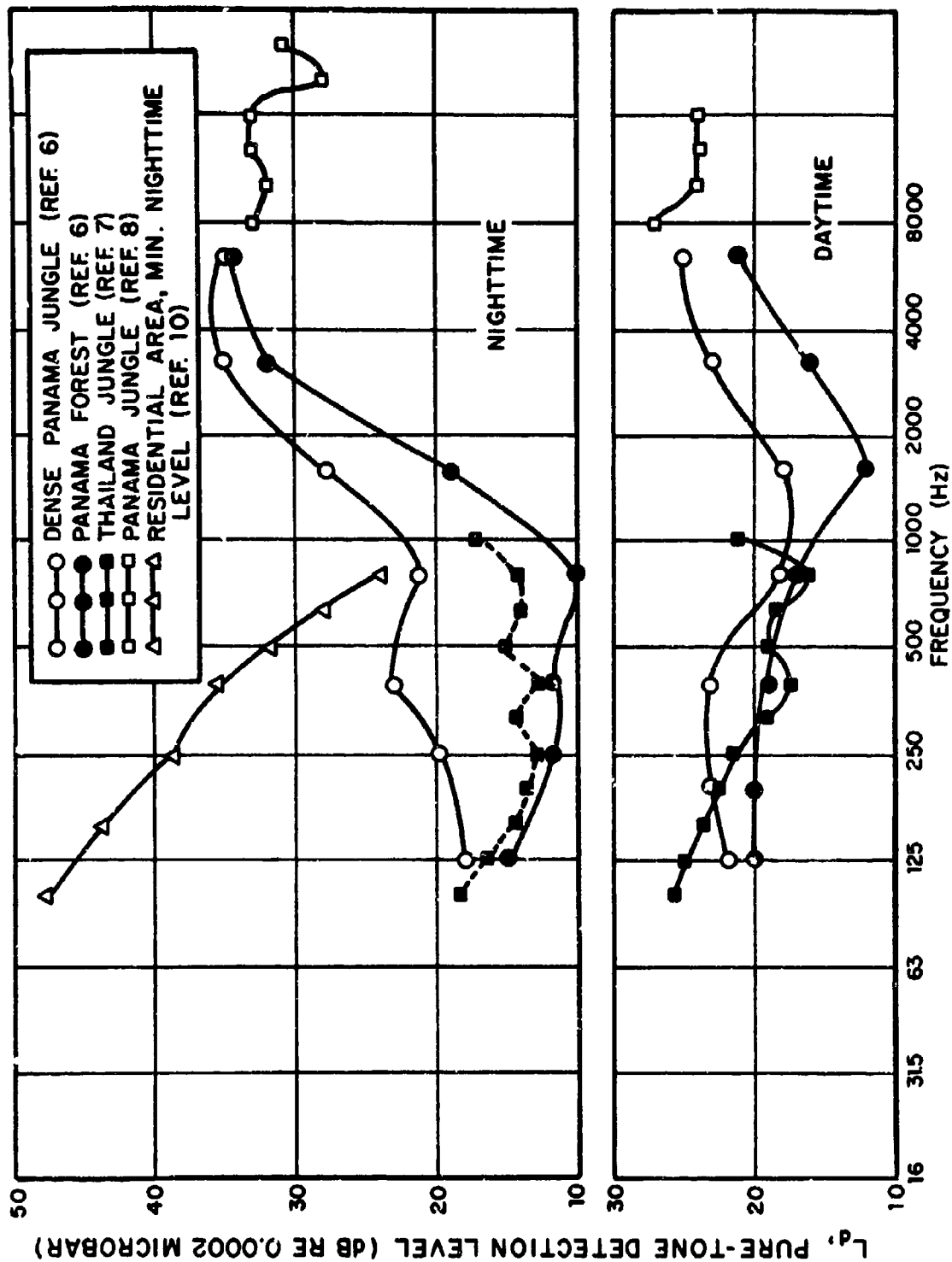
193

APPENDIX P

ALTERNATE METHOD FOR DETERMINING UNCORRECTED
DETECTION RANGE

INTRODUCTION

The "Detection Level Spectrum" discussion in the main body of this report, as well as the corresponding aural detectability estimation approach presented in Appendix N, are based on the results of psychoacoustic studies of the detectability of stationary (i.e., time-independent) pure-tone and broadband signals. Since different detectability criteria apply to pure-tone and to broadband signals, one must approximate the noise from any given source in terms of stationary pure-tone and broadband components, in order to apply the suggested approach.

However, the noise that reaches a listener on the ground due to an aircraft flyover is nonstationary and typically consists of many broadband and "pure-tone" components that change both in apparent frequency and amplitude. Thus, one faces the often very difficult problem of estimating equivalent stationary pure-tone and broadband levels. The various noise prediction schemes presented in the previous appendices suggest how these levels may be estimated for the various noise sources considered, and may be adequate for many purposes — particularly in the light of the often considerable uncertainties associated with the noise source predictions —; however, an alternate method, which does not require the user to differentiate *a priori* between pure-tone and broadband signal components, has been found useful for determining detectability, especially from recorded data (Ref. 1). This alternate method is described in the present appendix.

RESULTS OF SAILPLANE AURAL DETECTION STUDY

Reference 1 reports the results of a study of the flyby noise (as perceived on the ground) produced by three different sailplanes at various altitudes and speeds. This study served to characterize the noise, but also included some subjective determinations of when the sailplanes could just be heard.

It was found that the observed detection ranges agreed well with predictions obtained by comparing the spectrum levels of the received sound to an aural detection spectrum for pure tones, where the spectrum levels were determined (by means of an appropriate Fourier analyzer) with an effective averaging time of

50 milliseconds,* and were obtained by reducing the bandwidth of
the signal analysis until the level remained constant. Since this
analysis procedure resulted in signal levels that were 9 to 12 dB
greater than the spectrum levels calculated from the third-octave
levels using the usual bandwidth conversion relation,** which is
based on the assumption that the energy is uniformly distributed
in each band, it appears that for audibility estimation purposes
one should increase the "constant energy" spectrum levels $L_{S,1}$

obtained from broadband spectra by about 10 dB in order to account
for the ability of a listener to detect rapid changes in frequency
and amplitude.

ESTIMATION OF UNCORRECTED DETECTION RANGE FROM RECORDED FLYBY SOUND

In order to determine the uncorrected detection range of an
aircraft from tape-recorded flyover noise data, one may proceed
as described below. (An example, taken from Ref. 1, is shown in
Fig. P1.)

1. Determine the pure-tone detection level spectrum $L_d(f)$ from
   the pure-tone hearing threshold and the background noise
   spectrum, as indicated in Appendix N and Fig. 2 of the body
   of this report.

2. Determine the maximum sound pressure level in each one-third
   octave band during the flyover, using an averaging time no
   greater than 0.3 sec. Listen to the signal during the data
   reduction, and/or carry out preliminary narrow-band analyses,
   judge whether pure tones are dominant.

---

*This averaging time is within the 20 to 250 millisecond range
 of integration times of the ear, as reported in Ref. 2.

**i.e.,

$$L_{S,1} = L_{S,\Delta f} - 10 \log \Delta f \qquad (1)$$

where $L_{S,\Delta f}$ represents the level measured in a band of width Δf
(e.g., a third-octave band), and $L_{S,1}$ denotes the corresponding
"constant-energy" spectrum level.

3. Find the one-third octave band in which the difference between the detection level (Step 1) and the measured third-octave band signal level (Step 2) is greatest. (In the example of Fig. P1, this greatest difference occurs in the band centered at 315 Hz and amounts to 30.5 dB.)

4. Conduct a narrow-band analysis of the signal over a frequency range that includes the band selected in Step 3, using an averaging time for the analysis that does not exceed 0.1 sec.

   Repeat this analysis with narrower and narrower analysis bandwidths, until the peak level remains essentially unchanged. Note this peak level and the frequency at which it occurs. (In the example of Fig. P1, this spectrum level is 37 dB, at 285 Hz.)

5. Determine the difference between this peak level and the detection level spectrum $L_d(f)$ at the peak frequency. (In Fig. P1, this difference is 20.5 dB.)

6. If the received signal is not dominated by pure tones, and a narrow band analysis cannot be conducted.

   (a) Determine the effective signal spectrum levels $L_{S,1}$

   from the one-third octave band spectrum levels $L_{S,1/3}$

   $_{oct}$ found in Step 2, by use of

   $$L_{S,1} = L_{S,1/3 \text{ oct}} - 10 \log f + 16.5 \qquad (2)$$

   where f represents the center frequency of the third-octave bands (in Hz).

   (b) Consider the levels $L_{S,1}$ to occur at the center frequencies of the corresponding third-octave bands, and determine the greatest difference between these signal levels and the pure-tone detection level L_d. (In the example of Fig. P1, the greatest difference, 22 dB is obtained at 315 Hz).

7. Find the uncorrected detection range R_u from

   $$20 \log (R_u/R_{min}) = L_{S,1} - L_d \qquad (3)$$

where R_{min} is the minimum distance between the aircraft and the microphone during the flyby (and is equal to the altitude in the case where the aircraft passes directly over the microphone), and $L_{S,1}-L_d$ is the greatest difference between the signal spectrum and the detection spectrum levels, as obtained from Steps 3 and 4. (In the example of Fig. P1, uncorrected detection ranges of 1340 and 1580 ft were obtained.)

Note that this calculation of R_u does not take account of atmospheric and terrain attenuation effects. Corrections for these effects may be made by means of the data given in Appendix M. If R_{min} is large, one must also consider that these attenuation effects can affect the recorded signals.

ESTIMATION OF UNCORRECTED DETECTION RANGE FROM PREDICTED NOISE SOURCE CHARACTERISTICS

In order to determine the uncorrected detection range from the predictions of aircraft noise, as given in the various foregoing appendices, one may proceed as follows:

1. Determine the pure-tone detection level spectrum $L_d(f)$ from the pure-tone hearing threshold and the applicable background noise spectrum, as described in Appendix N and Fig. 2 of the body of this report.

2. Determine the power level and frequency for each pure-tone noise component from each source.

3. Determine the octave-band power level spectrum for each noise source, and combine the levels from all of the sources as described in the body of this report.

4. Find the corresponding effective signal spectrum level $L_{S,1}$ from

$$L_{S,1} = L_{S,oct} - 10 \log f + 11.5 \qquad (4)$$

where $L_{S,oct}$ represents the combined octave-band level (as found in Step 3) at the center frequency f.

5. Compare the power levels L_w of all pure tones (from Step 2) and the combined effective signal spectrum level $L_{S,1}$ (from

Step 4) with the pure-tone detection level spectrum L_d (from Step 1). Find the greatest differences L_w-L_d and $L_{S,1}-L_d$ and the corresponding frequencies.

6. Calculate the uncorrected detection range R_u from

$$20 \log R_u(ft) = (L-L_d)_{max}$$

where $(L-L_d)_{max}$ represents the greater of the two maximum differences, L_w-L_d and $L_{S,1}-L_d$.

REFERENCES FOR APPENDIX P

1. Smith, D.L. and R.P. Paxson, "Measurements of the Radiated Noise from Sailplanes", Air Force Flight Dynamics Laboratory TM-70-3-FDDA (1970).

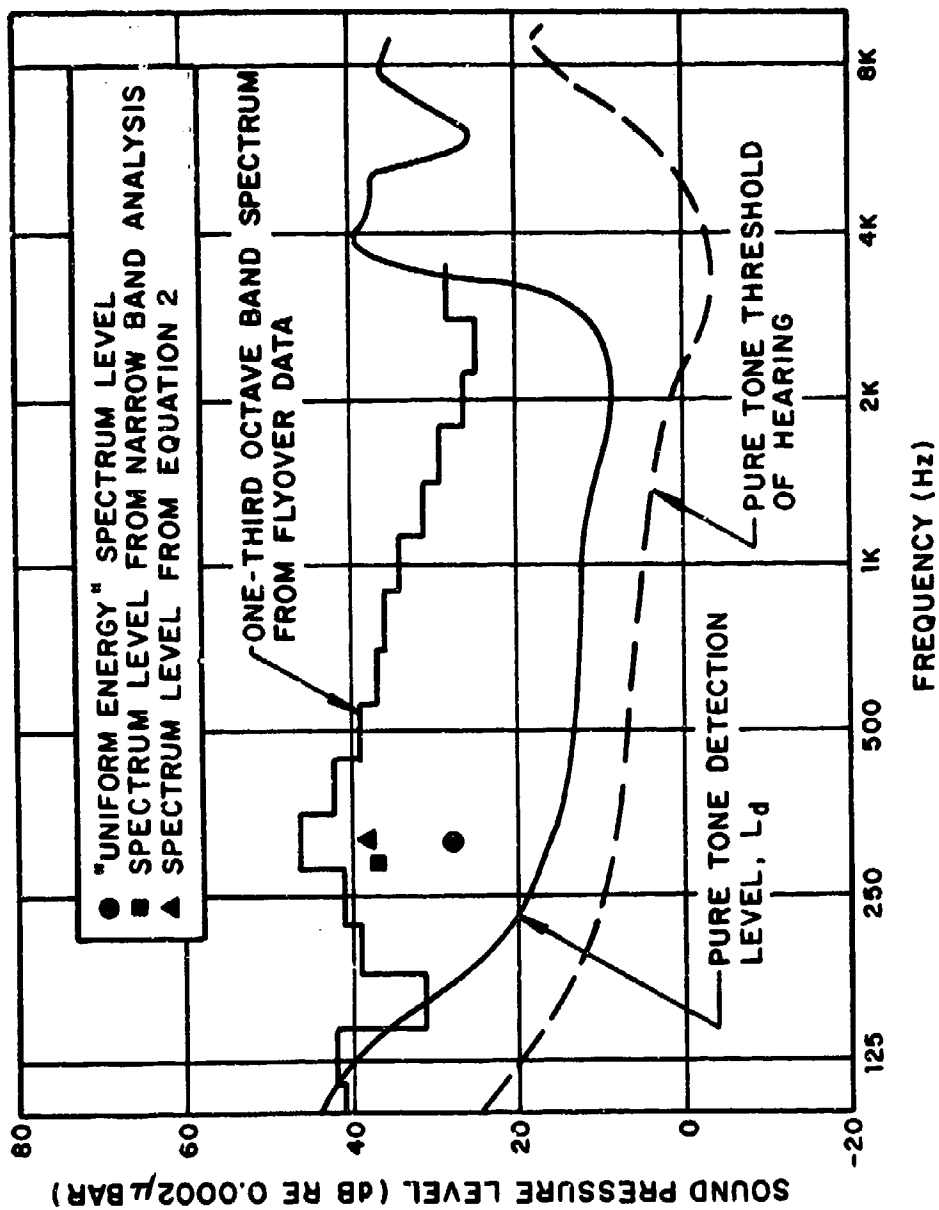2. Zwislocki, J., "Theory of Temporal Auditory Summation", *J. Acoust. Soc. Amer.* **32**, p. 1046 (1960).

FIGURE P1   SAMPLE AURAL DETECTION EVALUATION (FROM REFERENCE 1)

706

DOCUMENT CONTROL DATA · R & D

(Security classification of title, body of abstract and indexing annotation must be entered when the overall report is classified)

1. ORIGINATING ACTIVITY (Corporate author)	2a. REPORT SECURITY CLASSIFICATION
Bolt Beranek and Newman Inc. 50 Moulton Street Cambridge, Massachusetts 02138	Unclassified
	2b. GROUP

3. REPORT TITLE

A Guide for Predicting the Aural Detectability of Aircraft

4. DESCRIPTIVE NOTES (Type of report and inclusive dates)

Final Technical Report. Jan 70 - Jan 71,

5. AUTHOR(S) (First name, middle initial, last name)

Eric E. Ungar, Daniel L. Nelson, Joseph Smullin, Istvan Ver, Richard E. Hayden

6. REPORT DATE	7a. TOTAL NO. OF PAGES	7b. NO. OF REFS
MAR 72	229	105

8a. CONTRACT OR GRANT NO.	9a. ORIGINATOR'S REPORT NUMBER(S)
F33615-70-C-1276 NEW	BBN -2104
b. PROJECT NO. 1471	
c. AF Task No. 147102	9b. OTHER REPORT NO(S) (Any other numbers that may be assigned this report)
d.	AFFDL-TR-71-22

10. DISTRIBUTION STATEMENT

Distribution limited to U. S. Government agencies only; test and evaluation; statement applied 15 February 1972. Other requests for this document must be referred to AF Flight Dynamics Laboratory/FY, Wright-Patterson AFB, Ohio 45433.

11. SUPPLEMENTARY NOTES	12. SPONSORING MILITARY ACTIVITY
	Air Force Flight Dynamics Lab. Wright-Patterson Air Force Base Ohio

13. ABSTRACT

The concepts which underlie the detection of aircraft by the human ear are described. A scheme is delineated for predicting the range at which a given aircraft will first be heard by an "average" listener; this scheme is also applicable to comparing the aural detectabilities of alternate aircraft configurations and to identifying those components of the noise of a given configuration which bear prime responsibility for the aircraft's detectability. Means are presented for predicting the noise due to all sources likely to be significant for light aircraft, the attenuation of acoustic signals propagating from an aircraft to a listener on the ground, and the ability of a listener to detect an acoustic signal in the presence of background noise. (This report gathers)

This report gathers together for the first time from a diffuse literature of acoustics, engineering mechanics and aeronautical engineering knowledge and data on methods of predicting the source intensities, propagation and aural detection of sound radiated by military aircraft of the utility class. This report will be used for the design of quiet aircraft and discloses the detailed methods used by the Air Force in evaluating such aircraft from the acoustical standpoint.

UNCLASSIFIED
Security Classification

KEY WORDS	LINK A		LINK B		LINK C	
	ROLE	WT	ROLE	WT	ROLE	WT
Aural detection						
Aircraft noise						
Empire noise						
Propeller noise						
Aerodynamic noise						
Jet noise						
Ducts						
Sound propagation and attenuation						

DD FORM 1473 (BACK)
,NOV..